VOLUME 14 (1960) No. 3

NUCLEAR PHYSICS

JOURNAL DEVOTED TO THE EXPERIMENTAL AND THEORETICAL STUDY OF THE FUNDAMENTAL CONSTITUENTS OF MATTER AND THEIR INTERACTIONS

EDITOR: L. ROSENFELD - COPENHAGEN

TH. KANELLOPOULOS and K. WILDERMUTH, Antisymmetrization of "cluster model" wave functions and their expansion in "shell model" wave functions . . . 349
G. R. BISHOP, Application of the collective model to some nuclei in the d-shell . . . 376
EUGENE P. GROSS, Collective rotations of nuclei . . . 389
DIETER KURATH, Enhancement of E2 transition probability . . . 398
A. N. MITRA and V. L. NARASIMHAM, Role of spin-orbit force in nuclear interactions . . . 407
SHIGUEO WATANABE, Low energy elastic scattering of nucleons by deuterons . . . 429
N. M. ANTONIEVA, A. A. BASHILOV, B. S. DZHELEPOV and V. A. SERGIENKO, Decay of Gd^{146} and Eu^{146} . . . 438
E. P. GRIGORIEV and A. V. ZOLOTAVIN, On decay of Se^{75} . . . 443
D. BERÉNYI, GY. MÁTHÉ and T. SCHARBERT, Investigations of the decay-scheme of Fe^{59} . . . 459
H. DAVIES, On the convergence of the Born approximation . . . 465
R. L. CLARKE, E. ALMQVIST and E. B. PAUL, Properties of levels excited in (p, α) reactions on O^{18}, F^{31}, Cl^{35}, Cl^{37}, K^{39} and K^{41} . . . 472
KENNETH R. GREIDER, An approximation for nucleon-nucleus polarization effects . . . 498
GEOFFREY I. OPAT, The electric dipole sum rule . . . 506
P. H. STOKER and P. C. HAARHOFF, The creation of fast electron pairs by high energy muons . . . 512
PAUL DE CELLES and GORDON FELDMAN, Dispersion relations in the Lee model . . . 517
V. S. BARASHENKOV, V. A. BELIAKOV, V. V. GLAGOLEV, N. DALKHAZHAV, YAO TSYNG SE, L. F. KIRILLOVA, R. M. LEBEDEV, V. M. MALTSEV, P. K. MARKOV, M. G. SHAFRANOVA, K. D. TOLSTOV, E. N. TSYGANOV and WANG SHOU FENG, Mechanism of interaction of fast protons with nucleons and nuclei . . . 522
D. F. ZARETSKY and V. M. NOVIKOV, On excitation of nuclei by μ-mesons . . . 540
A. BERTHELOT, C. CHOQUET, A. DAUDIN, O. GOUSSU et F. LÉVY, Contribution à l'étude de l'annihilation des antiprotons dans les noyaux complexes . . . 545

NORTH-HOLLAND PUBLISHING COMPANY - AMSTERDAM

January (1) 1960

EDITORIAL BOARD

AUSTRALIA & NEW ZEALAND:	H. Messel (Sydney), M. L. Oliphant (Canberra)
AUSTRIA:	B. Karlik, (Vienna), H. Thirring (Vienna)
BELGIUM:	M. de Hemptinne (Louvain), J. Verhaeghe (Ghent)
CANADA:	G. Volkoff (Vancouver)
DENMARK:	C. Møller (Copenhagen), S. Rozental (Copenhagen), G. Brown (Copenhagen)
FINLAND:	L. Simons (Helsinki)
FRANCE:	A. Berthelot (Saclay), S. Gorodetzky (Strasbourg)
GERMANY (DEM. REP.):	G. Hertz (Leipzig)
GERMANY (FED. REP.):	W. Gentner (Freiburg i. B.), J. H. D. Jensen (Heidelberg)
GREAT BRITAIN:	S. Devons (Manchester), T. H. R. Skyrme (Harwell)
HUNGARY:	L. Janossy (Budapest)
INDIA:	H. Bhabha (Bombay), R. Ramanna (Trombay)
IRISH REPUBLIC:	J. McConnell (Maynooth)
ISRAEL:	G. Racah (Jerusalem)
ITALY:	E. Amaldi (Rome)
JAPAN:	S. Kikuchi (Tokyo), S. Tomonaga (Tokyo)
MEXICO:	M. Moshinsky (Mexico)
NETHERLANDS:	H. Brinkman (Groningen), S. R. de Groot (Leiden)
NORWAY:	E. Hylleraas (Oslo), A. Lundby (Oslo), H. Wergeland (Trondheim)
POLAND:	L. Infeld (Warsaw)
PORTUGAL:	J. M. Araújo (Porto), J. R. de Almeida Santos (Coimbra)
SOUTH AMERICA:	G. Beck (Saõ Paulo), J. Leite Lopes (Rio de Janeiro)
SPAIN:	J. M. Otero (Madrid), C. Sanchez del Rio (Madrid)
SWEDEN:	O. Klein (Stockholm), K. Siegbahn (Uppsala), I. Waller (Uppsala)
SWITZERLAND:	P. Huber (Basel), P. Scherrer (Zürich)
U.A.R. & ARAB COUNTRIES:	F. El Bedewi (Alexandria), M. G. Nooh (Cairo)
U.S.A.	H. H. Barschall (Madison, Wisconsin), V. Weisskopf (Cambridge, Mass.)
U.S.S.R.:	M. A. Markov (Moscow), I. S. Shapiro (Moscow), D. V. Skobeltzyn (Moscow)
YUGOSLAVIA:	I. Supek (Zagreb)

CONTRIBUTIONS may be sent to the Editor, Professor L. Rosenfeld, NORDITA, Blegdamsvej 17, Copenhagen Ø, either directly, or preferably through the intermediary of one of the members of the Editorial Board of the country or region in which the author is working. They may be written in English, French or German.

NUCLEAR PHYSICS is published in fortnightly issues. The subscription price per volume of 700 pages is fl 57.00; 114s; $ 15.00. Post-free.

SUBSCRIPTIONS should be sent to the publishers, NORTH-HOLLAND PUBLISHING COMPANY, P.O.Box 103, Amsterdam or to any subscription-agent.

BOOKS FOR REVIEW should be sent to Professor Rosenfeld.

No part of this issue may be reproduced in any form, by print, photoprint, microfilm or any other means without written permission from the publisher. Reprints, photoprints or microfilms are obtainable at cost from the publisher.

Printed in the Netherlands

1.D.3 *Nuclear Physics* **14** (1959/60) 349—375; © *North-Holland Publishing Co., Amsterdam*
Not to be reproduced by photoprint or microfilm without written permission from the publisher

ANTISYMMETRIZATION OF "CLUSTER MODEL" WAVE FUNCTIONS AND THEIR EXPANSION IN "SHELL MODEL" WAVE FUNCTIONS

TH. KANELLOPOULOS and K. WILDERMUTH †
Theoretical Division, CERN, *Geneva*

Received 20 August 1959

Abstract: A method is described whereby oscillator "Cluster Model" wave functions may be antisymmetrized and expressed as a superposition of "Shell Model" wave functions. Moreover, some ideas are presented concerning the antisymmetrization of wave functions in general. For the Cluster Model calculations, they are useful when passing from the oscillator wave functions to more general cluster wave functions.

1. Introduction

This paper deals with possible ways of antisymmetrizing oscillator "cluster model" wave functions [1,2,3]) and expressing them as a superposition of single particle wave functions. The reason why it is very useful to expand the cluster model wave functions in single particle wave functions, is that one can see directly their orthogonality and obtain their normalization factors very easily.

The choice of a convenient notation simplifies greatly the calculations. This is why in section 2 the notation is explained in some detail and properties of this notation are derived.

In section 3 we discuss a method by which one can readily obtain antisymmetrized cluster model wave functions for nuclear states in which there are no nucleons outside the 1p shell.

With the method which is described in section 4, it is possible to construct any antisymmetric oscillator "cluster model" wave functions. The antisymmetrization is carried out mainly in two steps; first we obtain the antisymmetric wave functions for the clusters, then we extend the antisymmetrization over all the particles. For the first step, the method of section 3 is generally very useful.

Finally, in section 5, we indicate how any wave function can be antisymmetrized, and arrive at some preliminary conclusions. One needs such a method if one wants to generalize the cluster model wave functions, i.e. if one builds them up of other than oscillator model wave functions.

† Now at Florida State University, Tallahassee, Florida, U.S.A.

January (1) 1960

2. Notation

2.1. SLATER DETERMINANTS

In the independent particle picture any antisymmetric wave function is a combination of Slater determinants. For brevity every such determinant is denoted by its first diagonal, written either as a row or as a column. Thus,

$$u_1^1(1)u_2^2(2)u_3^4(3) \equiv \begin{vmatrix} u_1^1(1)u_2^2(1)u_3^4(1) \\ u_1^1(2)u_2^2(2)u_3^4(2) \\ u_1^1(3)u_2^2(3)u_3^4(3) \end{vmatrix}. \tag{1}$$

In the determinant, the rows correspond to different particles and the columns to the states.

2.2. SPIN AND ISOSPIN STATES

For the spin and isospin states superscripts from 1 to 4 are used indicating

$$\ldots^{(1)} = \text{proton with spin "up"}$$
$$\ldots^{(2)} = \text{proton with spin "down"}$$
$$\ldots^{(3)} = \text{neutron with spin "up"}$$
$$\ldots^{(4)} = \text{neutron with spin "down".}$$

For example, in eq. (1) u_3^4 denotes a neutron with spin "down" in a spatial state u_3.

2.3. PROPERTIES OF SLATER DETERMINANTS

In writing down a Slater determinant, as in eq. (1), the order of the elements is irrelevant, because exchange of two diagonal elements in a determinant means exchange of two rows and two columns simultaneously. For example,

$$u_1^1(1)u_2^2(2)u_3^4(3) \equiv u_1^1(1)u_3^4(3)u_2^2(2).$$

This enables us to adopt the prescription that we always write the "representative" diagonal in such a way that the particles are arranged in increasing order of their lower indices and therefore, we can drop these indices. It is also convenient to extend the notation of § 2.2 to any positive integral index, by assuming that all indices of the form $4n+j$ belong to the same spin and isospin state as j.

Now, with this notation it is easy to verify that

$$\ldots u^i \ldots v^j \ldots = - \ldots v^j \ldots u^i \ldots \tag{3}$$

and that

$$\ldots u^i \ldots v^j \ldots \quad \text{and} \quad \ldots v^i \ldots u^j \ldots$$

are quite different functions unless $i \equiv j \pmod 4$, in which case

$$\ldots u^i \ldots v^j \ldots = - \ldots v^i \ldots u^j \ldots \text{ for } i \equiv j \pmod 4. \tag{4}$$

2.4. ANTISYMMETRIZED PRODUCTS OF SLATER DETERMINANTS

If we have a product of two (or more) Slater determinants with no common particles, the completely antisymmetric combination of such products can be expressed as a single Slater determinant whose principal diagonal is the product of the diagonals of the factor determinants. Thus,

$$\mathrm{A}\{(u^{\alpha}(1)u^{\beta}(2)\ldots u^{\tau}(n))\cdot(v^{\mu}(n+1)\ldots v^{\sigma}(N))\} = u^{\alpha}(1)u^{\beta}(2)\ldots u^{\tau}(n)v^{\mu}(n+1)\ldots v^{\sigma}(N), \quad (5)$$

where A denotes the antisymmetrization operator. The left-hand side of eq. (5) is the Lagrange expansion of the determinant of the right-hand side with respect to the first n columns.

2.5. SIMPLIFIED ANTISYMMETRIZATION

In a Slater determinant $D(n)$ for n particles, we may write the columns in four successive groups, corresponding to states of protons or neutrons with spin "up" or "down". Let n_1, n_2, n_3, n_4 be the numbers of columns in these groups $(n_1+n_2+n_3+n_4=n)$:

$$D(n)=\begin{vmatrix} u_1^1(1)u_2^1(1)\ldots u_{n_1}^1(1)v_1^2(1)\ldots v_{n_2}^2(1)w_1^3(1)\ldots w_{n_3}^3(1)t_1^4(1)\ldots t_{n_4}^4(1)\\ u_1^1(2)u_2^1(2)\ldots u_{n_1}^1(2)v_1^2(2)\ldots v_{n_2}^2(2)w_1^3(2)\ldots w_{n_3}^3(2)t_1^4(2)\ldots t_{n_4}^4(2)\\ u_1^1(3)u_2^1(3)\ldots u_{n_1}^1(3)v_1^2(3)\ldots v_{n_2}^2(3)w_1^3(3)\ldots w_{n_3}^3(3)t_1^4(3)\ldots t_{n_4}^4(3)\\ \ldots\ldots\ldots\ldots\ldots\ldots\ldots\ldots\ldots\ldots\ldots\ldots\ldots\ldots\ldots\ldots\ldots\ldots\ldots\ldots\ldots\ldots\\ \ldots\ldots\ldots\ldots\ldots\ldots\ldots\ldots\ldots\ldots\ldots\ldots\ldots\ldots\ldots\ldots\ldots\ldots\ldots\ldots\ldots\ldots\\ u_1^1(n)u_2^1(n)\ldots u_{n_1}^1(n)v_1^2(n)\ldots v_{n_2}^2(n)w_1^3(n)\ldots w_{n_3}^3(n)t_1^4(n)\ldots t_{n_4}^4(n)\end{vmatrix}. \quad (6)$$

Taking into account § 2.4 we may write

$$D(n)=\begin{pmatrix}u_1\\u_2\\\cdot\\\cdot\\u_{n_1}\end{pmatrix}\begin{pmatrix}v_1\\v_2\\\cdot\\\cdot\\v_{n_2}\end{pmatrix}\begin{pmatrix}w_1\\w_2\\\cdot\\\cdot\\w_{n_3}\end{pmatrix}\begin{pmatrix}t_1\\t_2\\\cdot\\\cdot\\t_{n_4}\end{pmatrix}, \quad (7)$$

each of the columns being the principal diagonal of one of the partial determinants in which the $D(n)$ can be expanded. Here we do not care about antisymmetrization in spin and isospin space, as each column corresponds to a definite spin and isospin wave function. This shows that we can take one distribution of the n particles over the four spin and isospin states and carry out the antisymmetrization only over the spatial co-ordinates in constructing the four partial determinants. The totally antisymmetric function is then obtained by

combining these four determinants, and in our notation, it is enough to write expression (7).

From the construction of (7) it is easy to see that by interchanging two states of the same column, the whole expression changes sign. If we interchange two states between two different columns, we obtain an expression which is a quite different wave function.

2.6. OPERATOR ACTING ON SLATER DETERMINANT

In this paragraph we shall show how, in our notation, we represent an operator symmetric in n particles acting on a Slater determinant. We start from the identity

$$\sum_{i<j<k<\ldots<r}^{n} \begin{vmatrix} a_{11} & a_{12} & \ldots & a_{1n} \\ \cdot & \cdot & \cdot & \cdot \\ a'_{i1} & a'_{i2} & \ldots & a'_{in} \\ \cdot & \cdot & \cdot & \cdot \\ a'_{j1} & a'_{j2} & \ldots & a'_{jn} \\ \cdot & \cdot & \cdot & \cdot \\ a'_{k1} & a'_{k2} & \ldots & a'_{kn} \\ \cdot & \cdot & \cdot & \cdot \\ \cdot & \cdot & \cdot & \cdot \\ a'_{r1} & a'_{r2} & \ldots & a'_{rn} \\ \cdot & \cdot & \cdot & \cdot \\ a_{n1} & a_{n2} & \ldots & a_{nn} \end{vmatrix} = \sum_{i<j<k<\ldots<r}^{n} \begin{vmatrix} a_{11} \ldots a'_{1i} \ldots a'_{1j} \ldots a'_{1k} \ldots a'_{1r} \ldots a_{1n} \\ a_{21} \ldots a'_{2i} \ldots a'_{2j} \ldots a'_{2k} \ldots a'_{2r} \ldots a_{2n} \\ \cdot \cdot \cdot \cdot \cdot \cdot \cdot \cdot \cdot \cdot \cdot \cdot \cdot \cdot \cdot \cdot \cdot \cdot \cdot \cdot \\ \cdot \cdot \cdot \cdot \cdot \cdot \cdot \cdot \cdot \cdot \cdot \cdot \cdot \cdot \cdot \cdot \cdot \cdot \cdot \cdot \\ a_{n1} \ldots a'_{ni} \ldots a'_{nj} \ldots a'_{nk} \ldots a'_{nr} \ldots a_{nn} \end{vmatrix} \tag{8}$$

which is easy to prove by expanding each determinant on the left-hand side over the $i, j, k, \ldots r^{\text{th}}$ rows and those on the right-hand side over the $i, j, k, \ldots r^{\text{th}}$ columns. Without loss of generality we can take a two-particle symmetric operator to illustrate its effect in the adopted notation. We have

$$\sum_{i<j}^{n} O_{ij}(u_1 u_2 \ldots u_n) = \sum_{i<j}^{n} O_{ij} \begin{vmatrix} u_1(1)u_2(1) \ldots u_n(1) \\ u_1(2)u_2(2) \ldots u_n(2) \\ \cdot \cdot \cdot \cdot \cdot \cdot \cdot \cdot \cdot \cdot \\ u_1(n)u_2(n) \ldots u_n(n) \end{vmatrix}$$

$$= \sum_{i<j}^{n} \begin{vmatrix} u_1(1)u_2(1) \ldots u_n(1) \\ \cdot \cdot \cdot \cdot \cdot \cdot \cdot \cdot \cdot \cdot \\ u'_1(i)u'_2(i) \ldots u'_n(i) \\ \cdot \cdot \cdot \cdot \cdot \cdot \cdot \cdot \cdot \cdot \\ u'_1(j)u'_2(j) \ldots u'_n(j) \\ \cdot \cdot \cdot \cdot \cdot \cdot \cdot \cdot \cdot \cdot \\ u_1(n)u_2(n) \ldots u_n(n) \end{vmatrix} = \sum_{i<j}^{n} \begin{vmatrix} u_1(1) \ldots u'_i(1) \ldots u'_j(1) \ldots u_n(1) \\ u_1(2) \ldots u'_i(2) \ldots u'_j(2) \ldots u_n(2) \\ \cdot \cdot \cdot \cdot \cdot \cdot \cdot \cdot \cdot \cdot \cdot \cdot \cdot \cdot \cdot \cdot \cdot \cdot \cdot \cdot \\ \cdot \cdot \cdot \cdot \cdot \cdot \cdot \cdot \cdot \cdot \cdot \cdot \cdot \cdot \cdot \cdot \cdot \cdot \cdot \cdot \\ u_1(n) \ldots u'_i(n) \ldots u'_j(n) \ldots u_n(n) \end{vmatrix}$$

$$= \sum_{i<j} (u_1 u_2 \ldots u'_i \ldots u'_j \ldots u_n), \tag{9}$$

with the convention

$$O_{ij} u_\alpha(i) u_\beta(j) = u'_\alpha(i) u'_\beta(j).$$

At this point we have to note that when an operator acts on the spin or isospin states, this sometimes corresponds to transferring a state from one column to another in expression (7). We have then to take into account the chance in sign, if the displacement is over an odd number of places.

2.7. ANTISYMMETRIZATION OF CERTAIN EXPRESSIONS

Another application of the identity (8)is the following: Suppose we want to antisymmetrize the expression

$$K = \{u_1(1)u_2(2) \ldots u_n(n)\} \cdot v(k),$$

where the expression in the bracket is a Slater determinant represented by its principal diagonal and k is one of the particles $1, \ldots, n$. Then,

$$AK = \{u_1(1)u_2(2) \ldots u_n(n)\} \sum_{k=1}^{n} v(k) = \sum_{k=1}^{n} u_1(1)u_2(2) \ldots [u_k(k)v(k)] \ldots u_n(n).$$

Similarly, if

$$K = \{u_1(1) \ldots u_n(n)\} v(k)w(l) \text{ with } k \text{ and } l \text{ in } 1, 2, \ldots n,$$

then

$$AK = \sum_{k<l}^{n} u(1) \ldots [u_k(k)v(k)] \ldots [u_l(l)w(l)] \ldots u_n(n).$$

2.8. LAGRANGE EXPANSION OF SLATER DETERMINANT

Suppose we have n elements

$$a_1, a_2, a_3, \ldots a_n$$

which are arranged in a definite order denoted by their indices. We call any combination of these elements in a group of l even or odd, according as the sum of the indices of the elements in the combination is even or odd.

For example, among the combinations of ${}^nC_3$, in l, in groups of 3, $a_1a_3a_5$ and $a_2a_3a_6$ are odd, while $a_1a_3a_5$ and $a_7a_9a_{10}$ are even. The sum of the indices in a given combination is denoted by $[{}^nC_l]$.

With this notation it is easy to write down an expression for the expansion of a determinant according to the Lagrange method:

$$\begin{vmatrix} a_{11}a_{12} \ldots a_{1l} \ldots a_{1n} \\ a_{21}a_{22} \ldots a_{2l} \ldots a_{2n} \\ \cdots\cdots\cdots\cdots \\ a_{n1}a_{n2} \ldots a_{nl} \ldots a_{nn} \end{vmatrix} = (-)^{\frac{1}{2}l(l+1)} \sum_{{}^nC_l} (-)^{[{}^nC_l]} \begin{vmatrix} a_{j1}a_{j2} \ldots a_{jl} \\ a_{i1}a_{i2} \ldots a_{il} \\ \cdots\cdots\cdots \\ a_{k1}a_{k2} \ldots a_{kl} \end{vmatrix} \times \begin{vmatrix} a_{ml+1} \ldots a_{mn} \\ \cdots\cdots\cdots \\ a_{sl+1} \ldots a_{sn} \end{vmatrix}, \quad (9a)$$

where $[{}^nC_l] = j+i+ \ldots k$, and $\sum_{{}^nC_l}$ means a sum over all combinations ${}^nC_l$.

3. Antisymmetrization of some Expressions involving Single Particle Wave Functions

3.1. THE METHOD

In this section we deal with the antisymmetrization of expressions of the form

$$f = (a_{11}u_1^1+a_{12}u_1^2+\ldots+a_{1n}u_1^n)^{m_1}(a_{21}u_2^1+a_{22}u_2^2+\ldots+a_{2n}u_2^n)^{m_2} \ldots (a_{\rho 1}u^1+\ldots+a_{\rho n}u^n)^{m_\rho} \quad (10)$$

where the m_j's are integers with

$$m_1+m_2+m_3+\ldots+m_\rho = n, \quad (11)$$

n being the number of particles. The u_i^l's are single particle functions and the a_{il}'s are numerical coefficients. The superscripts in u_i^l number the particles and at the same time denote the spin and isospin. In a given bracket of (10), the u's have all the same spatial part.

We can express many wave functions for the Cluster Model in the form (10). If we use the harmonic oscillator functions, the u_i^l's are Hermite Polynomials. The wave functions of nuclear states in which there are no nucleons outside the 1p shell can be directly represented by expressions similar to (10): these include the ground states of all nuclei up to O^{16}; for heavier nuclei there are difficulties in putting the wave functions in this form. In section 4, a more general method for antisymmetrization of the Cluster Model wave functions will be given. However, we think it is useful to explain here a method of antisymmetrization of (10) which can be easily extended to the case when the u's are any kind of single particle functions.

The antisymmetrization of (10) can be done by expanding this expression and considering each term of the expansion as the principal diagonal of a Slater determinant for n particles.

In this way, many terms of the expansion will vanish, while some will be equal to each other. However, the actual expansion of (10) is not practicable because the number of terms increases very rapidly with n. Our task is to give a method by which we can obtain directly the final result.

Because of (11) we have to consider only those terms of the expansion which are linear in the u's, as every term has to contain functions pertaining to all n particles. We write these terms as in (7). Let n_1, n_2, n_3, n_4 be the numbers of particles in the first, second, third and fourth columns. We have

$$n_1+n_2+n_3+n_4 = n.$$

Consider one term of the expansion:

$$m_1!m_2!\ldots m_\rho!\,a_{11}a_{25}\ldots a_{\tau,4\lambda+1}\cdots \begin{pmatrix} u_1^{\,1} \\ u_2^{\,5} \\ \cdot \\ \cdot \\ \cdot \\ u_\tau^{\,4\lambda+1} \\ \cdot \\ \cdot \\ \cdot \end{pmatrix} \begin{pmatrix} u_1^{\,2} \\ \cdot \\ \cdot \\ \cdot \\ \cdot \\ \cdot \\ \cdot \\ \cdot \\ \cdot \end{pmatrix} \begin{pmatrix} u_1^{\,3} \\ \cdot \\ \cdot \\ \cdot \\ \cdot \\ \cdot \\ \cdot \\ \cdot \\ \cdot \end{pmatrix} \begin{pmatrix} u_1^{\,4} \\ \cdot \\ \cdot \\ \cdot \\ \cdot \\ \cdot \\ \cdot \\ \cdot \\ \cdot \end{pmatrix}, \tag{12}$$

The functions in each column must have been taken from different brackets of (10), otherwise (12) is identically zero. Next consider all other terms in the expansion which differ from (12) in the first column only. Some of these arise from (12) by permutation of the superscripts in the first column, and hence are the same apart from their numerical coefficients. Collecting them together it is easy to see that they form the expansion of the determinant

$$Q_1^{\,i}\binom{n_1}{\rho} = \begin{vmatrix} a_{11}a_{15}\ldots a_{1,4r+1} \\ a_{21}a_{25}\ldots a_{2,4r+1} \\ \cdots\cdots\cdots\cdots \\ a_{\tau 1}a_{\tau 5}\ldots a_{\tau,4r+1} \end{vmatrix} \tag{13}$$

where $r = n_1 - 1$.

The indices of the u's in (12) are the same as the subscripts of the principal diagonal of (13). If we change the order of the elements in (12) we have a corresponding change in the order of the rows in (13) with the result that there is no change in sign in the final expression. Another choice of n_1 functions u from the ρ brackets will give another coefficient $Q_1^{\,j}\binom{n_1}{\rho}$. Similarly we can construct the coefficients $Q_2^{\,k}\binom{n_2}{\rho}$, $Q_3^{\,h}\binom{n_3}{\rho}$ and $Q_4^{\,g}\binom{n_4}{\rho}$ for the other columns. The coefficients of really distinct terms of Af are of the form

$$Q_1^{\,i}\binom{n_1}{\rho} Q_2^{\,k}\binom{n_2}{\rho} Q_3^{\,l}\binom{n_3}{\rho} Q_4^{\,m}\binom{n_4}{\rho}. \tag{14}$$

The functional part of any term is obtained by using the subscripts of the elements in the principal diagonals of the Q's as the indices of the u's in the corresponding columns.

The number of terms which one obtains is in principle ${}^{\rho}C_{n_1} \cdot {}^{\rho}C_{n_2} \cdot {}^{\rho}C_{n_3} \cdot {}^{\rho}C_{n_4}$. In practice, however, this number is reduced, because usually there exist some relations among the a_{ij}'s.

From the way (13) is constructed, one derives the following properties:

(i) We must have

$$n_i \leqq \rho \ (i = 1, 2, 3, 4). \tag{15}$$

If for one n_i we have $\rho < n_i$, then A$f \equiv 0$.

(ii) If all the coefficients a_{ij} in (10) are equal (or proportional), then A$f \equiv 0$.

(iii) If the coefficients a_{ij}, corresponding to the kth column in (12), for at least $\rho-n+2$ brackets are proportional, then $Af \equiv 0$, because in every determinant (13), for the kth column, there will be at least two rows with proportional elements. In practice we have many brackets with corresponding coefficients equal. This reduces the number of Q's and therefore the number of terms in the final expression.

(iv) Suppose that the ρ brackets can be divided, with respect to the ith column, in ν_i groups, so that in each group the coefficients of the different brackets are equal. Then we can put instead of (15)

$$n_i \leqq \nu_i < \rho \tag{15a}$$

and the number of the terms is reduced to

$$^{\nu_1}C_{n_1}\,{}^{\nu_2}C_{n_2}\,{}^{\nu_3}C_{n_3}\,{}^{\nu_4}C_{n_4}.$$

(v) In the expression (10), it is possible that two brackets contain the same functions u but with different coefficients a_{ij}:

$$u_l{}^i = u_h{}^i \quad \text{but} \quad a_{li} \neq a_{hi}.$$

In this case, terms containing states from both brackets l and h and referred to the same column vanish, not because the coefficients Q vanish, but because their adjusted Slater determinants contain two particles in the same state. This also will reduce the number of terms in the final expression.

3.2. NOTE

If we suppose that the s shell is filled, the coefficients (13) become, for harmonic oscillator wave functions,

$$Q_1\binom{n_1-1}{\rho} = (-)^{n_1-1}\begin{vmatrix} 1 & 1 & \dots & 1 \\ a_{11} & a_{15} & \dots & a_{1,4r+1} \\ \hline a_{r1} & a_{r2} & \dots & a_{r,4r+1} \end{vmatrix} \tag{13a}$$

with $r = n_1-1$. We obtain similar expressions for $Q_2{}^3\binom{n_2-1}{\rho}$, $Q_3{}^k\binom{n_3-1}{\rho}$, $Q_4{}^m\binom{n_4-1}{\rho}$. This is because we have n_i elements in the ith column of (12), of which one is always supposed to be the 1s state; thus one less is chosen from the u_{il}'s. We accordingly get as corresponding coefficient a sum of n_i determinants which is exactly the expansion of (13a).

3.3. EXAMPLES

We now illustrate the method by some examples of applications of the Cluster Model wave functions to light nuclei. We use harmonic oscillator wave functions.

For convenience, we put for the p-shell wave functions:

$$P_{10} \propto a = z,$$
$$P_{11} \propto b = x+iy, \tag{16}$$
$$P_{1-1} \propto c = x-iy.$$

a) Ground state of Be^8

We consider that the ground state of Be^8 is formed by two α-particles in a 3s relative oscillation. Thus, before antisymmetrization, we can write

$$\psi^{Be^8} = f_{1s}(\alpha_1) f_{1s}(\alpha_2) X_{3s}(\alpha_1-\alpha_2). \tag{17}$$

The exponential part of (17) is symmetric in all the particles. The polynomial parts of $f_{1s}(\alpha_1)$ and $f_{1s}(\alpha_2)$ reduce to constants. The polynomial part of (17), with which we shall be concerned, is therefore

$$X_{3s}(\mathbf{R}_{12}) \propto R_{12}^4 - \frac{5}{\alpha} R_{12}^2 + \frac{15}{4\alpha^2}, \tag{17a}$$

with

$$\mathbf{R}_{12} = \frac{\mathbf{r}_1+\mathbf{r}_2+\mathbf{r}_3+\mathbf{r}_4}{4} - \frac{\mathbf{r}_5+\mathbf{r}_6+\mathbf{r}_7+\mathbf{r}_8}{4}.$$

The second and the third terms of (17a) vanish after antisymmetrization, as they correspond to states with six and eight particles, respectively, in the 1s state. There remains, therefore, the antisymmetrization of the term

$$R_{12}^4 = (a_{12}^2 + b_{12}c_{12})^2 = a_{12}^4 + 2a_{12}^2 b_{12}c_{12} + b_{12}^2 c_{12}^2 \tag{17b}$$

where

$$a_{12} = \frac{a_1+a_2+a_3+a_4}{4} - \frac{a_5+a_6+a_7+a_8}{4},$$
$$b_{12} = \frac{b_1+b_2+b_3+b_4}{4} - \frac{b_5+b_6+b_7+b_8}{4},$$
$$c_{12} = \frac{c_1+c_2+c_3+c_4}{4} - \frac{c_5+c_6+c_7+c_8}{4}.$$

We have to antisymmetrize separately a_{12}^4, $a_{12}^2 b_{12}c_{12}$ and $b_{12}^2 c_{12}^2$:

1) Consider

$$a_{12}^4 = \frac{1}{4^4}\{(a_1+a_2+a_3+a_4) - (a_5+a_6+a_7+a_8)\}^4.$$

Here $\rho = 1$ and $n_1 = n_2 = n_3 = n_4 = 2$. Therefore,

$$Q_1\begin{pmatrix}1\\1\end{pmatrix} = Q_2\begin{pmatrix}1\\1\end{pmatrix} = Q_3\begin{pmatrix}1\\1\end{pmatrix} = Q_4\begin{pmatrix}1\\1\end{pmatrix} = (-)^1 \begin{vmatrix} 1 & 1 \\ 1 & -1 \end{vmatrix} = 2,$$

and

$$\mathrm{A}a_{12}^4 = 4!\,\frac{2^4}{4^4}\begin{pmatrix}s\\a\end{pmatrix}\begin{pmatrix}s\\a\end{pmatrix}\begin{pmatrix}s\\a\end{pmatrix}\begin{pmatrix}s\\a\end{pmatrix} = \frac{4!}{16}\begin{pmatrix}s\\a\end{pmatrix}\begin{pmatrix}s\\a\end{pmatrix}\begin{pmatrix}s\\a\end{pmatrix}\begin{pmatrix}s\\a\end{pmatrix},$$

where s in the bracket denotes the 1s state.

2) One has

$$a_{12}^2\, b_{12}\, c_{12} = \frac{1}{4^4}[(a_1+\ldots+a_4)-(a_5+\ldots+a_8)]^2 \times[(b_1+\ldots+b_4)-(b_5+\ldots+b_8)]\times[(c_1+\ldots c_4)-(c_5+\ldots c_8)].$$

Again $Q_1{}^i = Q_2{}^i = Q_3{}^i = Q_4{}^i = 2$. Therefore,

$$\mathrm{A}a_{12}^2 b_{12} c_{12} = \frac{2!}{4^4}\, 2^4 \overline{\binom{s}{a}\binom{s}{a}\binom{s}{b}\binom{s}{c}} = \frac{2!}{16}\overline{\binom{s}{a}\binom{s}{a}\binom{s}{b}\binom{s}{c}},$$

where the bar over the expression means that we have to take the sum of all the different permutations of the columns.

3) Similarly,

$$b_{12}^2 c_{12}^2 = \frac{1}{4^4}[(b_1+\ldots+b_4)-(b_5+\ldots+b_8)]\cdot[(c_1+\ldots+c_4)-(c_5+\ldots+c_8)]^2,$$

and we find

$$\mathrm{A}b_{12}^2 c_{12}^2 = \frac{2!\,2!}{4}\, 2^4 \overline{\binom{s}{b}\binom{s}{b}\binom{s}{c}\binom{s}{c}}.$$

The final expression for the antisymmetrized wave function of Be^8 in the ground state is thus

$$\Psi \propto 6\binom{s}{a}\binom{s}{a}\binom{s}{a}\binom{s}{a} + \overline{\binom{s}{a}\binom{s}{a}\binom{s}{b}\binom{s}{c}} + \overline{\binom{s}{b}\binom{s}{b}\binom{s}{c}\binom{s}{c}}.$$

It is a sum of 19 terms. If we now write a, b, c for the *normalized* wave functions P_{10}, P_{11}, $P_{1\,-1}$, we have

$$\Psi_{\text{normalized}} = \frac{1}{\sqrt{45}}\left\{3\binom{s}{a}\binom{s}{a}\binom{s}{a}\binom{s}{a} + \overline{\binom{s}{a}\binom{s}{a}\binom{s}{b}\binom{s}{b}} + 2\,\overline{\binom{s}{b}\binom{s}{b}\binom{s}{c}\binom{s}{c}}\right\}.$$

b) 2^+ *State of* C^{12}

We take $J = 2$, $J_z = 2$.

This state in the Cluster Model can be described as Be^8 oscillating against an α-particle. There are many expressions for this state as, for example,

$$F(\mathrm{Be}^8)_{3s} f_{1s}(\alpha)\, X(\mathrm{Be}^8 \leftrightarrow \alpha)_{2d},$$
$$F(\mathrm{Be}^8)_{2d} f_{1s}(\alpha)\, X(\mathrm{Be}^8 \leftrightarrow \alpha)_{3s},$$
$$F(\mathrm{Be}^8)_{2d} f_{1s}(\alpha)\, X(\mathrm{Be}^8 \leftrightarrow \alpha)_{2d}, \text{ etc.}$$

but after antisymmetrization, all lead to the same final expression.

We take the first one. The polynomial parts are

$$F(\mathrm{Be}^8)_{3s} \propto 15-20\alpha r'^2+4\alpha^2 r'^4 = 15-20\alpha(a'+b'c')+4\alpha^2(a'^2+b'c')^2,$$

$$f_{1s}(\alpha) \propto 1,$$

$$(\mathrm{Be}^8 \leftrightarrow \alpha)_{2d_z} \propto b''^3 c''+a''^2 b''^2,$$

where

$$b' = \frac{b_1 + \ldots + b_4}{4} - \frac{b_5 + \ldots + b_8}{4},$$

$$c' = \frac{c_1 + \ldots + c_4}{4} - \frac{c_5 + \ldots + c_8}{4},$$

$$a' = \frac{a_1 + \ldots + a_4}{4} - \frac{a_5 + \ldots + a_8}{4},$$

and

$$b'' = \frac{b_1 + \ldots + b_8}{8} - \frac{b_9 + \ldots + b_{12}}{4},$$

$$c'' = \frac{c_1 + \ldots + c_8}{8} - \frac{c_9 + \ldots + c_{12}}{4},$$

$$a'' = \frac{a_1 + \ldots + a_8}{8} - \frac{a_9 + \ldots + a_{12}}{4}.$$

From the F_{38} we keep only the highest term as the others lead to expressions which vanish after antisymmetrization, because there will be more than 4 particles in the 1s state.

We have to antisymmetrize the expression

$$(a'^2 + b'c')^2(b''^3c'' + a''^2b''^2) = (a'^4)(b''^3c'') + 2(a'^2b'c')(b''^3c'') + 2(a'^2b'c')(a''^2b''^2) + (b'^2c'^2)(a''^2b''^2) + (a'^4)(a''^2b''^2) + (b'^2c'^2)(b''^3c'').$$

The last two terms give zero after antisymmetrization because in the last one there are 5 states b and in the other 6 states a.

We have $n_1 = n_2 = n_3 = n_4 = 3$ and the Q's are 3×3 determinants. It is easy to see that they are all equal to

$$(-)^2 \times \begin{vmatrix} 1 & 1 & 1 \\ \frac{1}{4} & -\frac{1}{4} & 0 \\ \frac{1}{8} & \frac{1}{8} & -\frac{1}{4} \end{vmatrix} = \frac{6}{32}.$$

Then,

$$1) \quad \mathrm{A}(a'^4)(b''^3c'') = \frac{4!\,3!\,6^4}{32^4} \overline{\binom{S}{a}\binom{S}{b}\binom{S}{b}\binom{S}{b}\binom{S}{c}},$$

$$2)\dagger \quad A(a'^2b'c')(b''^3c'') = \frac{2!\,3!\,6^4}{32^4}\overline{\binom{S}{a\,b}\binom{S}{a\,b}\binom{S}{b\,c}\binom{S}{c\,b}}$$

$$= -2\,\frac{2!\,3!\,6^4}{32^4}\overline{\binom{S}{a\,b}\binom{S}{a\,b}\binom{S}{b\,c}\binom{S}{b\,c}},$$

$$3) \quad A(a'^2b'c')(a''^2b''^2) = \frac{2!\,2!\,2!\,6^4}{32^4}\overline{\binom{S}{a\,b}\binom{S}{a\,b}\binom{S}{b\,a}\binom{S}{c\,a}}$$

$$= 3\,\frac{2!\,2!\,2!\,6^4}{32^4}\overline{\binom{S}{a\,b}\binom{S}{a\,b}\binom{S}{a\,b}\binom{S}{a\,c}},$$

$$4) \quad A(b'^2c'^2)(a''^2b''^2) = \frac{2!\,2!\,2!\,2!\,6^4}{32^4}\overline{\binom{S}{b\,a}\binom{S}{b\,a}\binom{S}{c\,b}\binom{S}{c\,b}}$$

$$= \frac{2^4\,6^4}{32^4}\overline{\binom{S}{a\,b}\binom{S}{a\,b}\binom{S}{b\,c}\binom{S}{b\,c}}.$$

Finally we have

$$\psi_{2^+}^{C^{12}} \propto 6\,\overline{\binom{S}{a\,b}\binom{S}{a\,b}\binom{S}{a\,b}\binom{S}{a\,c}} - \overline{\binom{S}{a\,b}\binom{S}{a\,b}\binom{S}{b\,c}\binom{S}{b\,c}}.$$

Normalizing we have

$$\psi_{2^+\,\text{normalized}}^{C^{12}} = \frac{1}{\sqrt{42}}\left\{3\,\overline{\binom{S}{a\,b}\binom{S}{a\,b}\binom{S}{a\,b}\binom{S}{a\,b}} - \overline{\binom{S}{a\,b}\binom{S}{a\,b}\binom{S}{b\,c}\binom{S}{b\,c}}\right\}.$$

Here a, b, c are normalized, i.e. $a = (\alpha/\pi)^{\frac{1}{4}}\sqrt{2\alpha}z$, etc.

c) $\frac{3}{2}$ *State of* N^{15}

As a final example we shall find the wave function of the $\frac{3}{2}$ ground state of N^{15} when it is expressed as C^{12} oscillating against a triton.

The wave function for this state can be written immediately if we consider the $\frac{3}{2}$ state of N^{15} as the ground state of O^{16} with a proton hole with spin and

† The $-$ sign appears because we interchange the states b and c in the fourth column, and the factor 2 because

$$\overline{\binom{S}{a\,b}\binom{S}{a\,b}\binom{S}{b\,c}\binom{S}{c\,b}}$$

is the sum of 12 terms, while

$$\overline{\binom{S}{a\,b}\binom{S}{a\,b}\binom{S}{b\,c}\binom{S}{b\,c}}$$

is the sum of 6 terms.

angular momentum parallel. However, we use the above method in this case as a simple illustration only. The polynomial part of the N^{15} ground state wave function is of the 11th degree, while that of C^{12} is of the 8th degree, and the triton is the 1s state of 0 degree. Therefore, the relative oscillation must be either the (3, 1) or (3, 3) oscillation.

The spin of the triton is $\frac{1}{2}$, and if we take C^{12} in the 0^+ state, we have to take the (3, 1) oscillation, in order to obtain a total angular momentum $\frac{3}{2}$ for N^{15}.

We take also $J_z = \frac{3}{2}$. Then,

$$\psi^{N^{15}} \propto F(C^{12})_{3S} f_{1S}(H^3) X(C^{12} \leftrightarrow H^3)_{3,1}. \tag{17}$$

In (17) we retain the term of highest degree in the polynomial part (for reasons previously explained). Now we must antisymmetrize

$$\overbrace{(b'c'+a'^2)^2(b''c''+a''^2)^2}^{C^{12}_{0^+}} \overbrace{(b'''^2c'''+a'''^2b''')}^{X_{31}}, \tag{17a}$$

where

$$b' = \frac{b_1+b_2+b_3+b_4}{4} - \frac{b_5+b_6+b_7+b_8}{4},$$

and similarly for a' and c';

$$b'' = \frac{b_1+\ldots+b_8}{8} - \frac{b_9+b_{10}+b_{11}+b_{12}}{4},$$

and similarly for c'' and a'';

$$b''' = \frac{b_1+\ldots+b_{12}}{12} - \frac{b_{13}+b_{15}+b_{16}}{3},$$

and similarly for c''' and a'''.

Note that the number 14 which corresponds to a proton with spin "down" is missing. This is because in the H^3 we have a single proton with spin "up". Therefore we have

$$n_1 = n_3 = n_4 = 4 \quad \text{and} \quad n_2 = 3.$$

If we expand (17), all the terms which have at least one of the a, b, or c to a higher degree than the 4th will vanish, as they have at least in one column two or more identical states in their antisymmetrized expressions. The remaining terms are

$$\begin{aligned}(b'^2c'^2)(a''^4)(b'''^2c''')&+2(b'^2c'^2)(a''^2b''c'')(a'''^2b''')\\ &+4(b'c'a'^2)(a''^2b''c'')(b'''^2c''')+2(b'c'a'^2)(b''^2c''^2)(a'''^2b''')\\ &+(a'^4)(b''^2c''^2)(b'''^2c''').\end{aligned} \tag{17a}$$

We find that all the Q_1, Q_3 and Q_4 are equal to $5/2^6$, while all the Q_2 are equal

to $6/2^5$. Therefore, for every term, the product $Q_1^{\,i}Q_2^{\,j}Q_3^{\,k}Q_4^{\,l}$ is the same, $3 \cdot 5/2^{10}$, and we can neglect it.

Then we obtain

$$\mathrm{A}(b'^2c'^2)(a''^4)(b'''^2c''') \qquad \propto 3 \cdot 2!^3 \cdot 4! \cdot \begin{pmatrix} s \\ a \\ b \\ c \end{pmatrix}\begin{pmatrix} s \\ a \\ b \end{pmatrix}\begin{pmatrix} s \\ a \\ b \\ c \end{pmatrix}\begin{pmatrix} s \\ a \\ b \\ c \end{pmatrix},$$

$$\mathrm{A}(b'^2c'^2)(a''^2b''c'')(a'''^2b''') \quad \propto 2!^4 \cdot 6 \cdot \begin{pmatrix} s \\ a \\ b \\ c \end{pmatrix}\begin{pmatrix} s \\ a \\ b \end{pmatrix}\begin{pmatrix} s \\ a \\ b \\ c \end{pmatrix}\begin{pmatrix} s \\ a \\ b \\ c \end{pmatrix},$$

$$\mathrm{A}(b'c'a'^2)(a''^2b''c'')(b'''^2c''') \propto 2!^3 \cdot 12 \cdot \begin{pmatrix} s \\ a \\ b \\ c \end{pmatrix}\begin{pmatrix} s \\ a \\ b \end{pmatrix}\begin{pmatrix} s \\ a \\ b \\ c \end{pmatrix}\begin{pmatrix} s \\ a \\ b \\ c \end{pmatrix},$$

$$\mathrm{A}(b'c'a'^2)(b''^2c''^2)(a'''^2b''') \quad \propto 2!^4 \cdot 6 \cdot \begin{pmatrix} s \\ a \\ b \\ c \end{pmatrix}\begin{pmatrix} s \\ a \\ b \end{pmatrix}\begin{pmatrix} s \\ a \\ b \\ c \end{pmatrix}\begin{pmatrix} s \\ a \\ b \\ c \end{pmatrix},$$

$$\mathrm{A}(a'^4)(b''^2c''^2)(b'''^2c''') \qquad \propto 3!2^3 \cdot 4! \cdot \begin{pmatrix} s \\ a \\ b \\ c \end{pmatrix}\begin{pmatrix} s \\ a \\ b \end{pmatrix}\begin{pmatrix} s \\ a \\ b \\ c \end{pmatrix}\begin{pmatrix} s \\ a \\ b \\ c \end{pmatrix}.$$

Therefore, the antisymmetrized wave function of N^{15} for $\frac{3}{2}$ state is a single determinant

$$\psi_{\frac{3}{2}}^{N^{15}} = \begin{pmatrix} s \\ a \\ b \\ c \end{pmatrix}\begin{pmatrix} s \\ a \\ b \end{pmatrix}\begin{pmatrix} s \\ a \\ b \\ c \end{pmatrix}\begin{pmatrix} s \\ a \\ b \\ c \end{pmatrix}.$$

4. Antisymmetrization of Cluster Model Wave Functions

4.1. THE GENERAL METHOD

As we mentioned before, the method which is given in section 3 is not easily applicable to nuclei with particles occupying states higher than the 1p-shell. In the present section, we give a more general method, by which we can obtain antisymmetrized wave functions for any nucleus, provided its cluster structure is given. Here we again suppose that we have harmonic oscillator wave functions.

In the Cluster Model, a nucleus can be represented as two clusters † oscillating against each other. Each of the clusters is in a definite state and its wave function can be taken to be antisymmetrized. Therefore, the problem is to

† If there are more than two clusters, we can combine the small clusters in bigger and bigger ones, in order to obtain finally only two clusters. Cf. ref. [2]), § 3.

antisymmetrize expressions of the form

$$f_1(1, 2, \ldots n)f_2(n+1, \ldots, N)X(\mathbf{R}_1-\mathbf{R}_2), \tag{18}$$

where f_1 and f_2 are the antisymmetric wave functions of the two clusters, and X is the wave function of their relative motion, with

$$\mathbf{R}_1 = \frac{\sum_1^n \mathbf{r}_i}{n}, \quad \mathbf{R}_2 = \frac{\sum_{j=n+1}^N \mathbf{r}_j}{N-n}.$$

As previously for the antisymmetrization of (18), we omit the exponential part which is symmetric in all the particles, and we have just to antisymmetrize the polynomial part of (18).

The polynomial part X' of $X(\mathbf{R}_1-\mathbf{R}_2)$ has a definite degree n' and it is a sum of homogeneous polynomials in x, y, z of degrees ranging from n' to 0 or 1 (according as n' is even or odd). From these parts of X' it is usually sufficient to take into account the part of highest degree n'. It wili be necessary to take also the next one, which is of degree $n'-2$, when there are many unoccupied states in either or both of the wave functions f_1 and f_2 below the highest occupied one.

It is again convenient to put

$$z_i = a_i, \quad x_i+iy_i = b_i, \quad x_i-iy_i = c_i,$$

and express the polynomial X' (or the highest part of it) in terms of the a_i, b_i, c_i. Then from X' we take the terms

$$\sum_{k,\,l,\,m} a^k b^l c^m \tag{19}$$

(with $k+l+m = n'$, and if necessary $k+l+m = n'-2$, etc.), where

$$\begin{aligned} a &= \frac{a_1+a_2+\ldots+a_n}{n} - \frac{a_{n+1}+\ldots+a_N}{N-n}, \\ b &= \frac{b_1+b_2+\ldots+b_n}{n} - \frac{b_{n+1}+\ldots+b_N}{N-n}, \\ c &= \frac{c_1+c_2+\ldots+c_n}{n} - \frac{c_{n+1}+\ldots+c_N}{N-n}. \end{aligned} \tag{20}$$

The antisymmetrization of (18) is based on the results of sections 2.4 and 2.7.

The f_1 and f_2 in (18) are combinations of Slater determinants, with no common particles. If $X'(\mathbf{R}_1-\mathbf{R}_2)$ is a constant, i.e. if $X(\mathbf{R}_1-\mathbf{R}_2)$ is a 1s oscillation, the antisymmetric expression of (18) is, according to § 2.4, a determinant whose principal diagonal is the product of the diagonals of the determinants composing f_1 and f_2. If there exists at least one common state in the two Slater determinants which are joined together, the resulting determinant

vanishes. Usually, $X'(\mathbf{R}_1-\mathbf{R}_2)$ is not a constant. Then it can be written, using (19) and (20), as a sum of terms of the form $a_i^l b_i^m c_i^n$. Using § 2.7, we can insert this form into the determinants for the clusters 1 and 2, thus obtaining products of Slater determinants with no common particles. The final step is to join the diagonals in each product to obtain the antisymmetric expression for each term.

The number of terms is rather large in every expression (18), when, using (19) and (20), we write it as a sum of monomials in a_i, b_i, c_i, and it increases very rapidly when the clusters become larger. However, we can find from the beginning which of the terms of $X(\mathbf{R}_1-\mathbf{R}_2)$ contribute to the final result. Looking at the Slater determinants for the two clusters, we see that they have many states in common. The effect of the $X(\mathbf{R}_1-\mathbf{R}_2)$ part must be such that in the final determinant there are no two particles in the same state; therefore it has to be used to shift at least the states which are common in the two partial Slater determinants.

We give some examples below, in order to illustrate the method. Several short-cuts can be used, and especially we shall see that the explicit expansion of (19) in terms of (20) can be avoided.

4.2. EXAMPLES: THE WAVE FUNCTIONS OF THE 1^-, 2^-, AND 3^- STATES OF O^{16}

1) *The* 1^- *state*

Let $X(n, l)(\mathbf{R})$ denote oscillation with principal quantum number n and angular momentum l. Let

$$\mathbf{R}_1 = \frac{\mathbf{r}_1+\ldots+\mathbf{r}_{12}}{12}, \quad \mathbf{R}_2 = \frac{\mathbf{r}_{13}+\ldots+\mathbf{r}_{16}}{4}.$$

We consider the following wave-functions:

$$\begin{aligned}
&(\alpha) \quad \psi = (C^{12})_{3s} f_{1s}(\alpha) X_{(5,1)}(\mathbf{R}_1-\mathbf{R}_2)\\
&(\beta) \quad \psi = (C^{12})_{2d} f_{1s}(\alpha) X_{(5,1)}(\mathbf{R}_1-\mathbf{R}_2)\\
&(\gamma) \quad \psi = (C^{12})_{2d} f_{1s}(\alpha) X_{(5,3)}(\mathbf{R}_1-\mathbf{R}_2)\\
&(\delta) \quad \psi = (C^{12})_{1g} f_{1s}(\alpha) X_{(5,3)}(\mathbf{R}_1-\mathbf{R}_2)\\
&(\varepsilon) \quad \psi = (C^{12})_{1g} f_{1s}(\alpha) X_{(5,5)}(\mathbf{R}_1-\mathbf{R}_2),
\end{aligned}$$

and find that all of them, except (γ), give the same result. As to (γ), we find that it is identically zero. We shall give here in detail only case (α).

The unnormalized 3s wave function of C^{12} with $s = 1$, $z = a$, $x+iy = b$ and $x-iy = c$ is

$$(C^{12})_{3s} = 3\overline{\binom{s}{b}\binom{s}{b}\binom{s}{b}\binom{s}{c}} - 2\overline{\binom{s}{a}\binom{s}{b}\binom{s}{b}\binom{s}{c}} - 8\overline{\binom{s}{a}\binom{s}{b}\binom{s}{a}\binom{s}{c}},$$

where the bar indicates that we have to take the sum of the different permutations among the columns. We have

$$f(\alpha) = (s)\ (s)\ (s)\ (s)$$

and

$$X_{51} = b'^3c'^2 + 2a'^2b'^2c' + a'^4b'$$

with

$$b' = \frac{b_1 + b_2 \ldots + b_{12}}{12} - \frac{b_{13} + \ldots + b_{16}}{4}$$

and similarly for a' and c'.

We take successively

$$1)\quad Q_1 = \begin{pmatrix} s \\ b \\ c \end{pmatrix}\begin{pmatrix} s \\ b \\ c \end{pmatrix}\begin{pmatrix} s \\ b \\ c \end{pmatrix}\begin{pmatrix} s \\ b \\ c \end{pmatrix}(ssss)\ \ (b'^3c'^2 + 2a'^2b'^2c' + a'^4b'). \tag{1}$$

We have to use the terms of the expansion in the brackets to shift at least 4 particles from the 1s states from either cluster. From $b'^3c'^2$ and $2a'^2b'^2c'$ we get 0, because there will be, in one of the columns, at least twice the same state b or c. From

$$a'^4b' \rightarrow \begin{cases} \left.\begin{array}{l} aaaa \cdot b \rightarrow \overline{\begin{matrix} aaaa \\ b \end{matrix}} \\ aaab \cdot a \rightarrow \overline{\begin{matrix} aaab \\ a \end{matrix}} \end{array}\right\} & \text{the coefficient } \frac{24}{4 \cdot 3^5}, \\ aaa(ab) \rightarrow \overline{aaa(ab)} & \text{the coefficient } \frac{24 \times 2}{4 \cdot 3^5}. \end{cases}$$

Therefore,

$$A Q_1 = \frac{4!}{4 \cdot 3^5}\left\{\overline{\begin{pmatrix} s \\ a \\ b \\ c \end{pmatrix}\begin{pmatrix} s \\ a \\ b \\ c \end{pmatrix}\begin{pmatrix} s \\ a \\ b \\ c \end{pmatrix}\begin{pmatrix} s \\ a \\ b \\ bc \end{pmatrix}} - \overline{\begin{pmatrix} s \\ a \\ b \\ c \end{pmatrix}\begin{pmatrix} s \\ a \\ b \\ c \end{pmatrix}\begin{pmatrix} s \\ a \\ b \\ c \end{pmatrix}\begin{pmatrix} s \\ a \\ c \\ b^2 \end{pmatrix}} - 3\overline{\begin{pmatrix} s \\ a \\ b \\ c \end{pmatrix}\begin{pmatrix} s \\ a \\ b \\ c \end{pmatrix}\begin{pmatrix} s \\ a \\ b \\ c \end{pmatrix}\begin{pmatrix} s \\ b \\ c \\ ab \end{pmatrix}}\right\}$$

$$= \frac{4!}{4 \cdot 3^5}\left\{\overline{\begin{pmatrix} s \\ a \\ b \\ bc \end{pmatrix}} - \overline{\begin{pmatrix} s \\ a \\ c \\ b^2 \end{pmatrix}} - 3\overline{\begin{pmatrix} s \\ b \\ c \\ ab \end{pmatrix}}\right\},$$

if, of the four columns, we write only the one which differs from

$$\begin{pmatrix} s \\ a \\ b \\ c \end{pmatrix}.$$

In order to find the above coefficients we keep in mind that for the first cluster the coefficients are all equal to $\frac{1}{12}$ and for the second $-\frac{1}{4}$. The term $aaaa \cdot b$ means that the four a's will occupy the s states of either cluster and the

b will be combined with one of the other states of the first cluster only. The b for any column gives the factor $\frac{1}{12}$. For the a's we see that in every column they can occupy the s state, either of the first or the second cluster. For the first cluster they give $\frac{1}{12}$ and for the second $-\frac{1}{4}$, but changing the order in the last, we have to change the sign. Thus, finally, for every a-state we obtain a coefficient $\frac{1}{12}+\frac{1}{4}=\frac{1}{3}$. The total coefficient will then be $(\frac{1}{3})^4\times\frac{1}{12}=1/(4\cdot 3^5)$ which has to be multiplied by 4!.

For $aaa(ab)$, we obtain in a similar way the coefficient

$$\tfrac{1}{3}\times\tfrac{1}{3}\times\tfrac{1}{3}\times\left(\frac{1}{12^2}-\frac{1}{4^2}\right)=\frac{-2}{4\cdot 3^5}.$$

$$2)\quad Q_2=\overline{\begin{pmatrix}s\\a\\c\end{pmatrix}\begin{pmatrix}s\\b\\c\end{pmatrix}\begin{pmatrix}s\\b\\c\end{pmatrix}\begin{pmatrix}s\\a\\b\end{pmatrix}}\,(ssss)(b'^3c'^2+2a'^2b'^2c'+a'^4b'). \tag{2}$$

In this case,

(i) from $b'^3c'^2$ we get 0;

(ii) from $2a'^2b'^2c'$:

$$\left.\begin{array}{l} aabb\cdot c\to baab \\ \qquad\qquad\quad c \\ aabc\cdot b\to baac+baac+baac+baac \\ \qquad\qquad\quad b\quad b\qquad b\qquad b \\ abbc\cdot a\to babc+bbac \\ \qquad\qquad\quad a\quad a \end{array}\right\}\text{ the coefficient }\frac{8}{4\cdot 3^5},$$

$$\left.\begin{array}{ll} a^2bbc & \to 0 \\ aab^2c & \to b^2aac \end{array}\right\}\text{ the coefficient }-\frac{8}{4\cdot 3^5},$$

$$\left.\begin{array}{ll} aab(bc) & \to baa(bc) \\ abc(ab) & \to ba(ab)c+b(ab)ac \\ abb(ac) & \to 0 \end{array}\right\}\text{the coefficient }-\frac{16}{4\cdot 3^5},$$

from which we obtain

$$\text{(ii)}=-\frac{24}{4\cdot 3^5}\left\{2\overline{\begin{pmatrix}s\\a\\c\\b^2\end{pmatrix}}+4\overline{\begin{pmatrix}s\\b\\c\\ab\end{pmatrix}}\right\};$$

(iii) from a'^4b':

$$\left.\begin{array}{l} aaaa\cdot b\to 0 \\ aaab\cdot a\to baaa \\ \qquad\qquad\quad a \end{array}\right\}\text{the coefficient }\frac{24}{4\cdot 3^5},$$

$$\left.\begin{array}{ll} a^2aab & \to baaa^2 \\ aaa(ab) & \to 0 \end{array}\right\}\text{the coefficient }-\frac{24}{4\cdot 3^5},$$

therefore

$$\text{(iii)} \quad = -\frac{48 \cdot 3}{4 \cdot 3^5} \overline{\begin{pmatrix} s \\ a \\ b \\ a^2 \end{pmatrix}}.$$

Combining (i), (ii) and (iii), we have

$$Q_2 = -\frac{48}{4 \cdot 3^5}\left\{ 3\overline{\begin{pmatrix} s \\ a \\ b \\ a^2 \end{pmatrix}} + \overline{\begin{pmatrix} s \\ a \\ c \\ b^2 \end{pmatrix}} + 2\overline{\begin{pmatrix} s \\ b \\ s \\ ab \end{pmatrix}} \right\}.$$

3) $$Q_3 = \overline{\begin{pmatrix} s \\ a \\ b \end{pmatrix}\begin{pmatrix} s \\ a \\ b \end{pmatrix}\begin{pmatrix} s \\ a \\ c \end{pmatrix}\begin{pmatrix} s \\ a \\ c \end{pmatrix}} (ssss)(b'^3c'^2 + 2a'^2b'^2c' + a'^4b').$$

In this case,

(i) from $b'^3c'^2$ we get

$$\left.\begin{aligned} bbbc \cdot c &\to \underset{c}{bcbb} + \underset{c}{cbbb} \\ bbcc \cdot b &\to \underset{b}{ccbb} + \underset{b}{ccbb} + \underset{b}{ccbb} + \underset{b}{ccbb} \end{aligned}\right\} \text{ the coefficient } \frac{12}{4 \cdot 3^5},$$

$$\left.\begin{aligned} b^2bcc &\to ccb^2b + ccbb^2 \\ bbbc^2 &\to 0 \\ bbc(bc) &\to c(bc)bb + (bc)cbb \end{aligned}\right\} \text{ the coefficient } -\frac{24}{4 \cdot 3^5},$$

hence

$$\text{(i)} = \frac{72}{4 \cdot 3^5}\left\{ \overline{\begin{pmatrix} s \\ b \\ c \\ ab \end{pmatrix}} - \overline{\begin{pmatrix} s \\ a \\ b \\ bc \end{pmatrix}} \right\};$$

(ii) from $2a'^2b'^2c'$:

$$\left.\begin{aligned} aabb \cdot c &\to 0 \\ aabc \cdot b &\to 0 \\ bbca \cdot a &\to \underset{a}{acbb} + \underset{a}{cabb} \end{aligned}\right\} \text{ the coefficient } \frac{8}{4 \cdot 3^5},$$

$$\left.\begin{aligned} a^2bbc &\to a^2cbb + ca^2bb \\ ab^2ac &\to 0 \\ bba(ac) &\to 0 \end{aligned}\right\} \text{ the coefficient } -\frac{8}{4 \cdot 3^5},$$

hence

$$\text{(ii)} = -\frac{48}{4 \cdot 3^5} \overline{\begin{pmatrix} s \\ a \\ b \\ a^2 \end{pmatrix}};$$

(iii) from a'^4b' we get 0.

Thus

$$Q_3 = \frac{24}{4\cdot 3^5}\left\{3\overline{\begin{pmatrix}s\\b\\c\\ab\end{pmatrix}} - 3\overline{\begin{pmatrix}s\\a\\b\\bc\end{pmatrix}} - 2\overline{\begin{pmatrix}s\\a\\b\\a^2\end{pmatrix}}\right\}.$$

Then,

$$\psi^{1-} \propto 3\overline{\begin{pmatrix}s\\a\\b\\bc\end{pmatrix}} + \overline{\begin{pmatrix}s\\a\\c\\b^2\end{pmatrix}} - \overline{\begin{pmatrix}s\\b\\c\\ab\end{pmatrix}} + 4\overline{\begin{pmatrix}s\\a\\b\\a^2\end{pmatrix}}. \tag{21}$$

Putting now

$$d = (x+iy)^2 \propto d(2,2), \qquad g = z(x-iy) \propto d(2,-1),$$
$$f = z(x+iy) \propto d(2,1), \qquad e = (x-iy)^2 \propto d(2,-2),$$
$$h = 2z^2-x^2-y^2 \propto d(20), \quad i = 3/\alpha - 2_r^2 \propto 2s,$$

we find

$$\psi^{1-} \propto \tfrac{1}{3}\overline{\begin{pmatrix}s\\a\\b\\h\end{pmatrix}} - \tfrac{5}{3}\overline{\begin{pmatrix}s\\a\\b\\i\end{pmatrix}} + \overline{\begin{pmatrix}s\\a\\c\\d\end{pmatrix}} - \overline{\begin{pmatrix}s\\b\\c\\f\end{pmatrix}}.$$

Using the same notation for the normalized functions a, b, c etc., we have for the normalized wave function

$$\psi^{1-}_{\text{normalized}} = \frac{1}{12\sqrt{5}}\left\{\sqrt{3}\overline{\begin{pmatrix}s\\a\\b\\h\end{pmatrix}} - 5\sqrt{6}\overline{\begin{pmatrix}s\\a\\b\\i\end{pmatrix}} + 3\sqrt{2}\overline{\begin{pmatrix}s\\a\\c\\d\end{pmatrix}} - 3\overline{\begin{pmatrix}s\\b\\c\\f\end{pmatrix}}\right\}. \tag{22}$$

2) *The* 2^- *state*

Clustering into C^{12} and an α-particle, we can obtain the 2^- state of O^{16} from either of the following wave-functions:

$$(\alpha)\ (C^{12})_{2d} f_{1s}(\alpha) X_{(5,1)}(\mathbf{R}_1-\mathbf{R}_2)$$
$$(\beta)\ (C^{12})_{2d} f_{1s}(\alpha) X_{(5,3)}(\mathbf{R}_1-\mathbf{R}_2)$$
$$(\gamma)\ (C^{12})_{1g} f_{1s}(\alpha) X_{(5,3)}(\mathbf{R}_1-\mathbf{R}_2)$$
$$(\delta)\ (C^{12})_{1g} f_{1s}(\alpha) X_{(5,5)}(\mathbf{R}_1-\mathbf{R}_2),$$

all of which lead to the same result. We shall consider here only the wave-function (α).

We find that, taking a, b and c unnormalized,

$$\psi^{2-} \propto 4\left\{6\overline{\begin{pmatrix}s\\a\\b\end{pmatrix}\begin{pmatrix}s\\a\\b\end{pmatrix}\begin{pmatrix}s\\a\\b\end{pmatrix}\begin{pmatrix}s\\a\\c\end{pmatrix}} - \overline{\begin{pmatrix}s\\a\\b\end{pmatrix}\begin{pmatrix}s\\a\\b\end{pmatrix}\begin{pmatrix}s\\b\\c\end{pmatrix}\begin{pmatrix}s\\b\\c\end{pmatrix}}\right\}(ssss)\ (a'b'^2c'^2+2a'^3b'c'+a'^5)$$
$$+\left\{3\overline{\begin{pmatrix}s\\b\\c\end{pmatrix}\begin{pmatrix}s\\b\\c\end{pmatrix}\begin{pmatrix}s\\b\\c\end{pmatrix}\begin{pmatrix}s\\a\\b\end{pmatrix}} - 4\overline{\begin{pmatrix}s\\b\\c\end{pmatrix}\begin{pmatrix}s\\a\\b\end{pmatrix}\begin{pmatrix}s\\a\\b\end{pmatrix}\begin{pmatrix}s\\a\\b\end{pmatrix}}\right\}(ssss)[b'^3c'^2+2a'^2b'^2c'+a'^4b'].$$

Now,

(1)
$$\overline{\binom{s}{a}\binom{s}{a}\binom{s}{a}\binom{s}{a}}\begin{cases} a'b'^2c'^2 \to \dfrac{48}{4\cdot 3^5}\overline{\binom{s}{a}\binom{s}{b}\binom{s}{ab}} \\ 2a'^3b'c' \to 0 \\ a'^5 \to 0 \end{cases}$$

(2)
$$\overline{\binom{s}{a}\binom{s}{a}\binom{s}{b}\binom{s}{b}}\begin{cases} a'b'^2c'^2 \to -\dfrac{24}{4\cdot 3^5}\overline{\binom{s}{b}\binom{s}{c}\binom{s}{b^2}} \\ 2a'^3b'c' \to -\dfrac{12^2}{4\cdot 3^5}\overline{\binom{s}{a}\binom{s}{b}\binom{s}{ab}} \\ a'^5 \to 0 \end{cases}$$

(3)
$$\overline{\binom{s}{b}\binom{s}{b}\binom{s}{b}\binom{s}{a}}\begin{cases} b'^3c'^2 \to 0 \\ 2a'^2b'^2c' \to -\dfrac{48}{4\cdot 3^5}\overline{\binom{s}{b}\binom{s}{c}\binom{s}{b^2}} \\ a'^4b' \to -\dfrac{96}{4\cdot 3^5}\overline{\binom{s}{a}\binom{s}{b}\binom{s}{ab}} \end{cases}$$

(4)
$$\overline{\binom{s}{b}\binom{s}{a}\binom{s}{a}\binom{s}{a}}\begin{cases} b'^3c'^2 \to \dfrac{72}{4\cdot 3^5}\overline{\binom{s}{b}\binom{s}{c}\binom{s}{b^2}} \\ 2a'^2b'c' \to \dfrac{24\times 8}{4\cdot 3^5}\overline{\binom{s}{a}\binom{s}{b}\binom{s}{ab}} \\ a'^4b' \to 0. \end{cases}$$

Therefore,

$$\psi^{2^-}_{\text{unnormalized}} \propto 2\overline{\binom{s}{a}\binom{s}{b}\binom{s}{ab}} - \overline{\binom{s}{b}\binom{s}{c}\binom{s}{b^2}},$$

and for normalized $a, b, c,$ etc.,

$$\psi^{2^-}_{\text{normalized}} = \frac{1}{6}\left[\overline{\binom{s}{a}\binom{s}{b}\binom{s}{f}} - 2\sqrt{2}\,\overline{\binom{s}{b}\binom{s}{c}\binom{s}{d}}\right].$$

3) *The* 3^- *state*

We have six different combinations of C^{12} in 3s, 2d or 1g states and relative oscillations against α-particle X_{51}, X_{53} or X_{55}. All lead to the same final result. Taking, e.g., the combination $(C^{12})_{3s}f_{1s}(\alpha)X_{53}(\mathbf{R}_1-\mathbf{R}_2)$, we have

$$\psi^{3-} \propto \left\{ 3\begin{pmatrix}s\\b\\c\end{pmatrix}\begin{pmatrix}s\\b\\c\end{pmatrix}\begin{pmatrix}s\\b\\c\end{pmatrix}\begin{pmatrix}s\\b\\c\end{pmatrix} - 2\overline{\begin{pmatrix}s\\a\\c\end{pmatrix}\begin{pmatrix}s\\b\\c\end{pmatrix}\begin{pmatrix}s\\b\\c\end{pmatrix}\begin{pmatrix}s\\a\\b\end{pmatrix}} + 8\overline{\begin{pmatrix}s\\a\\b\end{pmatrix}\begin{pmatrix}s\\a\\b\end{pmatrix}\begin{pmatrix}s\\a\\c\end{pmatrix}\begin{pmatrix}s\\a\\c\end{pmatrix}} \right\}_{C_{12}}$$
$$\times (ssss)_\alpha \times [b'^4c' + a'^2b'^3]_{X_{53}}.$$

We see at once that the only non-vanishing term we can obtain is

$$\psi^{3-} = \overline{\begin{pmatrix}s\\a\\b\\c\end{pmatrix}\begin{pmatrix}s\\a\\b\\c\end{pmatrix}\begin{pmatrix}s\\a\\b\\c\end{pmatrix}\begin{pmatrix}s\\a\\b\\b^2\end{pmatrix}}.$$

5. General Considerations on Antisymmetrization and Symmetrization

5.1. PROPERTIES OF ANTISYMMETRIZATION AND SYMMETRIZATION OPERATORS

Suppose we have to antisymmetrize (symmetrize) the function $f(x_1, x_2, \ldots x_n)$ with respect to all coordinates x_i. We write

$$f(x_1, x_2, \ldots x_n) = \int f(x'_1, x'_2, \ldots x'_n)\delta(x_1-x'_1)\delta(x_2-x'_2)\ldots\delta(x_n-x'_n)\mathrm{d}\tau'_1\ldots\mathrm{d}\tau'_n \quad (22)$$

where x_i and $\mathrm{d}\tau'_i$ are extended to include spin and isospin coordinates. If A and S are the operators for antisymmetrization or symmetrization, we have †

$$\mathrm{A}f(x_1,\ldots x_n) = \frac{1}{n!}\int f(x'_1,\ldots x'_n)\begin{vmatrix}\delta(x_1-x'_1)\,\delta(x_1-x'_2)\ldots\delta(x_1-x'_n)\\ \delta(x_2-x'_1)\,\delta(x_2-x'_2)\ldots\delta(x_2-x'_n)\\ \ldots\ldots\ldots\ldots\ldots\\ \delta(x_n-x'_1)\delta(x_n-x'_2)\ldots\delta(x_n-x'_n)\end{vmatrix}\mathrm{d}\tau'_1\ldots\mathrm{d}\tau'_n, \quad (22a)$$

$$\mathrm{S}f(x_1\ldots x_n) = \frac{1}{n!}\int f(x'_1,\ldots x'_n)\begin{bmatrix}\delta(x_1-x'_1)\ldots\delta(x_1-x'_n)\\ \ldots\ldots\ldots\ldots\\ \delta(x_n-x'_1)\ldots\delta(x_n-x'_n)\end{bmatrix}\mathrm{d}\tau'_1\ldots\mathrm{d}\tau'_n, \quad (22b)$$

where [ ] denotes the permanent of the $\delta(x_i-x'_j)$'s. Obviously, the operators A and S are idempotent.

The following propositions are easily derived from (22a) or (22b):

(i) When $f(x_1\ldots x_n)$ is symmetric (antisymmetric), at least with respect to two particles, then

$$\mathrm{A}f(x_1\ldots x_n) \equiv 0, \quad [\mathrm{S}f(x_1\ldots x_n) \equiv 0].$$

† The expression (22a) for antisymmetric wave functions is already used in ref. [2]).

(ii) When a function $f(x_1 \ldots x_n)$ is symmetric with respect to two variables x_α and x_β and at the same time antisymmetric with respect to one of these (e.g. x_β) and a third one x_γ, it vanishes identically.

Indeed,

$$\begin{aligned} f(..x_\alpha..x_\beta..x_\gamma..) &= f(..x_\beta..x_\alpha..x_\gamma..) = -f(..x_\beta..x_\gamma..x_\alpha..) \\ &= -f(..x_\gamma..x_\beta..x_\alpha..) = f(..x_\gamma..x_\alpha..x_\beta..) = f(..x_\alpha..x_\gamma..x_\beta..) \\ &= -f(..x_\alpha..x_\beta..x_\gamma..), \end{aligned}$$

or

$$f(x_1 \ldots x_n) \equiv 0.$$

Therefore we can say that there is no "overlapping" between the symmetric and antisymmetric part of a function.

(iii) Let $f(x_1 \ldots x_l, x_{l+1} \ldots x_n)$ be antisymmetric with respect to $x_1 \ldots x_l$. We want to antisymmetrize it completely. From (22a) and (9a),

$$\mathrm{A}f = \frac{1}{n!}\int f(x'_1 \ldots x'_l, x'_{l+1} \ldots x'_n) \begin{vmatrix} \delta(x_1-x'_1)\ldots\delta(x_1-x'_l)\delta(x_1-x'_{l+1})\ldots\delta(x_1-x'_n) \\ \cdots\cdots\cdots\cdots\cdots\cdots\cdots\cdots \\ \delta(x_n-x'_1)\ldots\delta(x_n-x'_l)\delta(x_n-x'_{l+1})\ldots\delta(x_n-x'_n) \end{vmatrix} \mathrm{d}\tau'_1 \ldots \mathrm{d}\tau'_n$$

$$= \frac{1}{n!}\int f(x'_1 \ldots x'_l, x'_{l+1} \ldots x'_n)(-)^{\frac{1}{2}l(l+1)} \sum_{{}^nC_l} (-)^{[{}^nC_l]} \begin{vmatrix} \delta(x_k-x'_1)\ldots\delta(x_k-x_l) \\ \cdots\cdots\cdots\cdots \\ \delta(x_m-x'_1)\ldots\delta(x_m-x'_l) \end{vmatrix}$$

$$\times \begin{vmatrix} \delta(x_h-x'_{l+1})\ldots\delta(x_h-x'_n) \\ \cdots\cdots\cdots\cdots \\ \delta(x_j-x'_{l+1})\ldots\delta(x_j-x'_n) \end{vmatrix} \mathrm{d}\tau'_1 \ldots \mathrm{d}\tau'_n$$

$$= \frac{l!}{n!}(-)^{\frac{1}{2}l(l+1)} \int f(x_k \ldots x_m, x'_{l+1} \ldots x'_n) \sum_{{}^nC_l} (-)^{[{}^nC_l]} \begin{vmatrix} \delta(x_h-x'_{l+1})\ldots\delta(x_h-x'_n) \\ \cdots\cdots\cdots\cdots \\ \delta(x_j-x'_{l+1})\ldots\delta(x_j-x'_n) \end{vmatrix} \mathrm{d}\tau'_{l+1} \ldots \mathrm{d}\tau'_n$$

$$= \frac{l!(n-l)!}{n!}(-)^{\frac{1}{2}l(l+1)} \sum_{{}^nC_l} (-)^{[{}^nC_l]} \mathrm{A}(h, \ldots, j) f(x_k, \ldots x_m; x_h \ldots x_j). \tag{23a}$$

If $f(x_1 \ldots x_l, x_{l+1} \ldots x_n)$ is antisymmetric separately for the first l and the other $n-l$ variables, we have in particular

$$\mathrm{A}f = \frac{l!(n-l)!}{n!}(-)^{\frac{1}{2}l(l+1)} \sum_{{}^nC_l} (-)^{[{}^nC_l]} f(x_{i_1}, x_{i_2}, \ldots x_{i_l}; x_{i_{l+1}} \ldots x_{i_n}). \tag{23b}$$

(iiia) If $f(x_1 \ldots x_l; x_{l+1} \ldots x_n)$ is symmetric with respect to the l first variables and we want to symmetrize it completely, we get, in a similar way,

$$\mathrm{S}f(x_1 \ldots x_l, x_{l+1} \ldots x_n) = \frac{l!(n-l)!}{n!} \sum_{{}^nC_l} \mathrm{S}(i_{l+1} \ldots i_n) f(x_{i_1} x_{i_2} \ldots x_{i_l}, x_{i_{l+1}} \ldots x_{i_n}). \tag{23c}$$

Also, if $f(x_1 \ldots x_l, x_{l+1} \ldots x_n)$ is symmetric separately for the first l and the other $n-l$ variables, we have

$$Sf(x_1 \ldots x_l, x_{l+1} \ldots x_n) = \frac{l!(n-l)!}{n!} \sum_{{}^nC_l} f(x_{i_1}, x_{i_2} \ldots x_{i_l}; x_{i_{l+1}} \ldots x_{i_n}). \quad (23d)$$

(iv) If $f(x_1 \ldots x_n) = u(x_1 \ldots x_n)v(x_1 \ldots x_n)$ and $u(x_i)$ is antisymmetric, then

$$Af(x_i \ldots x_n) = u(x_1 \ldots x_n)[Sv(x_1 \ldots x_n)]; \quad (24)$$

if $u(x_i)$ is symmetric, then

$$Sf(x_1 \ldots x_n) = u(x_1 \ldots x_n)[Sv(x_1 \ldots x_n)]. \quad (24)$$

(v) It is easy to verify, using (22a) and (22b), that

$$\begin{aligned} (Au)(Av) &= S[u(Av)] = S[v(Au)], \\ (Au)(Sv) &= A[u(Sv)] = A[v(Au)]. \end{aligned} \quad (25)$$

Therefore, the expressions $u(Sv)$ and $v(Au)$ after antisymmetrization lead to the same result. Also

$$(Su)(Sv) = S[u(Sv)] = S[v(Su)]. \quad (25a)$$

(vi) If $f = u(x_1 \ldots x_l; x_{l+1} \ldots x_n)v(x_1 \ldots x_l)$, then

$$Af = \frac{l!(n-l)!}{n!} \sum_{{}^nC_l} (-)^{[{}^nC_l]} A(1, \ldots l)\{v(x_{i_1} \ldots x_{i_l})\, A(l+1, \ldots, n)u(x_{i_1}, x_{i_2} \ldots x_{i_n})\}, \quad (26a)$$

and if u is a function of $x_{l+1} \ldots x_n$ only,

$$Af = \frac{l!(n-l)!}{n!} \sum_{{}^nC_l} (-)^{[{}^nC_l]} (Au)(Av.) \quad (26b)$$

(vii) We can always write

$$A(1, 2, \ldots n) = \frac{l!(n-l)!}{n!} \sum_{{}^nC_l} (-)^{[{}^nC_l]} A(i_1 \ldots i_l) A(i_{l+1} \ldots i_n) \quad (27)$$

and

$$S(1, 2, \ldots n) = \frac{l!(n-l)!}{n!} \sum_{{}^nC_l} S(i_1, i_2, \ldots i_l) S(i_{l+1} \ldots i_n). \quad (27a)$$

Then, if we have

$$f = u(x_1 \ldots x_l)v(x_{l+1} \ldots x_n)X(x_1, \ldots x_{l1} x_{l+1} \ldots x_n), \quad (28)$$

where u and v are antisymmetric while X is symmetric separately for the first l and the last $n-l$ variables,

$$\mathrm{A}f = \frac{l!(n-l)!}{n!}\sum_{{}^{n}C_{l}}(-)^{[{}^{n}C_{l}]}\mathrm{A}(i_1 \ldots i_l)\mathrm{A}(i_{l+1} \ldots i_n)uvX \tag{28a}$$

$$= \frac{l!(n-l)!}{n!}\sum_{{}^{n}C_{l}}(-)^{[{}^{n}C_{l}]}u(x_{i_1} \ldots x_{i_l})v(x_{i_{l+1}} \ldots x_{i_n})X(x_{i_1} \ldots x_{i_l}; x_{i_{l+1}} \ldots x_n).$$

The form (28) is the general one for Cluster Model wave functions. With harmonic oscillator wave functions it reduces to the case with which we dealt in section 4.

5.2. MATRIX ELEMENT OF OPERATOR

The matrix element of an operator $O(1, \ldots n)$ is given by

$$O_{ij} = \frac{1}{N_i N_j}\int (\mathrm{A}f_i)^* O(\mathrm{A}f_j)\mathrm{d}\tau_1 \ldots \mathrm{d}\tau_n \tag{29}$$

where $1/N_i$ is the normalization factor of $(\mathrm{A}f_i)$.

When O is symmetric in all particles,

$$O_{ij} = \frac{1}{N_i N_j}\int f_i^*(1, 2, \ldots n)O(1, 2, \ldots n)[\mathrm{A}f_j(1, \ldots n)]\mathrm{d}\tau_1 \ldots \mathrm{d}\tau_n \tag{29}$$

and

$$|N_i|^2 = \int f_i^*(1, \ldots n)[\mathrm{A}f_i(1, \ldots, n)]\mathrm{d}\tau_1 \ldots \mathrm{d}\tau_n. \tag{30}$$

Therefore, using (22a), we obtain

$$O_{ij} = \frac{1}{n!N_i N_j}\int\int f_i^*(1, 2, \ldots n)O(1, 2, \ldots, n)$$

$$\cdot f_j(1', 2', \ldots n')\begin{vmatrix} \delta(1-1') \ldots \delta(1-n') \\ \cdots\cdots\cdots\cdots \\ \delta(n-1') \ldots \delta(n-n') \end{vmatrix}\mathrm{d}\tau_1 \ldots \mathrm{d}\tau_n \mathrm{d}\tau'_1 \ldots \mathrm{d}\tau'_n.$$

5.3. ANTISYMMETRIZATION OF ANALYTIC FUNCTIONS

Suppose we have a function $f(x_1, x_2 \ldots x_n)$ which is analytic in the neighbourhood of a point (ξ_i). Then we can expand it in a Taylor series

$$f(x_1, x_2, \ldots x_n)$$

$$= \sum_{\substack{i_1, i_2, \ldots i_n = 0 \\ i_1 + i_2 + \ldots + i_n = k}}^{\infty} \frac{(x_1-\xi_1)^{i_1}(x_2 \ldots \xi_2)^{i_2} \ldots (x_n-\xi_n)^{i_n}}{i_1! i_2! \ldots i_n!}\left[\frac{\partial^{(k)}}{\partial x_1^{i_1} \ldots \partial x_n^{i_n}} f(x_1 \ldots x_n)\right]_{x_i=\xi_i}. \tag{31}$$

After antisymmetrization we obtain

$$\mathrm{A}f = \frac{1}{n!}\sum_{\substack{i_\rho=0 \\ k=\sum_{\rho=1}^{n} i_\rho \geq \frac{1}{2}n(n-1)}}^{\infty} \frac{1}{i_1!\,i_2!\ldots i_n!} \begin{vmatrix} (x_1-\xi_1)^{i_1}(x_1-\xi_2)^{i_2}\ldots(x_1-\xi_n)^{i_n} \\ (x_2-\xi_1)^{i_1}(x_2-\xi_2)^{i_2}\ldots(x_2-\xi_n)^{i_n} \\ \ldots\ldots\ldots\ldots\ldots\ldots \\ (x_n-\xi_1)^{i_1}(x_n-\xi_2)^{i_2}\ldots(x_n-\xi_n)^{i_n} \end{vmatrix} \left\{ \begin{vmatrix} \frac{\partial^{i_1}}{\partial x_1^{i_1}} & \frac{\partial^{i_2}}{\partial x_1^{i_2}} & \cdots & \frac{\partial^{i_n}}{\partial x_1^{i_n}} \\ \ldots & \ldots & \ldots & \ldots \\ \frac{\partial^{i_1}}{\partial x_n^{i_1}} & \frac{\partial^{i_2}}{\partial x_n^{i_2}} & \cdots & \frac{\partial^{i_n}}{\partial x_n^{i_n}} \end{vmatrix} f(x_i) \right\}_{x_i=\xi_i}. \quad (32)$$

Thus, for every function analytic at a point (ξ_i) the operator of antisymmetrization takes the differential form

$$\mathrm{A}(1,\ldots,n) = \frac{1}{n!}\sum_{\substack{i_\rho=0 \\ \sum_{\rho=1}^{n} i_\rho = k \geq \frac{1}{2}n(n-1)}}^{\infty} \frac{1}{i'_1!\,i'_2!\ldots i_n!} \begin{vmatrix} (x_1-\xi_1)^{i_1}(x_1-\xi_2)^{i_2}\ldots(x_1-\xi_n)^{i_n} \\ (x_2-\xi_1)^{i_1}(x_2-\xi_2)^{i_2}\ldots(x_2-\xi_n)^{i_n} \\ \ldots\ldots\ldots\ldots\ldots\ldots \\ (x_n-\xi_1)^{i_1}(x_n-\xi_2)^{i_2}\ldots(x_n-\xi_n)^{i_n} \end{vmatrix} \times \begin{vmatrix} \frac{\partial^{i_1}}{\partial x_1^{i_1}} & \cdots & \frac{\partial^{i_n}}{\partial x_1^{i_n}} \\ \ldots & \ldots & \ldots \\ \frac{\partial^{i_1}}{\partial x_n^{i_1}} & \cdots & \frac{\partial^{i_n}}{\partial x_n^{i_n}} \end{vmatrix}_{x_i=\xi_i} \quad (33)$$

The lowest derivatives of $f(x_1 \ldots x_n)$ which appear in Af are of order $k = \frac{1}{2}n(n-1)$, because for $i_1+i_2+\ldots+i_n < \frac{1}{2}n(n-1)$ the determinant of $(x_i-\xi_i)$ vanishes, as one can see by expanding the elements of the determinant and splitting it in a sum of Vandermonde determinants in x_i(or ξ_i).

Suppose that a function $f(x_1 \ldots x_n)$ is analytic in a domain D. Then, eq. (32) gives the value of Af at a certain point $(x_1, x_2 \ldots x_n)$ as a function of the values of f and its derivatives at any point $(\xi_1, \xi_2, \ldots, \xi_n)$ of the domain D.

Theorem: If a function $f(x_i)$ of n variables is analytic in a domain D, its antisymmetric expression is independent of all derivatives of $f(x_i)$ of order lower than $\frac{1}{2}n(n-1)$.

This shows that one has to be careful in extending results obtained with a non-antisymmetrized wave function to the case where antisymmetrization is taken into account.

The above results are valid for the case in which we have n particles in one-dimensional space, without taking into account spin and isospin. The corresponding expressions for the general 3-dimensional case with spin and isospin accounted for, are

$$f(\mathbf{r}_1, \mathbf{r}_2, \ldots \mathbf{r}_n) = \sum_{\substack{i_1,\ldots i_n \\ j_1,\ldots j_n \\ k_1,\ldots k_n}=0}^{\infty} \frac{(x_1-\xi_1)^{i_1}(y_1-\eta_1)^{j_1}(z_1-\zeta_1)^{k_1}\ldots(x_n-\xi_n)^{i_n}(y_n-\eta_n)^{j_n}(z_n-\zeta_n)^{k_n}}{i_1!\ldots i_n!\,j_1!\ldots j_n!\,k_1!\ldots k_n!} \times \left\{ \frac{\partial^{(l)}}{\partial x_1^{i_1}\partial y_1^{j_1}\partial z_1^{k_1}\ldots\partial x_n^{i_n}\partial y_n^{j_n}\partial z_n^{k_n}} f(\mathbf{r}_1, \ldots \mathbf{r}_n) \right\}_{\substack{x_i=\xi_i \\ y_j=\eta_j \\ z_k=\zeta_k}} \quad (31a)$$

with $i_1+i_2+\ldots+i_n+j_1+\ldots+j_n+k_1+\ldots+k_n=l$,

$$\mathrm{A}f=\frac{1}{n!}\sum_{\substack{i_1,\ldots,i_n\\ j_1,\ldots,j_n\\ k_1,\ldots k_n}=0}^{\infty}\frac{1}{i_1!\ldots i_n!\,j_1!\ldots j_n!\,k_1!\ldots k_n!}$$

$$\times\begin{vmatrix}(x_1-\xi_1)^{i_1}(y_1-\eta_1)^{j_1}(z_1-\zeta_1)^{k_1}, & (x_1-\xi_2)^{i_2}(y_1-\eta_2)^{j_2}(z_1-\zeta_2)^{k_2}, & \ldots & (x_1-\xi_n)^{i_n}(y_1-\eta_n)^{j_n}(z_1-\zeta_n)^{k_n}\\ (x_2-\xi_1)^{i_1}(y_2-\eta_1)^{j_1}(z_2-\zeta_1)^{k_1}, & (x_2-\xi_2)^{i_2}(y_2-\eta_2)^{j_2}(z_2-\zeta_2)^{k_2}, & \ldots & (x_2-\xi_n)^{i_n}(y_2-\eta_n)^{j_n}(z_2-\zeta_n)^{k_n}\\ \cdots & \cdots & \cdots & \cdots\\ \cdots & \cdots & \cdots & \cdots\\ (x_n-\xi_1)^{i_1}(y_n-\eta_1)^{j_1}(z_n-\zeta_1)^{k_1}, & (x_n-\xi_2)^{i_2}(y_n-\eta_2)^{j_2}(z_n-\zeta_2)^{k_2} & \ldots & (x_n-\xi_n)^{i_n}(y_n-\eta_n)^{j_n}(z_n-\zeta_n)^{k_n}\end{vmatrix}$$

$$\times\left\{\begin{vmatrix}\frac{\partial^{m_1}}{\partial x_1^{i_1}\partial y_1^{j_1}\partial z_1^{k_1}} & \frac{\partial^{m_2}}{\partial x_1^{i_2}\partial y_1^{j_2}\partial z_1^{k_2}} & \cdots & \frac{\partial^{m_n}}{\partial x_1^{i_n}\partial y_1^{j_n}\partial z_1^{k_n}}\\ \frac{\partial^{m_1}}{\partial x_2^{i_1}\partial y_2^{j_1}\partial z_2^{k_1}} & \frac{\partial^{m_2}}{\partial x_2^{i_2}\partial y_2^{j_2}\partial z_2^{k_2}} & \cdots & \frac{\partial^{m_n}}{\partial x_2^{i_n}\partial y_2^{j_n}\partial z_2^{k_n}}\\ \cdots & \cdots & \cdots & \cdots\\ \frac{\partial^{m_1}}{\partial x_n^{i_1}\partial y_n^{j_1}\partial z_n^{k_1}} & \frac{\partial^{m_2}}{\partial x_n^{i_2}\partial y_n^{j_2}\partial z_n^{k_2}} & \cdots & \frac{\partial^{m_n}}{\partial x_n^{i_n}\partial y_n^{j_n}\partial z_n^{k_n}}\end{vmatrix} f(\mathbf{r}_1,\ldots\mathbf{r}_n)\right\}_{\substack{x_i=\xi_i\\ y_j=\eta_j\\ z_k=\zeta_k}} \qquad (32a)$$

with

$$m_\alpha=i_\alpha+j_\alpha+k_\alpha \quad (\alpha=1,2,\ldots,n).$$

Here we find again that $m_1+m_2+\ldots m_n\geqq N$, where N is a number depending on the number of particles n and their distribution in the four spin and isospin states. Thus, for O^{16}, one has $N=2$, for C_a^{40}, $N=3$, and so on. In order to include spin and isospin, we make the assumption that every column of the first determinant in (32a) corresponds to a definite spin and isospin state.

References

1) K. Wildermuth and Th. Kanellopoulos, Nuclear Physics **7** (1958) 150
2) K. Wildermuth and Th. Kanellopoulos, Nuclear Physics **9** (1958/59) 449
3) K. Wildermuth and Th. Kanellopoulos, The application of the Cluster Model to nuclear physics (CERN, June 1959)

1.D.2 *Nuclear Physics* **14** (1959/60) 376—388; ©*North-Holland Publishing Co., Amsterdam*

Not to be reproduced by photoprint or microfilm without written permission from the publisher

APPLICATION OF THE COLLECTIVE MODEL TO SOME NUCLEI IN THE d-SHELL

G. R. BISHOP

Laboratoire des Hautes Energies, Ecole Normale Supérieure, Orsay, France

Received 29 June 1959

Abstract: Eigenvalues and eigenfunctions have been recalculated for the Nilsson deformed potential well with the addition of a term $\mu \mathbf{l}^2$. Comparison of the results with the decay schemes of nuclei in the d-shell shows that some of the existing discrepancies are removed by the presence of this correction to the oscillator potential dependent on the orbital angular momentum.

1. Introduction

The decay schemes at low excitation energies of several odd-mass nuclei in the d-shell have been interpreted by the application of the rotational collective model [1]). The levels are grouped into rotational bands each based on an intrinsic single particle state calculated for a deformed nuclear potential. Analysis begins with an estimation of the nuclear shape, assumed cylindrically symmetric, from the measured quadrupole moments, magnetic moments or decoupling parameters. Once the magnitude and sign of the deformation are known, it is possible to make a detailed comparison of experimental and theoretical quantities using the eigenvalues and eigenfunctions corresponding to the single particle shell model. Such quantities are the excitation energies of the levels, the transition probabilities for gamma or beta radiations, the reduced nucleon widths characterizing nuclear reactions such as stripping or nuclear capture, the magnetic and quadrupole moments of nuclear levels and their spins and parities.

Although the most striking successes of the collective model are found [2]) for mass numbers $150 < A < 190$ and $A > 222$, a remarkable correlation of experimental data on light nuclei has been obtained by application of the model [1]) to F^{19}, Al^{25}, Mg^{25}, Si^{29}, P^{31} and Al^{26}. There is, however, room for improvement in details and it is the purpose of this discussion to suggest a possible modification of the existing calculations, which appears to reduce some discrepancies.

2. Calculation of Single Particle States

The interaction of a nucleon with the nuclear field is described in Nilsson's work by the Hamiltonian [3])

$$H = H_0 + C\,\mathbf{l}\cdot\mathbf{s} + D\,\mathbf{l}^2$$

where the H_0 is the oscillator potential, to which is added a spin orbit potential $C\,\mathbf{l}\cdot\mathbf{s}$ and the term $D\,\mathbf{l}^2$, a correction to the oscillator potential for higher angular momentum states. The strength of these two terms is adjusted to give the known order of the single particle levels of the shell model, for a spherically symmetric potential. Nilsson then studies the effect of a deformation of the nuclear potential with cylindrical symmetry. By neglecting temporarily the $\mathbf{l}\cdot\mathbf{s}$ and $\mathbf{l}^2$ terms he finds that the Hamiltonian with the deformed potential can be split into a spherically symmetric term $\mathring{H}_0$ and a term H_δ representing the coupling of the particle to the axis of deformation. A representation is then chosen with $\mathring{H}_0$ diagonal, together with $\mathbf{l}^2$, l_z and s_z. The total Hamiltonian is then

$$H = \mathring{H}_0 + H_\delta + C\,\mathbf{l}\cdot\mathbf{s} + D\,\mathbf{l}^2,$$

and Nilsson then treats the last three terms as a perturbation. By a suitable choice of parameters, reproduced here for convenience, Nilsson arrives at

$$H = \mathring{H}_0 + \kappa\hbar\mathring{\omega}_0 R$$

where $\kappa = -\frac{1}{2}C/\hbar\mathring{\omega}_0$, and R is given by

$$R = \eta U - 2\mathbf{l}\cdot\mathbf{s} - \mu\mathbf{l}^2.$$

Here $\mu = 2D/C$ and $\eta = (\delta/\kappa)\omega_0(\delta)/\mathring{\omega}_0$ ($\mathring{\omega}_0$ is the value of $\omega_0(\delta)$ for $\delta = 0$). The parameter δ is related to the deformation of the nuclear potential, and U is obtained from

$$H_\delta = \delta\hbar\omega_0 U = \kappa\hbar\mathring{\omega}_0\eta U$$

with

$$U = -\frac{4}{3}\sqrt{\frac{\pi}{5}}\,r^2 Y_{20}.$$

From the diagonalization of the operator R, Nilsson obtains the eigenvalues $r^{N\Omega}(\eta)$; the corresponding energy eigenvalues of the total Hamiltonian are then

$$E^{N\Omega} = (N+\tfrac{3}{2})\hbar\omega_0 + \kappa\hbar\mathring{\omega}_0 r^{N\Omega}.$$

The quantum number N represents the total number of oscillator quanta, whilst Ω is the quantum number corresponding to the operator $j_z = l_z + s_z$ which commutes with H. Thus, Ω is the component of the nucleon total angular momentum along the nuclear axis. The base vectors used are enumerated as $|Nl\Lambda\Sigma\rangle$ where Λ and Σ are the eigenvalues of the operators l_z and s_z and thus $\Omega = \Lambda + \Sigma$.

For the d-shell, which is the outer shell of the nuclei considered here, Nilsson performed the diagonalization of R with $\mu = 0$, for $N = 0$, 1, 2, although for higher N-values he used μ in the range from 0.35 to 0.55. It seemed worthwhile, however, to study the effect of the $\mu\mathbf{l}^2$ term on the

TABLE 1

Eigenvalues and eigenfunctions for the deformed field with $N = 2$.
The notation and arrangement of the table correspond to those adopted by Nilsson [3]). For each orbit and value of η, the eigenvalue $\epsilon^{N\Omega}$ is given first, followed by the coefficients of the base vectors $|1220+\rangle$, $|1200+\rangle$, $|1221-\rangle$.

$\mu = 0$						
η	-6	-4	-2	$+2$	$+4$	$+6$
Orbit 11	8.719	6.379	4.368	2.630	3.298	4.394
	1.000	1.000	1.000	1.000	1.000	1.000
	0.649	0.591	0.432	−0.717	−1.143	−1.287
	−0.428	−0.605	−0.907	−1.066	−0.675	−0.454
Orbit 9	2.568	1.693	0.667	0.120	−0.237	−0.853
	1.000	1.000	1.000	1.000	1.000	1.000
	2.203	2.227	2.828	−15.696	15.901	6.635
	5.672	3.827	2.449	11.489	−25.472	−16.609
Orbit 6	−4.287	−3.072	−2.035	−3.751	−6.069	−8.542
	1.000	1.000	1.000	1.000	1.000	1.000
	−1.319	−1.227	−0.927	0.503	0.622	0.662
	0.336	0.453	0.662	0.600	0.428	0.325
$\mu = 0.167$						
η	-6	-4	-2	$+2$	$+4$	$+6$
Orbit 11	8.000	5.607	3.484	1.892	2.82	4.000
	1.000	1.000	1.000	1.000	1.000	1.000
	0.707	0.672	0.541	−0.997	−1.335	−1.414
	−0.408	−0.573	−0.901	−0.957	−0.590	−0.408
Orbit 9	1.701	0.9506	0.2485	−0.272	−0.983	−1.725
	1.000	1.000	1.000	1.000	1.000	1.000
	3.325	3.967	7.587	6.932	3.838	3.278
	8.191	6.399	5.847	−6.184	−6.997	−6.531
Orbit 6	−4.900	−3.558	−2.733	−4.620	−6.837	−9.275
	1.000	1.000	1.000	1.000	1.000	1.000
	−1.154	−1.060	−0.690	0.408	0.552	0.609
	0.355	0.501	0.720	0.615	0.445	0.337

TABLE 1
(continued)

$\mu = 0.33$						
η	−6	−4	−2	+2	+4	+6
Orbit 11	7.322	4.892	2.667	1.334	2.434	3.655
	1.000	1.000	1.000	1.000	1.000	1.000
	0.772	0.771	0.707	−1.414	−1.549	1.547
	−0.3874	−0.537	−0.820	−0.612	−0.514	−0.368
Orbit 9	0.8462	+0.235	−0.127	−0.804	−1.781	−2.615
	1.000	1.000	1.000	1.000	1.000	1.000
	6.684	16.045	−14.846	2.345	2.118	2.163
	15.930	25.000	−11.894	−1.314	−4.437	−6.361
Orbit 6	−5.168	−4.127	−3.540	−5.529	−7.653	−10.040
	1.000	1.000	1.000	1.000	1.000	1.000
	−1.094	−0.914	−0.533	0.341	0.493	0.563
	0.397	0.550	0.764	0.634	0.460	0.348

$\mu = 0.5$						
η	−6	−4	−2	+2	+4	+6
Orbit 11	6.685	4.241	1.963	0.972	2.122	3.355
	1.000	1.000	1.000	1.000	1.000	1.000
	0.846	0.8893	0.943	−1.940	−1.777	−1.686
	−0.366	−0.499	−0.743	−0.673	−0.449	−0.334
Orbit 9	0.000	−0.468	−0.546	−1.509	−2.625	−3.522
	0.000	1.000	1.000	1.000	1.000	1.000
	1.000	−8.057	−3.453	1.250	1.435	1.606
	2.309	−12.307	−3.112	−2.115	−3.460	5.123
Orbit 6	−5.685	−4.773	−4.417	−6.463	−8.500	−10.833
	1.000	1.000	1.000	1.000	1.000	1.000
	−0.995	−0.790	−0.427	0.292	0.445	0.522
	0.431	0.596	+0.794	0.658	0.472	0.358

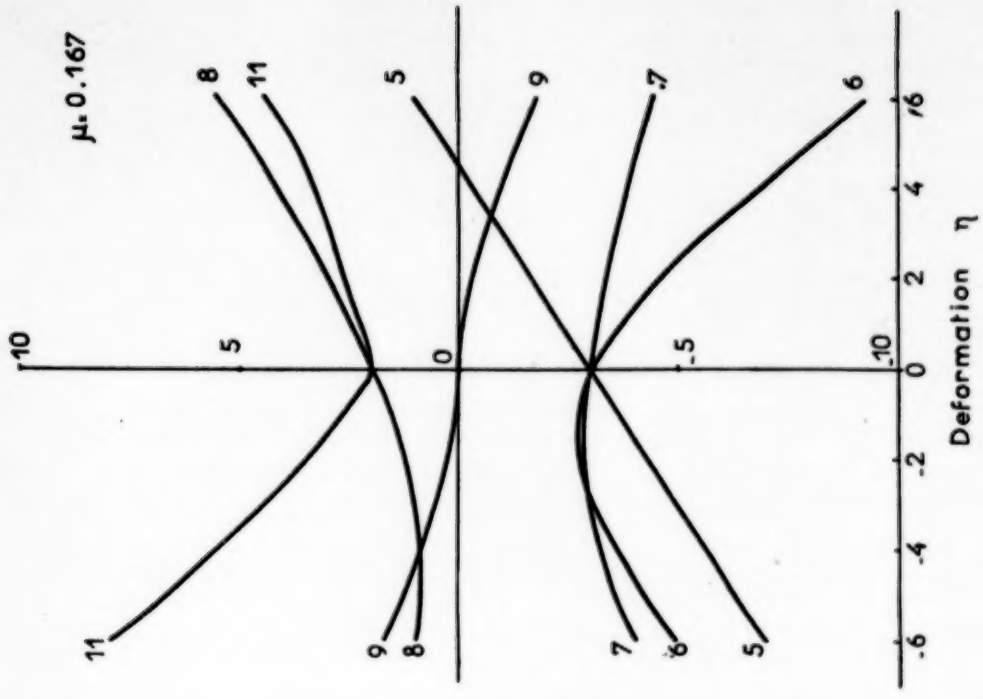
μ= 0.167
Deformation η

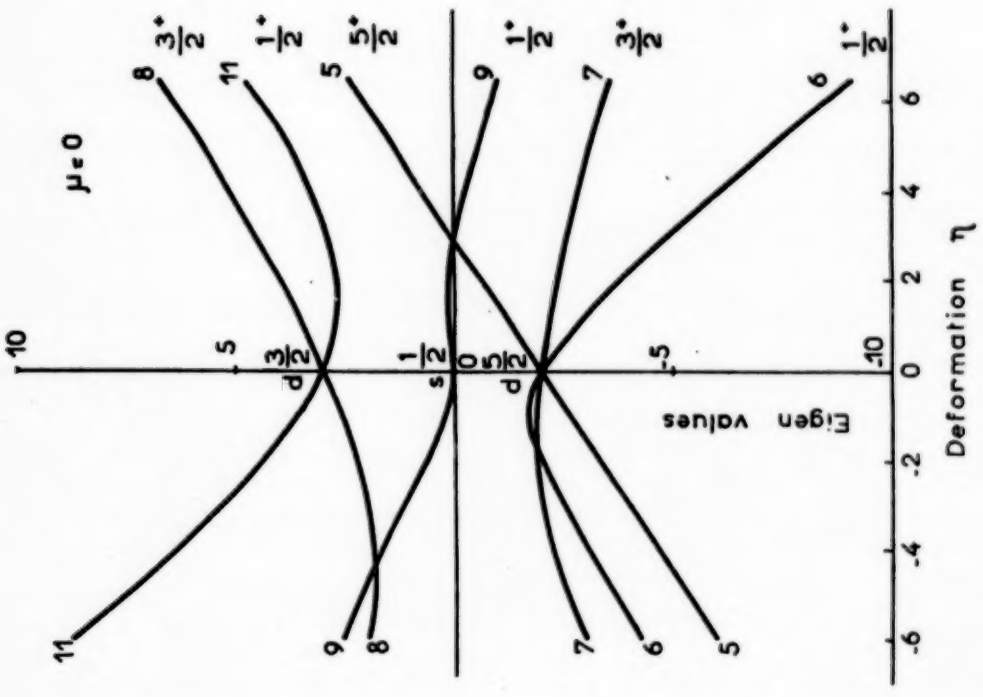
μ= 0
Eigen values
Deformation η

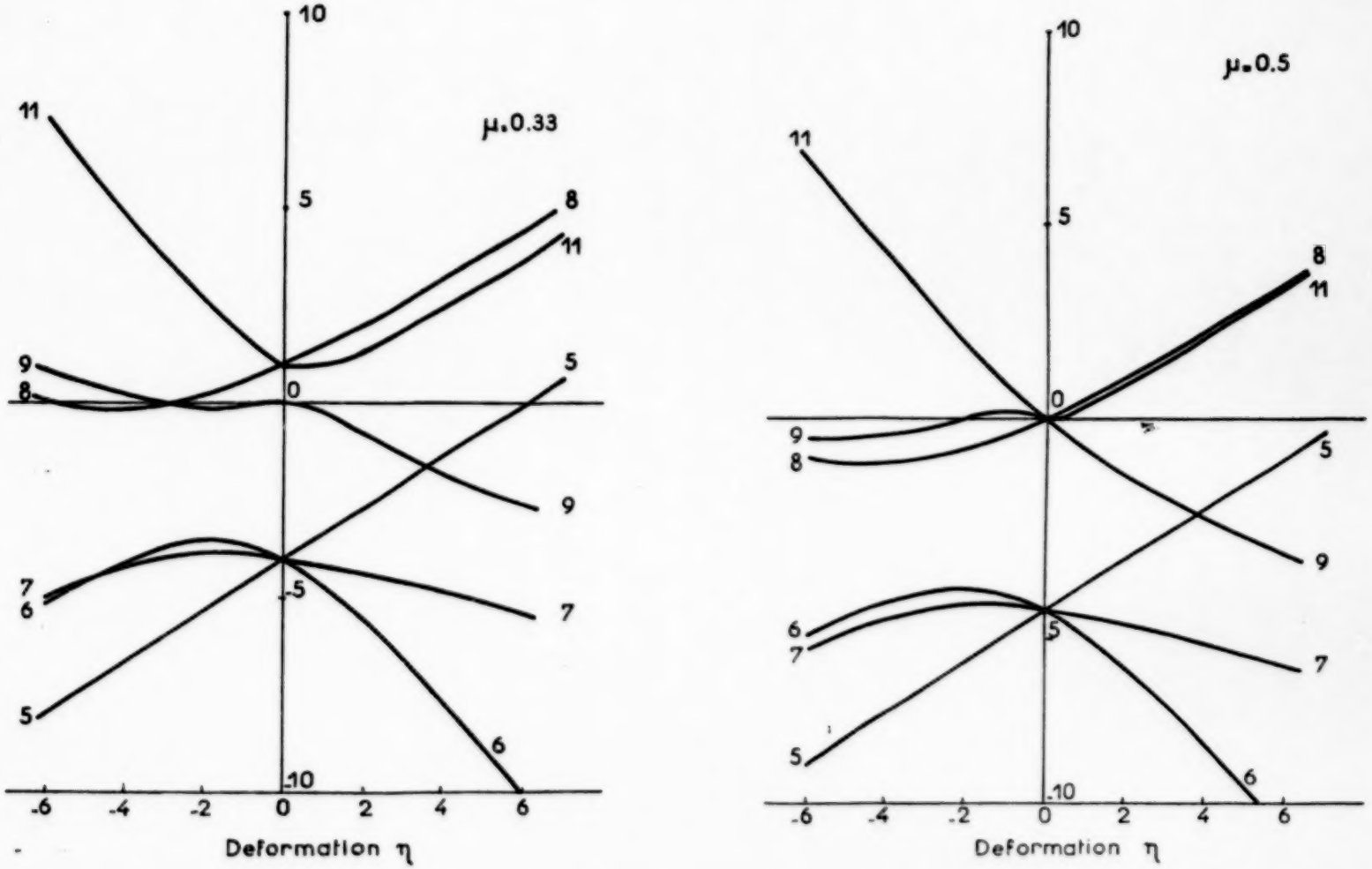

Fig. 1. (a, b, c, d). Eigenvalues $\epsilon^{N\Omega}$ of the operator R as a function of the deformation η and for four different values of the parameter μ. The ordinate must be multiplied by $\kappa\hbar\mathring{\omega}_0$ to give the energy of the individual orbits in excess of $3.5\hbar\omega_0(\delta)$.

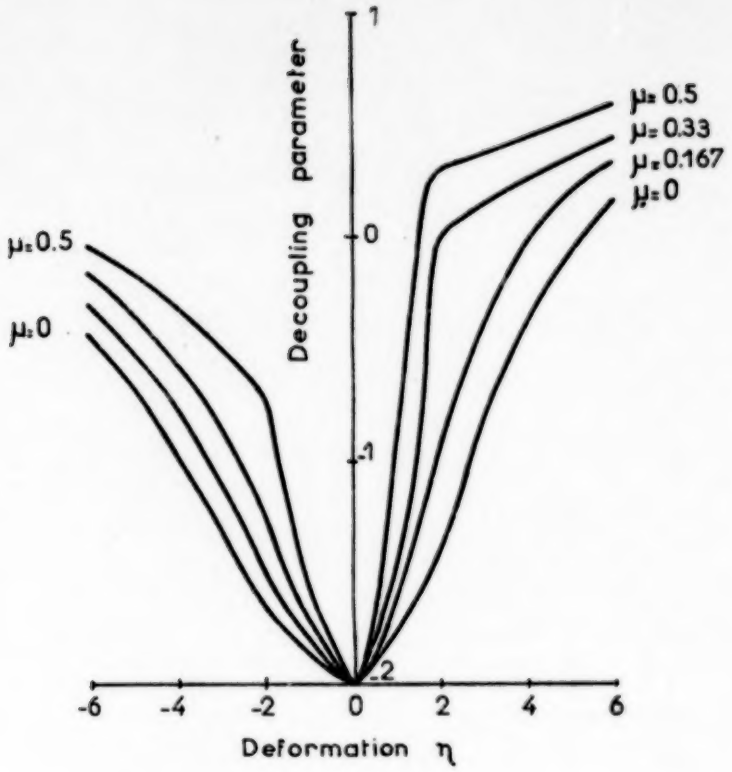
Decoupling parameter
1
0
-1
-2
μ=0.5
μ=0.33
μ=0.167
μ=0
μ=0.5
μ=0
-6
-4
-2
0
2
4
6
Deformation η

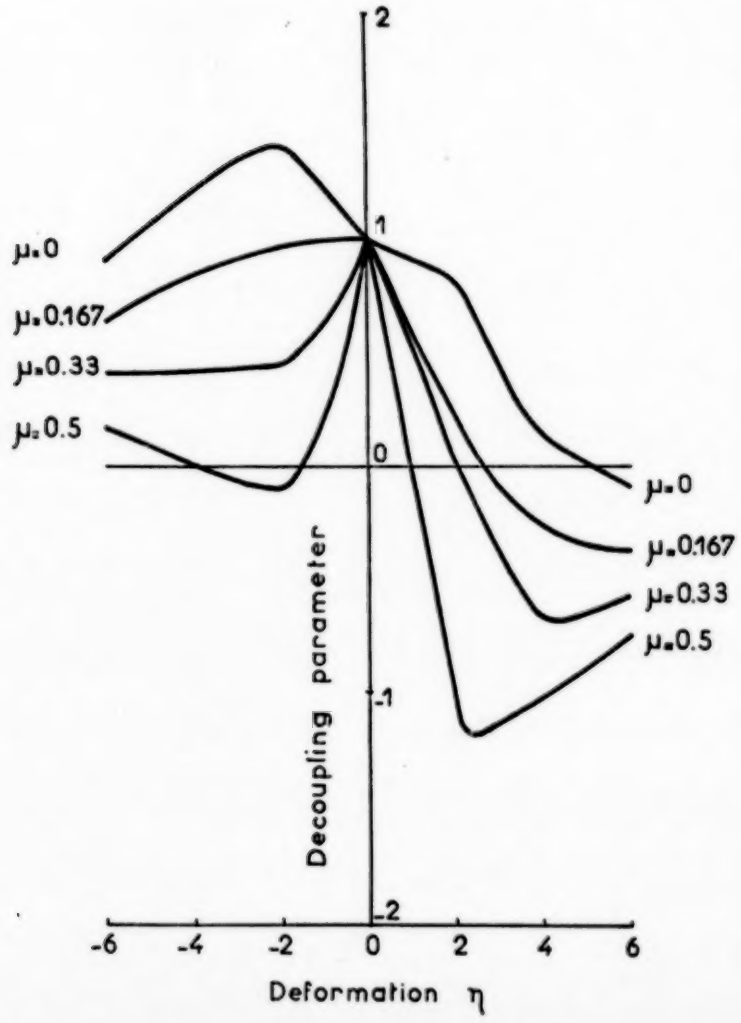
2
1
0
-1
-2
μ=0
μ=0.167
μ=0.33
μ=0.5
μ=0
μ=0.167
μ=0.33
μ=0.5
Decoupling parameter
-6
-4
-2
0
2
4
6
Deformation η

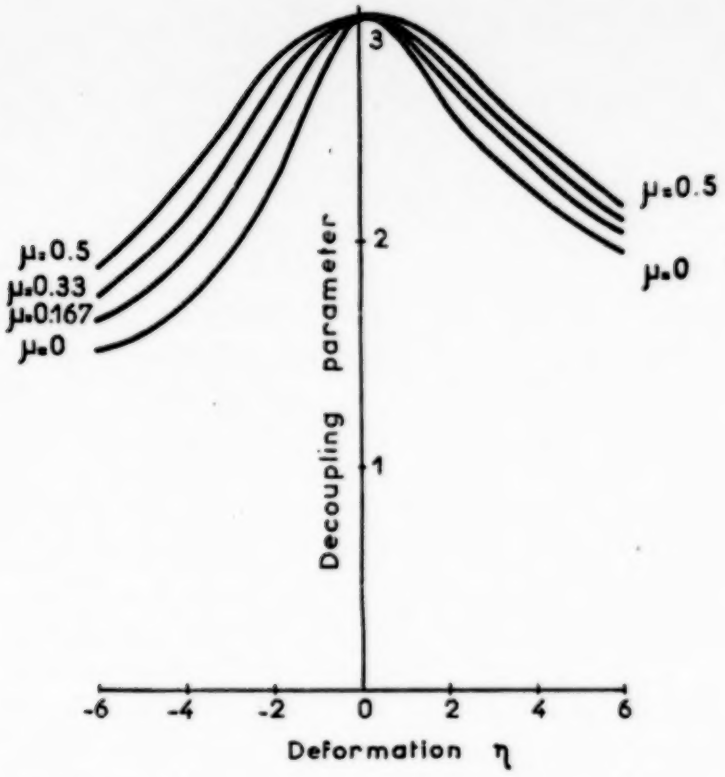

Fig. 2. (a, b, c). Plot of the decoupling parameter against deformation for orbits 11, 9 and 6, which each have $N = 2$ and $\Omega = \frac{1}{2}$.

eigenvalues and eigenfunctions corresponding to $N = 2$. For $N = 2$, $\Omega = \frac{5}{2}$ (Orbit 5), the only eigenvector is $|222+\rangle$ and the eigenvalue becomes $r = \frac{2}{3}\eta - 2 - 6\mu$. For $N = 2$, $\Omega_z = \frac{3}{2}$, the two eigenvectors are $|221+\rangle$ and $|222-\rangle$: since the term $\mu \mathbf{l}^2$ is diagonal and each of these eigenvectors has $l = 2$, the effect is simply to add a constant diagonal matrix, -6μ times the unit matrix, to the matrix diagonalized by Nilsson. Thus, the new eigenvalues are just those tabulated by Nilsson reduced by -6μ, and the eigenfunctions are unchanged for both orbit 8 and orbit 7.

For $N = 2$, $\Omega = \frac{1}{2}$, however, the eigenvectors are $|220+\rangle$, $|200+\rangle$ and $|221-\rangle$. The argument used for $\Omega = \frac{3}{2}$ is no longer valid, and the matrix must be diagonalized for each value of η and μ. The results of this calculation are displayed in table 1, giving the eigenvalues and eigenfunctions of orbits 11, 9 and 6. Figs. 1a—d, are a plot of the eigenvalues, and figs. 2a—c a plot of the decoupling parameters for the orbits with $\Omega = \frac{1}{2}$.

3. Application to Decay Schemes

We now discuss some examples of decay schemes for which the present calculations appear to give better agreement with experiment.

3.1. MAGNESIUM Mg^{25}

The ground state configuration for this nucleus is taken to be

$$\pi\{O^{16};d_{\frac{5}{2}}(\tfrac{1}{2}^2, \tfrac{3}{2}^2)\}$$
$$\nu\{O^{16};\ d_{\frac{5}{2}}(\tfrac{1}{2}^2, \tfrac{3}{2}^2, \tfrac{5}{2}^1)\},$$

corresponding to a prolate deformation as is found for the neighbouring nuclei Na^{23} and Al^{27}. The decoupling parameter for the band based on the first excited state is found to be $a = -0.2$. If this state is taken to correspond to orbit 9, a deformation of $\eta > +6$ is indicated from fig. 2b. However, from fig. 1a, one sees that for $\eta > +6$ the orbit 9 is lower in energy than orbit 5. No adjustment of the strength of the spin orbit coupling κ within the framework of the present type of calculation can eliminate this discrepancy.

If, now, one considers the other curves with $\mu \neq 0$, it is easily seen that a value of η compatible with both the above conditions can be found. The difference in eigenvalues for orbits 9 and 5 is given by $\Delta r = 0.58/(0.125 \times 41 \times 25^{-\frac{1}{3}}) = \Delta E/\kappa\hbar\mathring{\omega}_0 = 0.331$. From fig. 1b, for $\mu = 0.167$ this difference is obtained for $\eta = 3.2$, which from fig. 2b corresponds to $a = -0.15$. For $\mu = 0.33$, one has $\eta = +3.3$ and $a = -0.52$, so that for a value of μ slightly greater than 0.167 it would be possible to obtain very close agreement with experiment.

3.2. ALUMINIUM Al^{27}

The ground state configuration for this nucleus can be taken as

$$\nu\{O^{16};\ d_{\frac{5}{2}}(\tfrac{1}{2}^2, \tfrac{3}{2}^2, \tfrac{5}{2}^2)\}$$
$$\pi\{O^{16};\ d_{\frac{5}{2}}(\tfrac{1}{2}^2, \tfrac{3}{2}^2, \tfrac{5}{2}^1)\}.$$

The measured quadrupole moment is $Q = +0.15 \times 10^{-24}$ cm^2. The intrinsic quadrupole moment,

$$Q_0 = Q\,\frac{(I+1)(2I+3)}{3K^2 - I(I+1)},$$

is connected to the deformation $\delta \approx \Delta R/R_0$, by the relation

$$Q_0 = \tfrac{4}{3} Z R_0^2 \cdot \frac{\Delta R}{R_0},$$

which thus leads to a deformation $\delta = +0.35$

The first excited state $(\frac{1}{2}^+)$, is at an energy of 0.842 MeV, followed by states at 1.013 MeV $(\frac{3}{2}^+)$ and 2.729 MeV $(\frac{5}{2}^+)$. This sequence of states suggests a rotational band, based presumably on orbit 9. From the formula

$$E_{\text{rot}} = \frac{\hbar^2}{2\mathscr{I}}\{I(I+1) + a(-)^{I+\frac{1}{2}}(I+\tfrac{1}{2})\}$$

we deduce $\hbar^2/2\mathscr{I} = 218$ keV, and $a = -0.58$. A value of 218 keV for the

moment of inertia $\hbar^2/2\mathscr{I}$ is in good agreement with those obtained for neighbouring nuclei. Reference to fig. 2b then shows that the decoupling parameter is obtained for $\eta = +3.2$ and $\mu = 0.33$. It is evident also that no agreement could be obtained for $\mu = 0$.

The position of the first excited state relative to the ground state can then be calculated from fig. 1c and is 856 keV, if κ is taken to be 0.125, as for Mg^{25}. Thus, a consistent description of these lowest levels in Al^{27} can be given, which is not possible with the Nilsson calculations.

3.3. MAGNESIUM Mg^{27}

In the spirit of the Nilsson model we should suspect the deformation of this nucleus to be much the same as that of Al^{27}. The ground state spin is $\frac{1}{2}^+$ so the configuration must be taken as

$$\pi\{O^{16};\ d_{\frac{5}{2}}(\tfrac{1}{2}^2, \tfrac{3}{2}^2)\}$$
$$\nu\{O^{16};\ d_{\frac{5}{2}}(\tfrac{1}{2}^2, \tfrac{3}{2}^2, \tfrac{5}{2}^2)s_{\frac{1}{2}}(\tfrac{1}{2}^1)\}.$$

It is therefore necessary that orbit 9 lies above orbit 5 in energy, which is obtained, for the same value of deformation $\eta = +3.2$ as has been found for Al^{27}, for a value of $\mu = 0.167$. The first excited state can be taken as the second member of a rotational band with $K = \frac{1}{2}$. From fig. 2b this corresponds to a decoupling parameter $a \approx 0$, so that the moment of inertia $\hbar^2/2\mathscr{I}$ for the band is 330 keV. This compares favourably with $h^2/2\mathscr{I} = 305$ keV, obtained from the neighbouring even nucleus Mg^{26}. Finally the observed state at 3.50 MeV, $\frac{1}{2}^+$, is taken as corresponding to orbit 11.

3.4. SULPHUR S^{33}

The ground state configuration of this nucleus can be taken as

$$\pi\{O^{16};\ d_{\frac{5}{2}}(\tfrac{1}{2}^2, \tfrac{3}{2}^2, \tfrac{5}{2}^2),\ s_{\frac{1}{2}}^2 \text{ or } d_{\frac{3}{2}}^2\}$$
$$\nu\{O^{16};\ d_{\frac{5}{2}}(\tfrac{1}{2}^2, \tfrac{3}{2}^2, \tfrac{5}{2}^2),\ s_{\frac{1}{2}}^2,\ d_{\frac{3}{2}}(\tfrac{3}{2}^1)\}.$$

The measured quadrupole moment is $Q = -0.064 \times 10^{-24}$ cm^2. If the ground state is taken to have $I = \frac{3}{2}$, $K = \frac{3}{2}$, this corresponds to an intrinsic quadrupole moment Q_0 of -0.320×10^{-24} cm^2, and the deformation, $\delta = -0.17$. The magnetic moment has been measured as $\mu = +0.633$ nuclear magnetons, which corresponds, by fig. 3, to $\eta = -2$. Thus, these moments both indicate a negative deformation provided that the ground state is identified with orbit 8. Also $\kappa = \delta/\eta = 0.085$, somewhat smaller than the value of 0.125 used above in the middle of the d-shell.

We propose that a rotational band exists, based on orbit 8 taken as the ground state, with its second member at 1.96 MeV. The latter would thus have spin $\frac{5}{2}$, which is consistent with the recent demonstration [4]) that stripping to this level is mainly by d-wave; the value of the moment of inertia

is 392 keV, which is close to that of 373 keV deduced from the energies of excitation of the first 2^+ levels in S^{32} and S^{34}.

The first excited state at 841 keV ($\frac{1}{2}^+$) might, at first sight, be identified with orbit 11. However, reference to fig. 2a shows that the decoupling parameter is then large and negative, with the consequence that the next member of the rotational band, with spin $\frac{3}{2}$, would actually lie lower in energy than the parent level, fig. 4. Also if we use the calculated separation in eigenvalues of orbits 11 and 8, for $\eta = -2$, which is about 2.2, independently of the value of μ, we obtain an energy difference of $2.2 \times 0.085 \times 41 \times 33^{-\frac{1}{3}}$

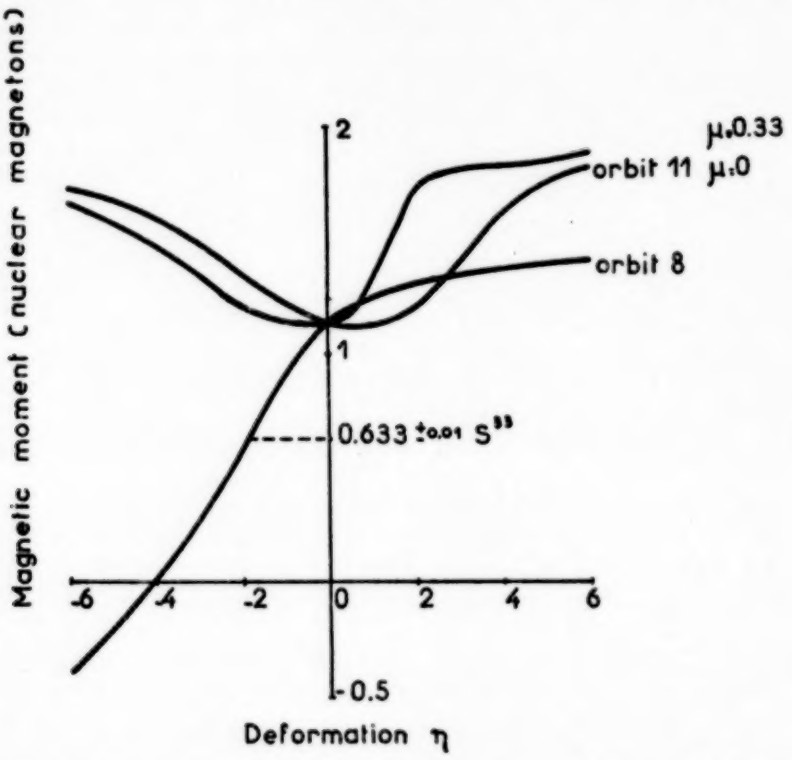

Fig. 3. The magnetic moment calculated for a single neutron occupying orbit 8, ($d_{\frac{3}{2}}$, $\frac{3}{2}^+$), of the Nilsson model, or orbit 11, ($d_{\frac{1}{2}}$, $\frac{1}{2}^+$) with $\mu = 0$ or 0.33. The dotted line corresponds to the measured magnetic moment of S^{33} in its ground state.

MeV = 2.34 MeV. This is almost three times the actual value of 841 keV.

The discrepancy can be avoided if we suppose that the 841 keV level corresponds to a core excitation, where one of the neutrons paired-off in the $s_{\frac{1}{2}}$ shell, or orbit 9, is raised to orbit 8 and pairs off to zero total angular momentum with the neutron already there. Thus, the properties of the band are determined by the remaining neutron in orbit 9. Comparison with fig. 1 then shows that the correct separation is obtained for $\eta = -2$ and $\mu = 0.33$.

We then propose that the state at 2.31 MeV (which is also formed by d-wave stripping [4]) and thus must have spin $\frac{3}{2}$ or $\frac{5}{2}$) might be identified with the second member of a rotational band based on the 841 keV state. Then a

decoupling parameter of $a = +0.4$ gives the correct energy separation, if the moment of inertia is taken as 370 keV. Reference to fig. 2b then shows that $a = 0.4$ is obtained at $\eta = -2$ and $\mu = 0.33$ in agreement with the above. It is evident that no such consistent interpretation could be given on the basis of the Nilsson calculations for this nucleus, although evidently much more experimental information for this nucleus must be obtained before a definite conclusion can be drawn.

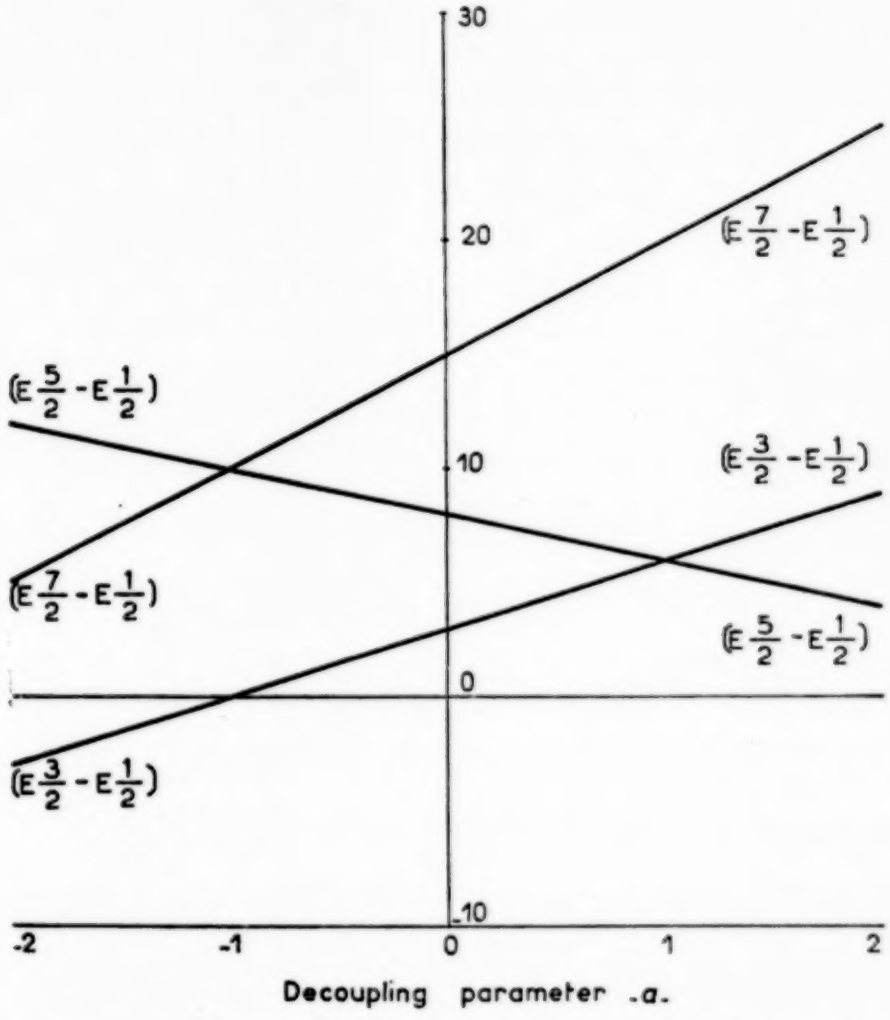

Fig. 4. A plot, as a function of the decoupling parameter, a, of the relative positions of the members of a rotational band with $K = \frac{1}{2}$. The ordinate is converted into energy separation through multiplication by the moment of inertia $\hbar^2/2\mathcal{I}$.

The large values of the decoupling parameter for orbit 11 suggest another possible interpretation of the ground state and first excited state as the inverted first two members of a $K = \frac{1}{2}$ band. If therefore the ground state is taken as $I = \frac{3}{2}$, $K = \frac{1}{2}$, the intrinsic quadrupole moment becomes $Q_0 = +0.320$ and the deformation is $+0.175$ instead of -0.175. Figs. 1 then suggest a neutron configuration with orbits 6, 7, 9 and 5, filled with paired-off

neutrons, and the odd neutron in orbit 11. Using $\hbar^2/2\mathscr{I} = 373$ keV, the observed separation is obtained for a decoupling parameter $a = -1.75$, fig. 4. Comparison with fig. 2a then shows that $\eta = +1$, for $\mu = 0$ and is even smaller for higher values of μ. This imposes rather a higher value on κ of approximately 0.175. However, this hypothesis is contradicted by the observed value of the magnetic moment of the ground state of S^{33}, which is much lower, fig. 3, than any calculated value for orbit 11. Another indication that the deformation is negative for this nucleus is the occurrence at quite low excitations of odd-parity levels with spin $\frac{5}{2}$ or $\frac{7}{2}$. These might conceivably correspond to the orbits 10 and 12 of the Nilsson model.

4. Conclusion

The modification proposed to the Nilsson calculations appears to lead to a more satisfactory agreement with some observed decay schemes. It seems worthwhile, then, to apply the eigenfunctions and eigenvalues listed above, in detailed fashion to the other better-established decay schemes for nuclei in the d-shell. This is now being done but we feel that the present results are likely to prove of value to experimentalists engaged on the study of such nuclei.

The author wishes to thank Professor Y. Rocard for making the facilities of the Laboratory available to him, and Professor H. Halban for his continued interest and encouragement.

He is indebted to the Commissariat à l'Energie Atomique for a bursary received whilst he performed the experimental work which provoked his interest in this subject.

References

1) a) Al^{25}, Mg^{25} A. E. Litherland, H. McManus, E. B. Paul, D. A. Bromley and H. E. Gove, Can. Jour. Phys. **36** (1958) 378
b) F^{19} E. B. Paul, Phil. Mag. **2** (1957) 311
c) Al^{26} R. K. Sheline, Nuclear Physics **2** (1956) 382
d) Si^{29} D. A. Bromley, H. E. Gove and A. E. Litherland, Can. Jour. Phys. **35** (1957) 1057
e) P^{31} C. Broude, L. L. Green and J. C. Willmott, Comptes Rendus Cong. Int. Phys. Nucl. Paris (1958) 724
2) B. R. Mottelson and S. G. Nilsson, Mat. Fys. Skr. Dan. Vid. Selsk. **1**, No. 8 (1959)
3) S. G. Nilsson, Mat. Fys. Medd. Dan. Vid. Selsk. **29**, No. 16 (1955)
4) P. Kossanyi-Demay, private communication

1.D.2 *Nuclear Physics* **14** (1959/60) 389—397; © *North-Holland Publishing Co., Amsterdam*
Not to be reproduced by photoprint or microfilm without written permission from the publisher

COLLECTIVE ROTATIONS OF NUCLEI

EUGENE P. GROSS
Brandeis University, Waltham, Mass. †

Received 31 August 1959

Abstract: An analysis is made of descriptions of collective motions of nuclei which involve the application of projection operators to a localized nuclear wave function ψ. This procedure leads to an incorrect description of centre of mass motion. The proposed remedy is to consider functions of the form $\psi e^{iS/\hbar}$, and to vary the functional form of the velocity potential S, subject to the constraint that the expectation value of the constant of motion has a given value for the state of collective motion. For translational motion this localized function already leads to the correct effective mass. The subsequent application of a projection operator mainly improves the zero momentum wave function. For rotational motion the velocity potential is expressed in terms of the excited states of a potential defined by ψ. The resulting moment of inertia is that of Inglis. The knowledge of the correct velocity potential for a given ψ suggests approximate trial functions S which express the moments of inertia solely in terms of properties of the ground state ψ.

1. Introduction

Recently, attempts have been made to calculate nuclear moments of inertia starting from wave functions describing nuclei with fixed positions and orientations in space [1, 2, 3]). The technique involves the application of a suitable projection operator to a localized approximate wave function, so as to obtain an eigenfunction of a constant of motion. In this note we examine some defects of this procedure and discuss the modifications necessary to obtain physically sensible wave functions.

2. Centre of Mass Motion

Consider first the treatment of centre of mass motion. We shall work with the Hamiltonian

$$H = \frac{1}{2M}\sum_{j=1}^{A} p_j^2 + \tfrac{1}{2}\sum_{i\neq j}^{A} V(\mathbf{x}_i - \mathbf{x}_j). \tag{1}$$

Starting from an approximate localized wave function $\psi_0(\mathbf{x}_1, \ldots \mathbf{x}_A)$, which for simplicity we take to be real, the procedure advocated is to construct a

† Work supported by Office of Scientific Research, U. S. Air Force.

wave function for a state of total momentum $\mathbf{P}$ by introducing the projection operator

$$\mathscr{P} = \frac{1}{(2\pi)^3}\int e^{i(\mathbf{P}-\mathbf{P}_{op})\cdot \mathbf{R}/\hbar} d^3R, \quad \mathbf{P}_{op} = \sum_{j=1}^{A} \mathbf{p}_j. \tag{2}$$

The projected wave function is

$$\Psi = \frac{\mathscr{P}\psi_0}{[\langle \mathscr{P}\psi_0, \psi_0\rangle]^{\frac{1}{2}}}, \quad \mathscr{P}\psi_0 = \frac{1}{(2\pi)^3}\int e^{i\mathbf{P}\cdot\mathbf{R}/\hbar}\psi_0(\mathbf{x}_1-\mathbf{R}, \ldots \mathbf{x}_A-\mathbf{R}) d^3R \tag{3}$$

and is an exact eigenfunction of $\mathbf{P}_{op}$ with eigenvalue $\mathbf{P}$. The energy is computed with this Ψ, and the coefficient of P^2 is identified with the effective mass. As remarked in ref. [1, 2]), this does not lead to the correct mass MA. That the procedure is defective is clear physically. The localized function ψ_0 is a wave packet of exact eigenfunctions of $\mathbf{P}_{op}$, and the projection operator picks out the momentum component $\mathbf{P}/\hbar$. The effective mass will therefore be sensitive to the detailed properties of ψ_0.

The remedy for the case of translational collective motion is to apply the projection operator to the modified wave function $\Phi = \psi_0(\mathbf{x}_1, \ldots \mathbf{x}_A) e^{iS/\hbar}$ with $S = M\mathbf{v}\cdot\sum_{j=1}^{A}\mathbf{x}_j$. The function Φ represents a wave packet for which the velocity of each particle is

$$\mathbf{v}_j = \int \psi_0^2 \frac{\nabla_j S}{M} d\tau = \mathbf{v}. \tag{4}$$

If ψ_0 is real and localized, Φ is not an eigenfunction of the total momentum operator $\sum_{j=1}^{A}\mathbf{p}_j$. The phase factor, however, insures that one satisfies the weaker condition that the average value $\langle \Psi, \sum_{j=1}^{A}\mathbf{p}_j\Psi\rangle$ equals a given c-number $\mathbf{P}$. In fact,

$$\langle \Psi, \sum_{j=1}^{A}\mathbf{p}_j\Psi\rangle = M\mathbf{v}A = \mathbf{P}. \tag{5}$$

If one now applies the projection operator to Φ, one obtains

$$\begin{aligned}\Psi' &= \frac{\mathscr{P}\Phi}{\langle \mathscr{P}\Phi, \Phi\rangle^{\frac{1}{2}}} = \frac{1}{(2\pi)^3}\frac{\int e^{i\mathbf{P}\cdot\mathbf{R}/\hbar}\psi_0(\mathbf{x}_1-\mathbf{R}, \ldots) e^{iM\mathbf{v}/\hbar\cdot\sum_{j=1}^{A}(\mathbf{x}_j-\mathbf{R})} d^3R}{\langle \mathscr{P}\Phi, \Phi\rangle^{\frac{1}{2}}} \\ &= e^{iM\mathbf{v}/\hbar\cdot\sum_{j=1}^{A}\mathbf{x}_j}\Psi'(0),\end{aligned} \tag{6}$$

$$\Psi'(0) = \frac{1}{(2\pi)^{\frac{3}{2}}}\frac{\int \psi_0(\mathbf{x}_1-\mathbf{R}, \ldots) d^3R}{\left[\int \psi_0(\mathbf{x}_1-\mathbf{R}, \ldots)\Psi_0(x_1, \ldots) d\tau d^3R\right]^{\frac{1}{2}}}.$$

Thus the wave function for the moving system is just $e^{iM\mathbf{v}/\hbar\sum_{j=1}^{A}\mathbf{x}_j}$ times the translation invariant function $\Psi'(0)$ for $\mathbf{P} = 0$. The energy computed with Ψ' is

$$E = \langle \Psi', H\Psi \rangle = \langle \Psi'(0), H\Psi'(0) \rangle + \frac{P^2}{2MA} \tag{7}$$

and has the correct effective mass MA, independently of the base function ψ_0. It is of interest, in addition, that the same correct value of the effective mass is obtained with the localized function Φ. The projection operator lowers the energy for the system when its mean velocity is zero.

The phase factor $S = M\mathbf{v} \cdot \sum_{j=1}^{A} \mathbf{x}_j$ is of course expected for the centre of mass problem. Nevertheless, we shall arrive at it by a method which can be used to treat constants of the motion other than the total momentum. We seek approximate eigenfunctions and eigenvalues of H. Since we may not be able to work easily with approximate eigenfunctions of H that are exact eigenfunctions of $\mathbf{P}_{op}$, we require only that $\langle \Psi, \mathbf{P}_{op}\Psi \rangle = \mathbf{P}$. To take this into account, we introduce the Lagrange multiplier $\boldsymbol{\lambda}$, and consider

$$\mathscr{E} = \langle \Psi, (H - \boldsymbol{\lambda} \cdot \mathbf{P}_{op} - E)\Psi \rangle. \tag{8}$$

The multiplier E is introduced to take account of the normalization condition $\langle \Psi, \Psi \rangle = 1$. The independent functional variations of Ψ and Ψ^* lead, of course, to the Schroedinger equation

$$(H - \boldsymbol{\lambda} \cdot \mathbf{P}_{op} - E)\Psi = 0 \tag{9}$$

and the complex conjugate equation. If we write $\Psi = \psi e^{iS/\hbar}$, where ψ and S are real functions, and isolate the real and imaginary parts of the Schroedinger equation, we find

$$\sum_{j=1}^{A} \frac{p_j^2}{2M}\psi + V\psi + \psi \sum_j \frac{(\nabla_j S)^2}{2M} - \boldsymbol{\lambda} \cdot \sum_j (\nabla_j S)\psi = E\psi, \tag{10}$$

$$\sum_j \operatorname{div}_j(\psi^2 \operatorname{grad}_j S) = M\boldsymbol{\lambda} \cdot \sum_j \operatorname{grad}_j(\psi^2). \tag{11}$$

The important point is that the second equation, a continuity equation referred to a moving coordinate system, also emerges as the condition on the function S, when a functional variation of $\mathscr{E}$ with respect to S is performed for fixed ψ. This is the case for any ψ, approximate or exact. In like manner the first equation is an eigenvalue equation resulting from functional variation of ε with respect to ψ for any S.

It is clear that an exact solution of the continuity equation is $S = M\boldsymbol{\lambda} \cdot \sum_{j=1}^{A} \mathbf{x}_j$. The operator on the left hand side of the equation (10) then differs from H by the constant $-\frac{1}{2}AM\lambda^2$. The Lagrange multiplier $\boldsymbol{\lambda}$ is determined by

$$\mathbf{P} = \langle \Psi, \mathbf{P}_{op}\Psi \rangle = \int \psi^2 \sum_{j=1}^{A} \nabla_j S \, d\tau = AM\boldsymbol{\lambda} \tag{12}$$

(if ψ is normalized). Thus $\boldsymbol{\lambda} = \mathbf{v}$. The energy is $\langle \Psi, H\Psi \rangle = \langle \psi, H\psi \rangle + P^2/2MA$ for any ψ.

The theory of the effective mass is of greater interest in a problem such as the properties of the polaron, where the answer is not known from general principles. In that case a moving particle has a different relation to the ionic motions than a particle at rest, so that one cannot invoke Galilean invariance. The above argument can be carried out and leads to a mass differing by a factor of the order of 2 from what one obtains by directly applying a projection operator to the wave function for a polaron at rest [4, 5]). Experience in that problem indicates that the procedure outlined here is more correct. The subsequent construction of a translationally invariant wave function leads only to small corrections.

3. Rotational Motion

Let us now consider the case of rotations. For simplicity we treat the rotations of even nuclei about a z axis perpendicular to the major symmetry axis. We take the ground state ψ_0 of the non-rotating nucleus to be real. For the rotating nucleus we write $\Psi = \psi e^{iS/\hbar}$ and consider the effective Hamiltonian $\mathscr{H} = H - \lambda J_z$, where λ is a Lagrange multiplier and J_z is the angular momentum operator. When the real functions ψ and S are varied independently to minimize $\langle \Psi, \mathscr{H}\Psi \rangle$ with $\langle \Psi, \Psi \rangle = 1$, they satisfy $\mathscr{H}\Psi = E\Psi$, or

$$H\psi + \psi \sum_{j=1}^{A} \frac{(\nabla_j S)^2}{2M} + \frac{\lambda}{i\hbar} \psi (J_z S) = E\psi \tag{13}$$

and

$$\sum_j \operatorname{div}_j(\psi^2 \operatorname{grad}_j S) = \frac{M\lambda}{-i\hbar} J_z(\psi^2) = M \sum_j \operatorname{div}_j(\psi^2 \boldsymbol{\lambda} \times \mathbf{r}_j). \tag{14}$$

Again, it is to be noted that the second equation, a continuity equation in a rotating coordinate system, is the condition for the best S, even for an approximate ψ. The first equation describes the modification of the real part of the wave function by the rotation.

Now, it is not hard to satisfy eq. (14), and thus to find the best function S for a given ψ. Introducing $S' = \psi S$, we find

$$-\frac{\hbar^2}{2M} \sum_{j=1}^{A} \nabla_j^2 S' + S' \left(\frac{\hbar^2}{2M} \sum_{j=1}^{A} \frac{\nabla_j^2 \psi}{\psi} \right) = \frac{\hbar\lambda}{i} (J_z \psi). \tag{15}$$

The solution S' may be found in the following way. Suppose ψ obeys the Schroedinger equation

$$-\frac{\hbar^2}{2M} \sum_{j=1}^{A} \nabla_j^2 \psi + U\psi = \varepsilon_0 \psi, \tag{16}$$

where $U(x_1, \ldots x_A)$ is some potential and ε_0 the lowest eigenvalue for U. Alternatively, any $\psi(\mathbf{x}_1 \ldots \mathbf{x}_A)$ *defines* a U by

$$U-\varepsilon_0 = \frac{\hbar^2}{2M}\sum_{j=1}^{A}\frac{\nabla_j^2\psi}{\psi}.$$

Then S' obeys an inhomogeneous equation with the left hand side governed by U, apart from a constant. We introduce the complete set of eigenvalues ε_n and eigenfunctions ψ_n of U. Then we can develop $S' = \sum_n S'_n\psi_n$. We find

$$S'_n = -\frac{i\hbar\lambda}{\varepsilon_n-\varepsilon_0}\int \psi_n^* J_z\psi \mathrm{d}\tau, \quad n \neq 0. \tag{17}$$

The $n = 0$ part is of the form $S'_0\psi$ and hence contributes only a constant to S.

To fix λ we use the condition

$$\langle \Psi, J_z\Psi\rangle = \hbar K \tag{18}$$

where K is an integer. Thus

$$\hbar K = \frac{i}{\hbar}\int \psi^2(J_z S)\mathrm{d}\tau = -\frac{2i}{\hbar}\int \psi(J_z\psi)S\mathrm{d}\tau. \tag{19}$$

Introducing the Green's function

$$G(\mathbf{x}, \mathbf{x}') = \sum_{n\neq 0}\frac{\psi_n(\mathbf{x})\psi_n^*(\mathbf{x}')}{\varepsilon_n-\varepsilon_0} \tag{20}$$

we can write

$$\hbar K = -2\lambda\int\int (J_z\psi)G(\mathbf{x}, \mathbf{x}')(J_z\psi(\mathbf{x}'))\mathrm{d}\tau\mathrm{d}\tau'. \tag{21}$$

Equation (13) shows that ψ and ψ_n should depend on λ^2. But for low values of K we may neglect this correction and take $\psi = \psi_0$, the ground state of the fixed nucleus. Then S'_n and thus S are proportional to λ, and λ is proportional to K.

With the above value of S we may compute the energy. It is simply

$$\langle \Psi, H\Psi\rangle = \langle \psi, H\psi\rangle + \tfrac{1}{2}\lambda\hbar K. \tag{22}$$

This leads to the moment of inertia

$$-2\int\int (J_z\psi)G(\mathbf{x}, \mathbf{x}')(J_z\psi(\mathbf{x}'))\mathrm{d}\tau\mathrm{d}\tau' = 2\sum_{n\neq 0}\frac{|\langle n|J_z|0\rangle|^2}{\varepsilon_n-\varepsilon_0}\hbar^2. \tag{23}$$

This result for the moment of inertia is just that of Inglis [6]). The present approach exhibits the velocity potential $S = \sum S'_n\psi_n/\psi$ that is appropriate to ψ. [We may note that the case of translational motion can be handled in the same way. It leads to

$$S = -i\hbar\boldsymbol{\lambda}\cdot\sum_n\frac{\psi_n}{\psi}\frac{\int\psi_n^*\mathbf{P}_{\mathrm{op}}\psi\mathrm{d}\tau'}{\varepsilon_n-\varepsilon_0}.$$

But the relation

$$\frac{i}{\hbar}(\varepsilon_n-\varepsilon_0)\int\psi_n^*\sum_{j=1}^{A}\mathbf{x}_j\psi d\tau=\frac{1}{M}\int\psi_n^*\sum\mathbf{p}_j\psi d\tau$$

allows us to write explicitly $S=M\boldsymbol{\lambda}\cdot\sum\mathbf{x}_j$.] The most direct method of evaluating the moment of inertia is to pick a potential U for which the Green's function and lowest eigenfunction are known. This is easily done when $U(\mathbf{x}_1,\ldots\mathbf{x}_A)$ is assumed to be additive, $U=\sum_{j=1}^{A}U(\mathbf{x}_j)$. However, it is not our purpose here to enter into applications of the Inglis formula [6, 7]).

If the nuclear orientation is changed by an angle φ_0, so that the real wave function is $\psi(x'_1,y'_1,\ldots z'_A)$, the appropriate S function is $S(x'_1,y'_1,\ldots y'_A,z'_A)$ where

$$\begin{aligned}x'_j&=\ \ x_j\cos\varphi_0+y_j\sin\varphi_0\\ y'_j&=-x_j\sin\varphi_0+y_j\cos\varphi_0\\ z'_j&=z_j.\end{aligned}$$

We may now superpose these functions with equal weights, i.e. form the projected wave function

$$\Psi=\frac{\mathscr{P}\Phi}{\langle\mathscr{P}\Phi,\Phi\rangle^{\frac{1}{2}}},\quad \mathscr{P}\Phi=\frac{1}{2\pi}\int e^{iK\varphi_0}\psi(\mathbf{x}'_j)e^{iS(\mathbf{x}'_j)/\hbar}d\varphi_0. \tag{24}$$

This Ψ can be used to calculate the moment of inertia of the system with this rotational eigenfunction. The energy is

$$\langle\Psi,H\Psi\rangle=\langle\mathscr{P}\Phi,H\Phi\rangle/\langle\mathscr{P}\Phi,\Phi\rangle \tag{25}$$

for a state of angular momentum $\hbar K$.

The Inglis moment of inertia has the disadvantage that it requires a knowledge of the excited states of the non-rotating nucleus. It does not appear possible to simplify S in a way similar to that for translational motion. Indeed the flow pattern in a rotating nucleus is expected to depend on the detailed interactions, and in addition there is a definite physical modification of the real part of the wave function arising from centrifugal and Coriolis forces. There is, therefore, some point in attempting to find approximate expressions for the moment of inertia directly in terms of simple properties of the ground state. For example we may introduce $S=\eta\sum_{j=1}^{A}x_jy_j$ which implies the flow pattern $(v_i)_x=\partial S/\partial x_i=\eta y_i$, $(v_i)_y=\partial S/\partial y_i=\eta x_i$. The requirement that the expectation value of J_z is given fixes η. We have

$$\langle\Psi,J\Psi\rangle=\eta\int\psi^2\sum_{j=1}^{A}(x_j^2-y_j^2)d\tau=\hbar K.$$

We also find

$$\langle\Psi,H\Psi\rangle=\langle\psi,H\psi\rangle+\frac{1}{2M}\eta^2\int\psi^2\sum_{j=1}^{A}(x_j^2+y_j^2)d\tau.$$

This results in a moment of inertia

$$\frac{M\left\{\int\psi^2\sum_j(x_j^2-y_j^2)\mathrm{d}\tau\right\}^2}{\sum_i\int\psi^2(x_i^2+y_i^2)\mathrm{d}\tau},$$

a result found by Bohr [8]). This choice of S is so simple that one can work with the projected wave function associated with $\psi e^{iS/\hbar}$. It is, however, not likely that a substantial improvement would result since the mean flow pattern is far from accurate. For distorted nuclei associated with a well-developed rotational spectrum, the quantum fluctuations and interference effects described by rotationally invariant wave functions are expected to be small compared to the mean flow effect. It is nonetheless interesting that, if the localized ψ is such that the projected wave function is exact for the non-rotating nucleus, the ground state energy is 'anchored'. Then, for a rotating state, the energy relative to the ground state is the least possible, i.e. the true moment of inertia is greater than that obtained with the projected wave function formed with any approximate S. The projected wave function for the above S would be expected to yield a moment of inertia somewhat larger than the incompressible flow result.

We must therefore try to improve the description of the flow pattern. Let us try $S=\sum_{j=1}^{A}\sigma(\mathbf{x}_j)$, varying the functional form of $\sigma(\mathbf{x}_j)$. [This is a form written down, but apparently not pursued, by Hill and Wheeler [9]).] We have

$$\langle\Psi, J_z\Psi\rangle=\hbar K=\int\psi^2\sum_{j=1}^{A}\left(x_j\frac{\partial}{\partial y_j}-y_j\frac{\partial}{\partial x_j}\right)\sigma(\mathbf{x}_j)\mathrm{d}\tau.$$

Now, the nuclear density distribution associated with $\psi(\mathbf{x}_1,\ldots\mathbf{x}_A)$ is

$$\rho(\mathbf{x})=\sum_{j=1}^{A}\int\psi^2\delta(\mathbf{x}-\mathbf{x}_j)\mathrm{d}\tau=A\int\psi^2(\mathbf{x},\mathbf{x}_2,\mathbf{x}_3\ldots\mathbf{x}_A)\mathrm{d}^3x_2\ldots\mathrm{d}^3x_A.$$

Thus, we can write

$$\langle\Psi, J_z\Psi\rangle=\int\frac{\rho(\mathbf{x})}{A}\left(x\frac{\partial}{\partial y}-y\frac{\partial}{\partial x}\right)\sigma(\mathbf{x})\mathrm{d}^3x.$$

We also have

$$\langle\Psi, H\Psi\rangle=\langle\psi, H\psi\rangle+\frac{1}{2M}\frac{1}{A}\int\rho(\mathbf{x})(\nabla\sigma)^2\mathrm{d}^3x.$$

The variational problem $(\delta/\delta\sigma(\mathbf{x}))\langle\Psi, (H-E-\lambda J_z)\Psi\rangle=0$ leads to

$$\mathrm{div}(\rho\ \mathrm{grad}\ \sigma)=M\lambda\left(x\frac{\partial}{\partial y}-y\frac{\partial}{\partial x}\right)\rho, \tag{26}$$

from which one can find $\sigma(\mathbf{x},\lambda)$ for given $\rho(\mathbf{x})$. The parameter λ is eliminated by

using the condition $\langle \Psi, J_z \Psi \rangle = \hbar K$. The earlier choice $S = \eta \sum_j x_j y_j$ led to a moment of inertia depending on the quadrupole moment of the nucleus. The present choice of S leads to results depending on the detailed density distribution $\rho(\mathbf{x})$. If ρ is taken to be a function of $\frac{x^2}{a^2} + \frac{y^2+z^2}{b^2}$ alone, the Bohr solution $\sigma(\mathbf{x}) = \eta xy$ satisfies the continuity equation exactly.

One can continue this line of argument. The additive form $S = \sum_{j=1}^{A} \sigma(\mathbf{x}_j)$ does not include correlations in the flow of nucleons. For example, if we add a term $\sum_{i \neq j} \tau(\mathbf{x}_i - \mathbf{x}_j)$ we can describe the type of backflow introduced by Feynman [10]) in the description of excitations in liquid helium. The moment of inertia will then depend on the correlation function for the nuclear ground state. By proceeding stepwise, one might hope to gain insight into the detailed nature of the flow pattern of a rotating nucleus and the most relevant features of the ground state wave function. The procedure of applying a projection operator directly to this wave function (with $S = 0$) of course selects certain features, but there is no physical reason to expect these features to be directly relevant to the determination of the moment of inertia.

Actually, the general expression for S suggests that the correlations are quite different. Let us assume an independent particle ground state $\psi = \prod_{j=1}^{A} \psi_j(\mathbf{x}_j)$, populating levels in accordance with the exclusion principle but neglecting antisymmetry, i.e. exchange contributions. Then $S = \sum_{j=1}^{A} \sigma_j(\mathbf{x}_j)$, with a different velocity potential for each particle. In addition, the density distribution is appreciably different from that assumed in the irrotational flow picture. For an oscillator potential $\sigma_j(\mathbf{x}_j)$ is the ratio of two polynomials in the space coordinates. If one invokes the exclusion principle for excited states, correlations appear. The use of an antisymmetrical ψ now brings in additional strong correlations between the particles taking part in the flow.

The general formula $S = \sum \psi_n S'_n / \psi$ suggests another trial function that involves strong correlations in the flow. If we replace ε_n by $\bar{\varepsilon}$, with the idea that many excited levels contribute about equally, we find

$$S = -i\hbar \sum_n \frac{\psi_n}{\psi} \frac{\lambda}{\bar{\varepsilon} - \varepsilon_0} \int \psi_n^* J_z \psi \, d\tau' = -i\hbar \frac{\lambda}{\bar{\varepsilon} - \varepsilon_0} \frac{1}{\psi} J_z \psi .$$

We may therefore try $S = \alpha J_z (\ln \psi)$, and determine α and the moment of inertia as in the preceding examples. An even simpler trial function is suggested by expanding $e^{iS/\hbar}$. This leads to $\Psi = a\psi + b J_z \psi$. The flow pattern involves strong correlations because of the many-body character of ψ. The moment of inertia depends on quantities such as $\langle \psi, H J_z \psi \rangle$.

In conclusion, we note that the Lagrange multiplier approach to the determination of collective properties is particularly appropriate when the low-lying states of the nucleus are analyzed by Bogolyubov's methods [11]). There the nucleus is described in the language of second quantization, and linear combi-

nations of creation and annihilation operators are introduced. Since a constant of the motion such as J_z involves a product of one creation and one annihilation operator, a term λJ_z will modify the appropriate normal mode transformation and make it depend on λ. The treatment of collective rotations is then formally very similar to the description of macroscopic flow of liquid helium [12]).

The stimulus for the present investigation was a lecture by Prof. F. Villars summarizing the present state of the theory of collective motions of nuclei. We are indebted to Dr. H. J. Lipkin for a stimulating discussion.

References

1) R. E. Peierls and J. Yoccoz, Proc. Phys. Soc. A **70** (1957) 388;
J. Yoccoz, Proc. Phys. Soc. A **70** (1957) 381;
R. E. Peierls, Proc. Rehovoth Conference on Nuclear Structure (North-Holland Publishing Co, 1958)
2) J. J. Griffin and J. A. Wheeler, Phys. Rev. **108** (1957) 311
3) F. Villars, Ann. Rev. of Nuclear Science **7** (1957) 185. (Reterences to other work are given)
4) G. R. Allcock, Advances in Physics **5** (1956) 412
5) E. P. Gross, Annals of Physics (1959)
6) D. R. Inglis, Phys. Rev. **96** (1954) 1059; **97** (1955) 701; **103** (1956) 1786
7) A. Bohr and B. Mottelson, Mat. Fys. Medd. Dans. Vid. Selsk. **30**, No. 1 (1955)
8) A. Bohr, Rotational States of Atomic Nuclei (E. Munksgaards Forlag, 1954)
9) D. L. Hill and J. A. Wheeler, Phys. Rev. **89** (1953) 1106
10) R. P. Feynman, Prog. Low Temp. Physics, Vol. 1 (North-Holland Publ. Co., 1955)
11) S. T. Belyaev, Mat. Fys. Medd. Dan. Vid. Selsk. **31**, No. 11 (1959)
12) E. P. Gross, Annals of Physics **4** (1958) 57

1.D.2:
1.E.4

Nuclear Physics **14** (1959/60) 398—406; © *North-Holland Publishing Co., Amsterdam*
Not to be reproduced by photoprint or microfilm without written permission from the publisher

ENHANCEMENT OF E2 TRANSITION PROBABILITY

DIETER KURATH
Argonne National Laboratory, Lemont, Illinois †

Received 17 August 1959

Abstract: The method of generator coordinates is applied to the calculation of E2 transition probabilities. Complete single-particle states in a deformed well are used as generator functions, and the transition from the first excited state to the ground state of C^{12} is computed as an example. The degree of enhancement is found to be of a magnitude consistent with experiment. The effect of centre-of-mass motion and other factors affecting the validity of the result are discussed.

1. Introduction

The method of generator coordinates [1]) serves to demonstrate collective properties of the wave functions of systems of interacting nucleons [2]). Recently it was found that for the 1p-shell the effect of interactions between nucleons can be simulated by using a potential field of quadrupole deformation in the generator Hamiltonian [3]). This method offers a direct, relatively simple procedure for evaluating the rather complicated configuration interaction needed to obtain enchancement of E2 transition probability.

The wave functions of independent nucleons in a harmonic oscillator well of quadrupole deformation are given by Nilsson [4]). For the 1s and 1p region one generally neglects the admixtures of states having a principal oscillator quantum number N differing by two units from that of the zero-order state. Such small admixtures are certainly unimportant for most properties but it is precisely because they are mixed in by means of a quadrupole operator that they can have an important effect on the E2 matrix elements. This is the effect we wish to calculate.

2. Procedure

The matrix elements needed for mixing in $\Delta N = 2$ contributions are given by Nilsson [4]). Perturbation theory is used to calculate these contributions from other shells, assuming that the energy separation of the pertinent oscillator levels, $2\hbar\omega_0$, adequately represents the actual separation of the low states from the admixed ones. The complete single-particle states are then

† Work performed under the auspices of the U. S. Atomic Energy Commission.

$$\psi_{k,\nu} = \psi^{(0)}_{k,\nu} + \frac{\delta m\omega_0}{\hbar}\sqrt{\frac{4\pi}{5}} \sum_{l,\Lambda,\Sigma} \langle N-2k\nu|r^2 Y_0{}^2|Nl\Lambda\Sigma\rangle \phi^{Nl}_{\Lambda\Sigma},$$
$$\psi_{k,\nu} = \psi^{(0)}_{k,\nu} + \sum_{l,\Lambda} \varepsilon^{Nl\Lambda}_{k,\nu} \phi^{Nl}_{\Lambda,k-\Lambda}. \tag{1}$$

Here $k = \Lambda + \Sigma$ is the projection of angular momentum on the nuclear symmetry axis; $\nu = 1, 2, 3, 4$ is Nilsson's label for the first-order wave functions considering only $\Delta N = 0$ interactions. The admixed states have orbital angular momentum l with projection Λ, spin angular momentum $\frac{1}{2}$ with projection Σ, and principal oscillator quantum number N. For $\nu = 1$, $N = 2$ and $N = 3$ for $\nu = 2, 3$ or 4; that is, we mix some 1d state into the 1s level ($\nu = 1$) and we mix 2p and 1f components into the 1p levels ($\nu = 2, 3, 4$). The quadrupole deformation is specified by the symbol δ.

The many-particle generator function is formed by putting nucleons into the lowest available levels and forming $X_K(R^{-1}x)$, an anti-symmetrized eigenfunction of isobaric spin, K being the projection of total angular momentum. The function is constructed in the nuclear coordinate system, $R^{-1}x$. From this generating function, the Hill-Wheeler integration will project eigenfunctions of the angular momentum in the laboratory coordinate system:

$$\Psi^I_{M(K)}(x) = N_K{}^I(2I+1)\int \mathrm{d}R D^{I*}_{KM}(R) X_K(R^{-1}x), \tag{2}$$

where $N_K{}^I$ is a normalization factor. These are the wave functions with which we shall calculate E2 matrix elements. If one uses only the first-order single-particle functions $\psi^{(0)}_{k,\nu}$ to form the generator function, one obtains $X_K{}^{(0)}$ and this is known [3]) to lead to the usual 1p-shell intermediate coupling functions. Since the admixtures included here are small, we shall expand X_K and keep only terms which are linear in the coefficients $\varepsilon^{Nl\Lambda}_{k\nu}$:

$$X_K \approx X_K{}^{(0)} + X_K{}^{(\varepsilon)}. \tag{3}$$

The matrix element needed for the E2 transition is $\langle I'M(K')|Q_0{}^2|IM(K)\rangle$, with

$$Q_\lambda{}^2 = e\sum_i r_i{}^2 Y_\lambda{}^2(\Omega_i)\tau_p{}^i,$$

where $\tau_p{}^i$ denotes the projection operator for protons. To terms linear in the ε's we obtain

$$\begin{aligned}\Delta Q &= \langle I'M(K')|Q_0{}^2|IM(K)\rangle - \langle I'M(K')|Q_0{}^2|IM(K)\rangle_{00} \\ &= N_{K'}{}^{I'} N_K{}^I (2I'+1)(2I+1)\int \mathrm{d}x\mathrm{d}R\mathrm{d}R' D^{I'}_{K'M}(R') D^{I*}_{KM}(R) E(R, R', x),\end{aligned} \tag{4}$$

where

$$E(R, R', x) = X^{(\varepsilon')*}_{K'}(R'^{-1}x) Q_0{}^2(x) X_K{}^{(0)}(R^{-1}x) + X^{(0)*}_{K'}(R'^{-1}x) Q_0{}^2(x) X_K{}^{(\varepsilon)}(R^{-1}x).$$

In order to evaluate the integral in eq. (4), we use the transformation properties of Q_0^2 and $X_K^{(0)}$ under rotation to transform both these functions to the $X_K^{(\epsilon)}$ coordinate system. Such a procedure requires knowledge of the angular momentum expansion of $X_K^{(0)}$ as in ref. [3]), namely,

$$X_K^{(0)}(R^{-1}x) = \sum_{I,s} C_{K(0)}^{Is} \Phi_K^{Is}(R^{-1}x). \tag{5}$$

Here the Φ_K^{Is} are a complete set of angular momentum eigenfunctions for the 1s, 1p shells. Then the transformations make it possible to integrate over dR and dR' so that the expression for enhancement of the matrix element becomes

$$\begin{aligned}\Delta Q = {} & N_{K'}^{I'} N_K^{I} \sum_{s,\lambda} C_{K(0)}^{Is} (2I-\lambda K'+\lambda|I'K')(2IOM|I'M) \int dy X_{K'}^{(\epsilon')*}(y) Q_{-\lambda}^{2}(y) \Phi_{K'+\lambda}^{Is}(y) \\ & + N_{K'}^{I'} N_K^{I} \sum_{s',\lambda} C_{K'(0)}^{I's'} (2I'-\lambda K+\lambda|IK)(2I'OM|IM) \int dy\, \Phi_{K+\lambda}^{I's'*}(y) Q_{-\lambda}^{2*}(y) X_K^{(\epsilon)}(y).\end{aligned} \tag{6}$$

Here the brackets are Clebsch-Gordan coefficients.

The evaluation of the integrals remaining in eq. (6) is simplified by the fact that the $\Phi^{Is}(y)$ are functions arising from configurations consisting of a full 1s-shell with the rest of the nucleons in the 1p-shell. Therefore, the only part of $[Q_\lambda^2 X_K^{(\epsilon)}]$ which contributes to the integral is that part with such configurations. This means that the single-particle functions which are necessary are those parts of $r^2 Y_\lambda^2(\psi_{k,\nu} - \psi_{k,\nu}^{(0)})$ which lie in the 1s and 1p shells. The effect of projecting out such parts for the four lowest Nilsson levels can be expressed in terms of the functions $\phi_{\Lambda,k-\Lambda}^{Nl}$ introduced in eq. (1):

$$\begin{aligned}
& r^2 Y_\lambda^2(\psi_{\pm\frac{1}{2},1} - \psi_{\pm\frac{1}{2},1}^{(0)}) \to g_{1,\lambda} \phi_{0,\pm\frac{1}{2}}^{0\ 0} = g_{1,\lambda} \psi_{\pm\frac{1}{2},1}^{(0)}, \\
& r^2 Y_\lambda^2(\psi_{\pm\frac{3}{2},2} - \psi_{\pm\frac{3}{2},2}^{(0)}) \to g_{2,\pm\lambda} \phi_{\lambda\pm1,\pm\frac{1}{2}}^{1\ 1}, \\
& r^2 Y_\lambda^2(\psi_{\pm\frac{1}{2},3} - \psi_{\pm\frac{1}{2},3}^{(0)}) \to L\, g_{2,\pm\lambda}^{1} \phi_{\lambda\pm1,\mp\frac{1}{2}}^{1\ 1} + A g_{3,\lambda} \phi_{\lambda,\pm\frac{1}{2}}^{1\ 1}, \\
& r^2 Y_\lambda^2(\psi_{\pm\frac{1}{2},4} - \psi_{\pm\frac{1}{2},4}^{(0)}) \to -A g_{2,\pm\lambda}^{1} \phi_{\lambda\pm1,\mp\frac{1}{2}}^{1\ 1} + L g_{3,\lambda} \phi_{\lambda,\pm\frac{1}{2}}^{1\ 1}.
\end{aligned} \tag{7}$$

The definitions of the coefficients are

$$g_{1,\lambda} = \frac{70}{\sqrt{5\pi}} \frac{\delta m \omega_0}{420\hbar} (\langle r^2 \rangle_{1d,1s})^2 \delta_{\lambda,0},$$

$$g_{2,\lambda} = \sqrt{\frac{(1-\lambda)(2-\lambda)}{10\pi}} \frac{\delta m \omega_0}{420\hbar} \{3(15\lambda^2+35\lambda+12)(\langle r^2 \rangle_{1f,1p})^2 + 14(\langle r^2 \rangle_{2p,1p})^2\},$$

$$g_{3,\lambda} = \sqrt{\frac{(2-\lambda)(2+\lambda)}{5\pi}} \frac{\delta m \omega_0}{420\hbar} \{9(3-5\lambda^2)(\langle r^2 \rangle_{1f,1p})^2 + 28(\langle r^2 \rangle_{2p,1p})^2\},$$

while A and B are the coefficients given by the Nilsson calculation for the 1p-shell:

$$\psi^{(0)}_{\pm\frac{1}{2},3} = A\phi^{1\ 1}_{0,\pm\frac{1}{2}} + I\,\phi^{1\ 1}_{\pm1,\mp\frac{1}{2}} \quad (A^2+B^2=1).$$
$$\psi^{(0)}_{\pm\frac{1}{2},4} = B\phi^{1\ 1}_{0,\pm\frac{1}{2}} - A\phi^{1\ 1}_{\pm1,\mp\frac{1}{2}} \tag{8}$$

From eq. (7) one sees that the effect of $[Q_\lambda{}^2 X_K{}^{(\epsilon)}]$ is to return a proton from the $\Delta N = 2$ shell to its orginal N shell, either to its original state or to any unoccupied state. The overlap integrals of the resulting functions with the $\Phi^{Is}_{k-\lambda}$ are needed for eq. (6). These overlap integrals depend on the importance of spin-orbit coupling relative to deformation as indicated by the Nilsson parameter η. The matrix elements $\langle r^2\rangle_{Nl,N'l'}$ are readily evaluated with the single-particle radial functions.

3. Application to C^{12}

As an example of such a calculation, consider the transition from the first excited state ($I = 2$, $T = 0$) to the ground state ($I' = 0 = T'$) in C^{12}. The wave functions for both these states are obtained by projection from the same generating function $X_{K=0}$. The generating function arises from the configuration with full Nilsson levels $\nu = 1$, 2 and 3. For this case eq. (6) becomes

$$\Delta Q = N_0{}^0 N_0{}^2 \left[\tfrac{1}{5}\sum_{s,\lambda} C^{2s}_{0(0)} \int dy [Q_\lambda{}^2 X_0{}^{(\epsilon)}]^* \phi_\lambda{}^{2s} + \sum_s C^{0s}_{0(0)} \int dy\, \phi_0{}^{0s^*} [Q_0{}^2 X_0{}^{(\epsilon)}]\right]. \tag{6'}$$

The components of $[Q_\lambda{}^2 X_0{}^{(\epsilon)}]$ which have non-vanishing overlaps with the Φ^{Is} are obtained by applying expression (7) and eq. (8). For the C^{12} example these components are either multiples of the original generating function $X_0{}^{(0)}$ or of a similar function which differs from $X_0{}^{(0)}$ in that a proton has gone from its original state (k_0, ν_0) into the state $(k = \pm\frac{1}{2}, \nu = 4)$. One then evaluates the coefficients

$$C_\lambda{}^{Is}(k_0\nu_0 \to k\nu) = \int dy \phi_\lambda{}^{I,s^*} X_\lambda(k_0\nu_0 \to k\nu) \tag{9}$$

and finally carries out the summation over s:

$$n_\lambda{}^{(I)}(k_0\nu_0 \to k\nu) = \sum_s C^{Is}_{0(0)} C_\lambda{}^{Is}(k_0\nu_0 \to k\nu). \tag{10}$$

Since the $n_\lambda{}^{(I)}$ are independent of the sign of λ for even I, terms can be combined to obtain the final expression for the enhancement ΔQ:

$$\begin{aligned}\Delta Q = \frac{2N_0{}^0 N_0{}^2}{5} \{&G(k_0\nu_0 \to k_0\nu_0)[5n_0{}^{(0)}(k_0\nu_0 \to k_0\nu_0) + n_0{}^{(2)}(k_0\nu_0 \to k_0\nu_0)] \\ &+G(\tfrac{1}{2}3 \to \tfrac{1}{2}4)[5n_0{}^{(0)}(\tfrac{1}{2}3 \to \tfrac{1}{2}4) + n_0{}^{(2)}(\tfrac{1}{2}3 \to \tfrac{1}{2}4)] \\ &+G(-\tfrac{3}{2}2 \to \tfrac{1}{2}4)n_1{}^{(2)}(-\tfrac{3}{2}2 \to -\tfrac{1}{2}4) \\ &+G(-\tfrac{1}{2}3 \to \tfrac{1}{2}4)n_1{}^{(2)}(-\tfrac{1}{2}3 \to \tfrac{1}{2}4) \\ &+G(-\tfrac{3}{2}2 \to \tfrac{1}{2}4)n_2{}^{(2)}(-\tfrac{3}{2}2 \to \tfrac{1}{2}4)\}.\end{aligned} \tag{6''}$$

The $G(k_0 v_0 \to kv)$ are combinations of the coefficients in expression (7):

$$G(k_0 v_0 \to k_0 v_0) = g_{1,0} + (1+B^2) g_{2,0} + A^2 g_{3,0},$$
$$G(\tfrac{1}{2}3 \to \tfrac{1}{2}4) = AB(g_{3,0} - g_{2,0}), \quad G(-\tfrac{3}{2}2 \to -\tfrac{1}{2}4) = B g_{2,-1},$$
$$G(-\tfrac{1}{2}3 \to \tfrac{1}{2}4) = B^2 g_{2,-1} - A^2 g_{3,-1}; \quad G(-\tfrac{3}{2}2 \to \tfrac{1}{2}4) = -A g_{2,-2}.$$

The expression for the enhancement can be compared to the zero-order matrix element, which is

$$\langle 00(0)|Q_0^2|20(0)\rangle_{00} = \frac{2N_0^2 N_0^0 \langle r^2\rangle_{1p,1p}}{\sqrt{20\pi}} \{(3A^2-2) n_0^{(0)}(k_0 v_0 \to k_0 v_0) + 3AB n_0^{(0)}(\tfrac{1}{2}3 \to \tfrac{1}{2}4)\}. \quad (11)$$

In order to evaluate these expressions one needs the quantities A, B and $n_\lambda^{(I)}(k_0 v_0 \to kv)$, which depend on the degree of spin-orbit coupling. These can be expressed in terms of the Nilsson parameter η, and are given numerically in table 1 for oblate deformation, appropriate to C^{12}. The matrix elements

TABLE 1

Numerical values of those quantities in the E2 matrix elements for C^{12} which depend on the Nilsson parameter η. They are given as functions of η which is proportional to the ratio of deformation to spin-orbit coupling

$\eta \to$	0	−4	−6	−8	$-\infty$ (LS-limit)
$n_0^{(0)}(k_0 v_0 \to k_0 v_0)$	1	0.332	0.250	0.225	0.200
$n_0^{(2)}(k_0 v_0 \to k_0 v_0)$	0	0.559	0.583	0.582	0.571
$n_0^{(0)}(\frac{1}{2}3 \to \frac{1}{2}4)$	0	0.112	0.059	0.037	0
$n_0^{(2)}(\frac{1}{2}3 \to \frac{1}{2}4)$	0	−0.052	−0.004	0.007	0
$n_1^{(2)}(-\frac{3}{2}2 \to -\frac{1}{2}4)$	0	−0.233	−0.232	−0.232	−0.247
$n_1^{(2)}(-\frac{1}{2}3 \to \frac{1}{2}4)$	0	−0.338	−0.308	−0.290	−0.247
$n_2^{(2)}(-\frac{3}{2}2 \to \frac{1}{2}4)$	0	−0.173	−0.092	−0.058	0
A	0.816	0.369	0.254	0.190	0
B	0.577	0.930	0.967	0.982	1

$\langle r^2\rangle_{Nl,N'l'}$ for harmonic oscillator functions are needed for the $G(k_0 v_0 \to kv)$; they are given in eq. (11) of ref. [4]), and lead to the following expressions for the $G(k_0 v_0 \to kv)$:

$$G(k_0 v_0 \to kv) = (11+3A^2)\rho,$$
$$G(\tfrac{1}{2}3 \to \tfrac{1}{2}4) = (3AB)\rho,$$
$$G(-\tfrac{3}{2}2 \to -\tfrac{1}{2}4) = (-2\sqrt{3}B)\rho,$$
$$G(-\tfrac{1}{2}3 \to \tfrac{1}{2}4) = \sqrt{3}(1-3B^2)\rho,$$
$$G(-\tfrac{3}{2}2 \to \tfrac{1}{2}4) = (-\sqrt{6}A)\rho,$$

where

$$\rho = \frac{\delta\langle r^2\rangle_{1p,1p}}{12\sqrt{5\pi}} = \frac{5\delta}{24\sqrt{5\pi}} \frac{\hbar}{m\omega_0}.$$

With the help of table 1 one can evaluate the ratio of enhancement to zero-order matrix element as a function of η, getting $\Delta Q/\langle Q\rangle_{00} = -2.24\delta$, -1.84δ and -1.72δ for $\eta = -4$, -6 and -8, respectively.

4. Numerical Estimate of the Enhancement

4.1. CORRECTIONS AND UNCERTAINTIES

There are three factors which affect the reliability of a numerical evaluation of the enhancement obtained above. In decreasing order of importance they are the estimate of δ, the effect of centre-of-mass motion and the magnitude of higher order contributions.

The largest uncertainty is the value of δ. A value of $\delta = -0.9$ was obtained [3]) for C^{12} by comparing the wave functions obtained from an interaction calculation with those generated from $\chi_0^{(0)}$, the generator within the 1p-shell only. An estimate which seems more reliable can be made by requiring self-consistency between the density distribution evaluated with the enhanced generator function and shape of the potential field. The shape of the field is given by eq. (3) of ref. [4]),

$$\frac{\omega_\perp^2}{\omega_z^2} = \frac{3+2\delta}{3-4\delta}. \tag{12}$$

For self-consistency, this should be the same as the ratio of the expectation values of $\langle z^2\rangle$ to $\langle x^2\rangle$ obtained from the generating function. Since only terms linear in the ε's were kept in the single-particle functions, and ε is proportional to δ, only the linear approximation to the ratio of expectation values is legitimate. This gives

$$\frac{\langle z^2\rangle}{\langle x^2\rangle} = \frac{3+2A^2}{5-A^2}\,\frac{3+2\delta}{3-\delta}, \tag{13}$$

where A, defined in eq. (8), depends on the Nilsson parameter η. By equating eqs. (12) and (13), one can obtain a value for δ which depends on η, and varies from $\delta = -0.86$ for $\eta = -\infty$ (the LS-limit) to $\delta = -0.58$ for $\eta = -4$. This is of the same magnitude as given by the wave-function comparison, but is in general smaller and a quite sensitive function of η, which causes uncertainty in estimating.

The effect of centre-of-mass motion must be investigated, since there is a question as to what degree the admixtures to the wave functions represent spurious effects arising from the fact that calculations are done with reference to an arbitrary fixed point rather than the centre-of-mass of the nucleons. Analysis [5, 6]) of such questions has shown that the physically meaningless effects of excitation of the centre of mass can be eliminated by using operators in which only coordinates relative to the centre of mass occur, i.e., by making

the transformation

$$\mathbf{r}_i \rightarrow \mathbf{r}'_i = \mathbf{r}_i - \mathbf{R},$$

where for A nucleons, $A\mathbf{R} = \sum_i \mathbf{r}_i$. Under this transformation, Q_0^2 becomes

$$Q_0^2(\mathbf{r}'_i) = Q_0^2(\mathbf{r}_i) - \sqrt{\frac{5}{16\pi}}\{(3Z^2 - R^2)\sum_i \tau_p{}^i + 2\sum_i (3Zz'_i - \mathbf{R}\cdot\mathbf{r}'_i)\tau_p'^i\}. \quad (14)$$

On taking matrix elements $Q_0^2(\mathbf{r}'_i)$ between $\chi^{(0)}$ and $\chi^{(\epsilon)}$, the cross terms (with matrix elements of Z and $\mathbf{R}$) will vanish. This leaves one term in the bracket, the centre-of-mass quadrupole operator, which in terms of the original coordinates is

$$(3Z^2 - R^2)\sum_i \tau_p{}^i = \frac{\mathscr{Z}}{A^2}\{\sum_i (3z_i^2 - r_i^2) + \sum_{i\neq j} (3z_i z_j - \mathbf{r}_i\cdot\mathbf{r}_j)\}, \quad (15)$$

where $\mathscr{Z}$ is the charge of the nucleus.

The first term on the right of eq. (15), when inserted in eq. (14), can be combined with $Q_0^2(\mathbf{r}_i)$ to give to good approximation $[1 - A^{-1}]Q_0^2(\mathbf{r}_i)$. This should hold because the neutrons and protons have about the same spatial distribution so the electric quadrupole matrix element should be about $\mathscr{Z}/A$ times the matrix element of the mass quadrupole.

In order to show that the second term of eq. (15) makes a relatively small contribution, we note that

$$\sum_{i\neq j} (3z_i z_j - \mathbf{r}_i\cdot\mathbf{r}_j) = \tfrac{4}{3}\pi \sum_{i\neq j} r_i r_j [2Y^1{}_0(\Omega_i)Y^1{}_0(\Omega_j) + Y^1{}_1(\Omega_i)Y^1{}_{-1}(\Omega_j) + Y^1{}_{-1}(\Omega_i)Y^1{}_1(\Omega_j)]. \quad (16)$$

The matrix element of eq. (16) is taken between $\chi^{(0)}$, which has a configuration $(1s)^4(1p)^8$, and $\chi^{(\epsilon)}$, which is a mixture of the configurations $(1s)^4(1p)^7(1f \text{ or } 2p)^1$ and $(1s)^3(1p)^8(1d)^1$ with intensities about 70 % and 30 %, respectively. From the form of eq. (16), we see that in operating on $\chi^{(0)}$ it can only raise a nucleon from 1s to 1p or from 1p to (1d or 2s). Therefore it can have no overlap with the bigger configuration in $\chi^{(\epsilon)}$, and can only give a contribution if it raises a 1p-nucleon to 1d and simultaneously raises another of the same charge from 1s to an unoccupied 1p-state. Therefore it is reasonable to expect that the contribution from eq. (16) is small.

The net result of estimating the centre-of-mass contribution is to reduce the matrix element by the factor $(1 - A^{-1})$, and bring in a further uncertainty due to the term given in eq. (16) which is probably of the order of 10 %.

Finally one must consider the importance of higher order terms since we have kept only the linear contribution of the wave-function admixture coefficients, the ε's of eq. (1). As the effect found is quite large it might be thought that the approximation is bad. However, as is discussed later, the large effect comes

from the large E2 matrix elements between the admixtures and the original states, and the ε's have magnitudes of about 0.2. Therefore keeping quadratic terms in the expansion in ε should give at most a 20 % change, so the magnitude of the enhancement obtained in the linear approximation we have used should be reliable.

4.2. EVALUATION

From the discussion in the preceding paragraphs, it is clear that the present calculation can only give a semi-quantitative estimate of the enhancement effect in the C^{12} case, primarily because of the large value of δ. The choice of $\eta = -6$ which seems appropriate [3]) for the spin-orbit strength in C^{12} gives $\delta = -0.71$. There is also the correction factor $(1-A^{-1})$ for the known centre-of-mass term, and an uncertainty of about 30 % for the remaining centre-of-mass term and higher order terms in ε. This gives an estimated value

$$\Delta Q \approx (1.2 \pm 0.3)\langle Q\rangle_{00}.$$

An earlier calculation [7]) of $\langle Q\rangle_{00}$ gave the gamma width for this transition (for $a/k \approx 5$ as the value of relative spin-orbit coupling strength)

$$(\Gamma)_{00} = 0.0103\langle r^2 \times 10^{25}\rangle^2 \text{ eV}.$$

The value of $\langle r^2\rangle$ can be taken from high-energy electron scattering as 5.8×10^{-26} cm^2. Since Γ is proportional to the square of the matrix element $[\langle Q\rangle_{00} + \Delta Q]$, the estimated numerical value with enhancement included is

$$\Gamma \approx 0.016 \text{ eV},$$

with an estimated uncertainty of 0.005 eV. The experimental value seems to lie near 0.011 eV, with about 0.002 eV uncertainty [8, 9]). The estimated value is compatible with observation, and has the feature that the mean-square radius can be taken as consistent with the electron scattering data, something that cannot be done without enhancement.

5. Discussion

An analysis of the way the enhancement is brought about in C^{12} is of interest for understanding and for rough estimates of other cases. About 90 % of the contribution comes from the $G(k_0\nu_0 \to k_0\nu_0)$ term of eq. (6''), which represents the process wherein $(Q_\lambda{}^2\chi_0{}^{(\epsilon)})$ raises a proton from its original state to a $\Delta N = 2$ level and then returns it to its original state. The overlap is then taken with a $\chi^{(0)}$ generating function, and since both $I = 2$ and $I' = 0$ come from the same generating function this means that such a contribution is much more important than from that part of $(Q_\lambda{}^2\chi_0{}^{(\epsilon)})$ which produces a different generating function. In this way we see that large enhancement arises for states within a "rotational band" (same generating function), and would not be

expected if the generating functions of I and I' differ. Such behaviour is a characteristic collective feature.

In the dominant $G(k_0 r_0 \rightarrow k_0 r_0)$ term, the contributions from the various excitation possibilities of the protons are 27 % for excitation from 1s to 1d, 65 % for excitation from 1p to 1f, and 8 % for excitation from 1p to 2p. Since there are only twice as many 1p protons as 1s protons, the indication is that the former are somewhat more effective in the enhancement.

While the admixtures to the zero-order wave functions are not large, they produce a large effect on the E2 matrix element. This is partly due to the fact that the zero-order matrix element is slightly smaller than the usual single-particle value, but it results chiefly from a combination of having more protons participating in the enhancement and having larger matrix elements between the $\Delta N = 2$ states than within the 1p shell. Such large matrix elements occur in these low states because $\Delta N = -2$ cannot occur for 1s and 1p nucleons, so the matrix element is concentrated into fewer states than in heavier nuclei. For operators other than the spatial $Y_\lambda^2(\Omega)$ type, one would not expect big effects, in fact they would generally be proportional to the square of admixture coefficients and so be quite small.

The conclusion is that the magnitude of E2 enhancement is given reasonably well by the procedure of this paper, and is of proper degree for the observations in the 1p-shell. A very good approximation can be simply obtained by keeping only the term analogous to $G(k_0 r_0 \rightarrow k_0 r_0)$ of eq. (6''). In order to obtain a more precise estimate, terms quadratic in the admixture coefficients should be included, and this would introduce another order of magnitude of difficulty into the calculation, since it would require complete angular momentum expansions of the $\chi^{(\epsilon)}$. Near the ends of the shell where smaller values of δ occur, the linear estimate is more accurate and provides an alternative for the usual weak-coupling or "effective neutron charge" approach.

The author wishes to thank Dr. B. Mottelson for helpful comments.

References

1) R. E. Peierls and J. Yoccoz, Proc. Phys. Soc. A **70** (1957) 381;
J. J. Griffin and J. A. Wheeler, Phys. Rev. **108** (1957) 311
2) J. P. Elliott, Proc. Roy. Soc. A **245** (1958) 128, 562
3) D. Kurath and L. Pičman, Nuclear Physics **10** (1959) 313
4) S. G. Nilsson, Mat. Fys. Medd. Dan. Vid. Selsk. **29**, No. 16 (1955)
5) J. P. Elliott and T. H. R. Skyrme, Proc. Roy. Soc. A **232** (1955) 561
6) S. Gartenhaus and C. Schwartz, Phys. Rev. **108** (1957) 482
7) D. Kurath, Phys. Rev. **106** (1957) 975
8) R. H. Helm, Phys. Rev. **104** (1956) 1466
9) Rasmussen, Metzger and Swann, Phys. Rev. **110** (1958) 154

1.B:1.C *Nuclear Physics* **14** (1959/60) 407—428; © *North-Holland Publishing Co., Amsterdam*

Not to be reproduced by photoprint or microfilm without written permission from the publisher

ROLE OF SPIN-ORBIT FORCE IN NUCLEAR INTERACTIONS

A. N. MITRA and V. L. NARASIMHAM

Department of Physics, Muslim University, Aligarh, U. P., India

Received 15 August 1959

Abstract: The two-body problem (scattering and bound state) has been solved exactly by considering an extension of Yamaguchi's non-local separable potential so as to include a two-body spin-orbit force. The parameters of the potential have been determined by obtaining their exact relationships with the low-energy experimental data (scattering length, effective range, deuteron binding energy, quadrupole and magnetic moments and the D-state probability). It is found that in order to fit the data, particularly the magnetic moment, the strength of the spin-orbit force must be comparable to that of the tensor force.

This potential has been applied to the evaluation of the spin-orbit energy splitting in the nuclei Ca^{41} and O^{17}. It is found that the tensor force by itself gives the wrong sign of the splitting and that it is overcompensated by a large contribution (of the correct sign) arising from the two-body spin-orbit force.

1. Introduction

While the presence of tensor forces in two-body interactions has long been established unambiguously, the same is unfortunately not true of direct two-body spin-orbit forces. The latter question has, however, received rather serious attention in recent times. The most direct experimental evidence in its favour came from the analysis of polarization in high energy p—p and n—p scattering, first by Gammel and Thaler [1]) and soon after by Signell and Marshak [2]). For low-energy processes, however, there never was any pressing need to harness such forces, since the number of ways in which such data can be fitted is almost unlimited. In particular the percentage of a direct two-body spin-orbit force is not known in any quantitative way.

One of the important low-energy data which is rather sensitive to such a force is perhaps the magnetic moment of the deuteron, which is very accurately known. A definite contribution to the deuteron magnetic moment arises from the spin-orbit force. Indeed, it was in this light that the Gammel-Thaler [1]) and Signell-Marshak [2]) potentials which fit the high energy data ideally were tested by Feshbach [3]) who found that both these potentials gave contributions of the wrong sign to the deuteron magnetic moment. Mesonic and other contributions which are of smaller (and uncertain) amounts were not thought to improve matters significantly. This led Feshbach even to suggest spin-orbit potentials of different types from the conventional ones †.

Among other low-energy nuclear properties which are sensitive to a two-body

† In order to meet Feshbach's objections, Signell and Marshak have recently suggested some changes in their earlier potential (see ref. [4])).

spin-orbit force is the spin-orbit splitting of energy levels in nuclei. This problem has assumed considerable importance in the present context of Brueckner's theory of nuclear structure. Attempts at explaining the magnitude of the observed splitting with the help of tensor forces alone have so far produced negative results (see Kisslinger [5]), and Nigam and Sundaresan [6])). In fact, apart from the small magnitude, even the sign of the calculated splitting due to tensor forces is not unambiguous. It has therefore been suggested that a direct spin-orbit force may have to be invoked in order to explain the observed splitting. Recently Sundaresan and Nigam [7]) have shown that the Signell-Marshak spin-orbit force improves the calculated splitting considerably when compared to that due to the tensor force alone.

It is thus seen that even an analysis of some low-energy nuclear properties can throw significant light on the role of a two-body spin-orbit force, and one has not to turn immediately to high energy scattering data for this purpose. Rather, the parameters of the two-body potential which are adjusted to fit all the low energy two-body data (both sensitive and insensitive to the spin-orbit force) may be *tested* against the high energy data. Keeping this sort of approach in mind, it was felt that an *exact* solution of the problem of two-body interaction at low energies, taking both tensor and spin-orbit forces into account, would, in addition to being free from the uncertainties of approximations, perhaps help to clarify some of the points raised in the earlier paragraphs. An exact solution, in turn, is known, from the work of Yamaguchi [8]) (referred to as A) to be greatly facilitated by considering a non-local potential of the separable type. We have, in this paper, considered an extension of the Yamaguchi potential so as to take into account a spin-orbit force as well.

In section 2, the choice of the two-body potential is discussed briefly, with particular reference to the determination of the various parameters from the observed data. In section 3, the Schrödinger equation is solved for the deuteron problem and the bound state parameters (quadrupole and magnetic moments, the binding energy and the D-state probability) are determined algebraically. In section 4, the corresponding scattering problem is solved and the low-energy parameters (scattering length and effective range) are calculated exactly. Section 5 is devoted to a detailed numerical evaluation (and also to an approximate determination of the range of variations) of the assumed parameters so as to fit all the observed low-energy data. Finally, in section 6, the spin-orbit energy splitting in some "doubly closed shell plus or minus one" nuclei is calculated in the "zeroth order" as a simple (but rather crude) application of our potential to the Brueckner theory of nuclear structure.

2. The Two-Body Potential

A most important characteristic feature of a separable potential, as the name implies, is that the interaction can be completely separated into individual

partial waves. This situation affords the possibility of adding various terms to the potential which would not interfere with one another. Thus singlet and triplet nucleon-nucleon scattering in a particular l-state which by the exclusion principle, would be associated with either triplet or singlet isobaric spins, can be considered separately. One can, by such reasoning, calculate separately the projections of the potentials on the isobaric-spin states 0 and 1 respectively. We are here particularly interested in the projection on to the state $I = 0$ which, for even l, is associated with n—p triplet spin-states and for odd l, with n—p singlet spin-states. Singlet spin-states are, however, not of immediate interest to our present problem since they are not affected by the spin-orbit force or even the tensor force.

As an extension of the Yamaguchi potential to include a spin-orbit force, we take the projection of the potential on the state $I = 0$ as

$$(\mathbf{p}|V|\mathbf{p}') = -\frac{\lambda}{M} g(\mathbf{p}) g(\mathbf{p}') + (\mathbf{p}|V_{LS}|\mathbf{p}'), \tag{2.1}$$

where

$$g(\mathbf{p}) = C(p) + 8^{-\frac{1}{2}} T(p) S(\hat{p}), \tag{2.2}$$

$$S(\hat{p}) = 3(\boldsymbol{\sigma}_1 \cdot \hat{p})(\boldsymbol{\sigma}_2 \cdot \hat{p}) - (\boldsymbol{\sigma}_1 \cdot \boldsymbol{\sigma}_2). \tag{2.3}$$

The direct spin-orbit term V_{LS} may be taken to be of the form

$$(\mathbf{p}|V_{LS}|\mathbf{p}') = \sum_l \sum_{m=-l}^{l} -\frac{4\pi\lambda_l}{M} v_l(p) v_l(p') \times Y^*_{lm}(\hat{p}) \tfrac{1}{2}(\mathbf{L} \cdot \mathbf{S} + \mathbf{L}' \cdot \mathbf{S}) Y_{lm}(\hat{p}'). \tag{2.4}$$

This term has all the features of a spin-orbit potential. The orbital angular momentum operators $\mathbf{L}$ and $\mathbf{L}'$ in (2.4) act on $\hat{p}$ and $\hat{p}'$ from the right and left respectively. It is easily verified by operating (2.4) on some arbitrary state $\psi(p) = \mathcal{Y}^M_{jlS}(\hat{p}) u_{jl}(p)$, where †

$$\mathcal{Y}^M_{jlS} = \sum_{m=-l}^{l} C_{lS}(jM; m, M-m) Y_{lm}(\hat{p}) \chi_1^{M-m},$$

that the effect of the operator $\frac{1}{2}(\mathbf{L} \cdot \mathbf{S} + \mathbf{L}' \cdot \mathbf{S})$ on this state is exactly the same as that of $\mathbf{L} \cdot \mathbf{S}$ or $\mathbf{L}' \cdot \mathbf{S}$ alone. Thus the term (2.4) can be simplified as

$$(\mathbf{p}|V_{LS}|\mathbf{p}') = \sum_l -\frac{\lambda_l}{M} (2l+1) v_l(p) v_l(p') (\mathbf{L} \cdot \mathbf{S}) P_l(\hat{p} \cdot \hat{p}'), \tag{2.5}$$

where P_l is the ordinary Legendre polynomial of degree l, and $\mathbf{L} \equiv +i\mathbf{p} \times \boldsymbol{\nabla}_p$, rather than the usual $-i\mathbf{p} \times \boldsymbol{\nabla}_p$, in (2.5) since it is now operating on $\hat{p}$ from the *left*. The expression (2.5) may be compared with an ordinary *local* spin-orbit potential which, apart from irrelevant factors, is

† The notation used here is that of ref. [9]); $\chi_1^m (m = 0, \pm 1)$ are the eigenfunctions of spin 1.

$$(\mathbf{L}\cdot\mathbf{S})\delta^3(\mathbf{p}-\mathbf{p}') = (4\pi pp')^{-1}\delta(p-p')\sum_l (2l+1)(\mathbf{L}\cdot\mathbf{S})P_l(\hat{p}\cdot\hat{p}'). \quad (2.6)$$

Our non-local potential thus differs from the conventional one in two respects, viz. (a) the weight factor $\lambda_l v_l(p)v_l(p')$ is different for each l and (b) the sum in (2.5) is not sought to be carried out over all l-values from 0 to ∞. Even for moderately high energies a few l-values should generally suffice in practice. This may sound a rather empirical approach at first sight, but it may be more conveniently suited for an experimental determination of the various l-parameters at successively higher energies, than one based on local potentials which was adopted by Gammel-Thaler [1]) or Signell-Marshak [2]). It may be noted that even in the analysis of these authors a large number of parameters for the various potentials had to be employed to give resonable fit with experiment. The present treatment may, in this respect, be regarded as a convenient alternative to the local-potential approach of these authors. From a calculational point of view, the main advantage of the present approach is that it is free from the singularities due to repulsive cores and is capable of exact treatment with relative ease. Its main disadvantage, on the other hand, is that the potentials used here do not have any direct physical significance (like range etc.), which local potentials enjoy.

For low and moderately high energies, it is sufficient to take only $l = 1$ and 2 in (2.5). For n—p triplet scattering in $I = 0$, only $l = 2$ can contribute by the exclusion principle with which $l = 1$ is incompatible. This implies that the parameters for $l = 1$ would not enter the expressions for the triplet scattering length and effective range. For the deuteron problem, $l = 1$ does not, of course, contribute at all. On the other hand, p—p or n—n triplet scattering which necessarily corresponds to $I = 1$, are governed solely by odd-l (on account of the exclusion principle), so that only $l = 1$ comes in at moderately high energies. These and similar considerations afford the possibility of determining the various parameters through essentially non-overlapping phenomena.

As we are interested only in low-energy triplet n—p phenomena corresponding to $I = 0$ in this paper, we need only consider $l = 2$ here.

3. The Deuteron Problem

Taking the total binding energy of the deuteron as α^2/M, the Schrödinger equation for the deuteron wave function $\psi(\mathbf{p})$ in momentum space is

$$(\alpha^2+p^2)\psi(\mathbf{p}) = -M\int (\mathbf{p}|V|\mathbf{p}')\psi(\mathbf{p}')\mathrm{d}^3\mathbf{p}', \quad (3.1)$$

where $(\mathbf{p}|V|\mathbf{p}')$ is now given by

$$(\mathbf{p}|V|\mathbf{p}') = -\frac{\lambda}{M}g(\mathbf{p})g(\mathbf{p}')-\frac{5\lambda_2}{M}v_2(p)v_2(p')\times(\mathbf{L}\cdot\mathbf{S})P_2(\hat{p}\cdot\hat{p}'). \quad (3.2)$$

We use here the notation of Blatt and Weisskopf [10]) for the orthonormal eigenstates of J, L and S, viz. $\mathscr{Y}^M_{jl1}$, so that $\psi(\mathbf{p})$ may be written as

$$\psi(\mathbf{p}) = u(p)\mathscr{Y}^M_{101} + w(p)\mathscr{Y}^M_{121}. \tag{3.3}$$

Eq. (3.2) is now substituted in (3.1) which can be simplified with the help of the following relations:

$$S(\hat{p})\mathscr{Y}^M_{101} = 8^{\frac{1}{2}}\mathscr{Y}^M_{121}; \tag{3.4}$$

$$S(\hat{p})\mathscr{Y}^M_{121} = 8^{\frac{1}{2}}\mathscr{Y}^M_{101} - 2\mathscr{Y}^M_{121}; \tag{3.5}$$

$$2(\mathbf{L}\cdot\mathbf{S})\mathscr{Y}^M_{jl1} = (j(j+1) - l(l+1) - 2)\mathscr{Y}^M_{jl1}; \tag{3.6}$$

$$\int S^2(\hat{p})\mathrm{d}\Omega = 32\pi; \tag{3.7}$$

$$\int P_2(\hat{p}\cdot\hat{p}')\mathscr{Y}^M_{jl1}(\hat{p}')\mathrm{d}\Omega' = \tfrac{4}{5}\pi\mathscr{Y}^M_{jl1}(\hat{p}). \tag{3.8}$$

Using these results and equating coefficients of the different $\mathscr{Y}$'s one obtains

$$(\alpha^2+p^2)u(p) = \lambda C(p)\int (u(p')C(p') + w(p')T(p'))\,\mathrm{d}^3\mathbf{p}' \tag{3.9}$$

and

$$\begin{aligned}(\alpha^2+p^2)w(p) = {}& \lambda T(p)\int (u(p')C(p') + w(p')T(p'))\,\mathrm{d}^3\mathbf{p}' \\ & - 3\lambda_2 v_2(p)\int v_2(p')w(p')\mathrm{d}^3\mathbf{p}'.\end{aligned} \tag{3.10}$$

The solutions of these equations are immediately seen to be

$$u(p) = \frac{N_0 C(p)}{\alpha^2+p^2}, \quad w(p) = \frac{N_0 T(p) + N_2 v_2(p)}{\alpha^2+p^2}, \tag{3.11}$$

where N_0 and N_2 are given by

$$\begin{aligned} N_0 &= \lambda N_0 I_{11} + \lambda N_2 I_{12}, \\ N_2 &= -3\lambda_2 N_0 I_{12} - 3\lambda_2 N_2 I_{22}, \end{aligned} \tag{3.12}$$

and I_{11}, I_{12}, I_{22} are defined by

$$\begin{aligned} I_{11} &= \int \frac{(C^2(p)+T^2(p))\mathrm{d}^3\mathbf{p}}{\alpha^2+p^2}, \\ I_{21} = I_{12} &= \int \frac{v_2(p)T(p)\mathrm{d}^3\mathbf{p}}{\alpha^2+p^2}, \\ I_{22} &= \int \frac{v_2^2(p)\,\mathrm{d}^3\mathbf{p}}{\alpha^2+p^2}. \end{aligned} \tag{3.13}$$

Eqs. (3.12) give the following relation between λ and λ_2:

$$(1-\lambda I_{11})(1+3\lambda_2 I_{22})+3\lambda\lambda_2 I_{12}^2=0. \tag{3.14}$$

Further, the D-state probability is given by either of the following equations:

$$1-P_D=\int_0^\infty u^2(p)p^2\mathrm{d}p=J_{00}N_0^2, \tag{3.15}$$

where

$$J_{00}=\int_0^\infty \frac{p^2\mathrm{d}p \quad C^2(p)}{(\alpha^2+p^2)^2}, \tag{3.16}$$

and

$$P_D=\int_0^\infty w^2(p)p^2\mathrm{d}p=N_0^2J_{11}+2N_0N_2J_{12}+N_2^2J_{22}, \tag{3.17}$$

where

$$\begin{aligned} J_{11}&=\int_0^\infty \frac{p^2\mathrm{d}p \quad T^2(p)}{(\alpha^2+p^2)^2},\\ J_{12}&=\int_0^\infty \frac{p^2\mathrm{d}p \quad v_2(p)T(p)}{(\alpha^2+p^2)^2},\\ J_{22}&=\int_0^\infty \frac{p^2\mathrm{d}p \quad v_2^2(p)}{(\alpha^2+p^2)^2}. \end{aligned} \tag{3.18}$$

Using (3.12), (3.15) and (3.17), one obtains the relation

$$\begin{aligned}(1-P_D)[\lambda^2(J_{11}I_{12}^2-2J_{12}I_{12}I_{11}+J_{22}I_{11}^2)\\ +2\lambda(I_{12}J_{12}-I_{11}J_{22})+J_{22}]=\lambda^2J_{00}I_{12}^2P_D.\end{aligned} \tag{3.19}$$

The quadrupole moment is given by

$$Q=-\frac{1}{4}\int \mathrm{d}^3\mathbf{p} \quad \psi^*(\mathbf{p})\left[3\frac{\partial^2}{\partial p_z^2}-\nabla_p^2\right]\psi(\mathbf{p}),$$

which simplifies to †

$$Q=\frac{\sqrt{2}}{10}\int_0^\infty \mathrm{d}p\left(pw\frac{\mathrm{d}u}{\mathrm{d}p}-p^2w\frac{\mathrm{d}^2u}{\mathrm{d}p^2}\right)-\frac{1}{20}\int_0^\infty \mathrm{d}p\left(6w^2+p^2\left(\frac{\mathrm{d}w}{\mathrm{d}p}\right)^2\right). \tag{3.20}$$

The extra magnetic moment contribution arising from the spin-orbit force is found in nuclear magneton units to be

$$\Delta\mu_{LS}=\tfrac{1}{2}\pi\lambda_2\,\mathscr{A}\mathscr{B}, \tag{3.21}$$

† This result has been taken over from ref. [8]). Yamaguchi's result had to be divided by 4π to take account of the difference in the two normalizations.

where

$$\mathscr{A} = \int_0^\infty p^2 \mathrm{d}p v_2(p) w(p) \tag{3.22}$$

and

$$\mathscr{B} = \int^\infty \mathrm{d}p \left[\frac{2}{3} \left(p \frac{\mathrm{d}w}{\mathrm{d}p} + 3w \right) \left(p \frac{\mathrm{d}v_2}{\mathrm{d}p} + 3v_2 \right) + p^2 \frac{\mathrm{d}v_2}{\mathrm{d}p} \frac{\mathrm{d}w}{\mathrm{d}p} + 6v_2 w \right]. \tag{3.23}$$

This result is derived in appendix 1.

At this stage, we must specify the form of the functions $C(p)$, $T(p)$ and $v_2(p)$. Following A again, we take them as

$$\begin{aligned} C(p) &= 1/(\beta^2+p^2), \\ T(p) &= -tp^2/(\gamma^2+p^2)^2, \\ v_2(p) &= p^2/(\delta^2+p^2)^2. \end{aligned} \tag{3.24}$$

These forms are consistent with the low-energy behaviour of the scattering phase shifts, viz $k^{2l+1} \cot \delta_l \approx a_l + b_l k^2$ for the l-th partial wave, keeping in mind that both $T(p)$ and $v_2(p)$ are associated with D-waves. The integrals occurring in eqs. (3.14) to (3.19) are now easily evaluated and they are listed along with a few others in appendix 2.

4. The n—p Scattering Problem

The scattering eq. for the n—p wave function for an initial momentum $\mathbf{k}$ in the C.M. system is

$$\psi_k(\mathbf{p}) = \phi_k(\mathbf{p}) + \frac{M}{k^2-p^2+i\varepsilon} \int (\mathbf{p}|V|\mathbf{p}')\psi_k(\mathbf{p}')\mathrm{d}^3\mathbf{p}', \tag{4.1}$$

with the normalizations

$$\phi_k(\mathbf{p}) = \delta^3(\mathbf{p}-\mathbf{k}) \tag{4.2}$$

and

$$(\mathbf{p}|V|\mathbf{p}') = \int \phi_p{}^*(\mathbf{q})(\mathbf{q}|V|\mathbf{q}')\phi_{p'}(\mathbf{q}')\mathrm{d}^3\mathbf{q}\mathrm{d}^3\mathbf{q}'. \tag{4.3}$$

The scattering operator T which is defined by

$$(\mathbf{p}|T|\mathbf{p}') = \int \phi_p{}^*(\mathbf{q})(\mathbf{q}|V|\mathbf{q}')\psi_{p'}(\mathbf{q}')\mathrm{d}^3\mathbf{q}\mathrm{d}^3\mathbf{q}', \tag{4.4}$$

is then seen from (4.1) and (4.3) to satisfy the equation

$$(\mathbf{p}|T|\mathbf{k}) = (\mathbf{p}|V|\mathbf{k}) + M \int \frac{(\mathbf{p}|V|\mathbf{p}')(\mathbf{p}'|T|\mathbf{k})}{k^2-p'^2+i\varepsilon} \mathrm{d}^3\mathbf{p}'. \tag{4.5}$$

Here $(\mathbf{p}|T|\mathbf{k})$ and $(\mathbf{p}|V|\mathbf{k})$ are still matrices in spin-space. We have now to solve (4.5) with $(\mathbf{p}|V|\mathbf{p}')$ defined by (3.2). The solution of this equation is

considerably more complicated compared with A because of the last term in (3.2). Thus it is clear that $(\mathbf{p}|T|\mathbf{p}')$ is not simply proportional to $(\mathbf{p}|V|\mathbf{p}')$, but that terms like $(\mathbf{L}\cdot\mathbf{S})^2 P_2(\hat{p}\cdot\hat{p}')$, $(\mathbf{L}\cdot\mathbf{S})S(\hat{p})$ etc. are likely to appear. However, terms like $(\mathbf{L}\cdot\mathbf{S})^3$ can be reduced to linear combinations of $(\mathbf{L}\cdot\mathbf{S})$ and $(\mathbf{L}\cdot\mathbf{S})^2$, by means of operator identities. By a process of trial and error, it has been possible to arrive at the following form of $(\mathbf{p}|T|\mathbf{p}')$:

$$\begin{aligned}(\mathbf{p}|T|\mathbf{p}') = {} & Ag(\mathbf{p})g(\mathbf{p}')+\tfrac{1}{8}Cv_2(p)v_2(p')S(\hat{p})S(\hat{p}') \\ & + 8^{-\frac{1}{2}}l\,v_2(p)S(\hat{p})g(\mathbf{p}')+8^{-\frac{1}{2}}B'g(\mathbf{p})S(\hat{p}')v_2(p') \\ & + 5v_2(p)v_2(p')[a+(\mathbf{L}\cdot\mathbf{S})b+(\mathbf{L}\cdot\mathbf{S})^2 c]P_2(\hat{p}\cdot\hat{p}').\end{aligned} \tag{4.6}$$

Here A, a, etc. are functions of the initial momentum and presumably also of the projection operator ρ for the triplet spin-state, which is defined by

$$\rho = \tfrac{1}{4}(3+\boldsymbol{\sigma}_1\cdot\boldsymbol{\sigma}_2). \tag{4.7}$$

In obtaining the form (4.6) for the scattering matrix, free use has been made of the following relations:

$$(\mathbf{L}\cdot\mathbf{S})^3 = L^2(\mathbf{L}\cdot\mathbf{S})-2(\mathbf{L}\cdot\mathbf{S})^2+L^2\rho-(\mathbf{L}\cdot\mathbf{S}); \tag{4.8}$$

$$(\mathbf{L}\cdot\mathbf{S})S(\hat{p}) = -S(\hat{p})(3+\mathbf{L}\cdot\mathbf{S})-2(\mathbf{L}\cdot\mathbf{S}); \tag{4.9}$$

$$S^2(\hat{p}) = 8\rho-2S(\hat{p}); \tag{4.10}$$

$$(\boldsymbol{\sigma}_1\cdot\boldsymbol{\sigma}_2)S(\hat{p}) = S(\hat{p})(\boldsymbol{\sigma}_1\cdot\boldsymbol{\sigma}_2); \tag{4.11}$$

$$(\mathbf{L}\cdot\mathbf{S})(\boldsymbol{\sigma}_1\cdot\boldsymbol{\sigma}_2) = -(\boldsymbol{\sigma}_1\cdot\boldsymbol{\sigma}_2)(\mathbf{L}\cdot\mathbf{S})+2(\mathbf{L}\cdot\mathbf{S}); \tag{4.12}$$

$$L^2P_2 = 6P_2, \quad L^2S(\hat{p}) = 6S(\hat{p}). \tag{4.13}$$

One has now to substitute (4.6) and (3.2) in (4.5) and obtain a set of equations for the constants A, a, etc. The correctness of our assumption (4.6) will be reflected in the self-consistency of the last set of equations. It may be remembered that the *order* in which the constants appear in (4.6) is important, since, according to (4.12), $\mathbf{L}\cdot\mathbf{S}$ does not commute with ρ. Finally, Eq. (4.13) shows that P_2 and $S(\hat{p})$ are eigenfunctions of L^2, which fact may be utilized to substitute $l(l+1)$ for L^2 whenever the latter operates on P_2 or $S(\hat{p})$ on the extreme right or left. Keeping these points in mind, the necessary relations between the various coefficients have been obtained in a straightforward manner, and these have been solved to give

$$A = -\frac{\lambda}{MD}(1+3\lambda_2\zeta_k); \tag{4.14}$$

$$B = B' = \frac{3\lambda\lambda_2\eta_k}{MD}; \tag{4.15}$$

$$C = -\frac{9\lambda_2^2\eta_k^2\lambda}{MD(1+3\lambda_2\zeta_k)}; \tag{4.16}$$

$$a = 6\lambda_2\zeta_k c; \tag{4.17}$$

$$b = \frac{(1+2\lambda_2\zeta_k)}{c\lambda_2\zeta_k}; \tag{4.18}$$

$$c = -\frac{\lambda_2^2\zeta_k}{M(1+3\lambda_2\zeta_k)(1+\lambda_2\zeta_k)(1-2\lambda_2\zeta_k)}; \tag{4.19}$$

where

$$D = (1-\lambda\xi_k)(1+3\lambda_2\zeta_k)+3\lambda\lambda_2\eta_k^2; \tag{4.20}$$

$$\xi_k = \int \frac{\mathrm{d}^3\mathbf{p}\,(C^2(p)+T^2(p))}{p^2-k^2-i\varepsilon}; \tag{4.21}$$

$$\eta_k = \int \frac{\mathrm{d}^3\mathbf{p}\,v_2(p)T(p)}{p^2-k^2-i\varepsilon}; \tag{4.22}$$

$$\zeta_k = \int \frac{\mathrm{d}^3\mathbf{p}\,v_2^2(p)}{p^2-k^2-i\varepsilon}. \tag{4.23}$$

It may be noted that

$$B^2 = AC. \tag{4.24}$$

Also, the equality of B and B', which is expected on grounds of symmetry, is a check on the consistency of these calculations.

One has now to calculate the differential unpolarized cross-section for triplet n−p scattering which is given by

$$\mathrm{d}\sigma/\mathrm{d}\Omega = \tfrac{1}{3}\,\mathrm{Tr}\,\rho(2\pi^2M)^2(\mathbf{p}|T|\mathbf{k})^*(\mathbf{k}|T|\mathbf{p}), \tag{4.25}$$

where the star in (4.25) stands merely for complex conjugation. The only complicated terms in the evaluation of (4.25) are of the type

$$\mathrm{Tr}\,\rho P_2(\hat{p}\cdot\hat{k})(\mathbf{L}'\cdot\mathbf{S})^{n'}(\mathbf{L}\cdot\mathbf{S})^n P_2(\hat{p}\cdot\hat{k}), \tag{4.26}$$

where n, $n' = 1, 2$ and $\mathbf{L}$ and $\mathbf{L}'$ are distinguished by their operations on the right and left respectively. Remembering this last point, the trace in (4.26) is easily evaluated, for $n' = 1$, $n = 2$, say, to give

$$P_2(\hat{p}\cdot\hat{k})(-\mathbf{L}\cdot\mathbf{L}')P_2(\hat{p}\cdot\hat{k}),$$

which simplifies to $-9\sin^2\theta\cos^2\theta$, where $\cos\theta = \hat{p}\cdot\hat{k}$. Other traces may be evaluated by means of the formulae listed in appendix 3. The final formula for (4.25) obtained in this way is an extremely unwieldy expression. However, the

contribution to $d\sigma/d\Omega$ arising from a pure S-state scattering may be picked out by dropping all the P_l-terms except for $l = 0$, and these give

$$(d\sigma/d\Omega)_{l=0} = (2\pi^2 M)^2[|A|^2(C_k^2+T_k^2)^2 + |Cv_k^2+2Bv_kT_k|^2+2\,\mathrm{Re}\,A^*T_k^2(Cv_k^2+2Bv_kT_k)], \quad (4.28)$$

where the symbols have their earlier meanings and $C(k)$, $T(k)$, $v_2(k)$ have been abbreviated as C_k, T_k, v_k respectively. Being interested in the low-energy parameters for scattering we have to consider (4.28) in the limit when k is small, with terms up to $O(k^2)$ retained. The following approximations for the basic quantities are then seen to hold when C_k, T_k, v_k have the forms (3.24)

$$C_k^2 \approx \beta^{-4}-2k^2\beta^{-6}, \quad T_k^2 \approx v_k^2 \approx 0; \quad (4.29)$$

$$\xi_k \approx \pi^2\beta^{-3}(1-3k^2\beta^{-2})+2i\pi^2k\beta^{-4}+\tfrac{1}{8}\pi^2t^2\gamma^{-3}(1+k^2\gamma^{-2}); \quad (4.30)$$

$$\eta_k \approx -\pi^2t(\gamma+\delta)^{-3}(1+k^2\gamma^{-1}\delta^{-1}); \quad (4.31)$$

$$\zeta_k \approx \tfrac{1}{8}\pi^2\delta^{-3}(1+k^2\delta^{-2}). \quad (4.32)$$

The approximations to the other quantities A, D, etc. may be evaluated from (4.14) to (4.20). Eq. (4.28) now reduces to

$$(d\sigma/d\Omega)_{l=0} = (2\pi^2M)^2|A|^2C_k^2. \quad (4.33)$$

For an evaluation for the S-phase shift δ_0, (4.33) must be compared with $(k\cot\delta_0-ik)^{-2}$, and this, after due simplifications, leads finally to

$$k\cot\delta_0 = -a^{-1}+\tfrac{1}{2}r_0k^2, \quad (4.34)$$

where

$$-a^{-1} = \tfrac{1}{2}\beta^4\pi^{-2}\lambda^{-1}-\tfrac{1}{2}\beta-\tfrac{1}{16}t^2\beta^4\gamma^{-3}+\tfrac{3}{2}\lambda_2\pi^2t^2\beta^4(\gamma+\delta)^{-6}\left(1+\frac{3\pi^2\lambda_2}{8\delta^3}\right)^{-1} \quad (4.35)$$

$$r_0 = 2\beta^2\pi^{-2}\lambda^{-1}+\beta^{-1}-\tfrac{1}{8}t^2\beta^2(\beta^2\gamma^{-5}+2\gamma^{-3}) + \frac{3\lambda_2\pi^2t^2\beta^4}{(\gamma+\delta)^6(1+\frac{3}{8}\pi^2\lambda_2\delta^{-3})}\left[\frac{2}{\gamma\delta}+\frac{2}{\beta^2}-\frac{3\pi^2\lambda_2}{8\delta^5}\left(1+\frac{3\pi^2\lambda_2}{8\delta^3}\right)^{-1}\right]. \quad (4.36)$$

5. Evaluation of the Parameters

Eqs. (3.14), (3.19)—(3.21), (4.35) and (4.36) determine the parameters λ, λ_2, β, γ, δ, t, of our two-body potential. Since these equations are extremely complicated it was not thought worth while at this stage solving them as such. They can, however, be considerably simplified by setting $\gamma = \delta$, in which case we have essentially 5 parameters to fit the data. Even so, this can be done in a variety of ways, particularly because of the uncertainty in the D-state probability. In this respect an attempt has been made to find the range of variations of these parameters that may be allowed without violating the observed data.

The physical meaning of $\gamma = \delta$ may, off-hand, be taken to be that the tensor and spin-orbit forces have the same range. In this respect the experimental information is not very clear. The analyses of Gammel-Thaler or Signell-Marshak seem to suggest that the spin-orbit force has a shorter range than the tensor force, but this statement is by no means rigorously true. Our potential, on the other hand, is non-local, so that it has a very different behaviour from the local potentials of Gammel-Thaler or Signell-Marshak, and it may at least be said that γ or δ do not bear any such obvious relation to the range (or rather the inverse range) as would be the case for a local potential. The choice of $\gamma = \delta$ was made essentially in the interest of the simplicity, and also to enable us to judge the implications of our potential in more detail.

For $\gamma = \delta$, eqs. (3.14) and (3.19) may be solved for λ and λ_2 to give

$$(\lambda\pi^2)^{-1} = \beta^{-1}(\alpha+\beta)^{-2} \mp \frac{t}{f}\left(\frac{P_D}{1-P_D}\right)^{\frac{1}{2}} \tag{5.1}$$

and

$$3\lambda_2\pi^2 = \mp tf\left(\frac{1-P_D}{P_D}\right)^{\frac{1}{2}} - 8\gamma(\alpha+\gamma)^4(5\alpha^2+4\alpha\gamma+\gamma^2)^{-1}, \tag{5.2}$$

where

$$f = 2(\alpha+\gamma)(\alpha+\beta)(5\alpha^2+4\alpha\gamma+\gamma^2)^{-1}[2\alpha\beta\gamma(\alpha+\beta)(\alpha+\gamma)(5\alpha+\gamma)]^{\frac{1}{2}} \tag{5.3}$$

and the results of appendix 2 have been used. Eqs. (5.1) and (5.2) show that λ^{-1} and λ_2 are linear functions of t. This result may be compared with one recently obtained by Vaidya [11]). The two solutions in each of (5.1) and (5.2) arise from the quadratic nature of eq. (3.19). The expression for the quadrupole moment (3.20) becomes, on substituting for λ, λ_2 from (5.1) and (5.2)

$$Q = \frac{\pi c N_0^2}{640}\left[\mp\chi\left(\frac{P_D}{1-P_D}\right)^{\frac{1}{2}} - bc\frac{P_D}{1-P_D}\right], \tag{5.4}$$

where

$$b = (7\alpha^3+49\alpha^2\gamma+91\alpha\gamma^2+33\gamma^3)\gamma^{-3}(\alpha+\gamma)^{-7}, \tag{5.5}$$

$$c = 2(\alpha+\gamma)^2(\alpha+\beta)^{-1}\left[\frac{2\gamma(\alpha+\gamma)}{\alpha\beta(\alpha+\beta)(5\alpha+\gamma)}\right]^{\frac{1}{2}}, \tag{5.6}$$

$$\begin{aligned}\chi = {} & 16\sqrt{2}(\alpha+\beta)^{-4}(\alpha+\gamma)^{-3}(\beta+\gamma)^{-2} \\ & \times[(\beta+\gamma)^{-2}\{2\alpha^3(\beta+4\gamma)+2\alpha^2(4\beta^2+19\beta\gamma+12\gamma^2)+2\alpha\gamma(12\beta^2+19\beta\gamma+4\gamma^2)+2\beta\gamma^2(4\beta+\gamma)\} \\ & +(\alpha+\gamma)^{-1}(\beta+\gamma)^{-1}\{8\alpha^2(\beta^2+3\beta\gamma+\gamma^2)+2\alpha(\beta^3+19\beta^2\gamma+19\beta\gamma^2+\gamma^3)+8\beta\gamma(\beta^2+3\beta\gamma+\gamma^2)\} \\ & +\alpha^{-1}(\alpha+\gamma)^{-2}\{5\alpha^3(\beta+\gamma)^2+5\beta^2\gamma(\beta+\gamma)^2 \\ & +\alpha^2(4\beta^3+33\beta^2\gamma+22\beta\gamma^2+\gamma^3)+\alpha\beta(\beta^3+22\beta^2\gamma+33\beta\gamma^2+4\gamma^3)\}].\end{aligned} \tag{5.7}$$

It is interesting to note that Q depends only on P_D and not on t, but this would not in general be the case if γ were not made equal to δ. At this stage, the upper

sign in (5.4) and hence also in (5.1) and (5.2) may be ruled out on the ground that it gives a negative quadrupole moment, since the parameters (5.5) to (5.7) are all positive. In the following we therefore work exclusively with the lower sign.

As for the magnetic moment, the quantity $\Delta\mu = \mu_d - \mu_n - \mu_p$ is given in nuclear magnetons, by

$$\Delta\mu = \Delta\mu_{LS} - \tfrac{3}{2}(\mu_p + \mu_n - \tfrac{1}{2})P_D, \tag{5.8}$$

where

$$\Delta\mu_{LS} = (\tfrac{1}{2}\pi\lambda_2)\mathscr{A}\mathscr{B}, \tag{5.9}$$

$$\mathscr{A} = \frac{N_0}{12\pi\lambda_2}\left[-t + c\left(\frac{P_D}{1-P_D}\right)^{\frac{1}{2}}\right], \tag{5.10}$$

$$\mathscr{B} = -\tfrac{5}{96}\pi N_0 dc\left(\frac{P_D}{1-P_D}\right)^{\frac{1}{2}}, \tag{5.11}$$

$$d = \gamma^{-3}(\alpha+\gamma)^{-6}(7\alpha^4 + 42\alpha^3\gamma + 77\alpha^2\gamma^2 + 36\alpha\gamma^3 + 6\gamma^4). \tag{5.12}$$

Experimentally,

$$\Delta\mu = -0.0224 \text{ n.m.}$$

In order, therefore, to prevent P_D from being negative, which would meet Feshbach's objections to the Gammel-Thaler or Signell-Marshak potentials, the contribution $\Delta\mu_{LS}$ to (5.8) should be algebraically larger than -0.0224. This requirement should serve as one of the guiding considerations for fixing up the numerical values of the parameters. Finally, the low-energy scattering parameters are given by (4.35) and (4.36) after setting $\gamma = \delta$ in them.

To ensure that a short-range spin-orbit or tensor force should have very little effect on the low-energy scattering parameters a^{-1} and r_0 one must require that very small contribution to (4.35) and (4.36) should come from the terms depending on t, λ_2 and γ.

Keeping these points in mind, the following procedure has been adopted. Assuming some convenient values of β and γ, eq. (5.4) is solved for P_D with

$$Q_{exp} = 2.74 \times 10^{-27} \text{ cm}^2 = 0.0147\alpha^{-2}, \tag{5.13}$$

since Q depends only on P_D, as stated above. Next, eq. (5.8), which is linear in t, is solved for t with

$$\Delta\mu_{exp} = -0.0224. \tag{5.14}$$

With the values of t and P_D so obtained, λ and λ_2 are calculated from (5.1) and (5.2). Finally, a^{-1} and r_0 are calculated by substituting for λ, λ_2, γ, β and t in (4.35) and (4.36), and comparing with the experimental values

$$a = (5.378 \pm 0.021) \times 10^{-13} \text{ cm}$$

and

$$r_0 = (1.72 \pm 0.035) \times 10^{-13} \text{ cm}. \tag{5.15}$$

If the calculated values tally with (5.15) within the limits of experimental error, the investigation with a particular set of values of β and γ is complete. Otherwise, the assumed values are altered suitably to give agreement with (5.15). Another set of values of β and γ is then taken and the same procedure repeated. As already mentioned, values of the parameters which do not conform to the requirements 1) $\Delta\mu_{LS} > -0.0224$ and 2) small spin-orbit and tensor contributions to a^{-1} and r_0, have been rejected. Table 1 gives the range of values of the parameters β, γ, t, P_D which fit the scattering parameters a^{-1} and r_0 within their experimental error.

TABLE 1

Values of the parameters which fit the low-energy data

β/α	γ/α	P_D in %	t	$(a\alpha)^{-1}$	$r_0\alpha$
5.7	5.8	2.8553	0.5593	0.7973	0.4056
5.8	6	3.0860	0.7541	0.8011	0.3970
6 †	5.5	2.6184	0.3154	0.8056	0.3879
6	5.7	2.8037	0.4589	0.8035	0.3936
6.1 †	5.3	2.4625	0.1957	0.8082	0.3814

† Do not fit the data.

It may be seen from table 1 that the "acceptable" values of β and γ seem to lie in rather small ranges, viz. $5.7\alpha \leqq \beta \leqq 6.0\alpha$ and $5.8\alpha \leqq \gamma \leqq 6.0\alpha$. The variation of P_D is also particularly narrow, being 2.8 % to 3.08 % for the "allowed" parameters. This result is definitely smaller than the 4 % value that is generally assumed for P_D. On the other hand, it is larger than the value obtained by Newton and Scofield [12]), viz. 1.37 %, to fit Q and $\Delta\mu$. As for the mixing ratio t of the tensor to the central force, it is seen to vary from 0.75 to 0.46. These limits, as expected, are considerably smaller than the value 1.78 obtained by Yamaguchi, who did not invoke the spin-orbit force and had to depend entirely on the tensor force for fitting the data. It thus seems that the presence of the spin-orbit force changes the picture of the interaction substantially: one needs both types of forces in comparable amounts.

An interesting feature of the proposed interaction may be noted. Numerical evaluation shows that the quadrupole moment arises almost entirely from the tensor interaction (terms proportional to N_0^2), the contributions from the spin-orbit ($\propto N_2^2$) and interference terms ($\propto N_0 N_2$) being much smaller. On the other hand, the magnetic moment contribution comes mainly from the spin-orbit force, tensor force effects being almost negligible. A neat separation between the functions of the tensor and spin-orbit forces is thus effected †.

† It is not yet clear if the same result would hold for the general case of $\gamma \neq \delta$, since the numerical figures are based only on the equality of these parameters.

This feature facilitates separate adjustments for each of these two forces to fit either moment without affecting the other.

Work on high energy n−p and p−p scattering and polarization with the above potential is in progress.

6. The Spin-Orbit Splitting in Nuclei

The results of the last few sections can now be applied to calculate the spin-orbit splitting in "doubly closed shell plus or minus one" nuclei in the lowest order Born approximation. Since the procedure has been already outlined by Kisslinger [5]) and subsequently by Nigam and Sundaresan[6]) (referred to as NS) we shall try here to omit as many details (including notational ones) as possible.

Let $\mathbf{k}_1$, $\mathbf{k}_2$ and $\mathbf{k}'_1$, $\mathbf{k}'_2$ be the momenta of the two particles before and after scattering and let $\mathbf{p}$, $\mathbf{p}'$ be the corresponding C.M. momenta. Then

$$2\mathbf{p} = \mathbf{k}_1 - \mathbf{k}_2, \quad 2\mathbf{p}' = \mathbf{k}'_1 - \mathbf{k}'_2 \tag{6.1}$$

and the V-matrix is given by

$$(\mathbf{p}|V|\mathbf{p}') = -\frac{\lambda}{M} g(\mathbf{p}) g(\mathbf{p}') - \left(\frac{5\lambda_2}{M}\right) v_2(p) v_2(p') \times (\mathbf{L}_p \cdot \mathbf{S}) P_2(\hat{p} \cdot \hat{p}'). \tag{6.2}$$

The element of the V-matrix in the (k_1, k_2) representation is given by

$$(\mathbf{k}_1 \mathbf{k}_2 | V | \mathbf{k}'_1 \mathbf{k}'_2) = \delta^3(\mathbf{K} - \mathbf{K}')(\mathbf{p}|V|\mathbf{p}') \tag{6.3}$$

where

$$\mathbf{K} = \mathbf{k}_1 + \mathbf{k}_2, \quad \mathbf{K}' = \mathbf{k}'_1 + \mathbf{k}'_2. \tag{6.4}$$

The sum of the spin-orbit energies arising from the two-body tensor and spin-orbit forces may now be written as

$$\begin{aligned} E_T + E_{LS} = \sum_c \int \psi_0^*(\mathbf{k}_1) \psi_c^*(\mathbf{k}_2) (\mathscr{I}_T + \mathscr{I}_{LS}) \\ \times \psi_0(\mathbf{k}'_1) \psi_c(\mathbf{k}'_2) d^3\mathbf{k}_1 d^3\mathbf{k}_2 d^3\mathbf{k}'_1 d^3\mathbf{k}'_2 \end{aligned} \tag{6.5}$$

where $\sum_c$ represents a summation over the core particles 2 and $\mathscr{I}_T$ and $\mathscr{I}_{LS}$ represent the contributions from the two-body tensor and spin-orbit forces respectively. These are given by

$$\begin{aligned} \mathscr{I}_T(\mathbf{p}, \mathbf{K}; \mathbf{p}', \mathbf{K}') = -\frac{27i\lambda}{16M} T(p) T(p') p^{-2} p'^{-2} \\ \times (\mathbf{p} \cdot \mathbf{p}')(\boldsymbol{\sigma}_1 \cdot \mathbf{p} \times \mathbf{p}') \delta^3(\mathbf{K} - \mathbf{K}') \end{aligned} \tag{6.6}$$

and

$$\mathscr{I}_{LS}(\mathbf{p}, \mathbf{K}; \mathbf{p}', \mathbf{K}') = -\frac{15\lambda_2}{4M} v_2(p) v_2(p') \times (\mathbf{L}_p \cdot \boldsymbol{\sigma}_1) P_2(\hat{p} \cdot \hat{p}') \delta^3(\mathbf{K} - \mathbf{K}') \tag{6.7}$$

Eq. (6.6) has already been derived by NS. The derivation of (6.7) is quite straightforward. A factor $\frac{3}{4}$ has been included in each of (6.6) and (6.7) to represent the 'weight' of the triplet spin-states which alone make a contribution in this regard. Since E_T has already been worked out by NS it need not be recalculated here. We shall now briefly indicate the steps leading to the final expression for E_{LS} only.

Introducing the spatial functions $\psi_c^*(\mathbf{r}_1)$, $\psi_c(\mathbf{r}_2)$ according to the normalizations

$$\begin{aligned}\psi_c^*(\mathbf{k}_2) &= (2\pi)^{-\frac{3}{2}}\int e^{i\mathbf{k}_2\cdot\mathbf{r}_1}\,\psi_c^*(\mathbf{r}_1)d^3\mathbf{r}_1,\\ \psi_c(\mathbf{k}'_2) &= (2\pi)^{-\frac{3}{2}}\int e^{-i\mathbf{k}_2\cdot\mathbf{r}'_2}\psi_c(\mathbf{r}_2)d^3\mathbf{r}_2,\end{aligned} \tag{6.8}$$

and the variables $\mathbf{r}$, $\mathbf{R}$ defined by

$$2\mathbf{R} = \mathbf{r}_1+\mathbf{r}_2, \quad \mathbf{r} = \mathbf{r}_1-\mathbf{r}_2, \tag{6.9}$$

we obtain

$$E_{LS}=-(2\pi)^{-3}\frac{15\lambda_2}{4M}\int\psi_0^*(\mathbf{k}_1)\rho(R)e^{i\mathbf{R}\cdot\mathbf{k}}\psi_0(\mathbf{k}'_1)I_{LS}(\mathbf{k}_1,\mathbf{k}'_1)d^3\mathbf{k}_1d^3\mathbf{k}'_1d^3\mathbf{R} \tag{6.10}$$

where

$$I_{LS} = \int d^3\mathbf{r}d^3\mathbf{k}_2e^{-\alpha r^2+i\mathbf{r}\cdot\mathbf{k}_1-2i\mathbf{r}\cdot\mathbf{p}}e^{-\frac{1}{2}i\mathbf{r}\cdot\mathbf{k}}v_2(p)v_2(p')(\boldsymbol{\sigma}_1\cdot\mathbf{L}_p)P_2(\hat{p}\cdot\hat{p}') \tag{6.11}$$

$$\mathbf{k} = \mathbf{k}'_1-\mathbf{k}_1, \tag{6.12}$$

and following Kisslinger, $\sum_c\psi_c^*(\mathbf{r}_1)\psi_c(\mathbf{r}_2)$ has been approximated as

$$\begin{aligned}\sum_c\psi_c^*(\mathbf{r}_1)\psi_c(\mathbf{r}_2) &= \rho(R)e^{-\alpha r^2},\\ \alpha = 4.61/R_0^2, \quad R_0 &= 1.18\times10^{-13}A^{\frac{1}{3}}\text{ cm}.\end{aligned} \tag{6.13}$$

It may be noted that in passing from (6.5) and (6.7) to (6.10) and (6.11), integration over $\mathbf{k}'_2$ has been carried out with the help of $\delta^3(\mathbf{K}-\mathbf{K}') = \delta^3(\mathbf{k}_1+\mathbf{k}_2-\mathbf{k}'_1-\mathbf{k}'_2)$. The integration over $\mathbf{k}_2$ in (6.11) with $\mathbf{k}_1$ fixed, can now be transformed into one over $\mathbf{p}$, according to the relation †

$$d^3\mathbf{k}_2 \equiv 8d^3\mathbf{p}. \tag{6.14}$$

Further, because of the rapid fluctuations of the factor $\exp(-\frac{1}{2}i\mathbf{k}\cdot\mathbf{r})$ in (6.11) for large $\mathbf{k}$, only small values of $\mathbf{k}$ are significant and the integrand may be expanded in powers of k. To simplify

$$\mathscr{F}(k) = e^{-\frac{1}{2}i\mathbf{r}\cdot\mathbf{k}}v_2(p)v_2(p')(\boldsymbol{\sigma}_1\cdot\mathbf{L}_p)P_2(\hat{p}\cdot\hat{p}'), \tag{6.15}$$

† In the calculation of NS the factor 8 of eq. (6.14) was replaced by -2, which explains the erroneous factor $\frac{2}{3}$ in their eq. (6) instead of the correct one -18. Private communication from these authors has confirmed this remark.

it is most convenient to change the variables from $\mathbf{p}$, $\mathbf{p}'$ to $\mathbf{p}$, $\mathbf{k}$ where $\mathbf{p}' = \mathbf{p}+\mathbf{k}$, so that

$$\boldsymbol{\nabla}_p \to \boldsymbol{\nabla}_p - \boldsymbol{\nabla}_k \quad \text{and} \quad \boldsymbol{\nabla}_{p'} \to \boldsymbol{\nabla}_k, \tag{6.16}$$

with the help of which the operator $\mathbf{L}_p \equiv +i\mathbf{p}\times\boldsymbol{\nabla}_p$† may be easily transformed. Substitution of (6.16) in (6.15) and straightforward simplification gives

$$\mathscr{F}(k) \approx +3ip^{-2}[(\mathbf{p}\times\mathbf{k})\cdot\boldsymbol{\sigma}_1]v_2^2(p)+\mathrm{O}(k^2). \tag{6.17}$$

Using (6.17) and (6.14) in (6.11), we obtain

$$I_{LS} \approx 8\int \mathrm{d}^3\mathbf{r}\mathrm{d}^3\mathbf{p}\,\exp(-\alpha r^2+i\mathbf{r}\cdot\mathbf{k}_1-2i\mathbf{r}\cdot\mathbf{p})\times 3ip^{-2}[(\mathbf{p}\times\mathbf{k})\cdot\boldsymbol{\sigma}_1]v_2^2(p). \tag{6.18}$$

Carrying out the angular integrations in (6.18), it can, with some manipulations after NS, be finally brought into the form

$$I_{LS} = 24i[\boldsymbol{\sigma}_1\cdot(\mathbf{k}_1\times\mathbf{k})]J(k_1), \tag{6.19}$$

where

$$\begin{aligned} J(k_1) = 16\pi^2\int_0^1 \mathrm{d}x\int_0^\infty \mathrm{d}y\,\exp\left(-\frac{\alpha y^2}{k_1^2}\right)\cdot\left(\frac{xy^2}{k_1^2}\right) \\ \times v_2^2(xk_1)\,\frac{\mathrm{d}}{\mathrm{d}y}\left(\frac{\sin y}{y}\right)\frac{\mathrm{d}}{\mathrm{d}(2xy)}\left(\frac{\sin 2xy}{2xy}\right), \end{aligned} \tag{6.20}$$

$$x = \frac{p}{k_1}, \quad y = k_1 r.$$

Eq. (6.20) has been evaluated numerically for $A = 16$ and 40 by taking the extra nucleon at the top of the Fermi-distribution, so that $k_1 \approx k_F$ where k_F is given by [13])

$$k_F = 1.524/(1.18\times 10^{-13})\ \mathrm{cm}^{-1}. \tag{6.21}$$

For a calculation of the level splitting of the extra nucleon at the top of the Fermi-distribution, we now take, in keeping with our earlier normalization,

$$\begin{aligned} \psi_0(\mathbf{k}_1') &= (k'_1)^{-\frac{1}{2}}\delta(k'_1-k_F)Y_{lm}(\hat{k}'_1), \\ \psi_0^*(\mathbf{k}_1) &= (k_1)^{-\frac{1}{2}}\delta(k_1-k_F)Y_{lm}^*(\hat{k}_1). \end{aligned} \tag{6.22}$$

Substituting (6.19) in (6.10) and using the relation

$$\begin{aligned} i\int[(\boldsymbol{\sigma}_1\times\mathbf{k}_1)\cdot\mathbf{k}'_1]\psi_0^*(\mathbf{k}_1)\mathrm{e}^{i\mathbf{R}\cdot\mathbf{k}}\rho(R)\psi_0(\mathbf{k}'_1)\mathrm{d}^3\mathbf{k}_1\mathrm{d}^3\mathbf{k}'_1\mathrm{d}^3\mathbf{R} \\ = (2\pi)^3\int\psi_0^*(\mathbf{R})\left(\frac{1}{R}\frac{\mathrm{d}\rho}{\mathrm{d}R}\right)(\boldsymbol{\sigma}_1\cdot\mathbf{L}_R)\psi_0(\mathbf{R})\mathrm{d}^3\mathbf{R}, \end{aligned} \tag{6.23}$$

† The positive sign before i comes about because $\mathbf{L}_p$ operates from the *left*, as has been mentioned already in section 2.

where $\mathbf{L}_R \equiv \mp i\mathbf{R}\times\boldsymbol{\nabla}_R$ (for right or left operations) and

$$\psi_0(\mathbf{R}) = (2\pi)^{-\frac{3}{2}}\int \psi_0(\mathbf{k'}_1)e^{i\mathbf{k'}_1\cdot\mathbf{R}}\,d^3\mathbf{k'}_1, \tag{6.24}$$

we obtain

$$E_{LS} = -\frac{15\lambda_2}{4M}\ 24\ J(k_F)\int \psi_0^*(\mathbf{R})\left(\frac{1}{R}\frac{d\rho}{dR}\right)(\boldsymbol{\sigma}_1\cdot\mathbf{L}_R)\psi_0(\mathbf{R})d^3\mathbf{R}. \tag{6.25}$$

Finally, substituting for $\psi_0(\mathbf{R})$ from (6.22) and (6.24) in (6.25), the energy level due to the two-body spin-orbit force works out to be

$$E_{LS} = -\frac{90\lambda_2}{M}J(k_F)\langle\boldsymbol{\sigma}\cdot\mathbf{L}\rangle F_l(R_0), \tag{6.26}$$

where

$$F_l(R_0) = \frac{\int_0^{R_0} j_l^2(k_F R)\frac{d\rho}{dR}R\,dR}{\int_0^{R_0} j_l^2(k_F R)R^2\,dR}. \tag{6.27}$$

In deriving (6.26) and (6.27) we have used the reduction factor

$$\frac{\int_0^\infty j_l^2(k_F R)R^2\,dR}{\int_0^{R_0} j_l^2(k_F R)R^2\,dR} = \tfrac{1}{2}\pi k_F^{-3}\left[\int_0^{R_0} j_l^2(k_F R)R^2\,dR\right]^{-1}, \tag{6.28}$$

to take care of the fact that the integration over R in the numerator of (6.27) extends only upto R_0, so that the denominator must also be correspondingly modified. It may be noted that in (6.26) $\lambda_2 < 0$ and so is $F_l(R_0)$ since $d\rho/dR<0$. Therefore it is clear that the state $j = l+\frac{1}{2}$, for which $\langle\boldsymbol{\sigma}\cdot\mathbf{L}\rangle$ is $(l+1)$, has the *lower energy*, as desired.

As for the tensor force contribution, it can be worked out, as in NS, to give

$$E_T = -\frac{27\lambda t^2}{2M}\langle\boldsymbol{\sigma}\cdot\mathbf{L}\rangle J_T(k_F)F_l(R_0), \tag{6.29}$$

where $F_l(R_0)$ is the same as in (6.26) and $J_T(k_F)$ is similar to (6.20) except for the replacement of $v_2(k_1x)$ by $-t^{-1}T(k_1x)$. In particular, for the special case of $\gamma = \delta$ that we have considered in sec. 5,

$$J_T(k_F) = J(k_F). \tag{6.30}$$

It may be noted that in (6.29) λ is positive and $F_l(R_0)$ is negative, so that E_T is positive for $j = l+\frac{1}{2}$. This shows that the tensor force by itself gives the *wrong* sign for the energy splitting. This result is in disagreement with that of NS and also of Kisslinger. The disagreement with NS, who also used the Yamaguchi potential, is of course due to an error in sign in their calculation (as pointed out in the footnote on p. 421).

The integral $F_l(R_0)$ has been evaluated with the help of the density curves for $\rho(R)$ that have been plotted by Kisslinger for the cases $A = 16$ and 40. The following values of the parameters have been taken for both $F_l(R_0)$ and $J(k_F)$:

$$\begin{aligned} &\beta = 5.8\alpha, \qquad \gamma = 6.0\alpha, \qquad t = 0.75, \\ &\lambda = 24.1\alpha^3, \quad \lambda_2 = -20.1\alpha^3, \quad P_D = 3.08\ \%. \end{aligned} \tag{6.31}$$

These values have been applied to the evaluation of the energy splitting ($E_{l+\frac{1}{2}}$ minus $E_{l-\frac{1}{2}}$, algebraically) to the nuclei O^{17} and Ca^{41}. The results for the tensor and spin-orbit contributions (with proper signs) to the energy splitting are shown in table 2 which also includes the experimental information and the calculations of Nigam and Sundaresan [7]) based on the Signell-Marshak potential.

TABLE 2

Spin-orbit splittings (in MeV) in the nuclei O^{17} and Ca^{41}

	Calculated			Observed	From Signell-Marshak potential
	Spin-orbit	Tensor	Total		
Ca^{41}, $l = 1$	2.6	−0.3	2.3	1.0	0.36
Ca^{41}, $l = 3$	6.8	−0.7	6.1	6.0	1.06
O^{17}, $l = 2$	4.8	−0.5	4.3	5.1	0.78

It may be seen from this table that the tensor contribution is much smaller than ($\approx 10\ \%$) and of opposite sign to, the spin-orbit contribution. The agreement with observation is rather good, the negative tensor contributions having generally improved matters. The results seem to be definitely better than those from the Signell-Marshak potential †.

It may be noted that though these splittings were worked out in the first order perturbation theory, the results are not likely to be much modified by using the exact T-matrix, since our potential does not have any singularities. On the other hand, calculation of the T-matrix in the presence of nuclear matter involves knowledge of many-body parameters like the effective mass and the Fermi momentum, which have still to be worked out in our present formalism ††. Qualitatively, at least, it may be emphasized that the tensor force by itself definitely gives the wrong sign for the energy splitting, and only

† Drs Nigam and Sundaresan have informed us that, as in their first paper [6]), the figures for the splitting given in ref. [7]) should be multiplied by 4, thus bringing agreement with observation substantially closer. However, even such an agreement is partially offset by the negative tensor contribution which must also be included.

†† The T-matrix of sec. 4, which was worked out for scattering of two *free* particles, is not applicable to the many-body problem.

the two-body spin-orbit force seems to save the situation. This result appears to be in harmony with some conclusions [14]) that the tensor force gives a low-energy spin-orbit force of the wrong sign, which is overcompensated by the actual spin-orbit force between nucleons. We regard this result of ours as a more compelling reason to invoke a direct two-body spin-orbit force than the more fact of the tensor force giving a numerically small contribution to the splitting.

We are grateful to Dr. S. P. Pandya for going through the manuscript and making useful suggestions. We are also indebted to Professor P. S. Gill for his interest in this work.

Appendix 1

We discuss here the extraction of the contribution to the magnetic moment of the deuteron from a potential of the type

$$(\mathbf{p}|v|\mathbf{p}') = -\frac{4\pi\lambda_2}{M} v_2(p)v_2(p')(\mathbf{L}_p \cdot \mathbf{S}) \sum_m Y^*_{2m}(\hat{p})Y_{2m}(\hat{p}'). \tag{A1.1}$$

The co-ordinate transform of (A1.1) is

$$(\mathbf{r}|v|\mathbf{r}') = -\frac{4\pi\lambda_2}{M} R_2(r)R_2(r')(\mathbf{L}_r \cdot \mathbf{S}) \sum_m Y^*_{2m}(\hat{r})Y_{2m}(\hat{r}'), \tag{A1.2}$$

where $\mathbf{L}_r$ operates on $\hat{r}$ alone, and

$$R_2(r) = \left(\frac{2}{\pi}\right)^{\frac{1}{2}} \int_0^\infty p^2 \mathrm{d}p j_2(pr)v_2(p). \tag{A1.3}$$

Now,

$$\mathbf{S} \cdot \mathbf{L} = \tfrac{1}{2}\mathbf{S} \cdot \mathbf{r} \times (\mathbf{p}_1 - \mathbf{p}_2) = \tfrac{1}{2}(\mathbf{S} \times \mathbf{r}) \cdot (\mathbf{p}_1 - \mathbf{p}_2), \tag{A1.4}$$

where $\mathbf{p}_1$ and $\mathbf{p}_2$ stand for the proton and neutron respectively, and $\mathbf{r} = \mathbf{r}_1 - \mathbf{r}_2$. The electromagnetic interaction is now introduced by the replacement $\mathbf{p}_1 \to \mathbf{p}_1 - (e/c)\mathbf{A}$, so that the additional Hamiltonian is

$$\frac{2\pi e\lambda_2}{M\hbar c} R_2(r)R_2(r') \sum_m Y^*_{2m}(\hat{r})Y_{2m}(\hat{r}')(\mathbf{S} \times \mathbf{r}) \cdot \mathbf{A}. \tag{A1.5}$$

Substituting $\mathbf{A} = -\frac{1}{2}\mathbf{r}_1 \times \mathbf{H}$ for a constant magnetic field $\mathbf{H}$ and expressing the result in the form $-\Delta\boldsymbol{\mu} \cdot \mathbf{H}$, the magnetic moment operator is deduced from (A1.5) to be

$$(\mathbf{r}|\Delta\boldsymbol{\mu}_{LS}|\mathbf{r}') = \frac{\pi e\lambda_2}{2\hbar cM} R_2(r)R_2(r') \times \sum_m Y^*_{2m}(\hat{r})Y_{2m}(\hat{r}')[(\mathbf{S} \times \mathbf{r}) \times \mathbf{r}]. \tag{A1.6}$$

The expectation value of the component (A1.6) in the direction **J** with respect to the deuteron state $\psi(\mathbf{r})$ is

$$\Delta\mu_{LS} = \int \psi^*(\mathbf{r})(\mathbf{r}|\Delta\boldsymbol{\mu}_{LS}\cdot\mathbf{J}/j(j+1)|\mathbf{r}')\psi(\mathbf{r}')\mathrm{d}^3\mathbf{r}\mathrm{d}^3\mathbf{r}'. \tag{A1.7}$$

Eq. (A1.7) must now be changed back to the momentum representation. The connection between the co-ordinate and momentum wave functions is

$$\psi(\mathbf{r}) = (2\pi)^{-\frac{3}{2}}\int \mathrm{e}^{i\mathbf{p}\cdot\mathbf{r}}\psi(\mathbf{p})\mathrm{d}^3\mathbf{p}, \tag{A1.8}$$

and the corresponding relation between the matrix elements of any operator A is

$$(\mathbf{p}|A|\mathbf{p}') = (2\pi)^{-3}\int \mathrm{e}^{-i\mathbf{p}\cdot\mathbf{r}+i\mathbf{p}'\cdot\mathbf{r}'}(\mathbf{r}|A|\mathbf{r}')\mathrm{d}^3\mathbf{r}\mathrm{d}^3\mathbf{r}'. \tag{A1.9}$$

Substituting (A1.3), (A1.6), (A1.8) and (A1.9) in (A1.7) and noting that $j = 1$, we have finally

$$\begin{aligned}\Delta\mu_{LS} = {} & \frac{\pi e\lambda_2}{4M\hbar c}\int \psi^*(\mathbf{p})[\nabla_p{}^2(\mathbf{S}\cdot\mathbf{J}) - (\boldsymbol{\nabla}_p\cdot\mathbf{S})^2]v_2(p)v_2(p') \\ & \times \sum_m Y^*_{2m}(\hat{p})Y_{2m}(\hat{p}')\psi(\mathbf{p}')\mathrm{d}^3\mathbf{p}\mathrm{d}^3\mathbf{p}'.\end{aligned} \tag{A1.10}$$

Integration over $\mathbf{p}'$ in (A1.10) is trivial and gives

$$\int v_2(p')\sum_m Y^*_{2m}(\hat{p})Y_{2m}(\hat{p}')\psi(\mathbf{p}')\mathrm{d}^3\mathbf{p}' = \mathscr{Y}^M_{121}(\hat{p})\mathscr{A}, \tag{A1.11}$$

where the results and notations of section 3 have been used and $\mathscr{A}$ is defined by eq. (3.22) of the text.

For the **p**-integration in (A1.10), we encounter

$$\int w(p)\mathscr{Y}^{M*}_{121}[\nabla_p{}^2(\mathbf{S}\cdot\mathbf{J}) - (\boldsymbol{\nabla}_p\cdot\mathbf{S})^2]v_2(p)\mathscr{Y}^M_{121}(\hat{p})\mathrm{d}^3\mathbf{p}. \tag{A1.12}$$

We now make a partial integration in the second term of (A1.12) and use the following result obtained by the techniques of ref. [9])

$$(\mathbf{S}\cdot\boldsymbol{\nabla}_p)v_2(p)\mathscr{Y}^M_{121} = (24)^{\frac{1}{2}}W(1211;11)\left(\frac{\mathrm{d}v_2}{\mathrm{d}p} + \frac{3}{p}v_2\right)\mathscr{Y}^M_{111}, \tag{A1.13}$$

where, in the notation of ref. [9]), $W(1211; 11)$ is a Racah coefficient having the value $-\frac{1}{6}$. Further,

$$\nabla_p{}^2 v_2(p)\mathscr{Y}^M_{121} = \left[\frac{1}{p^2}\frac{\mathrm{d}}{\mathrm{d}p}\left(p^2\frac{\mathrm{d}v_2}{\mathrm{d}p}\right) - \frac{6v_2}{p^2}\right]\mathscr{Y}^M_{121}, \tag{A1.14}$$

and

$$(\mathbf{S}\cdot\mathbf{J})\mathscr{Y}^M_{121} = -\mathscr{Y}^M_{121}, \tag{A1.15}$$

for the deuteron state. The expression (A1.12) is now immediately evaluated with the help of these relations. Substituting (A1.11) and (A1.12) in (A1.10) one finally arrives at eq. (3.21) of the text.

Appendix 2

We give here a list of integrals appearing in the text.

$$I_{11} = \frac{\pi^2}{\beta(\beta+\alpha)^2} + \frac{\pi^2 t^2(\gamma^2+4\alpha\gamma+5\alpha^2)}{8\gamma(\gamma+\alpha)^4}$$

$$I_{12} = -\pi^2 t(\gamma+\delta)^{-3}(\alpha+\gamma)^{-2}(\alpha+\delta)^{-2}[\alpha^2(\gamma^2+\delta^2+3\gamma\delta)+2\alpha\gamma\delta(\gamma+\delta)+\gamma^2\delta^2]$$

$$I_{22} = \tfrac{1}{8}\pi^2\delta^{-1}(\alpha+\delta)^{-4}(\delta^2+4\alpha\delta+5\alpha^2)$$

$$J_{00} = \tfrac{1}{4}\pi(\alpha\beta)^{-1}(\alpha+\beta)^{-3}$$

$$J_{11} = \tfrac{1}{32}\pi t^2\gamma^{-1}(\alpha+\gamma)^{-5}(\gamma+5\alpha)$$

$$J_{22} = \tfrac{1}{32}\pi\delta^{-1}(\alpha+\delta)^{-5}(\delta+5\alpha)$$

$$J_{12} = -\tfrac{1}{4}\pi t(\gamma+\delta)^{-3}(\alpha+\gamma)^{-3}(\alpha+\delta)^{-3}\times[\alpha^2(\gamma^2+\delta^2+3\gamma\delta)+3\alpha\gamma\delta(\gamma+\delta)+\gamma^2\delta^2]$$

$$\zeta_k = 2i\pi^2 k(C_k{}^2+T_k{}^2)+\pi^2\beta^{-1}(k^2+\beta^2)^{-1}[2\beta^2(k^2+\beta^2)^{-1}-1] - \frac{\pi^2 t^2}{4\gamma(k^2+\gamma^2)}\left[\frac{5}{2}-\frac{15\gamma^2}{k^2+\gamma^2}+\frac{20\gamma^4}{(k^2+\gamma^2)^2}-\frac{8\gamma^6}{(k^2+\gamma^2)^3}\right]$$

$$\eta_k = 2\pi^2 ikv_k T_k+\pi^2 t(\delta^2-\gamma^2)^{-2}\mathscr{F}(k,\gamma,\delta),$$

$$\mathscr{F}(k,\gamma,\delta) = \left[\frac{\gamma^3}{k^2+\gamma^2}\left(5-\frac{2\gamma^2}{k^2+\gamma^2}+\frac{4\gamma^2}{\delta^2-\gamma^2}\right)+\frac{\delta^3}{k^2+\delta^2}\left(5-\frac{2\delta^2}{k^2+\delta^2}+\frac{4\delta^2}{\gamma^2-\delta^2}\right)\right]$$

$$\zeta_k = 2\pi^2 ikv_k{}^2-\tfrac{1}{4}\pi^2\delta^{-1}(k^2+\delta^2)^{-1}g(k,\delta),$$

$$g(k,\delta) = \left[\frac{5}{2}-\frac{15\delta^2}{k^2+\delta^2}+\frac{20\delta^4}{(k^2+\delta^2)^2}-\frac{8\delta^6}{(k^2+\delta^2)^3}\right].$$

Appendix 3

We list here a few trace relations used in section 4 of the text.

$$\mathrm{Tr}\,\rho S(\hat{p}) = 0, \quad \mathrm{Tr}\,\rho S(\hat{p})S(\hat{k}) = 24P_2(\hat{p}\cdot\hat{k})$$

$$\mathrm{Tr}\,\rho S^2(\hat{p}) = 24;$$

$$\mathrm{Tr}\,\rho S(\hat{p})S^2(\hat{k}) = -48P_2(\hat{p}\cdot\hat{k})$$

$$\mathrm{Tr}\,\rho S^2(\hat{p})S^2(\hat{k}) = 192(1+\tfrac{1}{2}P_2)$$

$$\mathrm{Tr}\,\rho S(\hat{k})(a+b(\mathbf{L}\cdot\mathbf{S})+c(\mathbf{L}\cdot\mathbf{S})^2) = -\tfrac{2}{3}cL^2;$$

$$\mathrm{Tr}\,\rho(\mathbf{L}\cdot\mathbf{S})S(\hat{p})S(\hat{k}) = 0;$$

$$\mathrm{Tr}\,\rho(\mathbf{L}\cdot\mathbf{S})^2S(\hat{p})S(\hat{k}) = 12P_2L^2-18[(\hat{\mathbf{p}}\times\hat{\mathbf{k}})\cdot\mathbf{L}]^2+8L^2.$$

$$\mathrm{Tr}\,\rho(\mathbf{L}'\cdot\mathbf{S})(\mathbf{L}\cdot\mathbf{S}) = 2(\mathbf{L}\cdot\mathbf{L}').$$

$$\mathrm{Tr}\,\rho(\mathbf{L}'\cdot\mathbf{S})(\mathbf{L}\cdot\mathbf{S})^2 = -(\mathbf{L}\cdot\mathbf{L}')$$

$$\mathrm{Tr}\,\rho(\mathbf{L}'\cdot\mathbf{S})^2(\mathbf{L}\cdot\mathbf{S})^2 = L^2L'^2+(\mathbf{L}\cdot\mathbf{L}')^2+\tfrac{1}{2}(\mathbf{L}\cdot\mathbf{L})$$

$$(\mathbf{p}\times\mathbf{k}\cdot\mathbf{L})^2P_l(\cos\theta) = l(l+1)\sin^2\theta\,P_l(\cos\theta),$$

where $\cos\theta = \hat{p}\cdot\hat{k}$.

References

1) J. Gammel and R. Thaler, Phys. Rev. **107** (1957) 1337
2) P. Signell and R. Marshak, Phys. Rev. **109** (1957) 1229
3) H. Feshbach, Phys. Rev. **107** (1957) 1626
4) P. Signell and R. Marshak, Nuovo Cimento **6** (1957) 1189
5) L. S. Kisslinger, Phys. Rev. **104** (1956) 1077
6) B. P. Nigam and M. K. Sundaresan, Canadian J. Phys. **36** (1958) 571
7) B. P. Nigam and M. K. Sundaresan, Phys. Rev. **111** (1958) 284
8) Y. Yamaguchi, Phys. Rev. **95** (1954) 1635
9) M. E. Rose, Elementary Theory of Angular Momentum (John Wiley and Sons, New York, 1957)
10) J. Blatt and Weisskopf, Theoretical Nuclear Physics (John Wiley and Sons, New York, 1952)
11) S. M. Vaidya, Nuclear Physics **5** (1958) 179
12) R. Newton and J. Scofield, Phys. Rev. **110** (1958) 785
13) H. A. Bethe, Phys. Rev. **103** (1956) 1353
14) H. A. Bethe, Proc. Pittsburgh Conf. on Nuclear Structure (Pittsburgh Univ., 1957)

1.B:2.L *Nuclear Physics* **14** (1959/60) 429—437; © *North-Holland Publishing Co., Amsterdam*
Not to be reproduced by photoprint or microfilm without written permission from the publisher

LOW ENERGY ELASTIC SCATTERING OF NUCLEONS BY DEUTERONS

SHIGUEO WATANABE †
Palmer Physical Laboratory, Princeton University ††

Received 15 August 1959

Abstract: The elastic scattering of nucleons by deuterons at low energies is discussed. The interaction forces between two nucleons include the central exchange and spin-orbit ones. The inclusion of the two-body spin-orbit force leads to a set of coupled integro-differential equations.

1. Introduction

Several authors [1]) have discussed the elastic nucleon-deuteron scattering at low energies. They have used a two-body potential with central part only which contains the exchange forces. Since some measurements on the polarization [2]) of elastically scattered nucleons at low energies are becoming available it is interesting to include forces able to produce nucleons polarization. In a recent paper Bransden *et al.* [3]) have derived the coupled integro-differential equations which result from the addition of two-body tensor forces to the central ones; the numerical results have not been published yet. It is also interesting to investigate the effect of the two-body spin-orbit force [4]). It is the main purpose of this paper to carry out such an investigation.

In section 2 a set of coupled radial integro-differential equations, resulting from the inclusion of exchange forces, the spin-orbit force and the exclusion principle, is derived. In section 3 the specification to the Yukawa shape for both central and spin-orbit forces is considered. The method for solving coupled integro-differential equations of the form derived in this paper and the subsequent numerical results will be presented in a future paper.

2. Radial Equation

For definiteness let us take the proton-deuteron scattering. The incoming proton will be labelled with 3, the proton in the deuteron with 1 and the neutron with 2. Let

$$\boldsymbol{\varrho} = \mathbf{r}_1 - \mathbf{r}_2, \quad \mathbf{r} = \tfrac{1}{2}(\mathbf{r}_1 + \mathbf{r}_2) - \mathbf{r}_3. \tag{2.1}$$

† Guggenheim Fellow and on leave of absence from University of São Paulo, São Paulo, Brazil. Present address: Department of Physics, University of Washington, Seattle, Washington. This work was initiated when the author was a fellow of the National Research Council of Brazil.

†† This work was supported in part by the U. S. Atomic Energy Commission and The Higgins Scientific Trust Fund.

The wave equation is

$$\left\{\sum_{i=1}^{3} T_i+\sum_{i>j}\mathscr{V}(ij)+\frac{e^2}{r_{13}}+\hbar^{-2}\sum_{i>j}J(r_{ij})\mathbf{l}_{ij}\cdot\mathbf{s}_{ij}-E_0-E_d\right\}\Psi(123)=0 \quad (2.2)$$

where

$$\mathbf{s}_{ij}=\mathbf{s}_i+\mathbf{s}_j;\quad \mathbf{l}_{ij}=\tfrac{1}{2}(\mathbf{r}_i-\mathbf{r}_j)\times(\mathbf{p}_i-\mathbf{p}_j);$$

T_i is the kinetic energy operator of the particle i, $\mathscr{V}(ij)$ the central interaction potential between the particles i and j and it is given by

$$\mathscr{V}(ij)=V(r_{ij})(w+bP_{\mathrm{B}}{}^{ij}+mP_{\mathrm{M}}{}^{ij}+hP_{\mathrm{H}}{}^{ij}), \quad (2.3)$$

P_{B}, P_{M} and P_{H} being Bartlett, Majorana and Heisenberg exchange operators, respectively; w, b, m and h are constants normalized to

$$w+b+m+h=1$$

and they satisfy the relation $x=m-h+w-b$, where $x=0.6$ is the ratio of the singlet and the triplet central interactions between neutron and proton, in an even state; E_d is the deuteron binding energy and E_0 the incident proton energy in the centre of mass system ($E_0=\frac{2}{3}E_{\mathrm{lab}}$).

We shall consider only the S-state component of the deuteron ground state. The set of commuting operators is J^2, J_z and the parity operator. The properly symmetrized wave function is

$$\Psi(123)=(1-P_{\mathrm{H}}{}^{13})\psi(3,12); \quad (2.4)$$

$\psi(3, 12)$ can be expanded into eigenfunctions of the above set of operators:

$$\psi(3,12)=\sum_{J,M,l,\pi}\psi_{JM}^{l\pi}(3,12)\quad (J_z\equiv M) \quad (2.5)$$

with

$$\begin{aligned}\psi_{JM}^{l\pi}(3,12)=\sum_{\alpha=1}^{2}\Bigg\{&\frac{1}{r}F_{JM}^{l\alpha}(r)\mathscr{Y}_M^{Jl\alpha}(3,12)\psi_0(\rho)\\&+\int\frac{1}{r}F_{JMk'}^{l\alpha}(r)\mathscr{Y}_M^{Jl\alpha}(3,12)\psi_{k'}^{t}(\rho)\mathrm{d}k'\Bigg\}+\int\frac{1}{r}F_{JMk''}^{l\beta}(r)X_M^{Jl\beta}(3,12)\psi_{k''}^{s}(\rho)\mathrm{d}k''\end{aligned} \quad (2.6)$$

where

$$\mathscr{Y}_M^{Jl\alpha}(3,12)=\sum_{mm_\alpha}\begin{bmatrix}l & S_\alpha & J\\ m & m_\alpha & M\end{bmatrix}Y_{lm}(\theta,\varphi)\chi_{S_\alpha m_\alpha}(3,12), \quad (2.7a)$$

$$X_M^{Jl\beta}(3,12)=\sum_{mm_\beta}\begin{bmatrix}l & S_\beta & J\\ m & m_\beta & M\end{bmatrix}Y_{lm}(\theta,\varphi)\chi_{S_\beta m_\beta}(3,12); \quad (2.7b)$$

$\chi_{S_\alpha m_\alpha}$ for $\alpha=1, 2$ are, respectively, the quartet and the doublet spin functions, symmetric in the particles 1 and 2, whereas $\chi_{S_\beta m_\beta}$ is the doublet spin function antisymmetric in 1 and 2; $\psi_0(\rho)$ is the S-state deuteron ground state wave

function and $\psi^{t}_{k'}(\rho)$ and $\psi^{s}_{k''}(\rho)$ the triplet and singlet continuum state of the neutron-proton system, respectively.

Let us assume that only the first term in eq. (2.6) will contribute. The inclusion of the other terms will be discussed later.

We have the orthogonality relation

$$\int \mathrm{d}\boldsymbol{\varrho} \int \mathrm{d}\Omega(\theta, \varphi)[\psi_0(\rho)\mathscr{Y}^{Jl\alpha}_{M}(3,12)]^{*}[\psi_0(\rho)\mathscr{Y}^{J'l'\alpha'}_{M'}(3,12)] = \delta_{JJ'}\delta_{ll'}\delta_{\alpha\alpha'}\delta_{MM'} \tag{2.8}$$

and the equation

$$\int \mathrm{d}\boldsymbol{\varrho}\psi_0(\rho)\left\{-\frac{\hbar^2}{M_n}\Delta_\rho + \mathscr{V}(\rho) - E_d\right\}\psi_0(\rho) = 0 \tag{2.9}$$

where M_n is the nucleon mass. If we substitute (2,4), (2,5) and (2.6) into (2.3), multiply it by $[\psi_0(\rho)\mathscr{Y}^{Jl\alpha}_{M}(3,12)]^{*}$ and integrate over all coordinates with exception of $\boldsymbol{r}$, and carry out the product of spin functions, we obtain

$$\begin{aligned}\left(\frac{\mathrm{d}^2}{\mathrm{d}r^2} + k^2 - \frac{l(l+1)}{r^2}\right) F^{l\alpha}_{JM}(r) = \sum_{l'\alpha'}\int \mathrm{d}\boldsymbol{\varrho}\int \mathrm{d}\Omega(\theta,\varphi)\,\frac{4M_n}{3\hbar^2}\,r[\psi_0(\rho)\mathscr{Y}^{Jl\alpha}_{M}(3,12)]^{*} \\ \cdot\Bigg[\left\{\mathscr{V}(23)+\mathscr{V}(13)+\frac{e^2}{r_{13}}+\hbar^{-2}\sum_{i>j}J(r_{ij})\mathbf{l}_{ij}\cdot\mathbf{s}_{ij}\right\}\frac{1}{r}F^{l'\alpha'}_{JM}(r)\mathscr{Y}^{Jl'\alpha'}_{M}(3,12)\psi_0(\rho) \\ -\left\{\sum_{i=1}^{3}T_i - E_0 - E_d + \mathscr{V}(12)+\mathscr{V}(13)+\mathscr{V}(23)+\frac{e^2}{r_{13}}+\hbar^{-2}\sum_{i>j}J(r_{ij})\mathbf{l}_{ij}\cdot\mathbf{s}_{ij}\right\} \\ \cdot\frac{1}{r'}F^{l'\alpha'}_{JM}(r')\mathscr{Y}^{Jl'\alpha'}_{M}(1,23)\psi_0(\rho')\Bigg]\end{aligned} \tag{2.10}$$

where

$$\mathbf{r}' = P_M^{13}\mathbf{r} = -\tfrac{1}{2}\mathbf{r} - \tfrac{3}{4}\boldsymbol{\varrho}, \quad \boldsymbol{\varrho}' = P_M^{13}\boldsymbol{\varrho}.$$

We now perform the exchange operations included in the central force, carry out the product of spin functions, and use the relations

$$\sum_{i=1}^{3}T_i = -(\hbar^2/M_n)[\Delta_{23} + \tfrac{3}{4}\Delta_{r'}],$$

$$\{-(\hbar^2/M_n)\Delta_{23} - E_d + \mathscr{V}(23)\}\psi_0(|\mathbf{r}_2 - \mathbf{r}_3|) = 0,$$

and expansions of $V(|\mathbf{r}+\frac{1}{2}\boldsymbol{\varrho}|)$, $V(\frac{2}{3}|\mathbf{r}-\mathbf{r}'|)$, $V(\frac{2}{3}|2\mathbf{r}'+\mathbf{r}|)$, $V(\frac{2}{3}|\mathbf{r}'+2\mathbf{r}|)$, $\psi_0(\frac{2}{3}|2\mathbf{r}'+\mathbf{r}|)$, $\psi_0(\frac{2}{3}|\mathbf{r}'+2\mathbf{r}|)$ and $1/r_{13}$ in terms of Legendre polynomials, as for example

$$V(|\mathbf{r}+\tfrac{1}{2}\boldsymbol{\varrho}|) = \sum_{L=0}^{\infty}(-)^L V_L(r, \tfrac{1}{2}\rho)P_L(\cos\theta) \tag{2.11}$$

where θ is the angle between $\mathbf{r}$ and $\boldsymbol{\varrho}$. The right hand side of eq. (2.10), excluding the spin-orbit part, then becomes

$$\frac{4}{3}\frac{M_n}{\hbar^2}\left\{F_\alpha{}^l(r)f_1(r)+(\tfrac{4}{3})^3\frac{4\pi r}{2l+1}\sum_{L_1L_2L_3}(-1)^{L_1+L_3}\sum_{L'}\begin{bmatrix}L_1&L_2&L'\\0&0&0\end{bmatrix}^2\begin{bmatrix}L'&L_3&l\\0&0&0\end{bmatrix}^2 f_2(r)\right\}$$

$$+(\tfrac{4}{3})^3\frac{4\pi r}{2l+1}\mu(S_\alpha)\sum_{L_1L_2}(-1)^{L_1+L_2}\begin{bmatrix}L_1&L_2&l\\0&0&0\end{bmatrix}^2 f_3(r) \quad (2.12)$$

where $\mu(S_\alpha)=1-\frac{3}{2}\delta_{S_\alpha,\frac{1}{2}}$ and

$$f_1(r)=\int\left\{[(2w-h)+(2b-m)\mu(S_\alpha)]V_0(r,\tfrac{1}{2}\rho)+\frac{e^2}{r_>}\right\}\rho^2\psi_0{}^2(\rho)\mathrm{d}\rho \quad (2.13a)$$

$$f_2(r)=\int \mathrm{d}r'\,r'\psi_{0L_1}(\tfrac{4}{3}r',\tfrac{2}{3}r)\psi_{0L_2}(\tfrac{2}{3}r',\tfrac{4}{3}r)F_\alpha{}^l(r')$$
$$\times\left[[(2m-b)+(2h-w)\mu(S_\alpha)]V_{L_2}(\tfrac{2}{3}r',\tfrac{2}{3}r)-\tfrac{3}{2}e^2\frac{r_<{}^{L_2}}{r_>{}^{L_2+1}}\right. \quad (2.13b)$$
$$\left.+(-1)^{L_2+1}\mu(S_\alpha)V_{L_2}(\tfrac{4}{3}r',\tfrac{2}{3}r)+E_0\right]$$

$$f_3(r)=\int \mathrm{d}r'\,r'\psi_{0L_1}(\tfrac{4}{3}r',\tfrac{2}{3}r)\psi_{0L_2}(\tfrac{2}{3}r',\tfrac{4}{3}r)$$
$$\times\left[\frac{\mathrm{d}^2F_\alpha{}^l(r')}{\mathrm{d}r'^2}-\frac{l(l+1)}{r'^2}F_\alpha{}^l(r')\right]. \quad (2.13c)$$

In (2.13a) $r_>$ means the greater of r and $\frac{1}{2}\rho$, and in (2.13b) $r_>$ means the greater, and $r_<$ the lesser, of r and r'. The labels J and M were dropped from the F's, which will be denoted by $F_\alpha{}^l(r)$.

Let us now consider the integrals in eq. (2.10) containing spin-orbit forces. We split them into two parts, one resulting from the non-exchange term in eq. (2.4) and the other one from the exchange part. They will be denoted by $(LS)_1$ and $(LS)_2$, respectively.

If we

1) expand $J(|\mathbf{r}\pm\frac{1}{2}\boldsymbol{\rho}|)$ in a series of Legendre polynomials,
2) re-express $\mathbf{l}_{13}$ and $\mathbf{l}_{23}$ in terms of $(\mathrm{grad})_r$ and $(\mathrm{grad})_\rho$,
3) carry out the integral over $\mathrm{d}\Omega_\rho$,

we obtain

$$(LS)_1=\frac{\pi}{2}\frac{4}{3}\frac{M_n}{\hbar^2}f_4(r)\sum_{\alpha'=1}^{2}F^{l'}_{\alpha'}(r)\langle\mathscr{Y}^{Jl\alpha}_M(3,12)|\hbar^{-2}\mathbf{l}\cdot(\mathbf{s}_1+\mathbf{s}_2+2\mathbf{s}_3)|\mathscr{Y}^{Jl'\alpha'}_M(3,12)\rangle \quad (2.14)$$

where

$$f_4(r)=\int \mathrm{d}\rho\,\rho^2\psi_0{}^2\{6J_0(r,\tfrac{1}{2}\rho)+(\rho/r)J_1(r,\tfrac{1}{2}\rho)\}. \quad (2.15)$$

If we write

$$\mathbf{l}\cdot(\mathbf{s}_1+\mathbf{s}_2+2\mathbf{s}_3)=\mathbf{l}\cdot(\mathbf{s}_3+\mathbf{S});\quad \mathbf{S}=\mathbf{s}_1+\mathbf{s}_2+\mathbf{s}_3,$$

we have

$$\hbar^{-2}\langle \mathscr{Y}_M^{Jl\alpha}(3,12)|\mathbf{l}\cdot(\mathbf{s}_3+\mathbf{S})|\mathscr{Y}_M^{Jl'\alpha'}(3,12)\rangle$$
$$= \tfrac{1}{2}[J(J+1)-l'(l'+1)-S_{\alpha'}(S_{\alpha'}+1)]\delta_{\alpha\alpha'}\delta_{ll'}+(-1)^{\frac{1}{2}+l-J+2S_{\alpha'}}\{2S_{\alpha'}+1\}^{\frac{1}{2}} \quad (2.16)$$
$$\{\tfrac{3}{2}(2l+1)l(l+1)(2S_\alpha+1)\}^{\frac{1}{2}}W(l,S_{\alpha'},l,S_\alpha;J,1)W(\tfrac{1}{2},S_{\alpha'},\tfrac{1}{2},S_\alpha;1,1)\delta_{ll'};$$

the W's are Racah coefficients, and the formula which gives the matrix elements of the contraction of two irreducible tensors of rank L was used [6]). Substituting eq. (2.16) into (2.14) we obtain

$$(LS)_1 = \frac{\pi}{2}\frac{4}{3}\frac{M_n}{\hbar^2}f_4(r)\sum_{\alpha'=1}^{2}F_{\alpha'}^{l}(r)\{\tfrac{1}{2}[J(J+1)-l(l+1)-S_\alpha(S_\alpha+1)]\delta_{\alpha\alpha'}$$
$$+(-1)^{\frac{1}{2}+l-J}[\tfrac{3}{2}l(l+1)(2l+1)(2S_\alpha+1)(2S_{\alpha'}+1)]^{\frac{1}{2}}W(l,S_{\alpha'},l,S_\alpha;J,1) \quad (2.17)$$
$$W(\tfrac{1}{2},S_{\alpha'},\tfrac{1}{2},S_\alpha;1,1)\}.$$

Now consider the $(LS)_2$-term. If we write $\mathbf{l}_{12}$, $\mathbf{l}_{13}$ and $\mathbf{l}_{23}$ in terms of $(\mathrm{grad})_r$ and $(\mathrm{grad})_{r'}$ and use the equality

$$\int \mathbf{r}\times\nabla_r(\varphi(r)\psi(\mathbf{r},\mathbf{r}'))\mathrm{d}\mathbf{r}=0, \quad \text{if} \quad \varphi(r) \quad \text{and} \quad \psi(\mathbf{r},\mathbf{r}')\to 0 \quad \text{as} \quad r\to\infty,$$

the expression $(LS)_2$ becomes

$$(LS)_2 = \tfrac{3}{2}ir(\tfrac{4}{3})^6(M_n/\hbar^2)\sum_{l'\alpha'}\int \mathrm{d}\Omega(\theta,\varphi)\mathscr{Y}_M^{Jl\alpha*}(3,12)\int \mathrm{d}\mathbf{r}'\,\hbar^{-1}(\mathbf{r}\times\mathbf{r}')\cdot\mathbf{s}_{13}$$
$$\left[\frac{1}{\rho}\frac{\mathrm{d}\psi_0(\rho)}{\mathrm{d}\rho}\psi_0(\rho')+\frac{1}{\rho'}\frac{\mathrm{d}\psi_0(\rho')}{\mathrm{d}\rho'}\psi_0(\rho)\right]J(\tfrac{2}{3}|\mathbf{r}-\mathbf{r}'|)\frac{1}{r'}F_{\alpha'}^{l'}(r')\mathscr{Y}_M^{Jl'\alpha'}(1,23). \quad (2.18)$$

We now use the expansion

$$\frac{\mathrm{d}\psi_0(\rho)}{\rho\mathrm{d}\rho}\psi_0(\rho')+\frac{\mathrm{d}\psi_0(\rho')}{\rho'\mathrm{d}\rho'}\psi_0(\rho)=\sum_{L=0}^{\infty}[A_L(r,r')+B_L(r,r')]P_L(\cos\theta), \quad (2.19)$$

θ being the angle between $\mathbf{r}$ and $\mathbf{r}'$, and a similar expression for $J(\frac{2}{3}|\mathbf{r}-\mathbf{r}'|)$ in order to carry out the angular integration as well as the spin product. We obtain

$$(LS)_2 = i4\pi(\tfrac{4}{2})^5(M_n/\hbar^2)\sum_{l'\alpha'}\sum_{L_1L_2}\sum_{L'j'}\sum_{j}(-1)^{J+L'-j+1}\frac{2j+1}{(2L'+1)(2J+1)}$$
$$[(2J'+1)(2J+1)]^{\frac{1}{2}}\begin{bmatrix}L_1 & L_2 & L'\\ 0 & 0 & 0\end{bmatrix}^2 W(l',S_{\alpha'},j,L';J,J')f_5(r) \quad (2.20)$$
$$\langle j(L'J(lS_\alpha))|\sum_{\mu}(-)^{\mu}(\mathbf{r}')_{-\mu}(\mathbf{r}\times\boldsymbol{\sigma}_{13})_{\mu}|j(l'J'(L'S_{\alpha'}))\rangle$$

where $\mathbf{s}_{13}=\frac{1}{2}\hbar\boldsymbol{\sigma}_{13}$ and

$$f_5(r)=\int \mathrm{d}r' \quad r'^2 J_{L_2}(\tfrac{2}{3}r',\tfrac{2}{3}r)F_{\alpha'}^{l'}(r')[A_{L_1}(r,r')+B_{L_1}(r,r')]. \quad (2.21)$$

The matrix element of the product $\mathbf{r}' \cdot \mathbf{r} \times \boldsymbol{\sigma}_{13}$ which appears in eq. (2.20) can be calculated using the formula (6.21), p. 117 of ref. [6]). If we denote this matrix element by $b(J, S_\alpha, S_{\alpha'}, l)$, we obtain

$$b(J, S_\alpha, S_{\alpha'}, l) = (-)^{l'+J-j} \frac{9\sqrt{3}}{4\pi} \left[\frac{(2l'+1)(2S_\alpha+1)(2J'+1)(2L'+1)}{2J+1}\right]^{\frac{1}{2}} \begin{bmatrix} l' & 1 & L' \\ 0 & 0 & 0 \end{bmatrix}$$

$$\begin{bmatrix} L' & 1 & l \\ 0 & 0 & 0 \end{bmatrix} W(l', J', L', J; j, 1) X(L'1l; S_{\alpha'}1S_\alpha; J'1J) \langle S_\alpha(3,12) || \sigma_{13} || S_{\alpha'}(1,23) \rangle, \tag{2.22}$$

where $X(\ldots)$ is a Wigner 9-j symbol and $\langle S_\alpha || \sigma_{13} || S_{\alpha'} \rangle$ is the reduced matrix element of σ_{13}, which can be evaluated using the formula (6.22) of ref. [6]), after writing $S_\alpha(3,12)$ and $S_{\alpha'}(1,23)$ in terms of $S_\alpha(2,13)$ and $S_{\alpha'}(2,13)$, respectively We then obtain

$$b(J, S_\alpha, S_{\alpha'}, l) = (-)^{l'+J+\frac{1}{2}-j-S_{\alpha'}} \frac{81\sqrt{2}}{4\pi} (2S_{\alpha'}+1)(2S_\alpha+1) \begin{bmatrix} l' & 1 & L' \\ 0 & 0 & 0 \end{bmatrix} \begin{bmatrix} L' & 1 & l \\ 0 & 0 & 0 \end{bmatrix}$$

$$\left[\frac{(2l'+1)(2J'+1)(2L'+1)}{2J+1}\right]^{\frac{1}{2}} W(l', J', L', J; j, 1) W(\tfrac{1}{2}, \tfrac{1}{2}, \tfrac{1}{2}, S_\alpha; 1,1) \tag{2.23}$$

$$W(\tfrac{1}{2}, \tfrac{1}{2}, \tfrac{1}{2}, S_{\alpha'}; 1,1) W(1, S_{\alpha'}, 1, S_\alpha; \tfrac{1}{2}, 1) X(L'1l; S_{\alpha'}1S_\alpha; J'1J).$$

After the substitution of this expression into eq. (2.20) the summation over j and J' can be carried out if we use the relations [6, 7])

$$\sum_e (2e+1)(-)^{a+b-e} W(abcd; ef) W(bacd; eg) = W(afgb; cd) \tag{2.24a}$$

and

$$\sum_\lambda (2\lambda+1) X(ab\lambda; cde; fh) \begin{Bmatrix} a & b & \lambda \\ e & h & \mu \end{Bmatrix} = (-)^{2\mu} \begin{Bmatrix} c & d & e \\ b & \mu & g \end{Bmatrix} \begin{Bmatrix} f & g & h \\ \mu & a & c \end{Bmatrix}, \tag{2.24b}$$

where the Wigner 6-j symbol $\{\vdots\}$ is related to the Racah coefficient by [8])

$$\begin{Bmatrix} a & b & \mu \\ e & h & \lambda \end{Bmatrix} = (-)^{a+b+e+h} W(abeh; \mu\lambda). \tag{2.24c}$$

Thus we obtain

$$(LS)_2 = 216\pi(\tfrac{4}{3})^5 (M_n/\hbar^2) \sum_{l'\alpha'} \sum_{L_1 L_2} \sum_{L'} (-)^{J+S_{\alpha'}+S_\alpha+l+\frac{1}{2}}$$

$$\times \frac{(2S_{\alpha'}+1)(2S_\alpha+1)}{2J+1} \left[\frac{2l'+1}{2L'+1}\right]^{\frac{1}{2}} \begin{bmatrix} L_1 & L_2 & L' \\ 0 & 0 & 0 \end{bmatrix} \begin{bmatrix} l' & 1 & L' \\ 0 & 0 & 0 \end{bmatrix} \begin{bmatrix} L' & 1 & l \\ 0 & 0 & 0 \end{bmatrix} W(1,1,S_{\alpha'}, l'; 1, S_\alpha)$$

$$W(l, S_\alpha, l', L'; J, 1) W(\tfrac{1}{2}, \tfrac{1}{2}, \tfrac{1}{2}, S_\alpha; 1, 1) W(\tfrac{1}{2}, \tfrac{1}{2}, \tfrac{1}{2}, S_{\alpha'}; 1, 1) W(1, S_{\alpha'}, 1, S_\alpha; \tfrac{1}{2}, 1) f_5(r). \tag{2.25}$$

We see from eqs. (2.17) and (2.25) that the coupled integro-differential equations result essentially from the inclusion of the spin-orbit force. The coupling

due to the admixture of the quartet and doublet states is a purely spin-orbit effect, whereas the coupling resulting from the admixture of two l's differing by 2 is a combined effect of the spin-orbit force and the exclusion principle.

3. Choice of the Potential Shape and the Deuteron Wave Function

We want to consider a Yukawa potential for both central and spin-orbit forces, namely

$$V(r_{ij}) = V_c \frac{\exp(-\lambda r_{ij})}{\lambda r_{ij}} \tag{3.1}$$

and

$$J(r_{ij}) = V_{LS} \frac{\exp(-\mu r_{ij})}{\mu r_{ij}}. \tag{3.2}$$

The Yukawa potential was used by Haas and Robertson [1]) with

$$V_c = -68.01 \text{ MeV} \quad \text{and} \quad \lambda^{-1} = 1.18 \times 10^{-13} \text{ cm} \tag{3.3}$$

as determined by Burke [5]).

For the deuteron ground-state we choose Hulthén's function

$$\psi_0(\rho) = N\rho^{-1}[\exp(-\beta\rho) - \exp(-7\beta\rho)] \tag{3.4}$$

where $\beta^{-1} = 4.31 \times 10^{-13}$ cm and

$$N = (7\beta/9\pi)^{\frac{1}{2}}. \tag{3.5}$$

With this choice of the potentials and the deuteron wave function, we use the expansions

$$\frac{\exp(-\lambda|\mathbf{r}-\mathbf{r}'|)}{|\mathbf{r}-\mathbf{r}'|} = \sum_L (2L+1) \frac{I_{L+\frac{1}{2}}(\lambda r_<)}{\sqrt{r_<}} \frac{K_{L+\frac{1}{2}}(\lambda r_>)}{\sqrt{r_>}} P_L(\cos\theta) \tag{3.6}$$

where $r_<$ and $r_>$ mean the lesser and the greater of r and r', respectively, and

$$I_\omega(z) = e^{-\frac{1}{2}\omega\pi i} J_\omega(z e^{\frac{1}{2}\pi i}), \tag{3.7a}$$

$$K_\omega(z) = (\tfrac{1}{2}\pi i) e^{\frac{1}{2}\omega\pi i} H_\omega^{(1)}(iz), \tag{3.7b}$$

$J_\omega(z)$ and $H_\omega^{(1)}(z)$ being the ordinary Bessel function of order ω and first Hankel function of order ω, respectively. We may then write

$$V_L(r, \tfrac{1}{2}\rho) = \frac{V_c}{\lambda} \frac{2L+1}{\sqrt{\tfrac{1}{2}r\rho}} \begin{cases} I_{L+\frac{1}{2}}(\tfrac{1}{2}\lambda\rho) K_{L+\frac{1}{2}}(\lambda r) & \text{if } r > \tfrac{1}{2}\rho \\ K_{L+\frac{1}{2}}(\tfrac{1}{2}\lambda\rho) I_{L+\frac{1}{2}}(\lambda r) & \text{if } r < \tfrac{1}{2}\rho, \end{cases} \tag{3.8}$$

$$\psi_{0L}(\tfrac{4}{3}r', \tfrac{2}{3}r) = \tfrac{3}{2}N(2L+1)/\sqrt{2rr'}$$
$$\times \begin{cases} I_{L+\frac{1}{2}}(\frac{4}{3}\beta r')K_{L+\frac{1}{2}}(\frac{2}{3}\beta r) - I_{L+\frac{1}{2}}(\frac{28}{3}\beta r')K_{L+\frac{1}{2}}(\frac{14}{3}\beta r) & \text{if } 2r' < r \\ K_{L+\frac{1}{2}}(\frac{4}{3}\beta r')I_{L+\frac{1}{2}}(\frac{2}{3}\beta r) - K_{L+\frac{1}{2}}(\frac{28}{3}\beta r')I_{L+\frac{1}{2}}(\frac{14}{3}\beta r) & \text{if } 2r' > r. \end{cases} \quad (3.9)$$

Similar expressions hold for $V_L(\frac{2}{3}r, \frac{2}{3}r')$, $V_L(\frac{4}{3}r', \frac{2}{3}r)$, $\psi_{0L}(\frac{2}{3}r', \frac{4}{3}r)$, $J_L(\frac{2}{3}r', \frac{2}{3}r)$, etc.

For half odd integer ω, we have

$$K_{L+\frac{1}{2}}(z) = (\pi/2z)^{\frac{1}{2}} \sum_{r=0}^{L} \frac{(L+r)!}{r!(L-r)!(2z)^r} e^{-z}, \quad (3.10a)$$

$$I_{L+\frac{1}{2}}(z) = (2\pi z)^{-\frac{1}{2}} \left\{ e^{z} \sum_{r=0}^{L} (-)^r \frac{(L+r)!}{r!(L-r)!(2z)^r} + (-)^{L+1} e^{-z} \sum_{r=0}^{L} \frac{(L+r)!}{r!(L-r)!(2z)^r} \right\}. \quad (3.10b)$$

Then,

$$N^{-2} f_1(r) = \frac{e^2}{14\beta} \frac{1}{r} \{\tfrac{9}{2} - \exp(-28\beta r) + \tfrac{7}{2}\exp(-16\beta r) - 7\exp(-4\beta r)\}$$
$$+ 2e^2\{-\mathrm{Ei}(-4\beta r) + 2\mathrm{Ei}(-16\beta r) - \mathrm{Ei}(-28\beta r)\} + \frac{V_c}{\lambda}\{(2w-h) + (2b-m)\mu(S_a)\}$$
$$\cdot \left\{ \frac{\exp(-\lambda r)}{\lambda r} \log \frac{\omega_1 \omega_3 \omega_2'^2}{\omega_2^2 \omega'_1 \omega'_3} - \frac{\exp(-\lambda r)}{\lambda r}[-\mathrm{Ei}(-\omega'_3 r) + 2\,\mathrm{Ei}(-\omega'_2 r) - \mathrm{Ei}(\omega'_1 r)] \right.$$
$$\left. + \frac{\exp(\lambda r)}{\lambda r}[-\mathrm{Ei}(-\omega_1 r) + 2\,\mathrm{Ei}(-\omega_2 r) - \mathrm{Ei}(-\omega_3 r)] \right\} \quad (3.11)$$

where

$$-\mathrm{Ei}(-x) = \int_x^\infty \frac{\exp(-y)}{y}\,dy;$$
$$\omega_1 = 4\beta+\lambda, \quad \omega_2 = 16\beta+\lambda, \quad \omega_3 = 28\beta+\lambda,$$
$$\omega'_1 = 4\beta-\lambda, \quad \omega'_2 = 16\beta-\lambda, \quad \omega'_3 = 28\beta-\lambda.$$

Further,

$$\frac{1}{N^2}\frac{\mu}{3V_{LS}} f_4(r) = \frac{\exp(-\mu r)}{\mu r}\left\{ \left(\frac{1}{\mu r}\left(1+\frac{1}{\mu r}\right) - 1 \right) 2 \log \frac{\gamma_2 \gamma'_1 \gamma'_3}{\gamma_1 \gamma_3 \gamma'_2} \right.$$
$$+ \frac{2\mu}{\mu r}\left(1+\frac{1}{\mu r}\right)\left(\frac{1}{\gamma_1} - \frac{2}{\gamma^2} + \frac{1}{\gamma_3} + \frac{1}{\gamma'_1} - \frac{2}{\gamma'_2} + \frac{1}{\gamma'_3}\right)$$
$$- \frac{2\mu}{(\mu r)^2}\left(1+\frac{1}{\mu r}\right)\left(\frac{e^{-4\beta r}}{\gamma'_1} - \frac{2e^{-16\beta r}}{\gamma'_2} + \frac{e^{-28\beta r}}{\gamma'_3}\right) \quad (3.12)$$
$$\left. + \frac{2\mu}{(\mu r)^2}\left(1-\frac{1}{\mu r}\right)\left(\frac{\exp(-4\beta r)}{\gamma_1} - \frac{2\exp(-16\beta r)}{\gamma_2} + \frac{\exp(-28\beta r)}{\gamma_3}\right)\right\}$$

$$-\frac{2\exp(-\mu r)}{\mu r}\left(1-\frac{1}{\mu r}\left(1+\frac{1}{\mu r}\right)\right)(-\mathrm{Ei}(-\gamma'_1 r)+2\,\mathrm{Ei}(-\gamma'_2 r)$$
$$-\mathrm{Ei}(-\gamma'_3 r))+\frac{2\exp(\mu r)}{\mu r}\left(1+\frac{1}{\mu r}\left(1-\frac{1}{\mu r}\right)\right)(-\mathrm{Ei}(-\gamma_1 r) \qquad (3.12)$$
$$+2\,\mathrm{Ei}(-\gamma_2 r)-\mathrm{Ei}(-\gamma_3 r))$$

where

$$\gamma_1 = 4\beta+\mu, \quad \gamma_2 = 16\beta+\mu, \quad \gamma_3 = 28\beta+\mu;$$
$$\gamma'_1 = 4\beta-\mu, \quad \gamma'_2 = 16\beta-\mu, \quad \gamma'_3 = 28\beta-\mu.$$

Now

$$\frac{1}{\rho}\frac{\mathrm{d}\psi_0(\rho)}{\mathrm{d}\rho} = -\frac{1}{\rho^2}\psi_0(\rho)-\frac{\beta}{\rho}\psi_0(\rho)+\frac{6}{\rho}\frac{\exp(-7\beta\rho)}{\rho} \qquad (3.13)$$

and the left hand side of eq. (2.19) can be split into

$$A = -(\rho^{-2}+\rho'^{-2})\psi_0(\rho)\psi_0(\rho') \qquad (3.14a)$$

and

$$B = -\beta\left(\frac{1}{\rho}+\frac{1}{\rho'}\right)\psi_0(\rho)\psi_0(\rho')+\frac{6}{\rho}\psi_0(\rho')\frac{\exp(-7\beta\rho)}{\rho}$$
$$+\frac{6}{\rho'}\psi_0(\rho)\frac{\exp(-7\beta\rho')}{\rho'}; \qquad (3.14b)$$

after expansion into series of Legendre polynomials these expressions will give the coefficients $A_L(r, r')$ and $B_L(r, r')$, respectively. The integrals in $f_2(r)$, $f_3(r)$ and $f_5(r)$ will split into either four integrals, with the limits of integration $(0, \frac{1}{2}r)$, $(\frac{1}{2}r, r)$, $(r, 2r)$ and $(2r, \infty)$ or three integrals with the limits of integration $(0, \frac{1}{2}r)$, $(\frac{1}{2}r, 2r)$ and $(2r, \infty)$.

The author wishes to express his appreciation to Mr. H. Araki for several interesting comments on this paper.

References

1) R. A. Buckingham and H. S. W. Massey, Proc. Roy. Soc. A **179** (1941) 123;
R. A. Buckingham, S. J. Hubbard and H. S. W. Massey, Proc. Roy. Soc. A **211** (1952) 183;
P. G. Burke and H. H. Robertson, Proc. Phys. Soc. A **70** (1957) 777;
F. A. Haas and H. H. Robertson, Proc. Phys. Soc. A **73** (1959) 160
2) M. Brullmann, H. J. Gerber and D. Meier, Helv. Phys. Acta **31** (1958) 318, 580
3) B. H. Bransden, K. Smith and C. Tate, Proc. Roy. Soc. A **247** (1959) 73;
L. M. Delves and D. Brown, Nuclear Physics **11** (1959) 432
4) A. K. Bose, Dissertation, Göttingen (1957)
5) P. G. Burke, Thesis, University of London (1956)
6) M. E. Rose, Elementary Theory of Angular Momentum (John Wiley, 1957)
7) A. R. Edmonds, Angular Momentum in Quantum Mechanics (Princeton University Press, 1957)
8) E. P. Wigner, Group Theory (Academic Press, 1959)

1.E.1:
3.B

Nuclear Physics **14** (1959/60) 438—442; © *North-Holland Publishing Co., Amsterdam*
Not to be reproduced by photoprint or microfilm without written permission from the publisher

DECAY OF Gd^{146} and Eu^{146}

N. M. ANTONIEVA, A. A. BASHILOV, B. S. DZHELEPOV and V. A. SERGIENKO
Institute of Physics of the Leningrad University, Leningrad

Received 27 May 1959

Abstract: The spectra of conversion electrons of neutrino-deficient isotopes Gd^{146} and Eu^{146} are investigated. In the case of Gd^{146} three nuclear transitions with energies of 114.8, 115.5 and 155 keV are observed and the coincidences among their conversion electrons are studied. In the case of Eu^{146} transitions with energies of 630 and 742 keV are observed. Mechanisms of disintegration are suggested.

In studying the conversion electron spectrum of neutron-deficient isotopes of Gd [1]) produced by bombarding Ta nuclei with fast protons ($E_p = 680$ MeV) we observed conversion lines whose intensity decreased with the half-life period $T_{\frac{1}{2}} = 45$ days [2]). Murin and co-workers [3]) presented arguments indicating that the activity of $T_{\frac{1}{2}} = 45$ days belongs to Gd^{146}. To separate the gadolinium fraction we used first the usual chemical methods and then chromatography. The active substance was collected on a thin aluminium foil. In addition to the 45-day activity the source originally contained Gd^{147} (1.5 days), Gd^{149} (9 days), Gd^{151} (120 days), Gd^{153} ($\approx$ 200 days), as well as Eu^{147} (24 days) and Eu^{149} ($\approx$ 130 days) accumulated from the disintegration of corresponding isotopes of gadolinium [1]).

The conversion electron spectrum was examined in a magnetic spectrometer with resolution 0.5 % ("coetron" [4])), a photographic recording spectrograph and a double magnetic lens coincidence spectrometer.

Fig. 1 shows the portion of conversion electron spectrum of gamma rays from Gd^{146} obtained on the "coetron". ($E_\gamma = 114.8$, 115.5 and 155 keV).

The conversion electron spectrum of Gd^{146} was additionally investigated with the photographic recording magnetic spectrometer and it was established that the K 114.8 and K 115.5 lines have approximately equal intensity and that for both transitions the K : L ratio is great (≈ 7); besides, only L_1 lines were observable, while L_2 and L_3 lines did not appear on the photographic plate. The above facts are most naturally interpreted by assuming that the 114.8 and 115.5 keV transitions are transitions of M1 type and their total intensities are approximately equal.

The study of the 155 keV transition was complicated by the fact that our spectrum contained additional conversion electrons from a transition with the same energy (155 keV) belonging to Gd^{151} ($T = 120$ days).

The K : L ratio for the 155-keV transition was roughly estimated by means of the photographic recording β-spectrograph immediately after the source was prepared, when the K155 line of Gd^{146} was much more intense than the K155 line of Gd^{151}; It found to be ≈ 7, which indicates that the 155 keV transition of Gd^{146} most likely belongs to the M1 type. The intensity of the 155 keV transition can be calculated by using the theoretical value of the internal conversion coefficient β_1; it is rather close to the intensity of the 114.8 and 115.5 keV transitions.

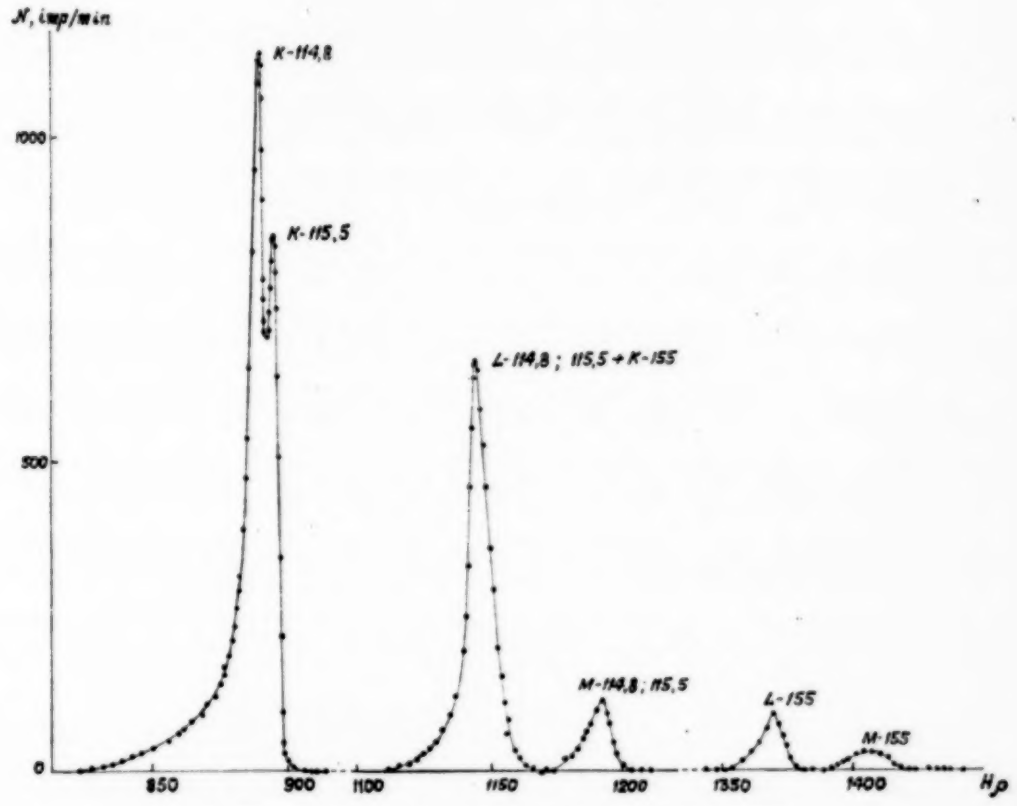

Fig. 1. Conversion electron spectrum of Gd^{146}.

Coincidences between conversion electrons of Gd^{146} were measured on a double magnetic lens spectrometer with scintillation counters [5]). The transmission of the spectrometer equalled $\Omega = 2\,\%$, the relative half-width of the lines $\Delta(H\rho)/H\rho$ was 3.5 %, and the resolution time of the coincidence circuit was $T = 1 \times 10^{-8}$ sec.

The coincidence measurements results (table 1) are illustrated in figures 2 and 3 and reduce to the following:

1) The transitions with $E_\gamma = 114.8$ keV and $E_\gamma = 115.5$ keV are in cascade (fig. 2, AA curve; fig. 3, AB and BB curves).

2) The transition with $E_\gamma = 155$ keV is in cascade with both the 114.8 and 115.5 keV transitions (fig. 2, AC curve). If it were not so, the number of coincidences should have been half the observed number.

The thorough qualitative analysis [6]) of the results shows that the possible

TABLE 1

Coincidence measurements results on conversion electrons in the decay of $Gd^{148} \rightarrow Eu^{148}$

Line obtained on first spectrometer (through the foil)	Line obtained on 2nd spectrometer	Total number on coincidences per hour	Number of real coincidences per hour
A	C	306	294
A	A	1884	1800
B	A	1060	994
B	B	244	202

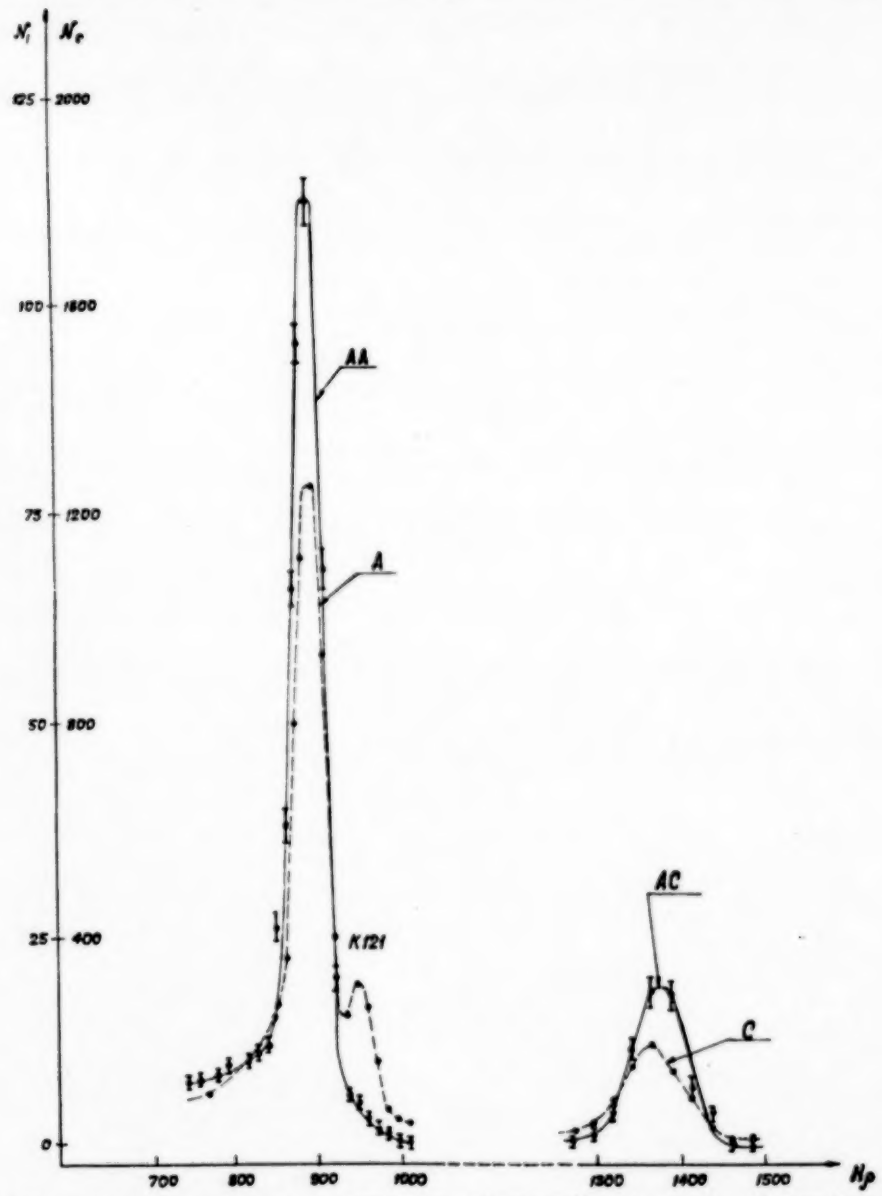

Fig. 2. Coincidence spectrum of electrons of K 114.8 with K 115.5 (AA curve) and of K (114.8+115.5) with (L+M) 155 (A.C. curve). The solid curve is the coincidence spectrum, the dotted curve is the single spectrum. Along the ordinate axis are N_1 and N_e, where N_1 is the counting rate on a single spectrometer in thousands pulses per minute and N_e is a coincidence counting rate in pulses per hour.

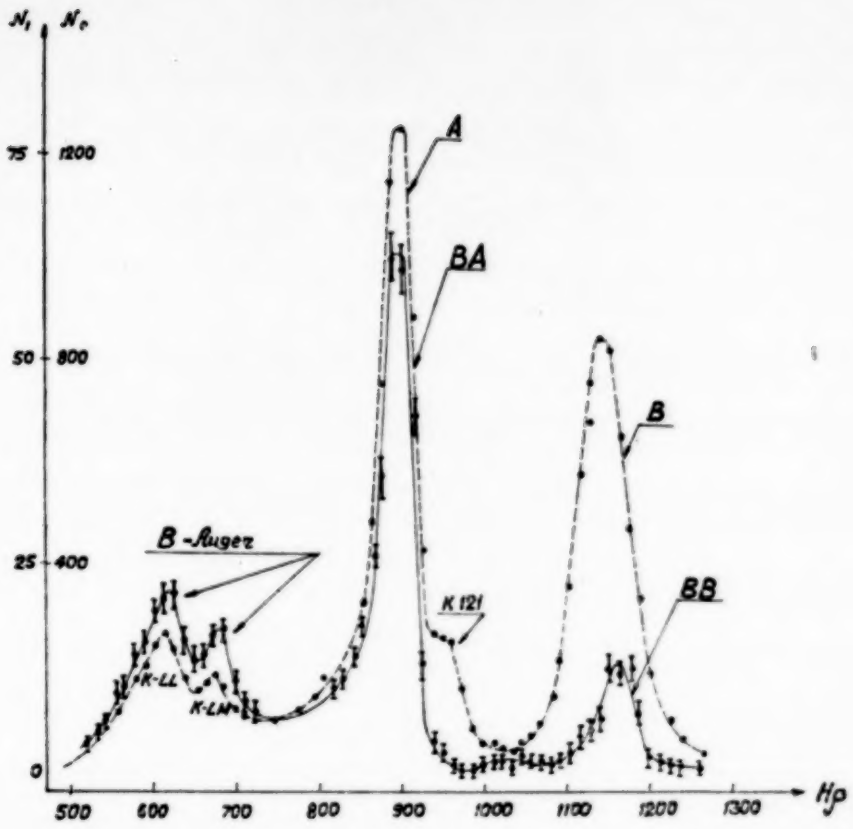

Fig. 3. Coincidence spectrum of electrons of (L+M) (114.8+115.5)+K 155 with K (114.8+115.5) (AB curve) and "self-coincidence" of lines (L+M) (114.8+115.5)+K 155. The solid curve is the coincidence spectrum, the dotted curve is the single spectrum. The ordinate axis is the same as in fig. 2.

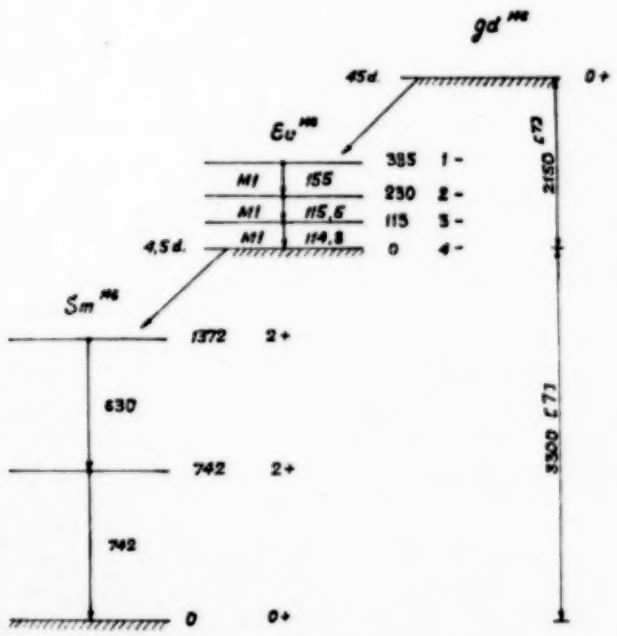

Fig. 4. Decay scheme of $Gd^{146} \rightarrow Eu^{146} \rightarrow Sm^{146}$.

small number of coincidences between conversion lines of other isotopes of Gd and Eu (contained in the source) cannot in any way affect the above conclusions.

On the basis of the results of the present investigation a proposed decay scheme is given for $Gd^{146} \rightarrow Eu^{146}$ (fig. 4).

Eu^{146}, the daughter nucleus of Gd^{146}, is also radioactive and decays into an even nucleus ${}_{62}Sm^{146}_{84}$ with a half-life of 4.5 days. In the course of the decay into Sm^{146} at least two transitions with $E = 630$ keV and 742 keV are excited.

The peaks corresponding to these transitions in the conversion electron spectrum of the gadolinium fraction (fig. 5) initially increase in time with a half-life of about 5 days. Some time later their intensity begins to decrease with

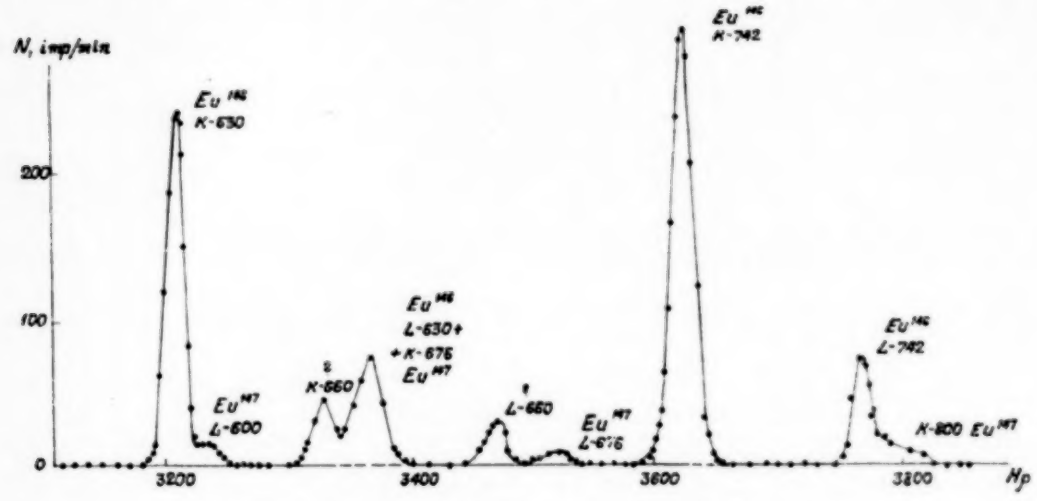

Fig. 5. Conversion electron spectrum of Eu^{146}.

a half-life of about 50 days. In the spectrum of the europium fraction the conversion lines of these transitions continously decrease with a half-life of 4.5 days. The enumerated features prove that the gamma rays of 630 and 742 keV belong to the daughter activity of Gd^{146} i.e., to Eu^{146}.

The above mentioned transitions probably correspond to the oscillatory system of the nuclear levels of ${}_{62}Sm^{146}_{84}$ (fig. 4).

References

1) N. M. Antonieva, A. A. Bashilov, B. S. Dzhelepov and B. K. Preobrazhensky, Izv. Acad. Nauk SSSR, Ser. Fiz. **22** (1958) 135, 895, 906
2) N. M. Antonieva, A. A. Bashilov, B. S. Dzhelepov and B. K. Preobrazhensky, Summaries of Reports at the VII Annual Conference on Nuclear Spectroscopy (Leningrad, 1957), p.22
3) G. M. Gorodinsky, A. M. Murin and V. N. Pokrovsky, Izv. Acad. Nauk USSR, Ser. Fiz. **22** (1958) 811
4) B. S. Dzhelepov and A. A. Bashilvov, Izv. Acad. Nauk SSSR, Ser. Fiz. **14** (1950) 263
5) V. A. Sergienko, Izv. Acad. Nauk USSR, Ser. Fiz. **22** (1958) 198
6) B. S. Dzhelepov and V. A. Sergienko, Izv. Acad. Nauk USSR, Ser. Fiz. **23** (1959) 211
7) A. G. W. Cameron, A revised semi-empirical atomic mass formula, CRP-690 (Ontario, 1957)

1.E.4:
3.B

Nuclear Physics **14** (1959/60) 443—458; © *North-Holland Publishing Co., Amsterdam*
Not to be reproduced by photoprint or microfilm without written permission form the publisher

ON DECAY OF Se^{75}

E. P. GRIGORIEV and A. V. ZOLOTAVIN
Physical Institute of Leningrad University, Leningrad

Received 26 May 1959

Abstract: The conversion and γ-ray spectrum of Se^{75} is investigated with a $\pi\sqrt{2}$ double focusing spectrometer possessing a line half width of 0.4 %. The relative conversion and γ line intensities, conversion coefficients and transition multipolarities are determined.

1. Introduction

Information available at present on the decay of Se^{75} and Ge^{75} and on the levels of As^{75} [1–24]) are depicted in the diagram in fig. 1. Existing models do not

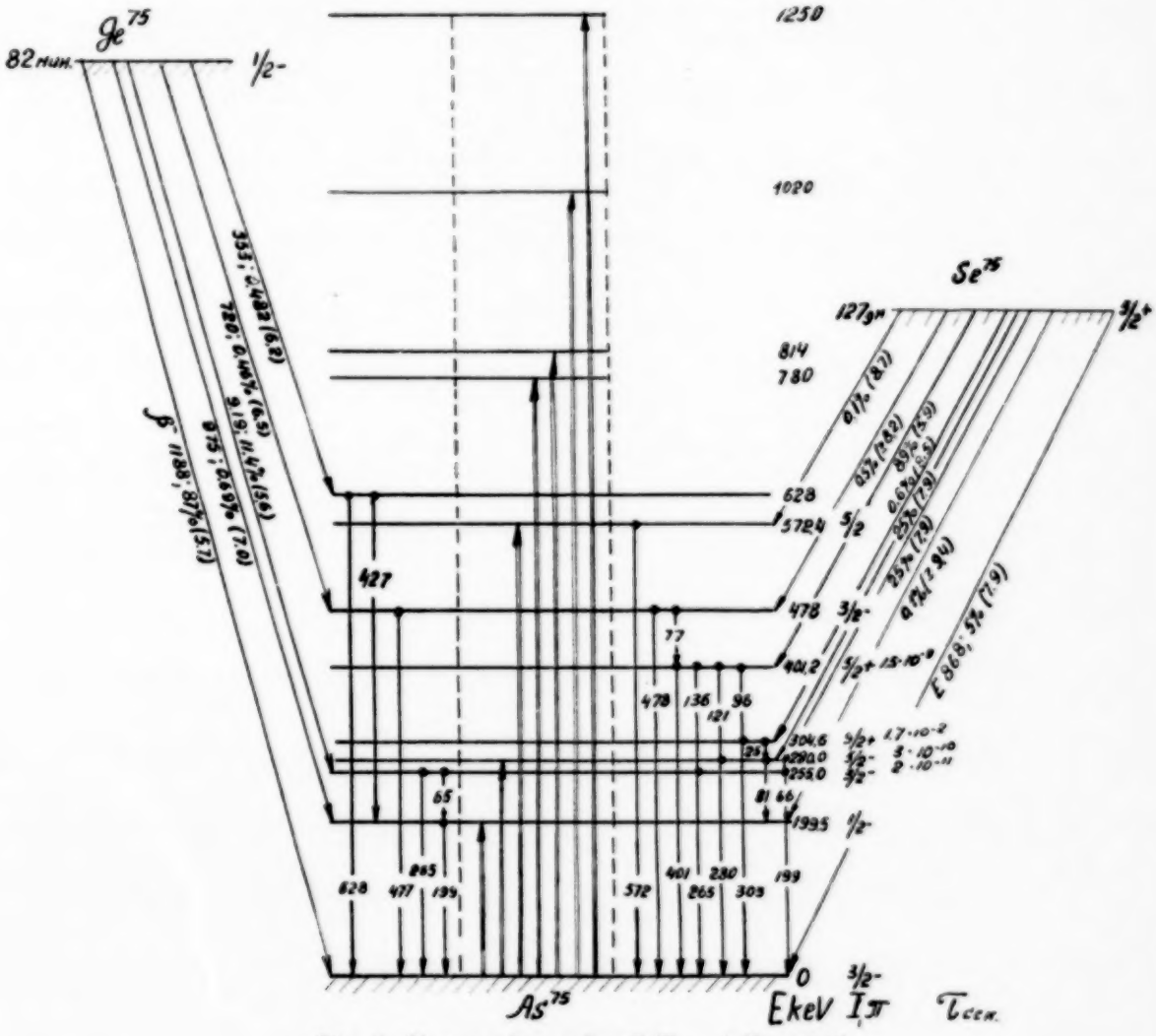

Fig. 1. Decay scheme for $Ge^{75} \rightarrow As^{75} \leftarrow Se^{75}$.

yield a simple explanation of the As^{75} level scheme which is of considerable interest to nuclear theory.

In view of the complexity of the β and γ ray spectra more accurate measurements of the relative γ transition intensities and of conversion coefficients are required to permit one to draw any reliable conclusions regarding the nature of the As^{75} levels. Investigations of the Se^{75} and Ge^{75} radiations carried out hitherto have been performed at conversion line half-width which exceeded 2 % (an exception is ref.[14]) in which the intensities were not determined) the resolution in the γ-ray spectrum studies being even poorer. In order to observe K and L shell internal conversion lines and to completely resolve the photoelectron lines in the γ-ray intensity measurements the Se^{75} spectrum should apparently be investigated with an instrument possessing a better resolving power. In our experiments the relative half-width of the lines did not exceed 0.5 %.

2. Spectrometer, Sources and Measurement Conditions

Our $\pi\sqrt{2}$ double focusing magnetic spectrometer [25]), in which improvements were introduced [26, 27]), was employed. The instrumental half-width of the electron lines in the spectrometer was 0.4 %. The Se^{75} isotope was obtained by irradiating a mixture of selenium isotopes enriched with Se^{74} in a reactor. The specific activity of the Se^{75} preparation was greater than 5 mc/mg.

The thin sources employed for measurement of the conversion spectrum were prepared by thermal evaporation in vacuum of radioactive selenium onto a thin aluminized collodion film. The selenium layer was then changed into the metallic state. In order to avoid sublimation, the selenium layer was covered by a thin collodion film slightly coated with aluminium.

Conversion electron spectrum measurements were performed with three sources; the surface density of two of the sources was not larger than 0.05 mg/cm^2, and 0.25 mg/cm^2 the thickness of the third source which was prepared by depositing selenious acid on the film did not exceed 5 mg/cm^2. All lines could be observed with a half-width equal to the instrumental half-width.

Lines of the photoelectron spectrum could also be observed with the instrumental half-width when thin targets were employed. The photoelectron source in this case was a small glass tube of 1 mm outer diameter, 0.3 mm inner diameter and 35 mm in length, with 50 mc Se^{75} inside.

Owing to the large luminosity of the instrument, $(\Omega S/\rho^2) \times 10^6 = 10$ (Ω, the mean solid angle employed in the spectrometer, was equal to 0.65 % of the total solid angle; $S = 30 \times 1\ mm^2$ is the source area, and $\rho = 140$ mm is the radius of the equilibrium orbit), and also thanks to the high quality of the sources it was possible to obtain high counting rates for many of the lines. The statistical error of the relative line intensity measurements was between several tenths of a percent for the strong lines and several percent for the weak ones. Measurements of the

Se^{75} spectrum continued over several months. The time variation of all observed lines corresponded to the accepted half life value $T = 127$ days.

3. Determination of Relative γ-line Intensities

3.1. METHOD

The relative γ transition intensities I_γ were determined by measuring the spectrum of photoelectrons produced in the interaction of γ rays with thin silver, lead, bismuth and other targets. The dependence of the angular distribution of the photoelectrons on energy of the quanta may influence the results of determination of I_γ by the method under discussion. The influence of the angular dependence of the photoelectrons can be avoided by employing a thin

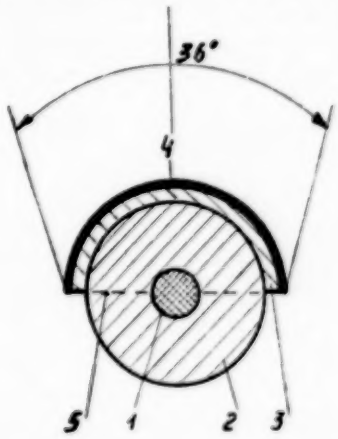

Fig. 2. Cross section of photoelectron source. 1 – Se^{75} preparation 2 – glass ampoule of 0.3 mm inner diameter and 1mm outer diameter; 3 – 0.2 mm thick aluminium backing; 4 – converter; 5 – position of conversion electron source.

source and an infinitely thin spherically symmetrical target. In our case a source possessing axial symmetry (fig. 2) and very thin targets were used. The first successful experiments with a source of such design were carried out by Bashilov, Antonieva and Dželepov [28, 29]) and subsequently also on our spectrometer [26, 27, 30, 31]).

3.2. MEASUREMENTS AND RESULTS

A target 1.1—1.2 mm in diameter was used to study the Se^{75} γ-spectrum. In order to elucidate the effect of thickness σ and atomic number Z of the target substance, targets with strongly different values of Z and σ were employed. Thus for Ag the values were $\sigma = 0.03$, 0.25 and 1.0 mg/cm^2 and for Bi: $\sigma = 0.03$ and 0.1 mg/cm^2. After introduction of various relevant corrections the relative γ transition intensities could be obtained. The values presented in table 1 are the average of experiments carried out with 8 different targets [22]). Parts of the photoelectron spectra are shown in fig. 3. The relative half-width of the line corresponding to the 66.5 keV transition obtained with an Ag target of

$\sigma = 0.03$ mg/cm² was found to equal 0.6 %; the hlaf-width of all other lines was the same as the instrumental half-width. Transitions with $h\nu = 77.1$ and 199.5 keV could be observed only with a thicker target. Similarly, the 304.6 keV

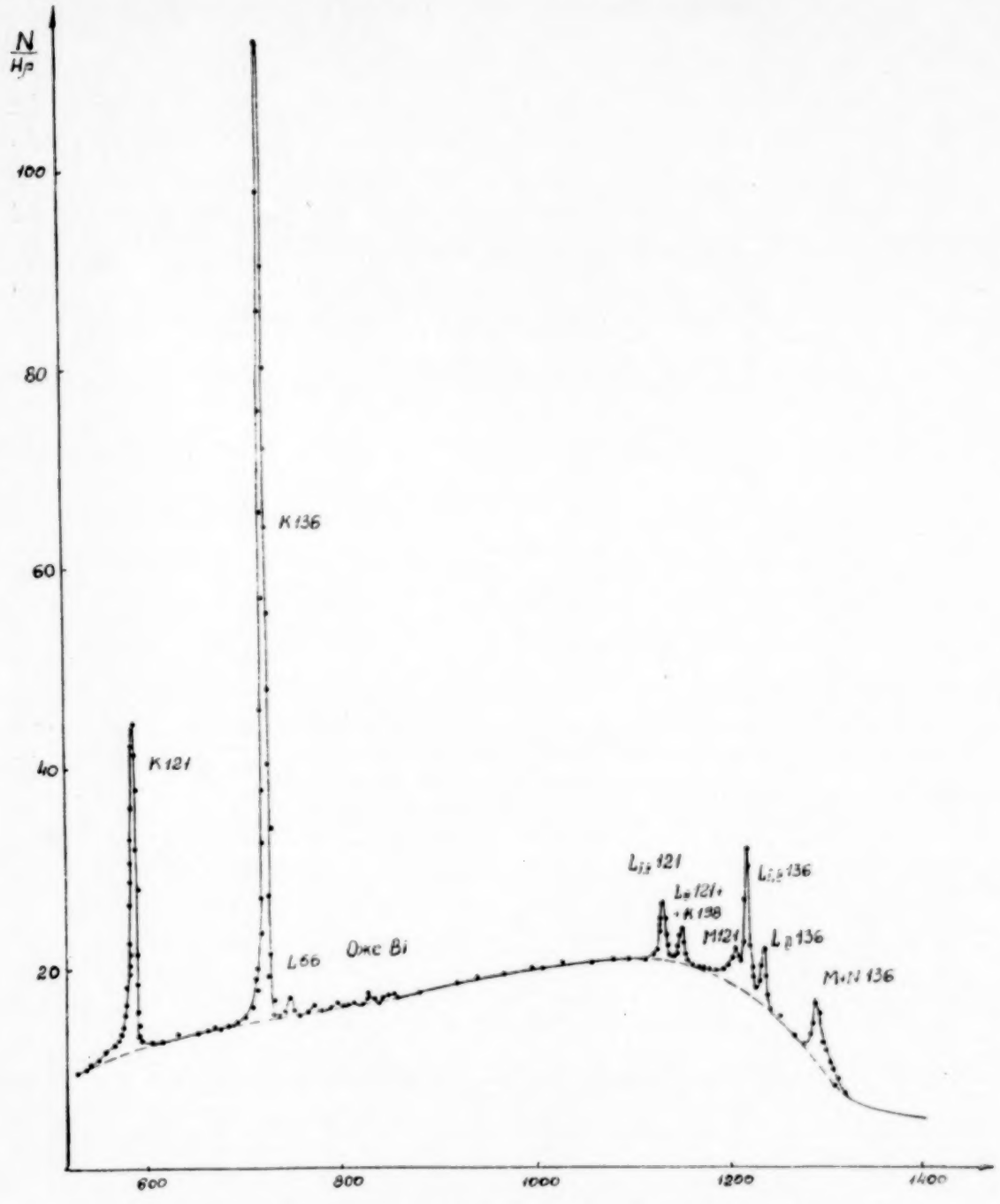

Fig. 3. Photoelectron spectrum of Se^{75} on $\tau = 0.1$ mg/cm² bismuth target.

transition could be observed with a Bi target of $\sigma = 0.1$ mg/cm². The very weak 572.4 keV transition was observed with thick Bi ($\sigma = 15$ mg/cm²), Pb($\sigma = 13$ and 18 mg/cm²) and Ta ($\sigma = 80$ mg/cm²) targets. The intensity of this

transition was expressed in terms of the 401 keV transition. In all measurement runs the 265 keV transition was used as a reference.

A careful study was made of the γ spectrum in the region in which lines from the possible transitions $h\nu = 81$, 370 and 478 keV were expected. Additional measurements of the spectrum with a tantalum target were carried out with the purpose of observing hard lines. A search of the 477 keV γ transition detected in the decay of Ge^{75} was impeded by the circumstance that in high Z targets

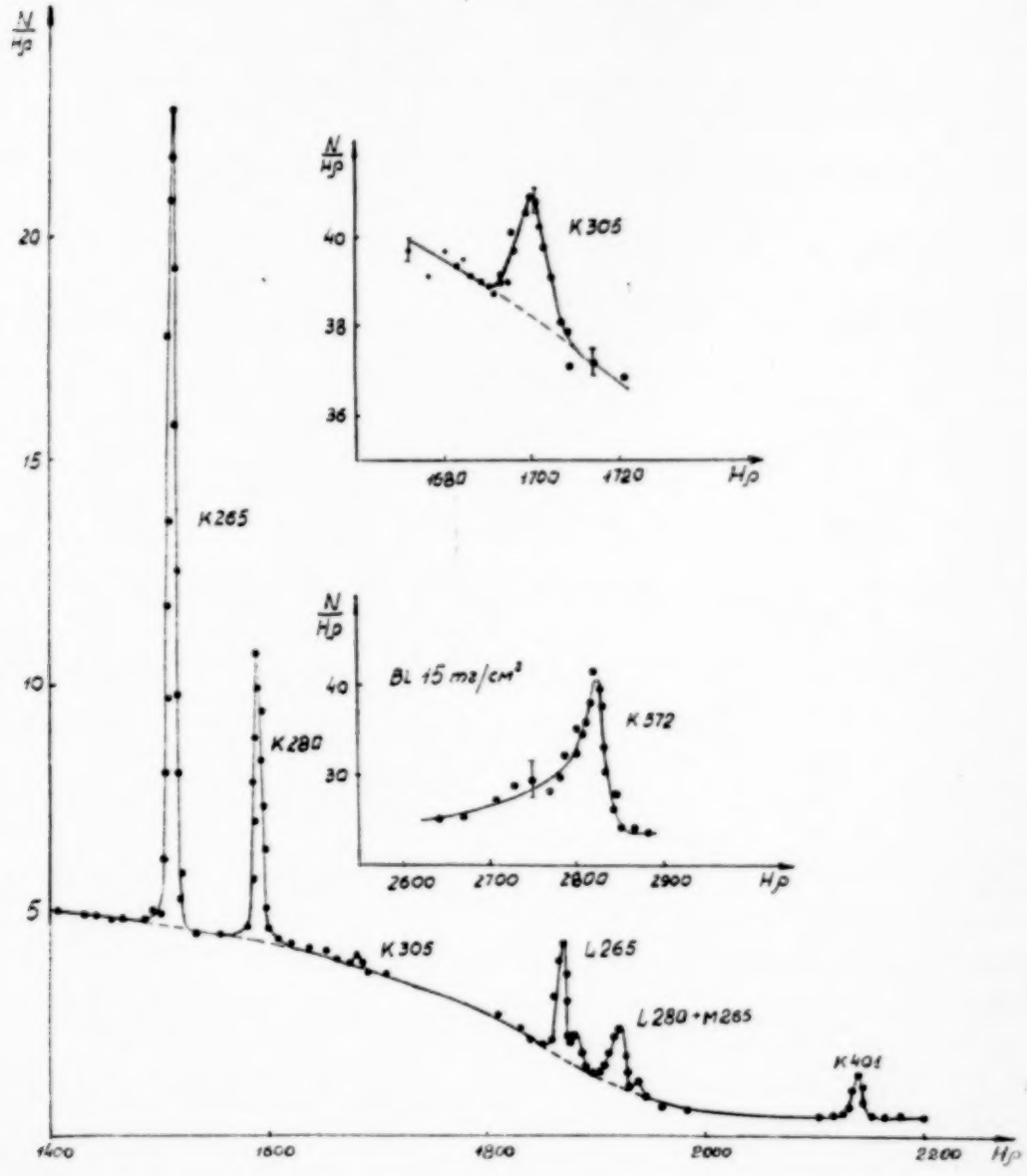

Fig. 3. (continued)

L and M photopeaks due to the 401 keV transition are located in this region. A search of a photoline produced by the 370 keV transition was difficult for the same reason. From our analysis of the experimental data we were only able to

indicate the uppler limit of the intensities of these transitions. The intensities of the soft lines obtained by employing a thick Ag($\sigma = 1$ mg/cm^2) target and high Z targets, e.g. Bi($\sigma = 0.03$ and 0.1 mg/cm^2) targets, were found to be lower compared with the intensities obtained by employing thin Ag targets. The intensities of the softest lines obtained with thin Ag targets were therefore assumed to be the most accurate.

3.3. COMPARISON WITH DATA OF OTHER AUTHORS

The γ ray intensities of Se^{75} obtained by us are in agreement with those measured by Schardt and Welker [13]) and Van den Bold *et al.* [19]) by using calibrated scintillation spectrometers. A certain discrepancy between the data in ref. [19]) and those of the two other investigations (ref. [13]) and the authors)

TABLE 1

Relative intensities of γ transitions in Se^{75}

Transition (keV)	Our data	Data of Voinova, Džhelepov and Zhukovsky [24])
66.5	1.53±0.15	–
77.1	0.3 ±0.1	–
81	<0.1	–
96.6	5.5 ±0.3	–
121.2	27.9 ±1.3	–
136.2	96 ±5	–
199.5	2.6 ±0.2	<6.4
265.0	100.0	100.0
280.0	41 ±2.5	44 ±7
304.6	2.5 ±0.3	3.2±1.1
370	<0.5	–
401.2	22.3 ±2.3	23 ±2
478	<0.5	1.1±0.7
572.4	0.18±0.06	0.7±0.5

can be explained by the fact that separation of the lines in ref. [19]) was not carried out with sufficient accuracy because of their appreciable broadening, whereas in ref.[13]) a lens spectrometer was used to revolve the close 97+121+136 and 265+280+305 keV lines. The data of Jensen *et al.* [21]) do not agree with any of the available results, the reason of this being that the thickness of the converters (22 and 37 mg/cm^2) affected the width and shape of the photoelectron lines.

Concurrent with our measurements Voinova, Dželepov and Zhukovsky [24]) determined the relative intensities of the 265 keV and higher energy Se^{75} γ rays by the recoil electron method as applied in the "elotron" and "ritron" calibrated spectrometers. The 478 keV transition observed in the decay of Ge^{75} was detected in these experiments. The γ transition intensities are indicated in table 1; they agree with our results.

The calibrated target method was employed by Bashilov and Ilyin [23]) to determine conversion coefficients of the 265, 280, 305 and 401 keV transitions occurring in the decay of Se^{75}. The relative γ ray intensities can also be determined by this method. Comparison of the results with those obtained by us show that they are equal to within 5—10 %. It should be mentioned here that with the source geometry indicated above the relative γ line intensities are reproduced by our instrument without appreciable distortion in the energy region from 0.1 to 2 MeV [22]).

Investigation of e^-—e^- coincidences due to Se^{75} decay was first carried out by Bunakov, Dželepov, Zvolsky and Sergienko [17]) simultaneoulsy with our work. The cascades first detected by γ—γ coincidences were confirmed by these authors.

4. Internal Conversion Electron Spectrum of Se^{75}

4.1. MEASUREMENTS AND RESULTS

We measured 26 conversion lines corresponding to 12 transitions in As^{75} These include the K—LL, K—LM and K—MM Auger electron lines which were resolved by us and whose intensities were estimated. Several measurement sets were carried out with each of the three sources and in each case the intense K-265 line which served as reference was measured. The results obtained after averaging and introduction of corrections are shown in figs. 4—7. The energies, intensities and origin of the lines are indicated in table 2. The L and M conversion lines were completely resolved only for the 24 keV transition. Since the L and M lines from transitions in the 66—265 keV region could not be resolved experimentally they were resolved in accord with the shape of the K peaks and a tentative estimation of their intensities was made on this basis.

An additional background due to electrons scattered in the source and spectrometer should be noted. It was carefully masured over the whole spectrum with the purpose of making a more accurate determination of the line areas. Since the soft lines are quite strong and scattering is small in the hard part of the spectrum this effect did not introduce any appreciable errors in the line area measurements. The background hindered observation of the weak K-77 line. Moreover the K-77 peak partially overlapped the M-66 peak. We could therefore estimate only the upper limit of the K-77 line intensity which was 0.7 of that of the K-81 line. By using a strong source it was possible to observe the K-572 line and to estimate its intensity. No conversion of the possible 477 keV transition was detected. Measurements in this region of the spectrum indicated that the K-477 line was at least 5 times weaker than the K-572 line. All these estimations are presented in table 2.

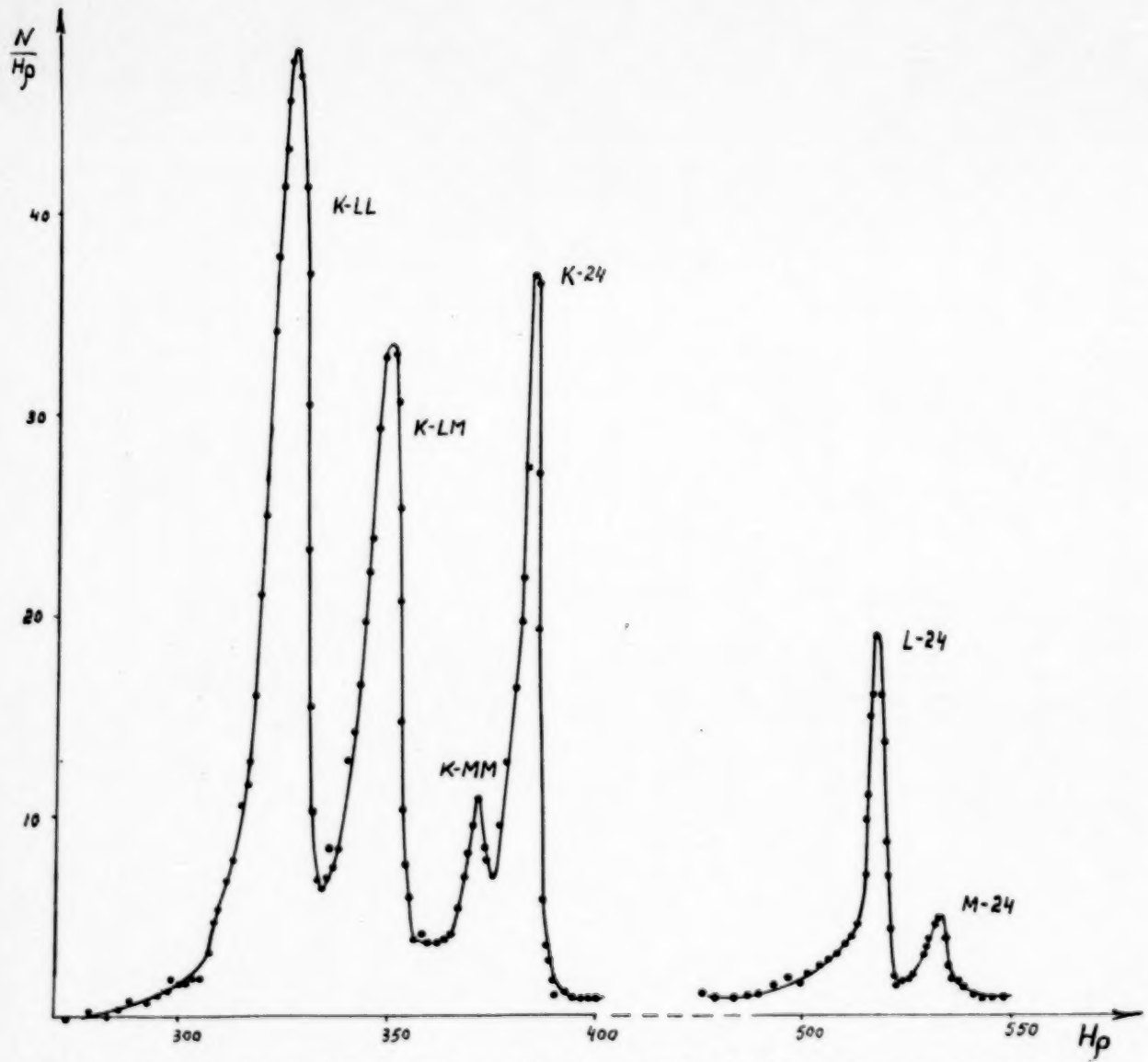

Fig. 4. Auger electron and 24.6 keV transition lines obtained with a 0.05 mg/cm² Se^{75} source.

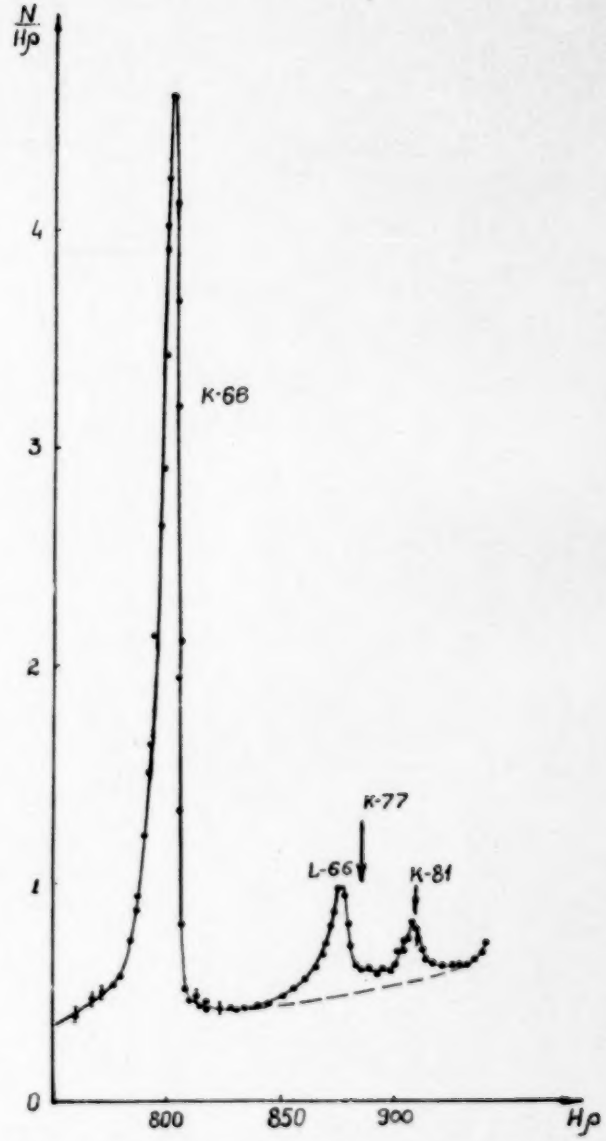

Fig. 5. Conversion lines of 66—81 keV transitions. The arrow indicates the position of the weak K-77 line.

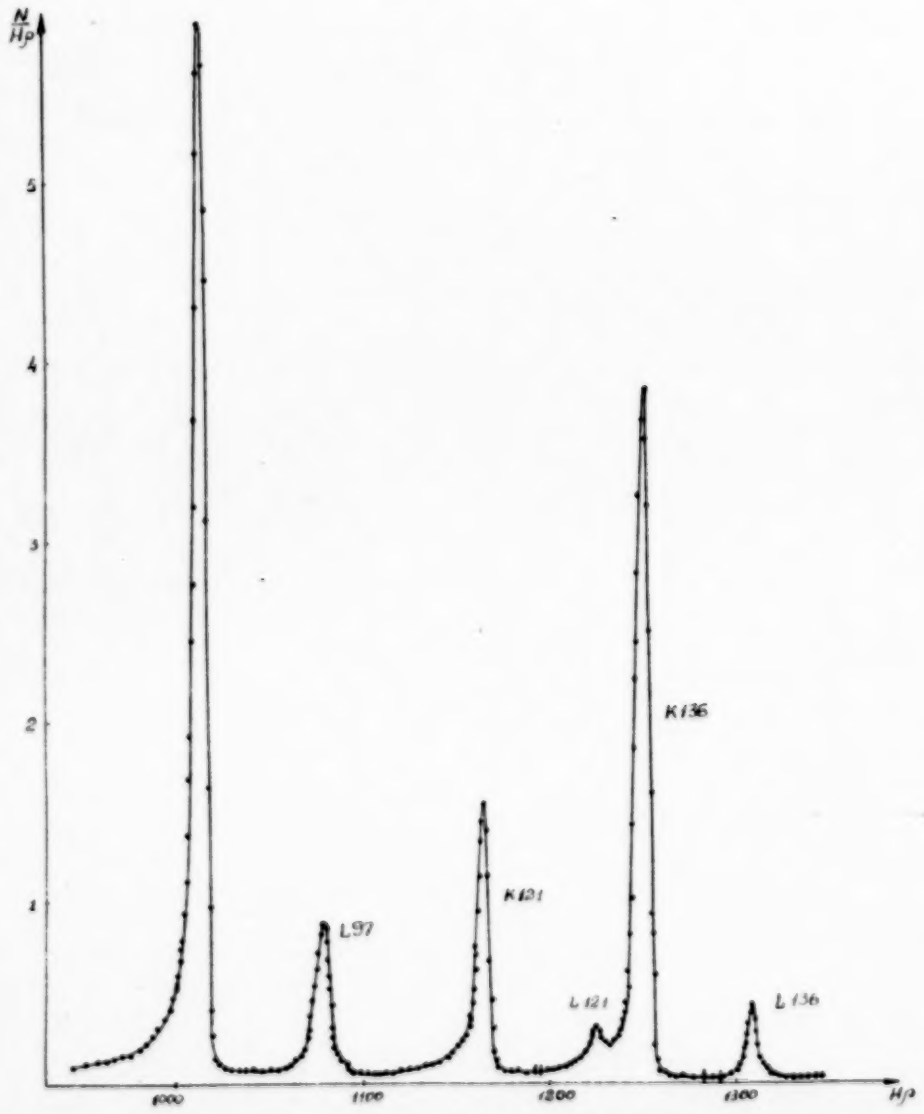

Fig. 6. Conversion lines of 96.6, 121 and 136 keV transitions.

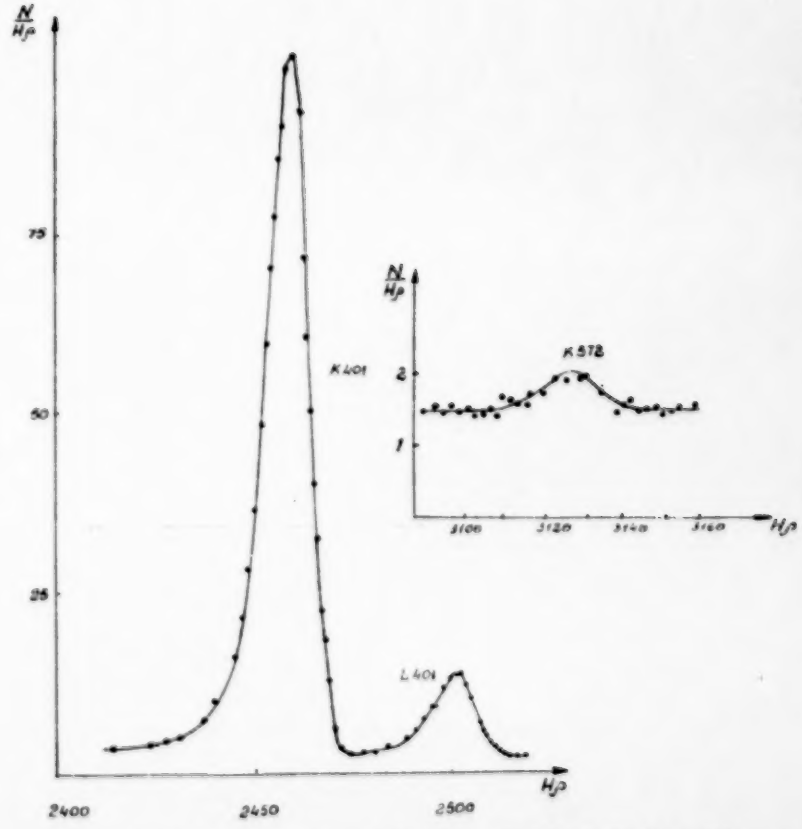

Fig. 7. Conversion lines of 401 and 572 keV transitions.

TABLE 2

Transition energies and relative intensities of conversion lines of Se^{75}

E (keV)	Line	Relative intensities	1. K/L 2. L/M 3. K/(L+M)
1	2	3	4
	K−LL	$(1.1 \pm 0.4) \times 10^4$	
	K−LM	$(3.7 \pm 0.8) \times 10^3$	
	K−MM	$(1.4 \pm 0.4) \times 10^2$	
24.6±0.2	K	1250 ±150	1. 4.0±0.9
	L	314 ± 31	2. 5.1±1.0
	M	61 ± 6	
66.5±0.5	K	73.7 ± 4.4	3. 5.9±1.5
	L+M	(12.4 ± 2.4)	
77 ±0.5	K	5	
81 ±0.6	K	7 ± 1	
96.6±0.5	K	645 ± 25	1. 7.5±0.7
	L	85.9 ± 4.3	2. 5.3±0.8
	M	15.9 ± 2.0	
121.2±1.0	K	154 ± 2	3. 7.2±0.6
	L+M	21.4 ± 1.3	
136.0±0.8	K	384 ± 5	1. 10.1±0.4
	L	38 ± 1	2. 5.9±0.7
	M	6.4 ± 0.6	
199.5±1.2	K	7.3 ± 0.3	3. 8.5±0.9
	L+M	0.82 ± 0.03	
265.0±1.0	K	100 ± 3	3. 7.4±0.8
	L+M	13.5 ± 1.0	
280.0±1.0	K	49.2 ± 3.0	3. 7.7±0.8
	L+M	6.4 ± 0.3	
304.5±1.3	K	16.1 ± 0.8	3. 6.9±0.2
	L+M	2.34 ± 0.16	
401.2±2.0	K	3.76 ± 0.26	3. 8.5±1.7
	L+M	0.44 ± 0.04	
477	K	<0.01	
572 ±3	K	0.055± 0.022	

4.2. CONVERSION COEFFICIENTS AND MULTIPOLARITIES OF TRANSITIONS

Two independent methods can be applied to determine the conversion coefficients from the measured relative intensities of the γ rays I_γ and conversion lines I_K. The first method consists in comparing the experimental ratios I_K/I_γ with the values of the conversion coefficients for the 265, 280, 305 and 401 keV transitions as measured by the calibrated target method by Bashilov and Ilyin [23]). The ratio of the quantities $A_K = \alpha_K/(I_K/I_\gamma)$ for these transitions was found to be constant. The average of these quantities was used to determine α_K for the other transitions.

The second possibility is to exploit the fact, established by other methods, that the transitions 121, 136 and 401 keV are of the E1 type. Then, by perfor-

TABLE 3

Determination of conversion coefficients of As^{75} transitions

Transition (keV)	I_K/I_γ	$\alpha_K \cdot 10^3$ According to ref.[23])	$A_K = \alpha_K/(I_K/I_\gamma)$	$\alpha_K = A_K \cdot (I_K/I_\gamma)$	α_K theor. for E1	$A = \alpha_{KT}(I_K/I_\gamma)$	$\alpha_K = A(I_K/I_\gamma)$	Multipolarity
1	2	3	4	5	6	7	8	9
66.5	48	–	–	0.30	–	–	0.30 ±0.03	M1, E1
77	≦15.6	–	–	≦0.1	–	–	≦0.10	E1(M1)
81	≧70	–	–	≧0.44	–	–	≧0.44	(E2)
96.6	117	–	–	0.75	–	–	0.78 ±0.05	E2
121.2	5.8	–	–	0.037	0.0371	0.0064	–	E1
136.2	4.0	–	–	0.026	0.0263	0.0066	–	E1
199.5	2.8	–	–	0.018	–	–	0.018 ±0.002	M1+E2
265.0	1.00	6.0±0.6	0.0060	0.0064	–	–	0.0065±0.0004	M1
280.0	1.20	7.9±1.0	0.0066	0.0077	–	–	0.0076±0.0008	M1(80 %)+E2(20 %)
304.6	6.7	42 ±6	0.0063	0.043	–	–	0.043 ±0.006	E3
401.2	0.17	1.1±0.2	0.0066	0.0011	0.00107	0.0064	–	E1
572.4	0.30	–	–	0.020	–	–	0.0020±0.0013	(M1+E2)
			$A_K = 0.0064$			$A = 0.0065$		

ming the same type of comparison, one can determine the conversion coefficients for other transitions.

The values of α_K determined by the two methods (columns 5 and 8 in table 3) were found to be identical. The errors in α_K lay between 6 and 14 %. The multipolarities of these transitions can be indicated by using the theoretical values of α_K.

An estimation of α_K for the 77 keV transition is presented in table 3. It was derived from the limiting values of the ratios for the 77 keV and 81 keV transitions i.e. from $I_{K-77}/I_{K-81} \leqq 0.7$ and $I_{\gamma-81}/I_{\gamma-77} \leqq 0.3$, whence it may be concluded that the 81 keV transition is converted by more than 4 times compared to the 77 keV transition. Thus, if the 81 keV transition is assigned as E2, a multipolarity of E1 or M1 should be assigned to the 77 keV transition.

TABLE 4

Determination of the multipolarities of the 24.6, 96.6 and 136.0 keV transitions from the value of $(K/L)_{exp}$

E (keV)	$(K/L)_{exp}$	$(K/L)_{theor}$						Multipolarity
		E1	E2	E3	M1	M2	M3	
24.6	4.0±0.9	7.8	1.7	0.36	8.8	4.6	1.5	M2(E2+M1) †
96.6	7.5±0.7	9.6	7.3	4.2	9.3	7.8	5.6	E2, M2, E2+M1
136.0	10 ±0.4	9.6	7.9	5.6	9.3	7.9	6.2	E1

† Analysis of the decay scheme permits one to choose M2 from the two possible multipolarity values.

The conversion coefficients determined quite recently by Schardt and Welker [13]) differ from ours on the average by a factor 2.5.

A multipolarity of M2 or M1+E2 can be assigned to the 24.6 keV transition on the basis of the measured value of the ratio $K/L = 4.0 \pm 0.9$. The experimental ratio K/L for this transition is compared with the theoretical value in table 4. The values of α_K were computed by G. F. Dranitsina by interpolating Rosés data and taking into account the effect of screening. The values of α_L for $Z = 33$ were communicated to us by Sliv and Band [32]). By making a similar comparison one can obtain information on the multipolarity of the 96.6 keV and 136.0 keV transitions. This yields a new and independent proof that the 136 keV transition is an E1 transition (see table 4).

5. Intensity Balance in Se^{75} Decay

The intensities of the K—X rays from As^{75} were measured by Schardt and Welker. From the data of these authors it can be concluded that transition between the ground states of Se^{75} and As^{75} is not a frequent event and is less than 20 % of the Se^{75} decay rate. A similar value can also be deduced on the

basis of the intensities of the Auger electron lines (tables 2 and 5). On the other hand, the decay scheme (fig. 1) and table 6 show that the 401 keV level becomes highly populated as a result of electron capture. This may happen if the parity of the Se^{75} ground level is the same as that of the 401 keV As^{75} level, that is, if the

TABLE 5

Intensity of Se^{75} transitions in percent of decay rate

$h\nu$ (keV)	I_γ	$I_{(K+L+M)}$	$I_{(\gamma+K+L+M)}$	
			Our data †	According to ref. [13])
1	2	3	4	5
KX + Auger	— ††	52	≈108	81 ±12
24	—	4.9	4.9	—
66	0.97	0.31	1.3	1.4
77	0.17	<0.018	<0.2	<0.2
81	<0.05	0.026	<0.07	0.13
96	3.1	2.66	5.8	11.5
121	15.1	0.64	15.7	17.3
136	53.6	1.54	55.1	56.7
199	1.45	0.029	1.5	1.8
265	55.9	0.39	56.3	57.0
280	22.9	0.20	23.1	26.2
305	1.39	0.066	1.5	1.2
370	<0.028	—	<0.03	—
401	12.5	0.015	12.5	14.0
478	<0.26	$\leqq 4 \times 10^{-5}$	<0.3	—
572	0.10	2.0×10^{-4}	~0.1	—

† The intensity of transitions to the ground level is assumed to be 95 %.
†† The intensity of KX is derived from the fluorescence yield $W_K = 52$ %.

TABLE 6

Intensity balance and determination of log τf for transitions of Se^{75} to As^{75} levels. The intensities are in percent of the total decay rate

Level	Intensities of incoming γ-transitions	Intensities of outgoing γ-transitions	Intensities of electron capture	log τf branches of electron capture
0	95	—	5	7.9
199	1.4	1.5	0.1	9.4
265	55.1	57.6	2.5	7.9
280	20.6	23.1	2.5	7.9
305	5.8	6.4	0.6	8.5
401	≦0.2	89.1	89	5.9
478	—	<0.5	<0.5	>8.2
572	—	0.1	0.1	8.7

allowed transition $\frac{5}{2}+ \rightarrow \frac{5}{2}+$ takes place. A rigorous proof of this conclusion can be obtained by calculating the log τf value for the transitions. The sum of the intensities of the γ transitions to the ground state of As^{75} is first assumed to

be 100 % and the intensities of the individual transitions are then determined. After this one may compute in accord with the decay scheme the probability of occupation of the As^{75} levels as a result of electron capture in Se^{75} and compute $\log \tau f$ for the respective transitions.

Since the spins and parities of the As^{75} ground state and 265 keV level are the same, the $\log \tau f$ value for transitions to these levels should be close. This signifies that about 5 % of the total number of Se^{75} decays involve transitions to the ground state. If we assume, in accord with the foregoing, that the total intensity of γ transitions to the ground state is 95 %, we obtain the absolute γ transition intensities and the intensity balance for Se^{75} decay presented in tables 5 and 6.

It should be noted that the $\log \tau f$ values for transitions to the 401 keV, 280 keV and 265 keV levels agree with the selection rules for these transitions i.e. $\Delta I = 0$, no; $\Delta I = 0$, yes; $\Delta I = 1$, yes, respectively.

6. Level Lifetimes

The following lifetimes have been estimated or measured:

Level (keV)	Lifetime (sec)	Reference
401	1.5×10^{-9}	[12])
305	1.7×10^{-2}	[6, 9, 10])
280	$\approx 3 \times 10^{-10}$	[11, 13])
265	2×10^{-11}	[12, 13])

Knowing the relative γ ray intensities and the conversion coefficients of the transitions from the indicated levels one can compute the partial lifetimes with respect to these transitions. The ratios thus obtained can be compared with

TABLE 7

Ratio of experimental $\tau_{\gamma e}$ and theoretical $\tau_{\gamma s.p.}$ lifetimes for Se^{75} γ transitions

Level (keV)	Transition (keV)	Multipolarity	$\tau_{\gamma exp}$ (sec)	$\tau_{\gamma s.p.}$ (sec)	$\tau_{\gamma e}/\tau_{\gamma s.p.}$	
					Our data	According to ref. [33])
401	401	E1	1.1×10^{-8}	6×10^{-15}	1.8×10^{6}	
	136	E1	2.4×10^{-9}	1.5×10^{-13}	1.6×10^{4}	
	121	E1	9×10^{-9}	2.1×10^{-13}	4×10^{4}	
	96	E2	4×10^{-8}	2.5×10^{-6}	1.6×10^{-2}	8×10^{-2}
305	305	E3	7×10^{-2}	7×10^{-3}	10	500
280	280	E2	3×10^{-10}	1×10^{-8}	3×10^{-2}	8×10^{-2}
		M1		1.6×10^{-12}	2×10^{2}	3×10^{2}
	81	E2	5×10^{-8}	6×10^{-6}	8×10^{-3}	8×10^{-2}
265	265	M1	2×10^{-11}	2×10^{-12}	10	300
	66	M1	6×10^{-9}	1.2×10^{-10}	50	300

those computed on basis of the single-particle model. The comparison is made in table 7. The mean values of the ratio of the experimental and theoretical lifetimes (last column in table 7) have been derived in ref. [33]). As a whole our values do not contradict the assignments made in ref. [33]).

At present it is difficult to draw any conclusions regarding the nature of the As^{75}, Se^{75} or Ge^{75} levels. If the As^{75} and Ge^{75} spins are those expected on basis on the shell model, the Se^{75} spin should rather be regarded as not being consistent with this model. The quadrupole moment of this nucleus is anomalously high: $Q = 1.1 \pm 0.2$ b [34, 35]). The magnetic moment of the ground state of As^{75} can better be explained by assuming that the nucleons of this nucleus form a configuration (see table 8). It is possible that the nature of the excited levels should be explained in a similar way.

TABLE 8

Magnetic moment of As^{75} computed for various configurations with $J = \frac{3}{2}-$ [36,37,38])

Proton configuration	μ calculated
$(p_{\frac{3}{2}})^2\ (f_{\frac{5}{2}})_{\frac{3}{2}}^3$	1.435
$(g_{\frac{9}{2}})^2\ (p_{\frac{3}{2}})^3$	1.62
$(f_{\frac{5}{2}})^2\ (p_{\frac{3}{2}})^3$	2.21

$\mu_{exp} = 1.44$.

Note: After our paper was sent to the editors two new studies of Se^{75} decay were published. In one of them [39]) the exact values of the energies of γ-transitions were determined through the crystal diffraction method: 66.054; 96.74; 121.12; 135.99; 198.60; 264.62; 279.57; 304.0 and 400.7 keV.

In the other [40]) the intensities of conversion and γ-transitions in the range of energies 136—402 keV were measured and the coefficients of the conversion of the relevant transitions determined. The paper offers a detailed study of possible mixed radiations in certain transitions. The results of our measurements [22]) are in good agreement with the data of this paper.

In conclusion the authors express their sincere appreciation to Prof. B. S. Džhelepov for useful remarks during the discussion of the paper. The authors are grateful to A. A. Bashilov, N. N. Zhukovsky, V. A. Sergienko, I. Zvolsky for communicating their results of investigation of Se^{75} prior to publication. Thanks are due to V. N. Klementiev, R. V. Sinitsyn, N. D. Novosiltseva, V. Zvolskaya, V. A. Mikhailov, V. O. Sergeyev and S. L. Sakharov for participating in the measurements and for aid during various stages of the investigation.

References

1) C. V. Kent, J. M. Cork and W. G. Wadey, Phys. Rev. **61** (1942) 389A
2) C. C. Trail and C. H. Jonson, Phys. Rev. **91** (1953) 474A
3) J. B. Butler and C. R. Gossett, Bull. Am. Phys. Soc. **2** (1957) 230
4) G. M. Temmer and N. P. Heydenburg, Phys. Rev. **93** (1954) 351; **100** (1955) 961A
5) E. B. Paul and H. E. Gove, Revs. Mod. Phys. **28** (1956) 432
6) E. C. Campbell and P. H. Stelson, Nucl. Sci. Abstr. **10** (1956) N 24B, 58
7) L. Cranberg and I. S. Levin, Phys. Rev. **103** (1956) 343
8) M. A. Rothom, H. S. Hans and C. E. Mandeville, Phys. Rev. **100** (1955) 83
9) A. W. Schardt, Phys. Rev. **108** (1957) 398
10) S. H. Wegors Jr. and P. Axel, Phys. Rev. **100** (1955) 1238A; **101** (1956) 1067
11) F. R. Metzger, Phys. Rev. **110** (1958) 123
12) H. Langevin-Joliot and M. Langevin, Jour. Phys. Rad. **19** (1958) 765
13) A. W. Schardt and J. W. Welker, Phys. Rev. **99** (1955) 810
14) J. M. Cork ,W. C. Rutledge and C. E. Branyan, Phys. Rev. **79** (1950) 889
15) A. W. Schardt and J. W. Welker, Phys. Rev. **93** (1954) 916A
16) D. C. Lu, W. H. Kelli and M. L. Wiedenbeck, Phys. Rev. **97** (1955) 139
17) V. E. Bunakov, B. S. Dželepov, I. Zvolsky and V. A. Sergienko, Izv. Akad. Nauk SSSR, Ser. Fiz. **23** (1959) 859
18) W. H. Kelli and M. L. Wiedenbeck, Phys. Rev. **102** (1956) 1130
19) H. J. Van den Bold, J. Van de Gein and P. M. Endt, Physica **24** (1958) 23
20) S. B. Burson, W. C. Jordan and J. M. Le Blanc, Phys. Rev. **95** (1954) 613
21) E. E. Jenesen, L. J. Lasslett, D. S. Martin Jr., F. J. Hughers and W. W. Pratt, Phys. Rev. **90** (1953) 557
22) E. P. Grigoriev, A. V. Zolotavin, V. N. Klementiev and R. V. Sinitsyn, Izv. Akad. Nauk SSSR, Ser. Fiz. **23** (1959) 159
23) A. A. Bashilov and V. V. Ilyin, Izv. Adad. Nauk SSSR. Ser. Fiz. **23** (1959) 154
24) N. A. Voinova, B. S. Dželepov and N. N. Zhukovsky, Izv. Akad. Nauk SSSR, Ser. Fiz. **23** (1959) 185
25) A. V. Zolotavin, Izv. Akad. Nauk SSSR, Ser. Fiz **18** (1954) 127
26) A. V. Zolotavin, E. P. Grigoriev and M. A. Abroyan, Izv. Akad. Nauk SSSR, Ser. Fiz. **20** (1956) 239
27) E. P. Grigoriev, A. V. Zolotavin, I. I. Kuzmin and E. D. Pavlitskaya, Izv. Akad. Nauk SSSR, Ser. Fiz. **22** (1958) 194
28) A. A. Bashilov, N. M. Antonieva, D. A. Broder and B. S. Dželepov, Izv. Akad. Nauk SSSR, Ser. Fiz. **17** (1953) 468
29) A. A. Bashilov, N. M. Antonieva, M. V. Blinov and B. S. Dželepov, Izv. Akad. Nauk SSSR Ser. Fiz. **18** (1954) 43
30) E. P. Grigoriev, L. V. Gustova, A. V. Zolotavin, B. Kracik, T. V. Polushchuk and O. V. Chubinsky, Vestnik LGU N 10 (1957) 37
31) M. P. Avotina, E. P. Grigoriev, A. V. Zolotavin and B. Kracik, Doklady Akad. Nauk SSSR **119** (1958) 1127
32) L. A. Sliv and I. M. Band, Tables of internal conversion coefficients of gamma rays
33) K. Way, D. N. Kundu, C. L. McGinnes and R. van Lieshout, Annual Review of Nuclear Science **6** (1956) 129
34) L. C. Aamodt, P. C. Fletcher, G. Silvey and C. H. Townes, Phys. Rev. **94** (1954) 789A
35) E. F. Kults, W. W. Coontz and V. T. Hartman, Uspekhi Fiz. Nauk **25** (1955) 537
36) M. G. Mayer and J. H. Jensen, Elementary Theory of Nuclear Shell Structure
37) A. Arima and H. Horia, Prog. Theoret. Phys. **12** (1954) 623
38) H. Kopferman, Kernmomente (Frankfurt am Main 1956)
39) W. F. Edwards, C. J. Gallagher and J. M. M. DuMond, Bull. Am. Phys. Soc. **4** (1959) 279
40) F. R. Metzger and W. B. Todd, Nuclear Physics **10** (1959) 220

4.E *Nuclear Physics* **14** (1959/60) 459—464; © *North-Holland Publishing Co., Amsterdam*

Not to be reproduced by photoprint or microfilm without written permission from the publisher

INVESTIGATIONS OF THE DECAY-SCHEME OF Fe^{59}

D. BERÉNYI, GY. MÁTHÉ and T. SCHARBERT

Institute of Nuclear Research of the Hungarian Academy of Sciences, Debrecen

Received 1 September 1959

Abstract: We have examined the gamma-ray spectrum and gamma-gamma coincidence spectrum of Fe^{59} by means of scintillation spectrometers. The two lines of high energy have been found to be 1.08 and 1.27 MeV respectively. Between these lines no genuine coincidence could be detected.

It was the analysis of beta spectrum and beta-gamma coincidence spectra which yielded the beta groups of 275 ± 5 and 455 ± 5 keV end-point energies. The intensity of these was 44.6 and 55.4 % respectively, and their corresponding log ft values were 5.3 and 6.1. The relative intensity of the high energy beta transition directly into the ground state was found not to attain 0.5 %.

1. Introduction

As early as in 1942, M. Deutsch and coworkers [1]), on investigating the decay of Fe^{59}, found that the beta-ray of the above isotope consisted of two groups, the end-point energy values of which were 257 and 460 keV. The same authors, while investigating the spectrum of secondary electrons obtained from the lead radiator, identified also two gamma-ray transitions (1.1 and 1.3 MeV). The latter gamma-lines were later measured also by several other authors, some of them using the above-mentioned method, some investigating the internal conversion electrons [2–5]). One of these authors [3]) examined again the beta-spectrum too, but he did not find the group of 257 keV end-point energy.

Subsequently, Metzger [6–7]), using a source of high specific activity, investigated in detail the decay of the isotope in question. He studied the beta-ray spectrum, the internal conversion electron spectrum and the photoelectron spectrum produced from gold foil by gamma-rays; furthermore, he carried out measurements for gamma-gamma coincidence and angular correlation by using scintillation counters. As a result of these measurements he corroborated the existence of the beta-group of lower end-point energy. He even proved the 0.3 per cent occurrence of a group of 1560 keV and-point energy. His further finding was the certitude of a gamma-line of 191 keV.

Considering that neither Metzger in any of his reports, nor other authors in any of their publications on Fe^{59}, have given account of beta-gamma coincidence measurements, we thought it desirable to contribute to the clarification and the corroboration of the decay scheme by such measurements. At the same time,

we wish to report somewhat more in detail on our scintillation spectrometer studies of the gamma spectrum of Fe^{59}, as well as on gamma-gamma coincidence spectrometric measurements, as these have only been briefly reported hitherto [6]).

2. Experimental

2.1. SOURCE

The preparation of Fe^{59} was obtained in the form of $FeCl_3$ from Harwell. Its specific activity was 4.22 c/g Fe. The source both for beta and gamma spectroscopic studies were prepared by drop method with a backing of ≈ 1 mg/cm^2 mylar foil.

For the gamma-gamma spectrometric investigations the mylar foil was placed in the middle of a suitably shaped lead disc. The lead disc served the purpose of eliminating (unfortunately not quite successfully) false coincidences arising from Compton scattering. When preparing the source for beta-spectrometric purposes in order to prevent charging of the backing, the plexi source holder skeleton, the foil, and the source spot itself were coated with vacuum evaporation of aluminium. To prevent dispersion of the radioactive substance, the source was covered with a Zapon foil of $\approx 10\ \mu$g/cm^2. The thickness of the source was 0.1 mg/cm^2 in order of magnitude.

The purity of the radioactive shipment was checked by half-life measurement.

2.2. GAMMA-RAY SPECTROMETER AND GAMMA-GAMMA COINCIDENCE SPECTROMETER

For studying the gamma-spectrum, a conventional scintillation spectrometer with NaI(Tl) crystal was used [8]). The multiplier was of RCA5819 type. The diameter of the cylinder-shaped crystal was 37 mm with a height of 29 mm. The line width at half height was 10 % in the case of gamma-rays of Cs^{137}.

For the coincidence measurements, two such spectrometers were used. The source was placed between the two crystals supported by the lead disc referred to in 2.1.

The coincidence unit was of Hayashi's gate-circuit design [9–10]), with a resolving time of 1.2×10^{-7} sec.

2.3. BETA-RAY SPECTROMETER AND BETA-GAMMA COINCIDENCE SPECTROMETER

The study of the beta-spectrum was made by a magnetic spectrometer of toroid-sector type [11–12]). The same was used for measuring beta-gamma coincidences, but combined with a NaI(Tl) crystal gamma-spectrometer [13]). During the measurements, the beta-spectrometer was set so that it had a transmission of ≈ 3.0 % and a resolution of ≈ 5.5 %.

For the beta-gamma coincidence measurements also, the coincidence unit referred to in 2.2 was used.

Results and Conclusion

3.1. MEASUREMENTS FOR THE GAMMA-RAY SPECTRUM

The presence of the two high energy lines (1.1) and 1.3 MeV) was clearly shown by the scintillation spectrum, but the line of 0.2 MeV was not demonstrable because of the position of the back-scattering peak.

Fig. 1 illustrates the scintillation gammaspectrum of Fe^{59} which was taken in such a way that a lead collimator of 90 mm length had been placed between the source and the crystal. The diameter of collimator channel was 5 mm. The two high energy lines of Fe^{59} were found to be 1.08 and 1.27 MeV respectively.

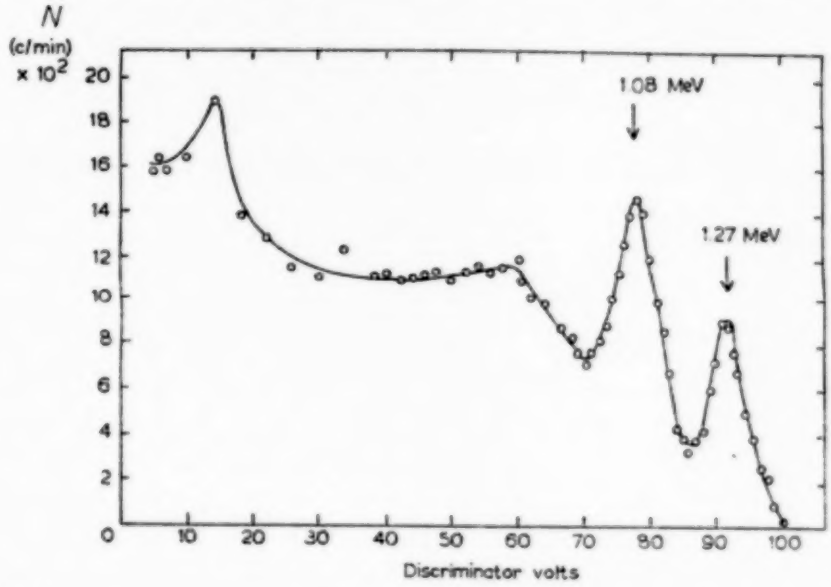

Fig. 1. Scintillation spectrum of Fe^{59} gamma-rays taken by using a lead collimator of 90 mm length and 5 mm channel diameter. (Channel width 1 volt.)

The gamma-gamma coincidence measurements definitely revealed that there was no coincidence between the lines of 1.1 and 1.3 MeV. In this range the number of coincidences surpassed nowhere the number of chance coincidences.

3.1. BETA-RAY SPECTRUM AND BETA-GAMMA COINCIDENCES

Even from the graphic illustration without any particular evaluation of the data of the beta-spectrum it became evident that we were confronted with a complex spectrum. On the basis of the Fermi-Kurie analysis (see fig. 2) two beta-groups may be distinguished: those of 455 ± 5 and 275 ± 5 keV end-point energies. Their relative intensities were found to be 55.4 % and 44.6 % respectively. As to the high energy betagroup, whose end point energy and relative intensity had been found by Metzger to be 1560 keV and 0.3 % respectively, we could only establish by our measurements that the relative intensity should be below 0.5 %.

The FK diagram is straight in the cases of both groups mentioned above.

This fact refers to allowed transition, though the log *ft* value of the higher energy group is 6.1, which is just about the highest limit of the *ft* value-range usually involving the comparative half-life of allowed transition in case of nuclei with odd mass numbers [14]). For the group of lower end point energy, log *ft* is 5.3. In computing these *ft* values we applied 45.4 days representing the mean of the values for the half-life of Fe^{59} reported in Strominger, Hollander and Seaborg's table of isotopes [15]).

The beta-gamma coincidence measurements were made at two different settings of the gamma-spectrometer. By means of one of these settings we

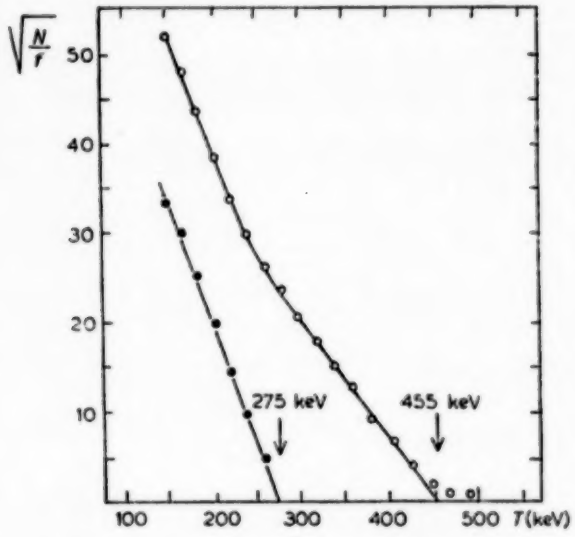

Fig. 2. Fermi-Kurie analysis of Fe^{59} beta-spectrum.

selected the beta-rays in coincidence with gamma-rays of higher energy (1.27 MeV) while by means of the other one we studied the coincidence of beta-rays with all the gamma-rays. The gamma-spectrometer was used in both cases at an integral setting.

Figs. 3 and 4 give good illustrations of the results in beta-gamma coincidence measurements. In fig. 3 the points of the coincidence spectrum were obtained by a measurement of 12×10 min and in fig. 4 by a measurement of 3×10 min. Fig. 3 shows that the gamma-ray of 1.27 MeV is in coincidence only with the beta-group of lower end point energy. If, however, we establish beta-gamma coincidences with all the gamma-rays, the shape of this coincidence spectrum and that of the beta-ray spectrum will completely agree (fig. 4).

These results definitely show, partly that only the beta particles of the beta group of lower end point energy coincide with the gamma line of higher energy; partly that a predominant number of beta-rays is in coincidence with gamma-rays.

The values obtained for the end point energies of the two beta-groups by the

FK analysis of beta-gamma coincidence spectra are in very good agreement with the values obtained by the analysis of beta-ray spectrum.

In this way, our investigations confirm the decay scheme set up by Metzger.

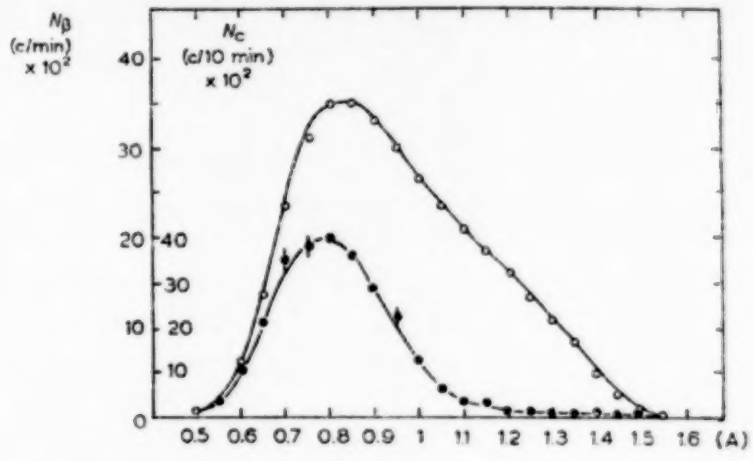

Fig. 3. Beta-ray spectrum (o empty dots) and beta-gamma coincidence spectrum (• black dots) of Fe^{59}. In this case, only gamma-radiation higher than 1.25 MeV was detected by the gamma-spectrometer.

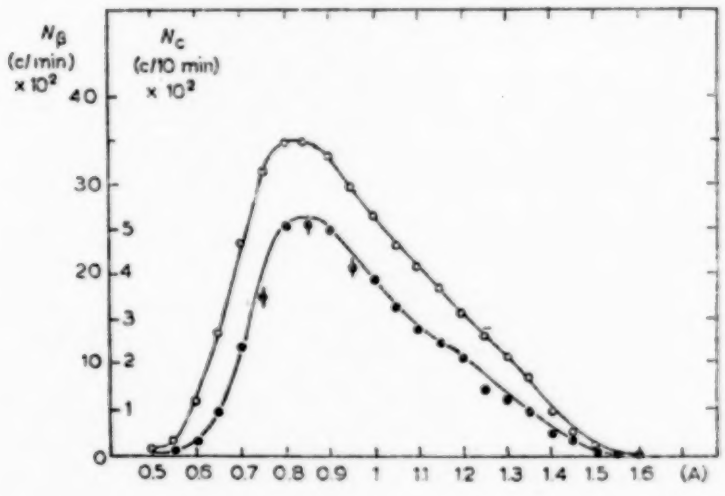

Fig. 4. Beta-ray spectrum (o empty dots) of Fe^{59} and its beta-gamma coincidence spectrum (• black dots) at the detection of all gamma lines in the gamma-spectrometer.

Acknowledgement is due to the director of this Institute, Prof. A. Szalay for his valuable help and the special interest he has taken in our work. Furthermore, the careful preparation of the source by our radio-chemist colleague, Mr. Cs. Ujhelyi is greatly appreciated.

References

1) M. Deutsch, J. R. Downing, L. G. Elliott, J. W. Irvine, Jr. and A. Roberts, Phys. Rev. **62** (1942) 3
2) A. Hedgran, K. Siegbahn and N. Svartholm, Proc. Phys. Soc. A **63** (1950) 960
3) K. Mann and G. Hanson, Phys. Rev. **83** (1951) 893
4) B. S. Dželepov and J. V. Hol'nov, Doklady Akad. Nauk, S.S.S.R. **86** (1952) 255, 497
5) D. Brower, G. Hinman, G. Lang, R. Leaner and D. Rose, Phys. Rev. **86** (1952) 1054
6) F. Metzger, Phys. Rev. **85** (1952) 727
7) F. Metzger, Phys. Rev. **88** (1952) 1360
8) Gy. Máthé and T. Scharbert, Mérés és Automatika **7** (1959) 1
9) T. Hayashi, Journ. Phys. Soc. of Japan **13** (1958) 117
10) T. Hayashi, M. Kawamura and A. Aoki, Sci, Rep. Saikyo Univ. **2A** (1957) 199
11) A. Szalay and D. Berényi, Izvest. Akad. Nauk S.S.S.R. Ser. Fiz. **22** (1958) 877
12) A. Szalay and D. Berényi, Acta Phys. Hungarica **10** (1959) 57
13) D. Berényi, Acta Universitatis Debreceniensis de L. Kossuth nom. (in course of publication)
14) M. E. Rose, in Beta and Gamma-Ray Spectroscopy, edited by Kai Siegbahn (North-Holland Publ. Co., 1955) Ch. IX, 288
15) D. Strominger, J. M. Hollander and G. T. Seaborg, Revs. Mod. Phys. **30** (1958) 585

2.L:).B *Nuclear Physics* **14** (1959/60) 465—471; © *North-Holland Publishing Co., Amsterdam*
Not to be reproduced by photoprint or microfilm without written permission from the publisher

ON THE CONVERGENCE OF THE BORN APPROXIMATION

H. DAVIES
Christ Church, Oxford, England

Received 6 November 1959

Abstract: It is shown that the Born series for the non-relativistic scattering amplitude $f(\mathbf{k})$ by a spherically symmetric static potential $V(r)$, which is bounded and has finite range, is convergent for all $\mathbf{k}$ if the potential $-|V(r)|$ cannot support a bound state.

1. Introduction

The Born approximation is one of the most extensively used methods in quantal scattering theory, and is essentially the expansion of the wave function as a power series in the potential. The first term in this series, i.e. the first Born approximation, is often easily calculated and sometimes gives good agreement with experimental results. Subsequent terms in the expansion are usually difficult to calculate and sometimes faith-shaking, as in the case of Coulomb scattering (cf. Dalitz [1])). The first Born approximation for the scattering of non-relativistic particles by a static potential is often presumed to be a good approximation, subject to the vague reservation that the potential be not too strong and that the energy of the incident particles be sufficiently high.

Some aspects of the convergence of the Born series have been considered by Jost and Pais [2]) and by Kohn [3]). Kohn has treated the case of non-relativistic scattering by a spherically symmetric static potential and has examined the convergence of the Born series for each partial wave, both for $\tan \eta_l$ and for $S_l = e^{2i\eta_l}$, where η_l is the usual phase shift for angular momentum l. He obtains criteria for convergence and some estimates of truncation errors.

Kohn criticizes the "rule of thumb" criterion which states that if a potential well is too weak to support a bound state, the Born expansions for $\tan \eta_l$ and S_l always converge, and in fact shows this to be a false criterion. It is the purpose of this work to show that, with some restrictive conditions on the potential, the "rule of thumb" is a valid rule for the complete three-dimensional scattering amplitude. These restrictions are not imposed in the work of Kohn, which is restricted to the analysis into partial waves. Once this splitting of the problem into partial waves is made, the Born approximation loses its power and uniqueness, because there then exist

always convergent expansions which are only a little more tedious to calculate than the Born series. However, such expansions do not appear to exist in three dimensions, apart from the Fredholm expansion, and here the Born approximation is invaluable.

2. The Born Series

The Schrödinger equation for non-relativistic scattering by a spherically symmetric static potential $\lambda V(r)$, where λ is a parameter, is

$$(\nabla^2+k^2)\psi = \lambda V\psi. \tag{1}$$

Suitable units have been chosen for $\hbar$ and for the mass of the particle. The scattering solution is given by

$$\psi(\mathbf{r}) = \exp(i\mathbf{k}_0\cdot\mathbf{r}) - \frac{\lambda}{4\pi}\int \frac{\exp(ik|\mathbf{r}-\mathbf{s}|)}{|\mathbf{r}-\mathbf{s}|} V(s)\psi(\mathbf{s})d\mathbf{s}, \tag{2}$$

where $\mathbf{k}_0$ is the direction of the incident particles.

We now impose the first restriction on the potential and suppose that $\lambda > 0$ and that $V = -U$ where $U > 0$. Then the scattering amplitude $f(\mathbf{k})$ in a direction $\mathbf{k}$ is given by the usual iterated expression

$$\begin{aligned} f(\mathbf{k}) &= \frac{\lambda}{4\pi}\int d\mathbf{r}\exp(-i\mathbf{k}\cdot\mathbf{r})\,U(r)\exp(i\mathbf{k}_0\cdot\mathbf{r}) \\ &+ \left(\frac{\lambda}{4\pi}\right)^2\int d\mathbf{r}\exp(-i\mathbf{k}\cdot\mathbf{r})\,U(r)\int d\mathbf{s}\frac{\exp(ik|\mathbf{r}-\mathbf{s}|)}{|\mathbf{r}-\mathbf{s}|}U(s)\exp(i\mathbf{k}_0\cdot\mathbf{s}) + \ldots \end{aligned} \tag{3}$$

This series will certainly be convergent, and in fact absolutely and uniformly convergent, if the corresponding series for $f(0)$ is convergent, where

$$f(0) = \frac{\lambda}{4\pi}\int d\mathbf{r}\,U(r) + \left(\frac{\lambda}{4\pi}\right)^2\int d\mathbf{r}\,U(r)\int d\mathbf{s}\,\frac{1}{|\mathbf{r}-\mathbf{s}|}U(s) + \ldots. \tag{4}$$

Performing the angular integrations in equation (4), we have

$$\begin{aligned} f(0) &= \lambda\int_0^\infty dr\,r^2U(r) + \lambda^2\int_0^\infty dr\,r^2U(r)\int_0^\infty ds\,s^2U(s)\mathrm{m}\left(\frac{1}{r},\frac{1}{s}\right) \\ &+ \lambda^3\int_0^\infty dr\,r^2U(r)\int_0^\infty ds\,s^2U(s)\mathrm{m}\left(\frac{1}{r},\frac{1}{s}\right)\int_0^\infty dt\,t^2U(t)\mathrm{m}\left(\frac{1}{s},\frac{1}{t}\right) + \ldots, \end{aligned} \tag{5}$$

where $\mathrm{m}(1/r, 1/s)$ denotes the smaller of the two quantities $1/r$, $1/s$.

We proceed now to connect this power series with similar expressions for S-wave scattering and for S-wave bound states.

3. S-Wave Scattering

Writing the wave function $\psi(r) = (1/r)\phi(r)$, we obtain the equation

$$\phi''+k^2\phi = \lambda V\phi = -\lambda U\phi. \tag{6}$$

This equation may be replaced by a Volterra integral equation

$$\phi(r) = \sin kr - \frac{\lambda}{k}\int_0^r ds \sin k(r-s)\, U(s)\phi(s), \tag{7}$$

and the iterated solution has the correct behaviour at the origin. Iteration gives

$$\begin{aligned}\phi(r) &= \sin kr - \frac{\lambda}{k}\int_0^r ds \sin k(r-s)U\ (s)\sin ks \\ &+ \left(\frac{\lambda}{k}\right)^2\int_0^r ds \sin k(r-s)\, U(s)\int_0^s dt \sin k(s-t)\, U(t)\sin kt + \ldots\end{aligned} \tag{8}$$

Equation (7) is a Volterra equation; therefore, if U is bounded, the iterated series will converge.

We now suppose that U is bounded, and furthermore that it is a finite range potential, i.e. $U(r) = 0$, $r > a$. Then, as $r \to \infty$,

$$\begin{aligned}\phi(r) &= \sin kr - \frac{\lambda}{k}\int_0^a ds \sin k(r-s)\, U(s)\phi(s) \\ &= \sin kr\left\{1 - \frac{\lambda}{k}\int_0^a ds \cos ks\, U(s)\phi(s)\right\} + \frac{\lambda}{k}\cos kr\int_0^a ds \sin ks\, U(s)\phi(s) \\ &= A(k,\lambda)\sin kr + B(k,\lambda)\cos kr.\end{aligned} \tag{9}$$

This Volterra expansion is not the one which we can relate to the series expansion for $f(0)$. The expansion which we require for this is obtained by using a different kernel in the integral equation. We write

$$\phi(r) = \sin kr + \frac{\lambda}{k}\int_0^a ds\, K(r,s)\, U(s)\phi(s), \tag{10}$$

where

$$K(r,s) = \begin{cases}\cos kr \sin ks, & s < r, \\ \sin kr \cos ks, & s > r.\end{cases} \tag{11}$$

Then, as $r \to \infty$, we have

$$\phi(r) = \sin kr + \frac{\lambda}{k}\cos kr\int_0^a ds \sin ks\, U(s)\phi(s) \tag{12}$$

$$= \sin kr + C(k,\lambda)\cos kr, \tag{13}$$

where

$$C(k,\lambda) = \frac{\lambda}{k}\int_0^a \mathrm{d}s\, \sin^2 ks\, U(s) + \left(\frac{\lambda}{k}\right)^2 \int_0^a \mathrm{d}s\, \sin ks\, U(s) \int_0^a \mathrm{d}t\, K(s,t)\, U(t) \sin kt + \ldots \tag{14}$$

The question of the convergence of this expansion for $C(k,\lambda)$ can now be answered by reference to the always convergent expansion (9), since

$$C(k,\lambda) = \frac{B(k,\lambda)}{A(k,\lambda)}; \tag{15}$$

therefore, the power series in λ for $C(k,\lambda)$ will be valid within $|\lambda| < |\lambda_m|$ where λ_m is that zero of $A(k,\lambda)$ which is nearest the origin.

From eq. (14) we have

$$\lim_{k\to 0} \frac{1}{k} C(k,\lambda) = \lambda\int_0^a \mathrm{d}r\, r^2 U(r) + \lambda^2 \int_0^a \mathrm{d}r\, rU(r) \int_0^a \mathrm{d}s\, \mathrm{sm}(r,s) U(s) + \lambda^3 \int_0^a \mathrm{d}r\, rU(r) \int_0^a \mathrm{d}s\, \mathrm{m}(r,s) U(s) \int_0^a \mathrm{d}t\, t\mathrm{m}(s,t) U(t) + \ldots, \tag{16}$$

which is identical with $f(0)$ of eq. (5) when we remember that $U(r) = 0$ for $r > a$, and observe that

$$r\mathrm{sm}\left(\frac{1}{r}, \frac{1}{s}\right) = \mathrm{m}(r,s). \tag{17}$$

The question of the convergence of the Born series is determined from consideration of the expression $\lim_{k\to 0}\{B(k,\lambda)/kA(k,\lambda)\}$, where, from eq. (9),

$$\frac{1}{k} B(k,\lambda) = \frac{\lambda}{k^2}\int_0^a \mathrm{d}r\, \sin^2 kr\, U(r) - \frac{\lambda^2}{k^3}\int_0^a \mathrm{d}r\, \sin kr\, U(r) \int_0^r \mathrm{d}s\, \sin k(r-s)\, \sin ks\, U(s) + \ldots,$$

$$A(k,\lambda) = 1 - \frac{\lambda}{k}\int_0^a \mathrm{d}r\, \cos kr\, \sin kr\, U(r) + \frac{\lambda^2}{k^2}\int_0^a \mathrm{d}r\, \cos kr\, U(r) \int_0^r \mathrm{d}s\, \sin k(r-s)\, \sin ks\, U(s) + \ldots. \tag{18}$$

Since these series are uniformly convergent, we can proceed term-wise to the limit, and therefore convergence will be decided by the zeros of the denominator $A(0,\lambda)$, where

$$A(0,\lambda) = 1 - \lambda\int_0^a \mathrm{d}r\, rU(r) + \lambda^2 \int_0^a \mathrm{d}r\, U(r) \int_0^r \mathrm{d}s\, s(r-s)\, U(s) + \ldots \tag{19}$$

4. S-Wave Bound States

The corresponding S-wave bound state problem can be solved similarly from the Schrödinger equation

$$\phi''-\alpha^2\phi = -\lambda U\phi, \tag{20}$$

where $-\alpha^2$ is the energy of the bound state. The solution of this equation which behaves properly at the origin is

$$\phi(r) = \sinh \alpha r - \frac{\lambda}{\alpha}\int_0^r ds \sinh \alpha(r-s)\, U(s)\, \phi(s), \tag{21}$$

which gives a convergent iterative series for a finite-range bounded potential. Then, as $r \to \infty$,

$$\phi(r) = \tfrac{1}{2}e^{\alpha r}\left\{1-\frac{\lambda}{\alpha}\int_0^a ds e^{-\alpha s}U(s)\phi(s)\right\} - \tfrac{1}{2}e^{-\alpha r}\left\{1-\frac{\lambda}{\alpha}\int_0^a ds e^{\alpha s}U(s)\phi(s)\right\} \tag{22}$$

$$= F(\alpha, \lambda)e^{\alpha r}+G(\alpha, \lambda)e^{-\alpha r}. \tag{23}$$

There exists a bound state if and only if $F(\alpha, \lambda) = 0$ for some $\alpha > 0$, i.e.

$$1-\frac{\lambda}{\alpha}\int_0^a ds\, e^{-\alpha s}\, U(s)\phi(s) = 0, \tag{24}$$

which iterated gives

$$\begin{aligned} &1-\frac{\lambda}{\alpha}\int_0^a dr\, e^{-\alpha r}U(r)\sinh \alpha r \\ &+\left(\frac{\lambda}{\alpha}\right)^2\int_0^a dr\, e^{-\alpha r}U(r)\int_0^r ds \sinh \alpha(r-s)\sinh \alpha s\, U(s)+ \ldots = 0. \end{aligned} \tag{25}$$

The values of α which satisfy this equation, for fixed λ, determine the S-wave bound states. The left hand side is uniformly convergent and is therefore a continuous function of λ, taking the value unity at $\lambda = 0$. There is a lower bound for λ, say λ_m, such that for $\lambda < \lambda_m$ there is no S-wave bound state, i.e.

$$F(\alpha, \lambda) > 0 \quad \text{for} \quad \lambda < \lambda_m \quad \text{and} \quad \alpha \geqq 0, \tag{26}$$

and in particular

$$F(0, \lambda) > 0 \quad \text{for} \quad \lambda < \lambda_m, \tag{27}$$

which is

$$\begin{aligned} &1-\lambda\int_0^a dr\, rU(r)+\lambda^2\int_0^a dr\, U(r)\int_0^r ds(r-s)s\, U(s) \\ &-\lambda^3\int_0^a dr\, U(r)\int_0^r ds(r-s)\, U(s)\int_0^s dt(s-t)t\, U(t)+ \ldots > 0 \end{aligned} \tag{28}$$

for $\lambda < \lambda_m$.

But this expression is precisely $A(0, \lambda)$ in eq. (19): therefore, the denomi-

nator $A(0, \lambda)$ does not have a zero in the real range $-\infty < \lambda < \lambda_m$. However we require to examine the behaviour of $A(0, \lambda)$ for complex λ as well. We now show that the only possible values of λ which satisfy $A(0, \lambda) = 0$ are in fact real. We consider the equation

$$\phi'' = -\lambda U\phi. \tag{29}$$

The solution which vanishes at $r = 0$ can be written in Volterra form

$$\phi(r) = r - \lambda \int_0^r \mathrm{d}s (r-s) U(s)\phi(s). \tag{30}$$

This is a special case of equations (9) and (21) and gives a convergent iterative series in the case of a finite-range bounded potential. For $r > a$,

$$\phi(r) = r\left\{1 - \lambda \int_0^a \mathrm{d}s\, U(s)\phi(s)\right\} + \lambda \int_0^a \mathrm{d}s\, sU(s)\phi(s) \tag{31}$$

$$= rA(0, \lambda) + c, \tag{32}$$

where c is independent of r. If $A(0, \lambda) = 0$, then $\phi(r)$ is a solution which vanishes at $r = 0$ and $\phi(r) = c$ for $r > a$. From eq. (29),

$$\int_0^\infty \bar{\phi}\phi'' \mathrm{d}r = -\lambda \int_0^\infty \bar{\phi} U\phi \, \mathrm{d}r, \tag{33}$$

where $\bar{\phi}$ is the complex conjugate of ϕ. Therefore,

$$[\bar{\phi}\phi']_0^\infty - \int_0^\infty \bar{\phi}'\phi' \mathrm{d}r = -\lambda \int_0^\infty \bar{\phi} U\phi \, \mathrm{d}r, \tag{34}$$

and so

$$\int_0^\infty \bar{\phi}'\phi' \mathrm{d}r = \lambda \int_0^\infty \bar{\phi} U\phi \, \mathrm{d}r. \tag{35}$$

Since U is real, therefore λ is real.

We have proved that $A(0, \lambda)$ is zero only for real λ and that it never vanishes for $\lambda < \lambda_m$. We conclude, then, that the Born series is convergent for $\lambda < \lambda_m$. If the spherically symmetric potential does not have an S-wave bound state, it will not have bound states of other angular momentum.

5. Conclusion

The result derived above can be conveniently put in the slightly more general form:

The Born series for the non-relativistic scattering amplitude $f(\mathbf{k})$ by a spherically symmetric static potential $V(r)$ which is bounded and has finite range is convergent for all $\mathbf{k}$ if the potential $-|V(r)|$ cannot support a bound state.

The restrictions on boundedness and finite range could probably be eased without much difficulty, but to do this here would only add details to the simple argument above.

References

1) R. H. Dalitz, Proc. Roy. Soc. A **206** (1951) 509
2) R. Jost and A. Pais, Phys. Rev. **82** (1951) 840
3) W. Kohn, Phys. Rev. **87** (1952) 539;
Carnegie Institute of Technology Report on the Convergence of Born Expansions;
Revs. Mod. Phys. **26** (1954) 292

2.A.1 *Nuclear Physics* **14** (1959/60) 472—497; © *North-Holland Publishing Co., Amsterdam*
Not to be reproduced by photoprint or microfilm without written permission from the publisher

PROPERTIES OF LEVELS EXCITED IN (p, α) REACTIONS ON O^{18}, P^{31}, Cl^{35}, Cl^{37}, K^{39} AND K^{41}

R. L. CLARKE, E. ALMQVIST and E. B. PAUL †
Chalk River Laboratories, Chalk River, Ontario

Received 12 August 1959

Abstract: Excitation functions and differential cross sections at 90° to the beam have been measured for the (p, α) ground state reactions in O^{18}, P^{31}, Cl^{35}, Cl^{37}, K^{39} and K^{41} from 1 to 3 MeV proton energy using a magnetic spectrometer to detect the alpha particles. Reduced widths and strength functions for protons and alpha particles are derived; the alpha-particle strength functions are a factor of five smaller than the proton values which agree with published results of (p, n) studies in the mass 40 region. The reduced widths of protons and alpha particles in units of $\hbar^2/\mu R^2$ are both 3×10^{-2} for P^{31} and decrease to 0.4×10^{-2} near mass 40. The equality of the proton and alpha-particle reduced widths suggests that these particles appear on the nuclear surface with equal probability. The measured mean level spacing runs from 78 keV for P^{31} to < 15 keV in the mass 40 region. These are larger than is predicted by the semi-empirical level spacing equation of Cameron. The measured Q-values of the (p, α) reaction on the isotopes shown are

$Cl^{35} = 1.865 \pm 0.015$ MeV, $Cl^{37} = 3.015 \pm 0.015$ MeV,
$K^{39} = 1.267 \pm 0.020$ MeV, $K^{41} = 4.002 \pm 0.020$ MeV.

1. Introduction

1.1. GENERAL

The results of investigations of (p, α) reactions in elements of $Z > 10$ have been summarized by Endt *et al.* and by Brostrøm *et al.* [1]). For these elements the levels found are in many cases so numerous and so narrow that a detailed study of each is impossible. However, the information that can be obtained about level densities and level widths for the compound states through which the (p, α) reaction can proceed is of interest. If the absolute yield of alpha particles is measured, some information on the partial widths for proton and alpha-particle emission can be computed. In addition accurate measurements of the Q-values of the reaction contribute to the knowledge of the mass differences of the target and residual nuclei.

The present paper gives results of a study of the excitation functions of the ground state (p, α) reactions up to 3 MeV on O^{18}, P^{31}, Cl^{35}, Cl^{37}, K^{39} and K^{41}. The results on O^{18} compare with those of Hill and Blair [2]) who have made measurements up to 3.5 MeV and the measurements on P^{31} overlap those of Freeman and Seed [3]) who used bombarding energies up to 1 MeV.

† Now at A.E.R.E., Harwell, England.

1.2. STRENGTH FUNCTIONS AND REDUCED WIDTHS

The areas under the thin target excitation curves have been used to compute values for proton and alpha-particle strength functions in a manner similar to that used by Schiffer and Lee [4]) in analysing the results of thick target neutron yields. In this derivation it is assumed that the net effect of interference terms in the total cross section is zero when averaging over a large number of levels and that a simple summation of single level Breit-Wigner resonance terms may be used. This gives for the area under the excitation curve over the energy range ΔE

$$A_{\Delta E} = 2\pi^2\lambda^2 \sum_i \frac{(2J+1)}{(2I+1)(2i'+1)} \sum_{s^1 l^1} \sum_{s^2 l^2} \frac{\Gamma^i_{Js^1 l^1} \Gamma^i_{Js^2 l^2}}{\Gamma^i}, \tag{1}$$

where the sum is taken over all resonances in the energy interval ΔE. Here $\Gamma^i_{Jl^1 s^1}$ is the ground state proton width for level i via a channel specified by channel spin s^1 and orbital momentum l^1; $\Gamma^i_{Js^2 l^2}$ is the similar alpha particle width and Γ^i is the total width. The spins of the target, the bombarding particle and the compound state are I, i' and J respectively.

Expression (1) is simplified by assuming either

$$\Gamma_p = \sum_{l^1 s^1} \Gamma^i_{Jl^1 s^1} = \Gamma^i \gg \sum_{l^2 s^2} \Gamma^i_{Jl^2 s^2} = \Gamma_\alpha \tag{2a}$$

or

$$\Gamma_\alpha = \sum_{l^2 s^2} \Gamma^i_{Jl^2 s^2} = \Gamma^i \gg \sum_{l^1 s^1} \Gamma^i_{Jl^1 s^1} = \Gamma_p. \tag{2b}$$

If either (2a) or (2b) is valid we get

$$A_{\Delta E} = 2\pi^2\lambda^2 \sum_i \frac{2J+1}{(2I+1)(2i'+1)} \sum_{ls} \frac{2kR}{A_l^2} \gamma^2_{Jls}, \tag{3}$$

where γ^2_{Jls} is the reduced width in energy units for either alpha particles (assumption a) or protons (assumption b), k and R are the corresponding wave number and nuclear radius respectively and A_l^2 is the Coulomb barrier penetration parameter. If D_J is used to denote the average spacing of levels with the same J, then $\Delta E/D_J$ is the number of such levels in the interval ΔE and one obtains from (3)

$$A_{\Delta E} = 2\pi^2\lambda^2 \sum_{J=0}^{\infty} \frac{(2J+1)}{(2I+1)(2i'+1)} \frac{\Delta E}{D_J} \left\langle \sum_{ls} \frac{2kR}{A_l^2} \gamma^2_{Jls} \right\rangle_J, \tag{4}$$

where the last term is an average value over all levels of the same J.

If γ^2_{Jsl} and D_J are assumed to be independent of s, and the ratio γ^2_{Jsl}/D_J is independent of J, eq. (4) may be written

$$\frac{A_{\Delta E}}{\Delta E} = 2\pi^2\lambda^2 \sum_{Js} \frac{2J+1}{(2I+1)(2i+1)} \frac{\left\langle \sum_l \frac{2kR}{A_l^2} \gamma^2_{Jls} \right\rangle_J}{D_J}. \tag{5a}$$

In the case of (p, α) reactions to a $J = 0$ final state the summations are restricted to the combinations of J, s and l that lead to "natural" parity (i.e. 0+, 1−, 2+, etc.) compound states; all other states have zero width for alpha particle emission and are omitted from the sum over J and s. Eq. (5a) then may be rewritten in the form

$$\frac{A_{\Delta E}}{\Delta E} = \pi\lambda^2 \sum_l (2l+1)\varepsilon_l T_l, \tag{5b}$$

where ε_l is the ratio given by dividing the sum over "natural" parity states by the sum over all states for a given l; the transmission factor T_l is defined by 2π times the bracket in (5a). For (pα) reactions to $J = 0$ final states, ε_l does not differ greatly from 0.5 and for all other cases is equal to 1. The level spacing D_J in the (pα) case is the average for levels of the same spin and parity.

The value of the average strength function over all l-values, $\bar{S}$, is obtained by fitting a curve of the form

$$\frac{A_{\Delta E}}{\Delta E} = 2\pi^2\lambda^2\left[\sum_l (2l+1)\varepsilon_l \frac{2kR}{A_l^2}\right]\bar{S} \tag{6}$$

to the measured areas in mb×keV per unit energy interval as a function of energy. Eqs. (5) and (6) combined define the average strength function, measured in this paper, to be

$$\bar{S} = \frac{1}{2\pi}\left\{\frac{\sum_l (2l+1)\varepsilon_l T_l}{\sum_l (2l+1)\varepsilon_l 2kR/A_l^2}\right\} \tag{7}$$

which is dimensionless. It should be noted that if a particular value of l predominates, $\bar{S} \approx \langle\gamma^2_{Jsl}\rangle/D_J$. The consequences of the assumptions used in deriving the strength functions and reduced widths are discussed for each individual case in the description of results. They depend on the particulars of the reaction being studied and on the bombarding energy used; in general conditions (2a) and (2b) if not fulfilled lead to lower limits being obtained. However, such experimental limits are of value since information about these average properties of nuclei is sparse. The proton strength functions obtained in this work agree with those obtained by Schiffer and Lee [4]) using (p, n) reactions where they can be compared; as regards alpha-particle strength functions there is no earlier data in this mass region with which to compare.

In the case of P^{31} where individual levels could be studied values of the product $\sigma\Gamma$ were obtained, where σ is the cross section at resonance and Γ is the total width which in some cases was directly measurable. From these measurements it was possible to obtain limits for the average reduced proton and alpha-particle widths of the compound state by making approximations which

are discussed in the section of results of the $P^{31}(p, \alpha)Si^{28}$ measurements.

In the computations in this paper the values of $2kR/A_l^2$ have been taken from the tables [5]) of Sharp *et al.* and of Tubis. The nuclear radius has been taken to be

$$R = (1.4A^{\frac{1}{3}} + \rho_\alpha) \times 10^{-31} \text{ cm}$$

where ρ_α is 0 for protons and 1.2 for alpha particles. The reduced widths γ^2 are expressed in keV; their value in keV cm may be obtained by multiplying by the radius R given above. For purposes of comparsion the reduced widths [6]) have also been expressed in single particle units defined as $\hbar^2/\mu R^2$.

1.3. LEVEL SPACINGS

From the measured distribution of spacings between resonances it is possible to derive information about the average level spacings in the compound nuclei. It has been shown recently [7]) that the spacing between levels for a given spin is not completely random. However, if levels arising from several values of the spin are observed, the distribution of spacings is probably not far from random. In this case, a plot of log N *vs.* D, where N is the number of spacings greater than D, should give a straight line with a slope inversely proportional to the average level spacing.

However, levels may also be missed because their reaction widths are too small to render them observable under the conditions of the experiment. At the low bombarding energies used in this work the angular momentum barrier reduces the yield of levels having large values of angular momentum J. In the analysis of the data an angular momentum cut-off is assumed; all levels of angular momentum equal to or greater than that which reduces the barrier penetrability to about 10 % of the value for $l = 0$ particles are considered unobservable. The exact value used in each case is given in the discussion of results. The measured level spacing for (p, α) reactions to a spin 0 final nucleus is therefore an average over all "natural" parity levels (0+, 1−, etc.) from $J = 0$ up to the maximum observable angular momentum. In order to estimate the average level spacing for given values of J to compare with theoretical values one must obtain some guide from theory about the variation of level density with J. In the analysis of the data it is assumed [8, 9]) that the level spacing varies as $(2J+1)^{-1}$. It is probable that this variation overestimates the number of levels of high J as suggested by the recent work of Cameron. This point is considered more fully in the discussion of results.

1.4. *Q*-VALUES

The Q-values of the reactions $Cl^{35}(p, \alpha_0)S^{32}$, $Cl^{37}(p, \alpha_0)S^{34}$, $K^{39}(p, \alpha_0)A^{36}$ and $K^{41}(p, \alpha_0)A^{38}$ were determined relative to the Q-value of the Na^{23} $(p, \alpha_0)Ne^{20}$ reaction which is precisely known [10]). These results which have been only briefly reported previously [11]) are here discussed in detail. They are in good agreement with the data of Van Patter *et al.* [12]) and Endt *et al.* [13]).

2. Experimental Apparatus and Procedure

2.1. GENERAL

The 3 MeV electrostatic accelerator at Chalk River was used to study the (p, α) reactions. The beam energy from this machine was stabilized to ± 3 keV, and was measured in terms of the magnetic field of the beam deflecting magnet. The current through the magnet was continuously controlled by a proton nuclear magnetic resonance system which was, in turn, calibrated by observation of the threshold of the Li^7(p, n)Be^7 reaction at 1.881 MeV [14]). This calibration was repeated several times during the course of the experiment, and no large changes in the calibration constant were observed except those associated with known alterations in the equipment.

2.2. TARGET ARRANGEMENTS

The target chamber was situated ten and a half feet from the beam deflecting magnet. For precise energy measurements a collimator two inches from the target defined the beam spot to $\frac{1}{8}$ inch diameter. For the measurement of excitation functions where the greatest possible yield was frequently necessary beam spots of up to $\frac{3}{8}$ inch diameter were used. The beam current, which was of the order of 1 μA, was measured with an integrator which was arranged to stop the counting equipment automatically when a pre-set amount of charge had bombarded the target. Secondary electrons were suppressed by surrounding the target by a copper cylinder which was held at a potential of -300 V with respect to the target. The targets were mounted at 45° to both the incident beam and the observed alpha particles.

2.3. SPECTROMETER ARRANGEMENT

The alpha particles emitted from the target at an angle of 90° to the incident beam were analysed in a magnetic spectrometer and counted with a scintillation detector. The magnetic spectrometer was one of the 180° double-focussing type developed at the Kellogg Radiation Laboratory [15]), having a radius of curvature of 16 inches and a target to magnet face distance of 16 inches. As in the case of the beam analysing magnet, the current through the magnetic spectrometer was continuously controlled by a proton nuclear magnetic resonance system. Since the field in this magnet is non-uniform in order to focus the particles, it was not possible to realize the full accuracy of the proton resonance system. In spite of this a short term reproducibility of better than 0.1 percent was found. Stability over long periods was achieved by comparing the frequency of the proton resonance system with a crystal standard. When the magnet was used with a source spot $\frac{1}{8}$ inch diameter and a counter slit $\frac{3}{8}$ inch wide the observed momentum spectrum of a mono-energetic particle group was a peak having a full width at half maximum of ≈ 0.7 percent, which may be compared with the calculated value of 0.6 percent for these conditions [15]).

Particles emerging from the magnet were counted in a scintillation counter using an RCA 5819 photomultiplier and a thallium activated KI crystal, and later a CsI crystal. Pulses from the counting system were displayed on a thirty-channel pulse height analyser where the particle group could be closely observed and separated from the background of pulses coming from K^{40} in the crystal.

In preliminary work it was found that the spectrometer could be accurately set by means of its proton resonance system to accept particles of a specified momentum. The accuracy of this setting was such that in taking an excitation curve with a thin target the magnet could be made to track the computed

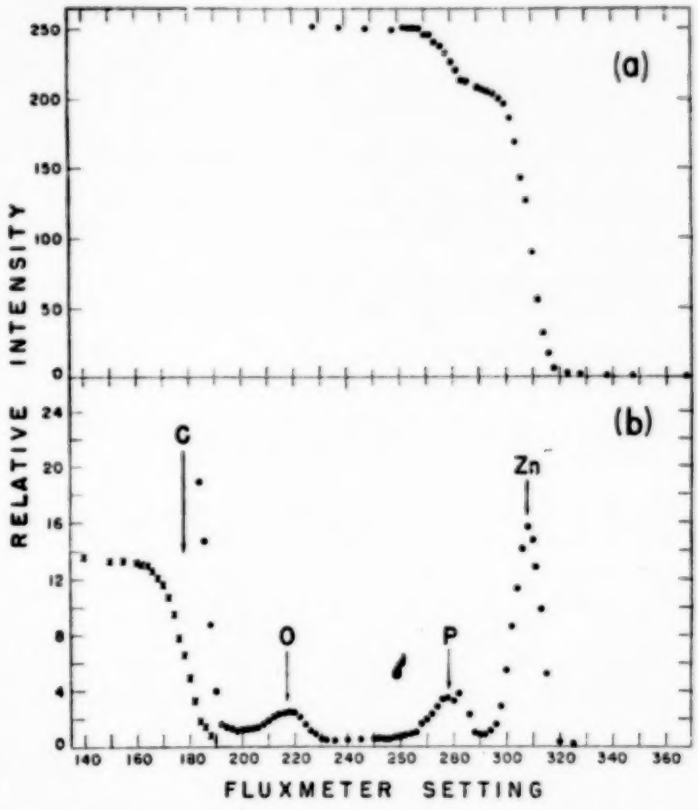

Fig. 1. The yield of scattered protons from Zn_3P_2 targets *vs* magnetic field of spectrometer given in terms of fluxmeter dial settings. The measurements were made at 90° to a 1.90 MeV proton beam.
(a) Thick Zn_3P_2 target
(b) 0.6 keV thick target on graphite backing

alpha particle energies to much better than the 1.5 percent energy "window" of the spectrometer as the bombarding energy was changed. Frequent checks of the tracking were made which showed that the spectrometer was operating satisfactorily and that the particles were from the reaction under study.

2.4. TARGET PREPARATION AND THICKNESS MEASUREMENT

The O^{18} target was prepared by bombardment of a tantalum sheet with mass 18 oxygen ions in the magnetic separator at A.E.R.E., Harwell †. The

† Prepared by E.M. Separator group, A.E.R.E. Harwell, England.

exact thickness of the target is not known, but it appeared from the resolution obtained in the excitation measurements to be less than 20 keV. The oxygen in the targets was estimated to contain 25 percent O^{18}. The other targets were prepared by the evaporation of Zn_3P_2, KCl and $SnCl_2$, the evaporation being carried out simultaneously on backings of tantalum and polished graphite. The measured thickness of the targets used varied from 0.3 to 10 keV for 1.9 MeV protons as indicated in the description of the results. For runs where the yield curves of alpha particles and gamma-rays were taken simultaneously tantalum backings were used to avoid the background from the $C^{12}(p, \gamma)N^{13}$ reaction.

The graphite backing permitted direct measurement of the thickness of the target material since protons elastically scattered by the heavy target atoms were clearly resolved from those scattered by the lighter carbon atoms of the backing, as illustrated in fig. 1b. The details of the use of the thick and thin targets in the measurement of target thickness are given in the Appendix.

The choice of 1.5 per cent for the energy resolution resulted in a magnet resolution curve which was wider than the spread of alpha-particle energies from the thin targets used in measuring excitation functions. This facilitated tracking, and in addition, made it unnecessary to correct for the change in absolute width of the magnet resolution curve as a function of alpha-particle energy when comparing intensities of peaks.

3. Results

3.1. $O^{18}(p, \alpha)N^{15}$

(i) *Yield Curve*

In the case of O^{18}, shown in fig. 2, the target thickness is not known but the appearance of sharp resonances separated by 20 keV (e.g. resonances 15 and 16) again suggests a resolution of 20 keV or less. The energy scale in this case was not independently determined but was fitted to that of Hill and Blair [2]) using the resonances at 838 keV and 2450 keV as reference points to fix the scale. The energies of the remaining peaks based on this calibration are summarized in table 1. The first and second columns of the table are taken from table 1 of Hill and Blair. The third and fourth columns list the resonances and their energies observed in the present work and it can be seen that there is general agreement between columns 2 and 4. The peaks are located relative to the energy scale with an accuracy of about 10 keV, with the exception of resonances 3 and 10 which are ill defined. It can be seen that the resonances observed by Hill and Blair at 2007, 2378, 2767 and 3064 keV are in each case resolved into two resonances in the present experiment. Since the observations of Hill and Blair and the present work were carried out at 90° to the incident beam, the relative yields found in the two sets of observations should be similar except for

effects due to differences in target thickness. This appears qualitatively to be the case, with the exception of resonances number 5 and 7 in fig. 2. The reasons for the large yield of the former and the small yield of the latter compared with the

TABLE 1

The energies of the resonances in the $O^{18}(p, \alpha)N^{15}$ reaction

Hill and Blair [2])		Present Work	
Resonance	E_p(keV)	Resonance	E_p(keV)
1	838	1	838 †
2	980	2	991
3	1271	3	1182
—	—	4	1308
4	1406	5	1390
5	1621	6	1639
6	1688	7	1676
7	1736	8	1740
8	1761	9	1760
—	—	10	1870
9	1934	11	1941
10	2007	12	2006
—	—	13	2037
11	2175	—	—
12	2232	—	—
13	2358	—	—
14	2291	14	2299
—	—	15	2369
15	2378	16	2389
16	2450	17	2450†
17	2635	18	2631
18	2712	19	2707
—	—	20	2737
19	2767	21	2771
20	2798	22	2803
21	2929	23	2922
22	3029	—	—
23	3064	24	3045
—		25	3075

† Energy scale normalized to Hill and Blair value at these points.

yields observed by Hill and Blair are not known. The large energy discrepancy for resonance 3 (1271 keV instead of 1215 keV) is probably due to its large width and to the poor counting statistics in that energy region.

(ii) *Strength Functions*

Since the amount of O^{18} in the target was not known, the values of $\sigma\Gamma$ in mb · keV were found by normalizing the area under the yield curve between 1.96 MeV and 2.12 MeV to the corresponding area under the curve of Hill and

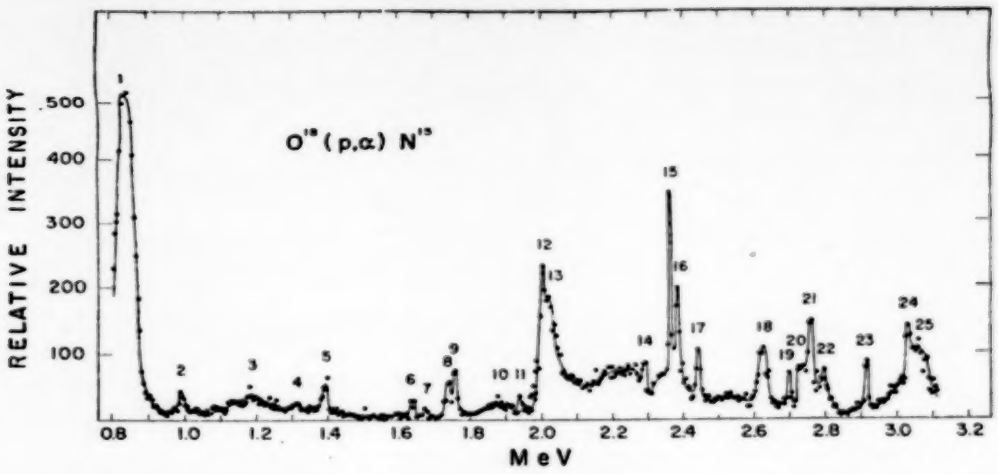

Fig. 2. The 90° excitation curve of the $O^{18}(p, \alpha)N^{15}$ reaction taken with a target estimated to be 20 keV thick.

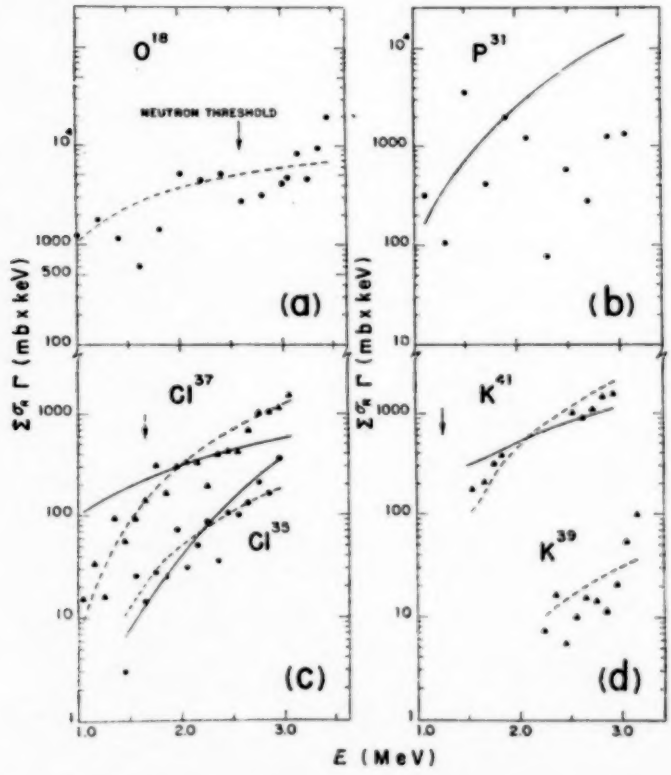

Fig. 3. The area in mb · keV under equal intervals of the yield curve plotted against mean bombarding energy. The curves are of the form of eq. (6); the dashed lines assume $\Gamma_\alpha \approx \Gamma \gg \Gamma_p$ while the solid curves assume $\Gamma_p \approx \Gamma \gg \Gamma_\alpha$. The positions of neutron thresholds are indicated; (a) is the O^{18} data including the measurements of Hill and Blair [2]) up to 3.5 MeV; (b) (c) and (d) are the present measurements with phosphorus, chlorine and potassium targets respectively.

Blair who made an absolute cross section measurement. Using this normalization the areas under the yield curve over 200 keV intervals could be obtained in mb · keV and plotted against the mean energy E as shown in fig. 3a. To obtain total yields in the absence of any knowledge of the angular distributions the differential cross sections measured at 90° were multiplied by 4π. Computations of the angular distributions made for various combinations of channel spins, orbital momenta and J values show that when averaging over many levels the yields obtained by assuming isotropy are probably good to better than a factor of two. The data were analysed by fitting a curve of the form of eq. (6) to the areas under 200 keV intervals of the yield curve as a function of energy (fig. 3a) between 1.0 and 2.5 MeV. This form implies the use of the approximations of eqs. (2) and leads to lower limits for the proton and alpha-particle strength functions; the factor by which the limit is low depends on the degree of validity of the approximations. Below 2.5 MeV proton energy the approximation (2b), $\Gamma_\alpha \approx \Gamma$, is probably valid because the penetration parameter $2kR/A_l^2$ for alpha particles is 50 times that for protons owing to the high Q-value of 3.69 MeV. At energies above the neutron threshold at 2.59 MeV [2]), a contribution to the total width by neutron emission is expected accompanied by an apparent drop in the measured strength function because of breakdown of the assumption $\Gamma_\alpha = \Gamma$. In fact no significant difference is observed in the two regions; the data below 2.6 MeV gave $S = 1.5 \times 10^{-2}$, the data of Hill and Blair covering 2.6—3.5 MeV give 1.8×10^{-2}. The absence of any apparent large change at the neutron threshold suggests that the levels involved in the (p, α_0) reaction have in general a neutron width which is similar to or less than the width for alpha particles at least in the region of 1 MeV above threshold. This probably reflects the fact that most of these levels have spins and parities that forbid s-wave neutron emission; for higher angular momenta the barrier penetration factor favours the emission of high energy alpha particles over that of low energy neutrons. If indeed the density of levels is greater for higher spins as has been suggested [8, 9]), then the result that s-wave neutron emission is not possible from most levels is not surprising.

The average values of the strength function found by fitting all the data are given in rows 7 and 10 of table 2 where the results for various elements are compared. As was noted for eq. (7), if a particular value of l predominates then the product of the strength function and the level spacing for the appropriate J gives an estimate of the average width $\langle \gamma^2_{Jl\alpha} \rangle$ which is shown in rows 9 and 12 for alpha particles and protons respectively.

(iii) *Level Spacings*

A level spacing plot such as discussed in section 1.3 is shown in fig. 4a for the O^{18}(p, α)N^{15} reaction. It can be seen that the slope of log N versus D is constant corresponding to an average level spacing of 70 keV, down to the smallest

TABLE 2

The average properties of the levels studied

1. Target	O^{18}	P^{31}	Cl^{35}	Cl^{37}	K^{39}	K^{41}
2. Compound Nucleus	F^{19}	S^{32}	A^{36}	A^{38}	Ca^{40}	Ca^{42}
3. Excitation (MeV)	9.9	10.9	10.7	12.1	10.3	12.3
4. D (keV)	70	78	26	20	<15	<15
5. D_0 (keV)	840 †	1250	420	320	<240	<240
6. Empirical Spacing (keV)		29	18	6	5	8
7. S_α	$\gg 0.0006$	$\lesssim 0.027$	$\lesssim 0.0083$	>0.0012	≈ 0.0029	$\lesssim 0.0019$
8. $S_\alpha D_0$ (keV)	$\gg 0.5$	$\lesssim 33$	$\lesssim 3.5$	>0.38	≈ 0.69	$\lesssim 0.46$
9. $\theta_\alpha^2 \times 10^2$	$\gg 0.08$	$\lesssim 8.2$	$\lesssim 1$	$\lesssim 0.1$	≈ 0.2	$\lesssim 0.14$
10. S_p	$\lesssim 0.017$	>0.040	$\gg 0.0028$	$\lesssim 0.014$	$\gg 0.0005$	$\lesssim 0.036$
11. "Black Nucleus" Strength Function	0.0441	0.0387	0.0375	0.0370	0.0364	0.0360
12. $S_p D_0$ (keV)	$\lesssim 14$	>50	$\gg 1.1$	$\lesssim 4.5$	$\gg 0.12$	$\lesssim 8.7$
13. $\theta_p^2 \times 10^2$	$\lesssim 0.4$	>2	$\gg 0.06$	$\lesssim 0.2$	$\gg 0.007$	$\lesssim 0.47$

† Spacing in this case refers to $J = \frac{1}{2}$ of a given parity.

Row 4 is the measured level spacing in keV; row 5 is the derived spacing of $J = 0$ levels (see text for assumptions); row 6 is the level spacing of $J = 0$ levels given by Cameron's semi-empirical formula [9]; row 7 is the alpha-particle strength functions; row 8 is the estimate of the reduced alpha-particle width given by taking the product of the strength function and spacing; row 9 is this reduced width expressed in single particle units. Rows 10, 12 and 13 are the quantities for protons which have already been defined for alpha particles in rows 7, 8 and 9. Row 11 gives the "black nucleus" value of the strength function, $1/\pi Ka$, where K is the wave number appropriate for a 40 MeV well depth.

observed spacing, 18 keV. Thus the resolution of the system is equal to or better than 18 keV. Extrapolation of the slope to zero level spacing suggests that there were 30 resonances in the region examined, of which 25 were recorded.

As discussed in the introduction the measured value of D cannot be directly compared with theoretical estimates without assumptions about the angular momentum distribution among the levels. On inspection of the O^{18} excitation

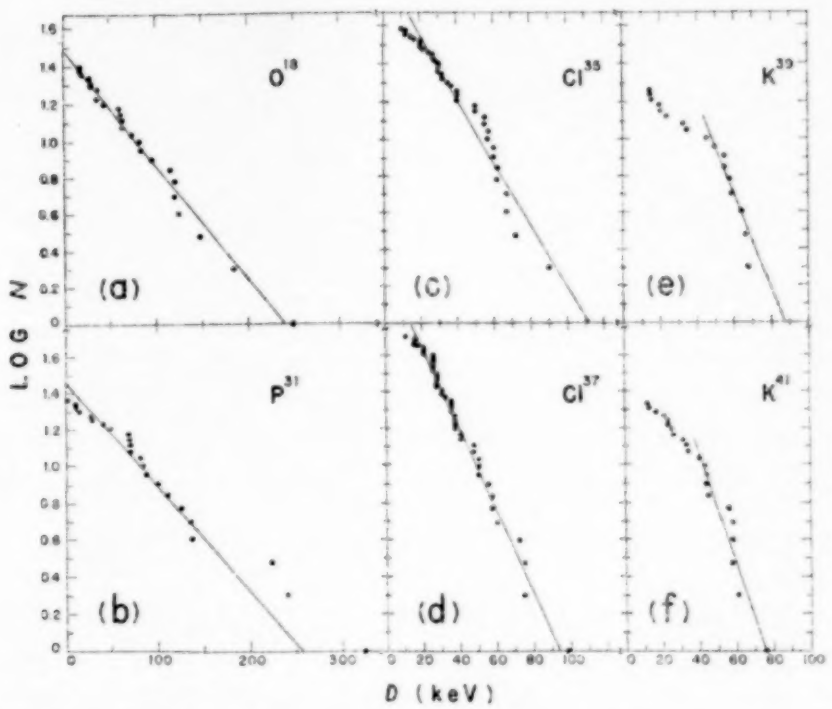

Fig. 4. A plot of the logarithm of the number of occurrences of a level spacing greater than D between adjacent levels *vs* the spacing D. The target nucleus is indicated in each case.

function it appears that resonances of area less than 15 % of the average value would be lost in the general background. Computation of the angular momentum barrier penetrations then shows that only levels with $J = \frac{5}{2}$ or less are observed. Assuming that the spacing varies as $(2J+1)^{-1}$ the average spacing of $J = \frac{1}{2}$ levels is computed to be 840 keV. This is compared to the spacing of $J = 0$ levels for other elements in row 5 of table 2. An uncertainty in the maximum observable J value of one unit leads to an error of ± 50 % in these values.

3.2. $P^{31}(p, \alpha)Si^{28}$

(i) *Yield Curve and Cross Sections*

The excitation curve for phosphorus shown in fig. 5 is composed of portions taken from many runs to get the best results for each part. The yield is given in arbitrary units. The results of these measurements are summarized in table 3.

The first column gives the resonant energy. Here the results are accurate to 10 keV; small differences may be good to 2 or 3 keV. The differential cross sections which are given in the second column were obtained by comparing the yield of alpha particles with the yield of protons elastically scattered from phosphorus which were clearly resolved from those scattered by other elements in the target (fig. 1). Since a target thickness less than five percent of the spectrometer line width was used the peak counting rate is given by eq. (A1). Hence, for a given target and spectrometer, the ratio of peak counting rates is

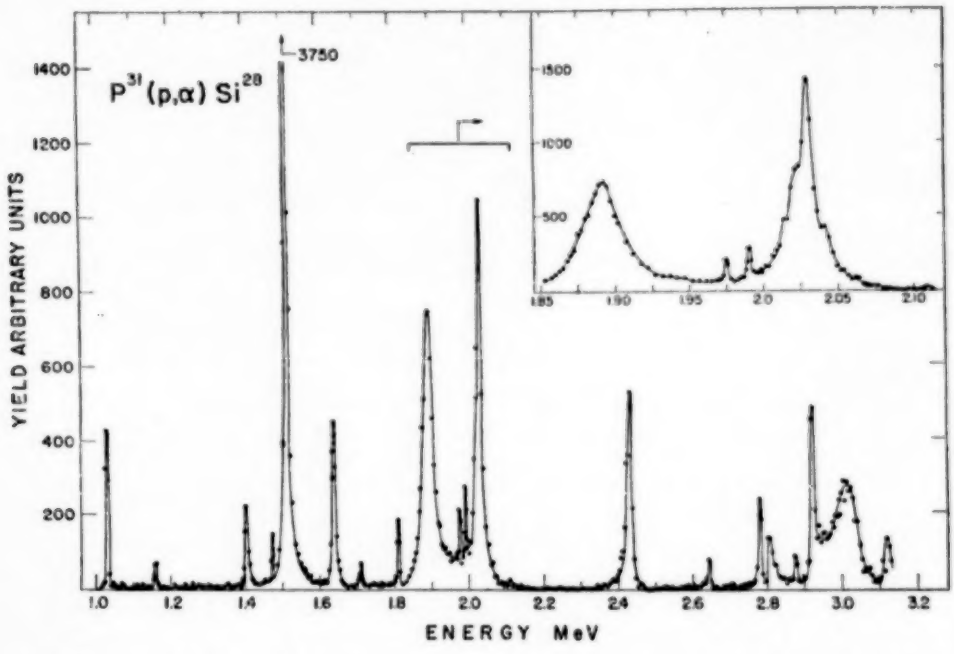

Fig. 5. The 90° excitation curve of the $P^{31}(p, \alpha)Si^{28}$ reaction taken with a target 0.6 keV thick.

directly equal to the ratio of differential cross sections for the (p, α) and (p, p) reactions on phosphorus, provided the resonance is wide compared with the energy spread introduced by the beam and the target thickness. The measured ratio together with the assumption that the (p, p) process is Coulomb scattering only, allows one to compute the value for the (p, α) cross section. As a check on the validity of this assumption, the yield of elastically scattered protons was observed at six points between 1.5 MeV and 2.7 MeV. It was found that to within 10 percent the yield followed the Coulomb law for both Zn and P. Relative errors in $d\sigma/d\omega$ are estimated to be 20 percent; absolute errors are estimated to be $\pm$ 25 percent.

In order to correlate the (p, α_0) resonances observed in the present work with the resonances observed by Paul *et al.* [16]) in the $P^{31}(p, \gamma)S^{32}$ reaction, yield curves of the alpha particles and gamma-rays were taken simultaneously using a somewhat thicker target. The gamma-rays were detected in a scintillation

counter using a two-inch by two-inch NaI crystal. The bias of the counting system selected those gamma-rays leading to the ground and first excited states of S^{32}. The only resonances found common to both reactions were those at 1.892, 2.029 and 2.109 MeV.

TABLE 3

The properties of the levels of S^{32} near 11 MeV excitation which were studied via the $P^{31}(p, \alpha)$ reaction

E (keV)	$\frac{d\sigma}{d\omega}$ (mb/sr)	Γ (keV)	$\sigma\Gamma$ (mb · keV)	$\omega\gamma$ (eV)	Γ_α (eV)	γ_α^2 (keV)	γ_p^2 (keV)	$\theta_\alpha^2 \times 10^{-2}$	$\theta_p^2 \times 10^2$
1024	>1.8	$\gtrsim 3$	70	26	35	11.2	$\gtrsim 3100$	2.9	<141
1161	≈ 0.29	≈ 4	15	6.1	3.1	1.4	≈ 1800	0.35	≈ 83
1404	≈ 0.87	≈ 6	65	33	44	3.3	≈ 930	0.82	≈ 42
1474	>0.53	$\gtrsim 2.4$	16	8.5	11.3	0.7	<288	0.18	<13
1514	16.1	7	1410	770	1030	56.6	483	1.41	22
1640	≈ 1.9	≈ 4.2	98	58	77	2.9	≈ 252	0.72	≈ 11
1710	>0.21	$\gtrsim 5.5$	15	9	12	0.37	$\gtrsim 258$	0.09	<12
1811	≈ 0.68	≈ 4.7	40	26	35	0.84	≈ 164	0.21	≈ 7
1892	3.2	27	1070	730	970	19.4	741	4.8	34
1976	$\lesssim 0.68$	$\gtrsim 2.8$	24	17	23	0.37	$\gtrsim 60$	0.09	<3
1990	$\lesssim 0.94$	$\gtrsim 3.6$	43	30	40	0.64	$\gtrsim 75$	0.17	<3.5
2018	$\lesssim 0.85$	$\gtrsim 3$	32	23	31	0.47	$\gtrsim 60$	0.12	<3
2029	2.74	18	620	450	600	8.6	350	2.1	17
2031	≈ 2.2	≈ 6	160	120	160	2.3	≈ 114	0.6	≈ 5
2041	≈ 0.36	≈ 6	27	20	27	0.39	≈ 115	0.98	≈ 5
2109	$\lesssim 0.07$	$\gtrsim 4$	2	1.3	1.7	0.02	$\gtrsim 76$	0.004	3.5
2434	2.5	17	540	407	540	3.5	149	0.87	6.8
2644	≈ 0.39	≈ 5	25	23	31	0.14	≈ 29	0.03	≈ 1.3
2779	1.2	8	120	120	160	0.58	38	0.146	1.7
2805	0.63	17	130	136	180	0.63	78	0.16	3.6
2874	≈ 0.34	≈ 5	21	22	29	0.09	≈ 20	0.023	≈ 0.9
2922	2.1	10	260	273	360	1.04	38	0.26	1.6
3008	1.3	75	1250	1370	1830	4.75	255	1.18	11.6
3119	0.55	20	140	156	208	0.47	58	0.12	2.7
		Mean for $Er < 1.5$ MeV				5.20	170.7	1.30	7.76

The various column headings are defined in the text in section 3.2.

(ii) *Widths*

The third column gives the observed value of the total width, Γ. For many resonances only an approximate value or an upper limit would be found due to the finite resolution of the equipment; consequently for these resonances the value of $d\sigma/d\omega$ is only a lower limit. For the remaining cases an error of ± 2 keV is generally applicable.

Column 4 lists the values of $\sigma\Gamma$ in mb · keV which is a measure of the strength of the resonance. It can be shown that if the target is thin and the beam energy spread is small compared with the line width of the spectrometer, the observed

area under a resonance is proportional to $\sigma\Gamma$. Hence, even for resonances whose widths were too small to be observed directly, the value of $\sigma\Gamma$ could be derived from the area under the curve of observed $d\sigma/d\omega$ vs. bombarding energy. Isotropy was assumed and 4π times the differential cross section used to compute $\sigma\Gamma$.

The quantity, $\omega\gamma$, tabulated in column 5 is defined by the relation

$$\omega\gamma = \frac{(2J+1)}{2(2I+1)} \frac{\Gamma_\alpha \Gamma_p}{\Gamma} = \frac{\sigma\Gamma}{4\pi\lambda^2}, \tag{9}$$

where I is the spin of the target nucleus. $\omega\gamma$ is then computed from the measured value of $\sigma\Gamma$. To obtain Γ_p and Γ_α two assumptions are made for all the levels: (a) $J = 1-$ and (b) $\Gamma_p \approx \Gamma \gg \Gamma_\alpha$. Assumption (b) gives an upper limit to the proton width. Moreover for narrow resonances the effect of finite target thickness and beam energy spread yields an apparent width greater than the true width. Consequently the derived proton widths tend to be high. This assumption also leads to an underestimate of the alpha-particle widths for those cases where the alpha-particle width is of magnitude similar to or greater than the proton width. However, without knowledge of the extent to which assumption (b) is true it is difficult to make any estimate of the uncertainty introduced into the mean widths and the error so introduced is ignored in the discussion of the results. The values are tabulated in column 6 of table 3. From these individual widths, the reduced widths γ_p^2 and γ_α^2 were calculated from the relation

$$\Gamma = \frac{2kR}{A^2}\gamma^2 \tag{10}$$

and are tabulated in columns 7 and 8 of table 3. In columns 9 and 10 they are expressed in the single particle units defined in the introduction.

The lack of knowledge of most of the J values and of all the angular distributions will introduce random uncertainties of factors of three or four into the values of γ_α^2 and γ_p^2 obtained in this manner, but the average values over all the resonances should be much better known, apart from systematic errors such as are introduced by the choice of nuclear radius used in computing Coulomb penetration factors. The effect on the average values of γ^2 and θ^2 of different choices of nuclear radius and average J are seen in table 4. In calculating these averages, resonances below a bombarding energy of 1.5 MeV have been omitted because at low energies the very large Coulomb factor unduly weights the proton widths where only upper limits are known; for example for the level at 1.024 MeV, $\Gamma_p < 3.1$ keV corresponds to $\theta_p^2 < 94$ %, whereas for the level at 1.99 MeV, $\Gamma_p < 3.6$ keV corresponds to $\theta_p^2 < 2.3$ %.

The average value of γ^2 given in table 3 is a measure of the average $\langle \sum_{ls} \gamma_{jls}^2 \rangle$ over all the resonances. This is related to the product of the strength function and the level spacing listed in rows 9 and 12 in table 2; as already noted it

appears from eq. (7) that this product becomes equal to $\langle \gamma^2_{Jls} \rangle$ if a single value of l predominates in the sums. It is of interest to see how this product compares with the more directly measured widths because in the elements where resonances were not resolved it provides the only measure of the magnitude of the reduced widths. For alpha particles γ^2 is $\lesssim$ 5.2 keV, $S_\alpha D_1$ is 11 keV; for protons

TABLE 4

The derived average values of the reduced widths for proton and alpha-particle emission from the S^{32} states studied in the $P^{31}(p, \alpha)Si^{28}$ reaction for different assumptions about level spins and nuclear radius.

Radius (10^{-13} cm)	J	γ_p^2 (keV)	γ_α^2 (keV)	$\theta_p^2 \times 10^2$	$\theta_\alpha^2 \times 10^2$
$1.5\,A^{\frac{1}{3}}$	0	$\lesssim$ 43	$\lesssim$46	$\lesssim$2.3	$\lesssim$8.1
$1.4\,A^{\frac{1}{3}}+\rho_\alpha$	0	$\lesssim$ 58	$\lesssim$10.8	$\lesssim$2.7	$\lesssim$2.7
$1.4\,A^{\frac{1}{3}}+\rho_\alpha$	1	$\lesssim$171	$\lesssim$ 5	$\lesssim$7.8	$\lesssim$1.3
$1.4\,A^{\frac{1}{3}}+\rho_\alpha$	1	$>$ 17*	$\approx$11*	$>$0.8*	2.7

The asterisk indicates the values that were obtained by taking the product of the strength function and the level spacing for $J = 1$ levels.

γ^2 is $<$ 171 keV, while $S_p D_1$ is $>$ 17 keV. The spacing for $J = 1$ levels has been used since this corresponds to the $J = 1$ assumption used in computing the γ^2. For alpha particles both methods yield similar reduced widths; for protons the assumption $\Gamma = \Gamma_\alpha$ which is used to obtain the strength function is probably not valid (see section 4) and leads to an underestimate while the use of directly measured widths assumes $\Gamma = \Gamma_p$ which leads to an overstimate.

(iii) *Level Spacings*

A plot of log N versus D, similar to that made for O^{18}, is shown in fig. 4b. It can be seen that the slope is approximately constant above $D \approx 20$ keV. This slope corresponds to an average level spacing of 78 keV. The divergence of the average slope and the experimental points for small values of D indicates that the experimental resolution was approximately 20 keV. Extrapolation of the slope to zero level spacing suggests that there were $\approx$ 30 resonances in the region examined, of which 24 were seen. In finding the range of J values observed in the excitation function as described in the O^{18} case, it was assumed that resonances of area greater than 10 % of the average would be seen. This gave the result $J_{0bs} \leqq 3$, from which D_0, the spacing for $J = 0$, becomes 1250 keV.

(iv) *Strength Functions*

In order to make a direct comparison between the P^{31} results and the other nuclei studied, the area under the P^{31} yield curve was measured in 200 keV intervals and the strength function obtained by fitting the results to a curve

(fig. 3b) of the form of eq. (6) as was described for O^{18} with the exception that the summation over Jsl only included "natural" parity states, 0+, 1−, 2+, etc. because only these contribute to the yield. The result for protons is $S_p \gtrsim 0.040$ and for alpha particles $S_\alpha \gtrsim 0.027$. In this case the barrier penetration parameter $2kR/A_l^2$ is of the same order of magnitude for protons and alpha particles and the degree of validity of the approximations of eqs. (2) are difficult to estimate directly but a guide is provided by the analysis of level widths given in subsection (ii). There it was assumed that the measured width $\Gamma = \Gamma_p$ which gives an upper limit for Γ_p and a lower limit for Γ_α as already discussed. This assumption is supported by the fact that the derived reduced widths in single particle units are reasonable. For example, if the assumption $\Gamma_\alpha = \Gamma$ had been used the reduced alpha-particle widths would have averaged nearly 30 % of a single particle unit while the proton reduced widths would have been less than 0.1 % which appears less likely. Approximation (2a) therefore appears to be the more valid and $S_\alpha \approx 0.027$ while $S_p \gg 0.040$.

3.3. CHLORINE ISOTOPES

(i) *Yield Curves*

The excitation functions at 90° to the beam shown in figs. 6 and 7 were obtained using targets measured to be 10 keV thick for 2 MeV protons. For both Cl^{35} and Cl^{37} the level density was too large to permit individual resonances to be studied.

(ii) *Strength Functions*

The areas under 100 keV intervals of the yield curve were measured in mb · keV and the results plotted against energy are shown in fig. 3c. To obtain the strength functions, isotropic angular distributions were assumed. The curves have the form of eq. (6); the solid line uses the assumption $\Gamma_p \approx \Gamma$ and $\Gamma_\alpha \ll \Gamma_p$ of eq. (2a) while the dashed curve uses the opposite assumption (2b). The data are summarized in table 2.

In these cases it is not clear which assumption is favoured. In the case of Cl^{35} the barrier penetration factors are about equal for protons and alpha particles while in Cl^{37} the higher Q-value favours the alpha particles. Because of this uncertainty the values derived for either S_p or S_α are lower limits. In the case of Cl^{37} there is the possibility of neutron emission which makes the observed value of S an even lower limit although as discussed for O^{18} the effect may not be large in the region near threshold.

(iii) *Level Spacing*

Plots of log N versus D for the chlorine isotopes are shown in figs. 4c and 4d. The data look quite normal, in that the points fall on straight lines down to an energy of ≈ 20 keV. The straight lines correspond to values of $\langle D \rangle$ of 26 keV

and 20 keV for Cl^{35} and Cl^{37} respectively. The intercepts of these lines with the log N axis indicate that in the interval of observation there were, for Cl^{37},

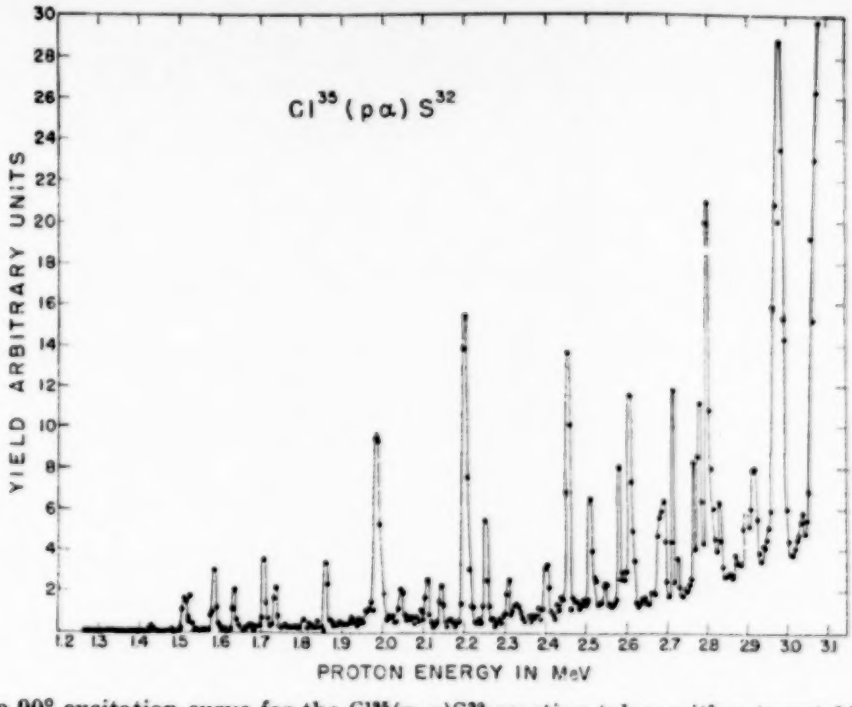

Fig. 6. The 90° excitation curve for the $Cl^{35}(p, \alpha)S^{33}$ reaction taken with a target 10 keV thick.

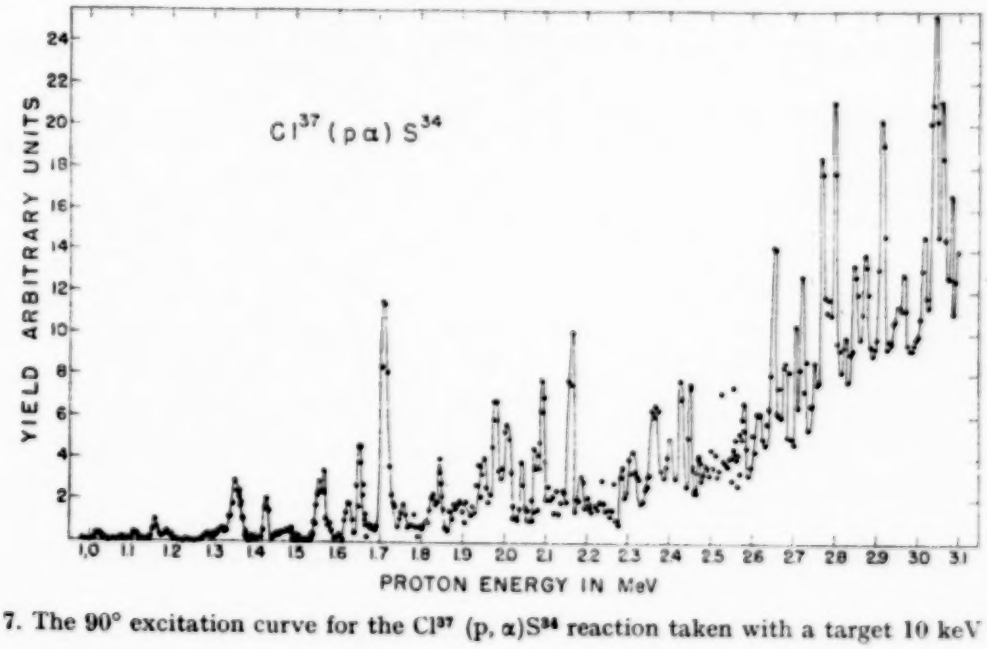

Fig. 7. The 90° excitation curve for the Cl^{37} $(p, \alpha)S^{34}$ reaction taken with a target 10 keV thick.

$\approx$ 120 resonances, of which 51 were observed, and for Cl^{35}, 77 resonances, of which 38 were observed.

The data are summarized in table 2. The values of D_0 are computed assuming no levels with $J > 3$ are observed and that the level density is proportional to $(2J+1)$ as discussed in the introduction.

3.4. POTASSIUM ISOTOPES

(i) *Yield Curves*

The excitation function at 90° to the beam for K^{39} is shown in fig. 8. For both this and K^{41} a large number of closely spaced levels were found so that it was impractical to deal with individual resonances and the comments made for the chlorine isotopes apply. The target thickness was measured to be 10 keV for 2 MeV protons.

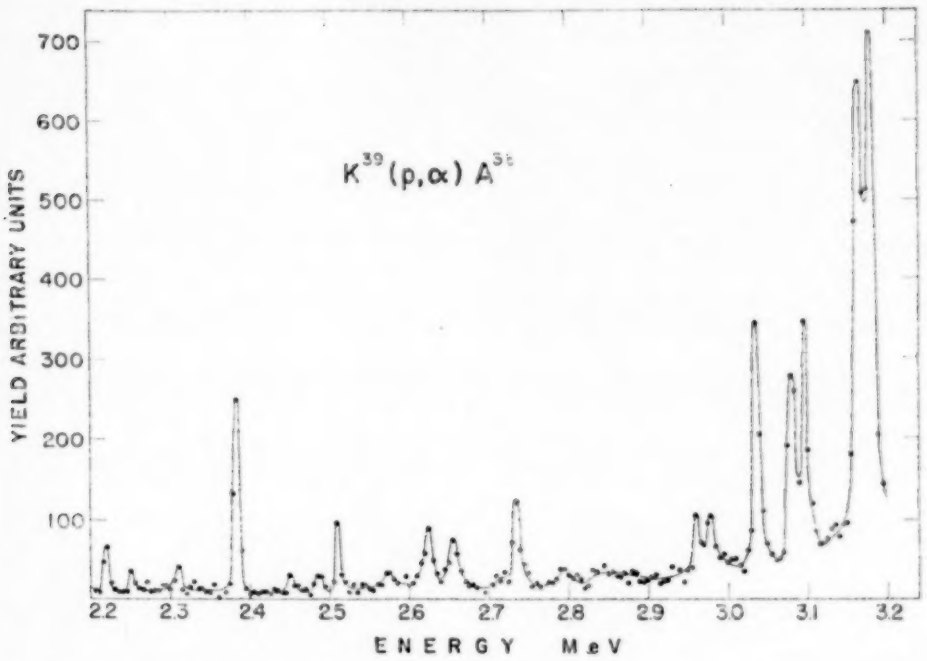

Fig. 8. The 90° excitation curve of the $K^{39}(p, \alpha)A^{36}$ reaction taken with a target 10 keV thick.

(ii) *Strength Functions*

The plots of the areas under 100 keV intervals of the yield curve are shown in fig. 3d. Again isotropy was assumed when deriving the strength functions given in table 2. In the case of K^{39} the barrier penetrability favours the proton width over the energy range examined and it is probable that assumption (2a), $\Gamma \approx \Gamma_p$ is fair, so that the result, 0.0029, is a reasonable estimate of S_α.

For K^{41} the barrier penetration favours the alpha particle relative to the proton so that a fair estimate of the proton strength function might be expected. Again neutron competition makes this result a lower limit but as discussed for O^{18} it may not greatly affect the results near threshold.

(iii) *Level Spacing*

Plots of log N versus D for the potassium isotopes are given in figs. 4e and 4f. Here the data do not give any appreciable straight portion. This could be interpreted as indicating that the overall resolution of the system is about 40 or

50 keV, due to target thickness, or it could be a result of real overlapping of levels which would cause many small resonances to be lost if they are near large ones. In this case, the value of $\langle D \rangle$ that is obtained should be considered as an upper limit. The straight lines shown on the figures represent only estimates based on what appeared to be widely separated pairs of resonances. For the potassium isotopes it appears that only about $\frac{1}{5}$ of all the resonances in the region of observation have been resolved. The results are summarized in table 2. The level spacings for $J = 0$ listed there have been computed from the measured D assuming $J_{max} = 3$ and a level density which is proportional to $(2J+1)$.

3.5. Q-VALUES

For the accurate measurement of the Q-values of the chlorine and potassium isotopes a sharp resonance was chosen from the excitation curves. The energies of the alpha particles from these reactions were compared with the energy of the alpha particles from the $Na^{23}(p, \alpha)Ne^{20}$ reaction, which has a Q-value of 2.378 ± 0.003 MeV [10]). The comparison was made in terms of the frequency of the proton resonance fluxmeter of the spectrometer. A General Radio comparison oscillator which had an accuracy of 0.01 percent was used to measure frequencies. The resonances used were chosen so that with the exception of the K^{41} case, both the comparison and the unknown frequencies fell within a small range. Hence any lack of proportionality between the measured field and the field through which the reaction products passed would have a small effect.

Targets less than 1 keV thick were used for the Q-value measurements. The accumulation of carbon on the targets was not measured directly. However, the target chamber was well pumped, with liquid air traps in both the beam tube and over the pump, which kept the carbon deposit small. Actual measurements of the carbon deposit produced in similar running conditions indicate that less than one kilovolt of carbon may be expected. No allowance was made for this in the calculations, but the errors given do take it into account.

The final results are shown in table 5, where the results of the present

TABLE 5

The measured Q-values

Reaction	(a)	Q-value (MeV)	
		(b)	(c)
$Cl^{35}(p\alpha)S^{32}$	1.865 ± 0.015	1.851 ± 0.007	1.863 ± 0.008
$Cl^{37}(p\alpha)S^{34}$	3.015 ± 0.015	3.015 ± 0.011	3.026 ± 0.008
$K^{39}(p\alpha)A^{36}$	1.267 ± 0.020		
$K^{41}(p\alpha)A^{38}$	4.002 ± 0.020		

Column (a) gives the results of the present work, column (b) the results of Van Patter *et al.*[12]) and column (c) the results of Endt *et al.*[13])

experiment are compared with the observations of Van Patter *et al.*[12]), and those of Endt *et al.* [13]). These final values are the same as those reported at the Chicago A.P.S. Meeting, 1954 [11]).

4. Discussion

4.1. STRENGTH FUNCTIONS

The present measurements of the proton strength function may be compared with the results of Schiffer and Lee [4]), and Johnson *et al.* [17]), whose measurements of average (p, n) cross sections cover the range $37 \leqq A \leqq 130$. In addition, strength functions determined from average (p, pn) cross sections have been given by Schiffer *et al.* [18]) for roughly the same range of A. Their results are expressed in a form related to the present results through the radius of the nucleus which for the region of interest, $A \approx 40$, has been taken to be 4.8×10^{-13} cm. With this radius the average value of the strength function from the above determinations is 0.035 ± 0.020, in satisfactory agreement with the present work which yields $\lesssim 0.036 \pm 0.02$ and $\lesssim 0.014 \pm 0.02$ for K^{41} and Cl^{37} respectively. The calculations of Johnson *et al.* [17]) indicate that a p-wave resonance in the proton strength function should appear at about the region of P^{31}, which is consistent with the limiting value $\gg 0.040$ found here.

The fact that the proton strength functions computed from the (p, α) data are in agreement with the values obtained from (p, n) measurements, supports the assumption $\Gamma_\alpha \approx \Gamma$ for Cl^{37} and K^{41} bombardment below the neutron threshold. In these two cases therefore the alpha-particle strength function is underestimated. For K^{39} and Cl^{35} the very low values obtained for the proton strength functions favours the assumption that $\Gamma_p \approx \Gamma \gg \Gamma_\alpha$ as is expected from the computation of the barrier penetrabilities, hence these cases give a fair estimate of the alpha-particle strength functions. The mean value obtained is $S_\alpha = 0.006$. If the possibility that $\Gamma_p \approx \frac{1}{2}\Gamma$ is allowed this value is increased by a factor of two which is the estimated reliability of the result. The alpha-particle strength functions are a factor of five smaller than the proton strength functions in the same mass region.

In the case of P^{31} a much larger value of $S_\alpha = 0.027$ is obtained suggesting a rise in the alpha-particle strength function in this mass region. There are no published data with which to compare these results.

4.2. LEVEL SPACINGS

Recently Cameron [9]) has given a semi-empirical level spacing formula which reproduces the spacings obtained from slow neutron measurements with a root mean square error of a factor of 1.74. This formula includes explicitly the $(2J+1)^{-1}$ dependence of the level spacings also used in the analysis of the experimental data. The predictions of this formula for $J = 0$ are given in row 6 of table 2 for comparison with the spacings observed in the present work. It is

seen that in every case there is a large discrepancy, with a tendency for the discrepancy to be largest for heavier nuclei.

Cameron has recently improved his level spacing formula by assuming a linear dependence of nuclear density on radius at the nuclear boundary. This revision predicts a dependence of level density on J that is slower than the $(2J+1)$ dependence used previously. This causes the values of D_0 calculated from the observed level spacing to be decreased by a factor of approximately 2 which, although it improves the agreement between observed and calculated spacings, leaves a discrepancy of a factor of 10 to 20.

The experimental results in row 4 of table 2 are believed to be correct to a factor of two except for the potassium isotopes where the result is an upper limit. It should be noted, however, that the derived spacings of levels with $J = 0$ and same parity listed in row 5 of table 2 depends on the choice of J_{max} used in reducing the data. For example, if it happens that a particular l value is dominant in the strength function then the J values formed by combining this l with the channel spins will most likely occur. As an extreme example this might result in only levels with $J = 0$ or 1 being observed in which case a value of D_0 about $\frac{1}{4}$ that given in table 2 would be obtained from the measured distributions. To obtain a unique answer it would be necessary to determine the spins and parities of a large number of levels but experimentally this is difficult when the levels are not well resolved. However, the studies by Paul *et al.* [16]) of the $P^{31}(p\gamma)$ reaction showed eight levels with $J = 1$ in an energy interval of 1.5 MeV. Assuming these to have either parity, a spacing of 375 keV is obtained for levels with $J = 1$ and the same parity which is in good agreement with the value 420 keV obtained in the present work and lends support to the assumptions made in deriving the results given in table 2.

At first sight it appears that the large discrepancy between the level spacings seen in the present work and those seen in neutron scattering, as reflected in Cameron's formula, might arise because only a small fraction of all levels have a large enough alpha-particle width to be seen. However, the agreement between proton strength functions obtained from (p, n) measurements and (p, α) measurements is then surprising; it suggests that the (p, α) reaction shows a smaller number of levels each with a large average proton width.

4.3. REDUCED WIDTHS

Although the reduced widths, except for P^{31}, are derived from the strength functions and level spacings, it is of interest to discuss them separately because of their theoretical interest. We have assumed the strength functions to be independent of J whereas the level spacing D has a J dependence; these assumptions imply a J dependence of the reduced widths similar to that of D. As already discussed in section 1.1 the product SD_0 provides an order of magnitude estimate of the reduced widths and these products are tabulated

in table 2 using the observed D_0 which applies to $J = 0$ levels. For purpcses of comparison they are expressed in "single particle" units $\hbar^2/\mu R^2$ in rows 8 and 13.

For protons in the mass 40 region the best values are given by the Cl^{37} and K^{41} measurements for which θ_p^2 are $\lesssim 0.2\times10^{-2}$ and $\lesssim 0.4\times10^{-2}$ respectively for an excitation of about 12 MeV. This may be compared with the average value for neutrons incident on sulphur [6]) and calcium [19]) of $\theta_n^2 \approx 1.0\times10^{-2}$ at $\approx$ 10 MeV excitation. For a P^{31} target a much higher value $\theta_p^2 \lesssim 2\times10^{-2}$ is obtained from the strength function analysis while the measured individual resonance widths yield the result $\theta_p^2 < 2.7\times10^{-2}$; the corresponding excitation energy is $\approx$ 11 MeV. These results suggest a decrease in the value of θ_p^2 in going from mass 30 to mass 40 of a factor of five.

The alpha-particle reduced widths expressed in single particle units in table 2 show a similar trend. Varying from 8×10^{-2} for P^{31} to 1×10^{-2} for Cl^{35} and 0.2×10^{-2} for K^{39}. The magnitudes of the alpha-particle reduced widths in single particle units are the same as those for protons for the mass region studied. For P^{31} the individual level analysis which is summarized in table 3 gives $\theta_\alpha^2 \lesssim 2.7\times10^{-2}$ for $J = 0$ assumptions while assuming $J = 1$ yields a result a factor of two smaller. The only comparable data on alpha-particle widths of which we are aware are the measurements in lighter nuclei summarized by Wilkinson [20]) who gives $\theta_\alpha^2 \approx 5\times10^{-2}$ for masses below 20.

The similar magnitude of the alpha-particle and proton or neutron reduced widths suggests that the probability of a configuration of the nucleus in which an alpha particle appears at the nuclear surface is similar to the probability of finding a single nucleon separated from the residual nucleus at least for the even-even compound nuclei studied.

5. Summary

In (p, α) reactions the observed mean level spacing is a factor of ten greater than predicted from Cameron's semi-empirical formula [9]) which has its constants adjusted to fit neutron measurements. The measured proton strength functions however agree with those derived from (p, n) studies. Together these observations suggest that the (p, α) reaction proceeds through relatively few levels which have large average proton widths. No evidence is found for any large decrease in the (p, α) yield in the first MeV above the neutron threshold owing to competition with the (p, n) reaction; this may be because the emission of low energy neutrons is inhibited by the angular momentum barrier. Extending the studies to higher energies is then expected to show a decrease in the (p, α) yield.

The alpha particle strength functions are a factor of five smaller than those of protons but the reduced widths in single particle units are equal for both.

It therefore seems that the appearances at the nuclear surface of an alpha particle or of a single nucleon separated from the residual nucleus have equal probability. The reduced widths for both protons and alpha particles decrease by a factor of about eight in going from mass 31 to mass 41.

Q-values for (p, α) reactions on the chlorine and potassium isotopes were measured. In those cases where comparison can be made with other work agreement is found.

We are indebted to Dr. A. G. W. Cameron for discussions of level densities and for the use of his revised work before publication. The cooperation of the operating staff of the electrostatic accelerator is gratefully acknowledged.

Appendix

TARGET THICKNESS MEASUREMENT

The ratio of the peak yield of protons scattered from the thin target to the yield of protons scattered from a thick target of the same material can be shown to give the thin target thickness in terms of the line width of the spectrometer.

If the particles are emitted at 90° to the beam and the line width of the spectrometer is greater than the spread in energy due to the target thickness then the maximum yield observed in elastic scattering from a particular type of atom is given by

$$C_1 = n\sigma_s \Omega \sqrt{2}t, \tag{A1}$$

where

C_1 is the maximum counting rate in a peak expressed as counts per incident particle,
n is the number of atoms of the particular type selected per cm^3 in the target,
σ_s is the differential elastic scattering cross section at 90°,
Ω is the solid angle of the spectrometer,
t is the target thickness in cm; the target is assumed at 45° to the beam.

Similarly for a thick target the height of the step corresponding to elastic scattering from a particular type of atom (see fig. 1a) is given by

$$C_2 = n\sigma_s \Omega \sqrt{2}t',$$

where

C_2 is the increase in counting rate in the step corresponding to scattering from the particular atoms selected,

t' is the effective thickness in cm measured normal to the target surface which just gives a spread in energy of the outgoing particles equal to that accepted by the spectrometer collecting slit. The target surface is assumed at 45° to the beam.

A simple calculation shows that for elastic scattering

$$\sqrt{2}t' = W\frac{A+1}{2Ak}, \tag{A2}$$

where

W is the line width in energy units of the spectrometer determined by the detector slit,

A is the mass of the scattering nucleus,

k is the energy loss per cm in the target material and is assumed constant over the small energy range determined by the spectrometer line width.

Combining the three relations we get the ratio of the thin target thickness to the spectrometer line width for the case of elastic scattering from a thin and a thick target both of the same source material:

$$\frac{kt}{W} = \frac{1}{2\sqrt{2}}\frac{A+1}{A}\frac{C_1}{C_2}, \tag{A3}$$

where kt is the thickness of the thin target in energy units. A knowledge of the energy loss per cm, k, in the target material is required to obtain the actual thickness of the target in cm or mg/cm².

References

1) P. M. Endt and J. C. Kluyver, Revs. Mod. Phys. **26** (1954) 95;
P. M. Endt and C. M. Braams, Revs. Mod. Phys. **29** (1957) 683;
Brostrøm, Madsen and Madsen, Phys. Rev. **83** (1951) 1265
2) H. A. Hill and J. M. Blair, Phys. Rev. **104** (1956) 198
3) J. M. Freeman and J. Seed, Proc. Phys. Soc. A **64** (1951) 3136
4) Schiffer, Lee, Davis and Prosser, Phys. Rev. **107** (1957) 547;
J. P. Schiffer and L. L. Lee, Phys. Rev. **107** (1957) 640;
J. P. Schiffer and L. L. Lee, Phys. Rev. **109** (1958) 2098
5) Sharp, Gove and Paul, Graphs of Coulomb Functions, Chalk River Report T.P.I.-70 (July 1953);
A. Tubis, Tables of Non-relativistic Coulomb Wave Functions, LA 2150 (April 1958)
6) T. Teichmann and E. P. Wigner, Phys. Rev. **87** (1952) 123;
A. M. Lane and R. G. Thomas, Revs. Mod. Phys. **30** (1958) 257
7) E. P. Wigner, International Conf. on the Neutron Interactions with the Nucleus, TID-7547, September 1957;
N. Rosenzweig, Phys. Rev. Letters **1** (1958) 24;
Rosen, Havens, Rainwater and Desjardins, Bull. Am. Phys. Soc. **4** (1959) 33
8) T. D. Newton, Can. J. Phys. **34** (1956) 804
9) A. G. W. Cameron, Can. J. Phys. **35** (1957) 1021;
A. G. W. Cameron, Can. J. Phys. **37** (1959) 244

10) D. M. Van Patter and W. Whaling, Revs. Mod. Phys. **26** (1954) 402
11) R. L. Clarke, E. Almqvist and E. B. Paul, Phys. Rev. **99** (1955) 654;
E. Almqvist, R. L. Clarke and E. B. Paul, Phys. Rev. **100** (1955) 1265
12) D. M. Van Patter, Swann, Porter and Mandeville, Phys. Rev. **103** (1956) 656
13) P. M. Endt, C. H. Paris, A. Sperduto and W. W. Buechner, Phys. Rev. **103** (1956) 961
14) Shoupp, Jennings and Jones, Phys. Rev. **76** (1949) 502;
Jones, Douglas, McEllistrem and Richards, Phys. Rev. **94** (1954) 947
15) Snyder, Rubin, Fowler, Lauritsen, Rev. Scient. Instr. **21** (1950) 852;
D. L. Judd, Rev. Scient. Instr. **21** (1950) 213
16) Paul, Gove, Litherland and Bartholomew, Phys. Rev. **99** (1955) 1339
17) Johnson, Galonsky and Ulrich, Phys. Rev. **109** (1958) 1243
18) Schiffer, Lee, Davis and Prosser, Phys. Rev. **107** (1957) 547
19) B. T. Feld, N.Y.O. (1953) 3978
20) D. H. Wilkinson, Proceedings of the Rehovoth Conference on Nuclear Structure, Editor H. J. Lipkin (North-Holland, 1958) Ch. IV

2.F

Nuclear Physics **14** (1959/60) 498—505; © *North-Holland Publishing Co., Amsterdam*

Not to be reproduced by photoprint or microfilm without written permission from the publisher

AN APPROXIMATION FOR NUCLEON-NUCLEUS POLARIZATION EFFECTS

KENNETH R. GREIDER †

Lawrence Radiation Laboratory, University of California, Berkeley, California ††

Received 25 August 1959

Abstract: A simple, approximate method of incorporating the effects of a nuclear spin-orbit potential in the wave function has been developed. When used with the appropriate optical-model wave function for the central potential, it permits closed-form solutions for polarizations and cross sections that are about as simple to obtain as the Born-approximation solutions. Its application is discussed in two types of problems: the elastic scattering of nucleons by nuclei, and the "direct" interaction type of nuclear rearrangement collision. In this latter problem it is found that the elastic scattering of initial and final state particles from the nuclear spin-orbit potential is primarily responsible for the observed polarization effects.

1. Introduction

In recent years the theoretical description of both the elastic and the inelastic scattering of nucleons by nuclei has achieved considerable success by the use of the optical model [1]) and the direct-interaction picture [2]), respectively. The aim of an earlier paper [3]) (hereafter designated as I) was to combine these two models to obtain a simple description of nuclear rearrangement collisions. To accomplish this, the direct-interaction picture was modified by representing the initial and final state particles by elastic scattering states rather than by Born-approximation plane wave states.

In order to avoid the usual calculational difficulties of such problems, a major goal of I was to derive closed-form wave functions to represent these elastic scattering states. By means of a high-energy WKB approximation, simple forms were obtained for the wave functions that describe the scattering from the nuclear central potential. The rather important effects of including elastic scattering were shown for a particular inelastic process — the deuteron pickup reaction.

The purpose of the present note is to describe briefly the results of an analysis, similar to that of I, that incorporates the nuclear spin-orbit potential. An approximate elastic wave function that includes the effects of both the central and spin-orbit potentials is given in section 2. A simple example that shows its utility is given in section 3, where the polarization due to the elastic scattering of nucleons by nuclei is calculated with this wave function, and is compared

† Present address: University of California, La Jolla, California.

†† Work done under the auspices of the U. S. Atomic Energy Commission.

with the more exact computer results. Finally in Section 4, the approximate wave functions are used to obtain the polarization of particles produced by an inelastic nuclear process — the deuteron pickup reaction considered in I.

2. The Spin-Orbit Wave Function

We consider the non-relativistic Schroedinger equation for a nucleon of mass m and energy E_0 interacting elastically with a nucleus. Eq. (18) of I can be generalized to read

$$\left(-\frac{\hbar^2}{2m}\nabla_r^2+\mathscr{V}_c(\mathbf{r})+\mathscr{U}_c(\mathbf{r})\boldsymbol{\sigma}\cdot\mathbf{l}-E_0\right)\psi(\mathbf{r},\lambda)=0 \tag{1}$$

where $\mathscr{V}_c$ and $\mathscr{U}_c\boldsymbol{\sigma}\cdot\mathbf{l}$ are the central and spin-orbit potentials, respectively, $\boldsymbol{\sigma}$ is the nucleon spin operator, and λ the nucleon spin variable. We define the two potentials to be of the usual form [4])

$$\mathscr{U}_c(\mathbf{r})=\frac{\mu a^2}{\hbar}\frac{1}{r}\frac{\partial}{\partial r}\rho(\mathbf{r})=\gamma\frac{\rho'(\mathbf{r})}{r}, \tag{2}$$

$$\mathscr{V}_c(\mathbf{r})=\beta\rho(\mathbf{r}), \tag{3}$$

where $\rho(\mathbf{r})$ is the nuclear density distribution. An approximate solution of eq. (1) can now be obtained by considering a simplified two-dimensional solution similar to the one-dimensional WKB approximation used in I, but where the spin-orbit potential here is a function of the coordinate perpendicular to the direction of motion of the incoming nucleon. Although such a two-dimensional model is a rather crude approximation, we can test the validity of the solution by examining the extent to which it satisfies eq. (1).

The three-dimensional form of this approximate solution turns out to be

$$\psi(\mathbf{r})\approx[1+\alpha f(\mathbf{r})\rho(r)\boldsymbol{\sigma}\cdot\mathbf{l}]\psi_0(\mathbf{r}), \tag{4}$$

where α is a constant and $\psi_0(\mathbf{r})$ is the WKB solution for the central potential alone [see eqs. (23), (24), and (25) of I]. The function $f(\mathbf{r})$ approaches unity at low energies and, provided the angular momentum $L=\hbar kR_0$ is not too large, depends only weakly on $\mathbf{r}$ at higher energies. We shall assume that at the energies used in the applications below, we may set $f(\mathbf{r})=1$. Now, the form of eq. (4) is made physically reasonable by considering an argument due to Fermi [5]); upon entering the nucleus, the particle feels two potentials: the central potential, which acts everywhere inside the nucleus and which changes the local wave number of the particle in accordance with the approximate WKB solution, and the spin-orbit potential, which acts only at the nuclear surface. Incoming particles feel the effect of this latter potential only while traversing the nuclear boundaries. A mathematical description of this physical effect is provided by the use of the density function $\rho(\mathbf{r})$ in eq. (4).

To test the validity of eq. (4) and find the value of α, we substitute the wave function of eq. (4) into eq. (1) and make the following assumptions:

(a) $\rho(r)$ falls from its maximum value to zero in a distance 2ε, where $\varepsilon \ll R_0$, the radius of the density distribution,

(b) $\rho'(r) = \rho''(r) = 0$ for $r < R_0 - \varepsilon$,

(c) the average value of ρ'' from $R_0-\varepsilon$ to $R_0+\varepsilon$ is zero.

(d) $f(\mathbf{r}) = 1$, and

(e) $(-\hbar^2\nabla^2/2m+\mathscr{V}_c(\mathbf{r})-E_0)\psi_0(\mathbf{r}) = 0$, where $\psi_0(\mathbf{r})$ is given by eq. (24) of I.

We then obtain an approximate solution, provided

$$\alpha = \frac{2m}{\hbar}\frac{\gamma}{4} = \frac{m\mu a^2}{2\hbar^3}. \tag{5}$$

Using this value of α together with $\psi_0(\mathbf{r})$ given in I, we obtain our approximate analytic wave function for the case of a square-well potential:

$$\psi(\mathbf{r}) = \left(1 + \frac{m\mu a^2}{2\hbar^3}\boldsymbol{\sigma}\cdot\mathbf{l}\right)\exp\{i(n-1)k_0\sqrt{R_0^2 - r^2\sin^2\theta} + in\mathbf{k}_0\cdot\mathbf{r}\} \text{ for } r < R_0, \tag{6}$$

$$\psi(\mathbf{r}) = \exp\{i\mathbf{k}_0\cdot\mathbf{r}\} \qquad \text{for } r > R_0. \tag{7}$$

The index of refraction n of eq. (6) is defined in I:

$$n^2 = 1 - \frac{\mathscr{V}_c}{E_0}. \tag{8}$$

3. Elastic Scattering Polarization

The polarization of nucleons scattered elastically from nuclei has been investigated by a number of authors [6]), and the more recent theoretical results have usually been in good agreement with experiments. In this section we describe the results of using the wave function of eq. (6) to calculate the polarization. We are not primarily interested in an exact calculation, but merely want to show the effects of the spin-orbit term. Therefore we shall keep the analysis simple and use only the *zero-order* term in the central potential, i.e., we let $n = 1$ in eq. (6), but include the *higher-order* effects in the spin-orbit potential.

The general form of the matrix element for a spin-$\frac{1}{2}$ particle and a spin-zero nucleus is

$$f(\theta) = A(\theta) + B(\theta)\boldsymbol{\sigma}\cdot\hat{\mathbf{n}}, \tag{9}$$

where $\hat{\mathbf{n}}$ is a unit vector perpendicular to the plane of scattering. In our approximation, with $n = 1$, the scattering amplitude is

$$f(\theta) \propto \int_0^{R_0} d\mathbf{r}\, e^{-i\mathbf{k}_f\cdot\mathbf{r}}\,(\mathscr{V}_c + \mathscr{U}_c\boldsymbol{\sigma}\cdot\mathbf{l})\{1+\alpha\boldsymbol{\sigma}\cdot\mathbf{l}\}e^{i\mathbf{k}_0\cdot\mathbf{r}}, \tag{10}$$

where $\mathbf{k}_0$ and $\mathbf{k}_f$ are the intial and final nucleon momenta, respectively, and $|\mathbf{k}_0| = |\mathbf{k}_f|$. The only difference between eq. (10) and the usual Born-approximation analysis [7]) is the addition of the term involving α, which yields results of higher order than the Born approximation only for the spin-orbit term. To show the effect of this term, we first set $\alpha = 0$ to obtain the Born-approximation amplitudes:

$$A(\theta) \propto 4\pi R_0^3 \mathscr{V}_c \frac{j_1(\Delta k R_0)}{\Delta k R_0}, \tag{11}$$

and

$$B(\theta) \propto i\mu a^2 k^2 \sin\theta 4\pi R_0^3 \frac{j_1(\Delta k R_0)}{\Delta k R_0}, \tag{12}$$

where $\Delta\mathbf{k} = \mathbf{k}_0 - \mathbf{k}_f$ is the momentum transfer. The polarization is defined by the relation

$$P = \frac{2\,\mathrm{Re}\,(AB^*)}{|A|^2 + |B|^2}. \tag{13}$$

The Born approximation gives the correct polarization for small angles [8]), but does not predict the observed diffraction effects near the first zero of the spherical Bessel function, since this is a common factor to $A(\theta)$ and $B(\theta)$ and therefore cancels in eq. (13). (See fig. 1.) However, if we go beyond the Born approximation and use the higher-order spin-orbit term ($\alpha \neq 0$), $B(\theta)$ will include a contribution in addition to that given in eq. (12), of the form

$$\alpha \mathscr{V}_c \int_0^{R_0} \mathrm{d}\mathbf{r}\; \mathrm{e}^{-i\mathbf{k}_f \cdot \mathbf{r}} \boldsymbol{\sigma} \cdot \mathbf{l}\, \mathrm{e}^{i\mathbf{k}_0 \cdot \mathbf{r}} = -i \frac{m\mathscr{V}_c}{2\hbar^2} k^2 \sin\theta\, 4\pi R_0^3 \frac{j_2(\Delta k R_0)}{(\Delta k R_0)^2}. \tag{14}$$

By adding the contribution of eq. (14) to $B(\theta)$ in eq. (12), we obtain an expression for the polarization that exhibits diffraction effects; the angle-dependent Bessel function no longer cancels, and the polarization shows a remarkable similarity to the exact calculation. (See fig. 1.)

We may also calculate $f(\theta)$ more exactly by using the complete wave function $\psi_0(\mathbf{r})$ of eq. (6), instead of a plane wave. This calculation gives spherical Bessel functions $j_1(\Delta k' R_0)$ and $j_2(\Delta k' R_0)$, where the argument $\Delta k' R_0 = |\mathbf{k}_f - n\mathbf{k}_0| R_0$ is complex due to the imaginary part of the index of refraction †. The results are in good agreement with the exact WKB calculation for the polarization in high-energy scattering problems.

It should be emphasized again that in our first example we have investigated the higher-order terms in the spin-orbit potential alone, and not the central potential. Other analyses that yield simple results for polarization effects [10]) have proceeded from the opposite point of view, i.e., they include the higher-order terms in the central potential only and neglect them in the spin-orbit

† Tables of spherical Bessel functions for complex argument have been compiled by the author [9]).

potential. However, as the calculation above suggests, the higher-order spin-orbit terms are not negligible. In fact, at least in the high-energy WKB approximation used here, it can be shown that the contributions from higher-order terms in each potential are of the same order of magnitude.

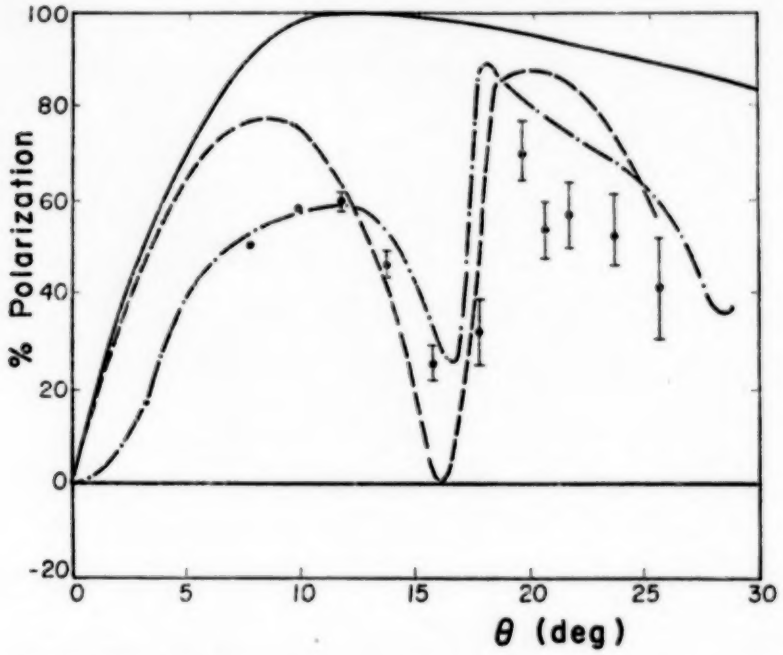

Fig. 1. The polarization from the elastic scattering of 300-MeV protons on aluminium. The solid curve is the Born approximation and the dashed curve shows the results of the simplified calculation in the text. The nuclear radius was chosen as $1.3\ A^{\frac{1}{3}} \times 10^{-13}$ cm. Coulomb effects have been neglected in both these curves. The dot-and-dash curve shows the results of the exact computer calculation of Bjorklund *et al.*[6]).

Although the approximate methods described above are able to yield adequate results for the scattering of nucleons in an energy region where the kinetic energy is much larger than the potential, they cannot be expected to be as generally useful as the computer calculations in which the Schroedinger equation is solved exactly. However, it is interesting that the main qualitative features of the scattering and polarization can be obtained from the very simple Born-approximation type of calculation, and that a detailed analysis is not necessary to afford at least a physical understanding of the experimental results.

4. Polarization from Inelastic "Direct" Processes

We have seen the usefulness of our optical-model wave functions in the calculation and physical interpretation of elastic nuclear scattering processes. A more important application, however, is found in the description of high-energy inelastic nuclear processes for which even computer calculations become

exceedingly cumbersome. The description of a rearrangement collision which proceeds via a "direct" interaction can be improved considerably over the Born approximation by the inclusion of elastic scattering effects. We require only a formal expression for the transition matrix in which the initial and final scattering states can be approximated by elastic scattering states.

For our example here, we consider the deuteron pickup reaction in which a high-energy proton enters a nucleus, picks up a neutron, and emerges as a final-state deuteron. We wish to include in our treatment the elastic nuclear scatterings of the initial-state proton and of the final-state deuteron. The formalism for use in an optical-model approximation has been derived in I, and the calculation of the differential cross section (excluding spin-orbit scattering effects) can also be found there.

In considering the polarization of final-state deuterons, we include only the effects of the nuclear spin-orbit potential on the initial and final scattering states, and we neglect the spin effects of the two-body potential through which the "direct" pickup process occurs, and also the spin effects of the nuclear potential in which the picked up neutron is initially bound. These latter effects are neglected since they lead to polarizations [11]) considerably smaller than those predicted by our spin-orbit scattering effects. For a complete treatment these terms should be included, but our purpose here is to show that the spin-orbit scattering is the major factor in producing polarized deuterons.

It can be shown from invariance arguments [12]) that, for two spin-$\frac{1}{2}$ particles and a spin-zero nucleus, the most general form of the transition matrix M is

$$M = A(\theta)+B(\theta)\boldsymbol{\sigma}_{\mathrm{p}} \cdot \hat{\mathbf{n}}+C(\theta)\boldsymbol{\sigma}_{\mathrm{n}} \cdot \hat{\mathbf{n}}+ \ldots, \tag{15}$$

where $\hat{\mathbf{n}}$ is a unit vector perpendicular to the plane defined by the momenta of the incoming proton and outgoing deuteron, and $\boldsymbol{\sigma}_{\mathrm{p}}$ and $\boldsymbol{\sigma}_{\mathrm{n}}$ are the spin vectors for the proton and neutron respectively. In this application higher-order terms in $\boldsymbol{\sigma}_{\mathrm{p}}$ and $\boldsymbol{\sigma}_{\mathrm{n}}$ are small and can be neglected.

We calculate M by replacing the optical-model wave functions ψ_0 in eq. (36) of I by the ψ given in eq. (6) above. The spin function for the outgoing deuteron is assumed to be characterized by the neutron spin function, in accordance with the formalism derived by Francis and Watson [13]) and discussed at some length in I. The details of the calculation are not given here, but the method is straightforward and is exactly the same as that used in I, i.e., the functions in the integrands are approximated by Gaussians, which allows closed-form expressions for the integrals over momentum space.

Once we have found A, B and C of eq. (15), we can use the matrix notation of Wolfenstein and Ashkin [12]) to evaluate the polarization. Specific applications of this formalism to deuteron problems have been investigated by Lakin [14]) and Stapp [15]). However, since the tensor terms in the deuteron formalism turn out to be small for the pickup reaction, it is simpler for the purposes here to

consider just the formalism for two spin-$\frac{1}{2}$ particles, and at the end to project out the states that do not give deuterons.

Following Wolfenstein [7]), we write the differential cross section for the deuterons resulting from the scattering of initially polarized protons:

$$I = \tfrac{1}{4}\,\mathrm{Tr}[T(MM^\dagger)] + \tfrac{1}{4}P\boldsymbol{\mu}\cdot\mathrm{Tr}[T(M\boldsymbol{\sigma}_\mathrm{p}M^\dagger)], \tag{16}$$

where $P\boldsymbol{\mu}$ gives the amount and direction of the initial proton polarization, and the operator T projects out the singlet spin state of the n—p system and leaves only triplet deuteron states:

$$T = \frac{3+\boldsymbol{\sigma}_\mathrm{p}\cdot\boldsymbol{\sigma}_\mathrm{n}}{4}. \tag{17}$$

For the specific case we wish to compare with experiment, we assume that the initial proton polarization is in a direction normal to the plane of scattering. Then eq. (16) becomes

$$I = \tfrac{3}{4}(|A|^2+|B|^2+|C|^2)+\tfrac{1}{2}\mathrm{Re}(BC^*)+P\{\mathrm{Re}[A(\tfrac{3}{2}B^*+\tfrac{1}{2}C^*)]\}\cos\phi, \tag{18}$$

and the left-right asymmetry is

$$\varepsilon = \frac{\mathrm{Re}[A(\frac{3}{2}B^*+\frac{1}{2}C^*)]}{\frac{3}{4}(|A|^2+|B|^2+|C|^2)+\frac{1}{2}\mathrm{Re}(BC^*)}. \tag{19}$$

A comparison of the results obtained by using eq. (19) with recent experiments from the bombardment of C^{12} by 145-MeV protons [16]) is given in fig. 2. The values for the optical-model parameters for the central potential are the same as those tabulated in I, and the spin-orbit parameter chosen is $\mu a^2 = 5\times10^{-26}\,\mathrm{MeV}\cdot\mathrm{cm}^2$, which is the value used in ref. [4]).

It can be seen that the main features of the data are predicted by our theory. Particularly, it is clear that the major contribution to the polarization must come from the spin-orbit scatterings, since the results obtained by considering just the effect of the initial state of the bound neutron [11]) lead to a maximum asymmetry of $\frac{1}{3}$, which is much too small to account for the experimental results.

Because of the simplicity of the wave functions used, the analysis here allows a qualitative explanation of the form of the observed polarization, as it also did for the elastic-scattering case of section 3. The increasing positive slope for small angles can be understood from the fact that the effects of the optical potential (spin-orbit elastic scattering) become increasingly important as the angle increases away from the forward direction. A maximum in the polarization is reached, however, since for very large angles, inelastic initial- and final-state

scatterings (which are not considered in the theory here) contribute to the cross section.

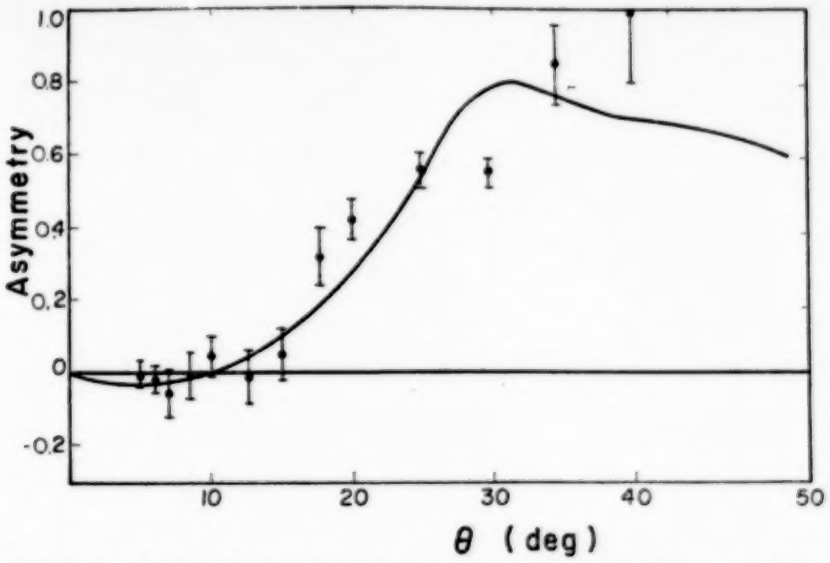

Fig. 2. The asymmetry of outgoing deuterons from the pickup reaction on carbon. The smooth curve gives the results of the calculation in section 4.

The author is deeply indebted to Professor Kenneth M. Watson for his support and many helpful suggestions during the course of this work. Particular thanks are also due to Dr. Henry Stapp for many stimulating discussions.

References

1) Fernbach, Serber and Taylor, Phys. Rev. **75** (1949) 1352
2) R. Serber, Phys. Rev. **72** (1947) 1114
3) K. R. Greider, Phys. Rev. **114** (1959) 786
4) See, for example, Fernbach, Heckrotte, and Lepore, Phys. Rev. **97** (1955) 1059
5) E. Fermi, Nuovo Cimento Supp. **10** (1955) 17
6) See ref.[4]), and also F. Bjorklund, I. Blandford and S. Fernbach, Phys. Rev. **108** (1957) 795; R. Sternheimer, Phys. Rev. **97** (1955) 1314
7) See, for example, E. Fermi, Nuovo Cimento **11** (1954) 407; L. Wolfenstein, Ann. Rev. Nuclear Sci. **6** (1956) 43
8) H. A. Bethe, Ann. Physics **3** (1958) 113
9) University of California Radiation Laboratory Report UCRL-8415 (August 12, 1958) (unpublished)
10) H. S. Köhler, Nuclear Physics **9** (1958) 49
11) B. J. Malenka, Phys. Rev. **98** (1955) 843
12) L. Wolfenstein and J. Ashkin, Phys. Rev. **85** (1952) 947
13) N. C. Francis and K. M. Watson, Phys. Rev. **93** (1954) 313
14) W. Lakin, Phys. Rev. **98** (1955) 139
15) H. P. Stapp, Phys. Rev. **107** (1957) 607
16) P. F. Cooper, thesis, Harvard University, 1958 (unpublished)

2.1 *Nuclear Physics* **14** (1959/60) 506—511; © *North-Holland Publishing Co., Amsterdam*
Not to be reproduced by photoprint or microfilm without written permission from the publisher

THE ELECTRIC DIPOLE SUM RULE

GEOFFREY I. OPAT
Physics Department, University of Melbourne, Australia

Received 14 August 1959

Abstract: A derivation of the electric dipole sum rule is given, which takes nuclear recoil into account and eliminates redundant coordinates.

1. Introduction

The electric dipole sum rule of Thomas, Reiche and Kuhn [1]), as developed by Levinger and Bethe [2]), is one of the strongest rules used in the analysis of photo-nuclear experiments, because it gives an essentially model-independent expression for the integrated cross-section for electric dipole photon absorption. The presence of redundant coordinates together with the nuclear recoil effect leaves the status of this rule open to doubt. In this paper the rule, in the Levinger and Bethe form, is shown to hold by giving an exact treatment of recoil and redundant coordinates. Levinger and Bethe have discussed the effect of exchange potentials on the dipole sum and so this point is not considered below.

In using particle coordinates relative to the centre of mass of the system under consideration, an equation of constraint exists which is not present for laboratory coordinates.

If ξ_i is the coordinate of the ith particle relative to centre of mass, and m_i its mass, then

$$\sum_i m_i \xi_i = 0 \tag{1}$$

is the equation of constraint, the summation being over all particles. The effect of this equation is to limit the domain of integration in configuration space employed in the formation of matrix elements.

In the past the distinction between centre-of-mass and laboratory coordinates has not always been made explicitly, with the result that a "hybrid" system has been used, expressing the operators in centre-of-mass coordinates but forming the matrix elements by integration over laboratory coordinates. This is particularly true of the effective charge concept (Bethe [3])), which rightly belongs only to the centre-of-mass system, and its relation to the sum rule.

One further point of objection that may be raised is that the solutions of Schrödinger equation (2) below are not localised even for bound nuclear

systems, but extend into a region of macroscopic size. It is doubtful therefore if the matrix element of a position vector of a nucleon exists in the mathematical sense. Furthermore, the use of the electric dipole approximation implies that the system considered has a small extension. Thus the electric dipole approximation strictly applies to the interaction operator after centre-of-mass motion is removed.

2. Derivation of the Sum Rule

2.1. THE COORDINATE TRANSFORMATION

Let m_i be the mass of the ith particle with laboratory coordinates $\mathbf{x}_i$. The Schrödinger equation for the system is given by

$$\{-\tfrac{1}{2}\hbar^2 \sum_i \nabla_{x_i}^2/m_i + \mathscr{V}(\substack{\text{coordinate}\\\text{differences}})\}\Psi(\mathbf{x}) = E\Psi(\mathbf{x}). \tag{2}$$

We carry out the transformation to internal or centre-of-mass coordinates $\boldsymbol{\xi}_i$ and the coordinate of the centre-of-mass $\mathbf{X}$. It is to be noted that only $(N-1)$ vectors $\boldsymbol{\xi}_i$ are employed below; the position operator of the Nth particle, which is left unused, can always be found from eq. (1).

Explicitly we have the transformation

$$\boldsymbol{\xi}_j = \mathbf{x}_j - \sum_i m_i \mathbf{x}_i/M, \quad (i = 1, 2, \ldots, N;\ j = 1, 2, \ldots, N-1), \tag{3}$$

$$\mathbf{X} = \sum_i m_i \mathbf{x}_i/M, \tag{4}$$

where

$$M = \sum_i m_i. \tag{5}$$

The wave-function $\Psi(\mathbf{x})$ expressed in the new coordinates is denoted $\Phi(\mathbf{X}, \boldsymbol{\xi})$. Thus we find

$$\nabla_{x_i} \to \frac{m_i}{M}\nabla_X + \sum_j{}' \left(\delta_{ij} - \frac{m_i}{M}\right)\nabla_{\xi_j}, \tag{6}$$

where $\sum'$ indicates a sum over all particles other than the Nth and ∇_{x_i} is the gradient operator for coordinate $\mathbf{x}_i$ etc.

The Schrödinger equation becomes

$$\left\{-\tfrac{1}{2}\hbar^2\left[\frac{1}{M}\nabla_X{}^2 + \sum_j{}'\left(\frac{1}{m_j} - \frac{1}{M}\right)\nabla_{\xi_j}^2 - \frac{2}{M}\sum_j{}'\sum_{k>j}{}'\nabla_{\xi_k}\cdot\nabla_{\xi_j}\right] + \mathscr{V}(\boldsymbol{\xi})\right\}\Phi(\mathbf{X}, \boldsymbol{\xi})$$
$$= E\Phi(\mathbf{X}, \boldsymbol{\xi}). \tag{7}$$

The function $\Phi(\mathbf{X}, \boldsymbol{\xi})$ can be shown to be separable into centre-of-mass and internal coordinates:

$$\Phi(\mathbf{X}, \boldsymbol{\xi}) = \phi(\mathbf{X})\psi(\boldsymbol{\xi}), \tag{8}$$

where $\phi(\mathbf{X})$ satisfies

$$-\frac{\hbar^2}{2M}\nabla^2_X\phi(\mathbf{X}) = E^0\phi(\mathbf{X}), \tag{9}$$

and has the solution

$$\phi(\mathbf{X}) = V^{-\frac{1}{2}}e^{i\mathbf{K}\cdot\mathbf{X}}, \tag{10}$$

where $K^2 = 2ME^0/\hbar^2$ and V is the volume of a box on the surfaces of which $\phi(\mathbf{X})$ satisfies periodic boundary conditions.

The internal wave function satisfies

$$\left\{-\tfrac{1}{2}\hbar^2\left[\sum_j{}'\left(\frac{1}{m_j}-\frac{1}{M}\right)\nabla^2_{\xi_j}-\frac{2}{M}\sum_j{}'\sum_{k>j}{}'\nabla_{\xi_k}\cdot\nabla_{\xi_j}\right]+\mathscr{V}(\xi)\right\}\psi(\xi) = E'\psi(\xi), \tag{11}$$

where $E'+E^0 = E$, E' being interpreted as the internal energy of the nucleus and E^0 as the kinetic energy of gross nuclear motion.

It can readily be shown that the eigensolutions of equation (11) form a set of orthogonal normalisable functions in the coordinates $\xi_j (j = 1, \ldots N-1)$.

We now consider the matrix elements of ξ_j defined by

$$\langle \mathrm{f}|\xi_j|0\rangle \equiv \int \psi_\mathrm{f}^*(\xi)\xi_j\psi_0(\xi)\mathrm{d}\tau_\xi.$$

From eq. (11), remembering the non-exchange character of $\mathscr{V}(\xi)$ we may show that

$$\frac{1}{\hbar^2}(E'_\mathrm{f}-E'_0)\langle \mathrm{f}|\xi_j|0\rangle = \frac{-1}{m_j}\langle \mathrm{f}|\nabla_{\xi_j}|0\rangle+\frac{1}{M}\sum_k{}'\langle \mathrm{f}|\nabla_{\xi_k}|0\rangle. \tag{12}$$

It follows that

$$\frac{1}{m_j}\langle \mathrm{f}|\nabla_{\xi_j}|0\rangle = -\frac{(E'_\mathrm{f}-E'_0)}{\hbar^2}\left[\langle \mathrm{f}|\xi_j|0\rangle+\frac{1}{m_\mathrm{N}}\sum_k{}' m_k\langle \mathrm{f}|\xi_k|0\rangle\right]. \tag{13}$$

2.2. INTEGRATED CROSS-SECTION

The expression for the integrated cross-section is given by Heitler [4]) as

$$I \equiv \int_0^\infty \sigma \mathrm{d}E = \frac{2\pi}{\hbar}\sum_\mathrm{f}|H_{\mathrm{f}0}|^2, \tag{14}$$

where

$$H_{\mathrm{f}0} = \int \Psi_\mathrm{f}^*(\mathbf{x})\left[\sqrt{\frac{\mu_0\hbar}{2k_{\mathrm{f}0}}}i\hbar\sum_i\frac{q_i}{m_i}e^{i\mathbf{k}_{\mathrm{f}0}\cdot\mathbf{x}_i}\,\mathbf{u}\cdot\nabla_{x_i}\right]\Psi_0(\mathbf{x})\mathrm{d}\tau_x. \tag{15}$$

In this expression the photon field has been normalised to one photon per unit area per unit time and has polarisation in the direction of the unit vector **u**. The photon field is chosen to have periodic boundary conditions on the surface of the box referred to above. The volume of this box is made sufficiently large, so that the separation of the energy states is very much smaller than the width

of the excited nuclear states. That this last condition is required is implicit in the derivation of eq. (14). The wave number k_{f0} is the magnitude of the photon propagation vector, $\mathbf{k}_{\mathrm{f0}}$ which has the direction of the photon beam; k_{f0} corresponds to the energy $(E'_{\mathrm{f}}-E'_{0})$. The charge of the ith particle q_i has been expressed in rationalised MKS units and μ_0 is the permeability of the vacuum in these units. The summation over f is over all final states of the system.

The matrix element H_{f0} is expressed in terms of $\mathbf{X}$ and $\boldsymbol{\xi}$, by using eqs. (6) and (8) together with the inverse of eqs. (3) and (4), namely,

$$\mathbf{x}_j = \mathbf{X}+\boldsymbol{\xi}_j \quad (j = 1, 2, \ldots, N-1), \tag{16}$$

$$\mathbf{x}_{\mathrm{N}} = \mathbf{X}-\sum_k{}' m_k \boldsymbol{\xi}_k/m_{\mathrm{N}}. \tag{17}$$

We find

$$H_{\mathrm{f0}} = i\hbar\sqrt{\frac{\mu_0\hbar}{2k_{\mathrm{f0}}}}\int \phi_{\mathrm{f}}^*(\mathbf{X})\psi_{\mathrm{f}}^*(\boldsymbol{\xi})\left[\sum_j{}'\frac{q_j}{m_j}\mathrm{e}^{i\mathbf{k}_{\mathrm{f0}}\cdot(\mathbf{X}+\boldsymbol{\xi}_j)}\mathbf{u}\cdot\left(\frac{m_j}{M}\nabla_X+\sum_k{}'\left(\delta_{jk}-\frac{m_j}{M}\right)\nabla_{\xi_k}\right)\right.$$
$$\left.+\frac{q_{\mathrm{N}}}{m_{\mathrm{N}}}\mathrm{e}^{i\mathbf{k}_{\mathrm{f0}}\cdot(\mathbf{X}-\sum_k{}' m_k\boldsymbol{\xi}_k/m_{\mathrm{N}})}\mathbf{u}\cdot\left(\frac{m_{\mathrm{N}}}{M}\nabla_X-\sum_k{}'\frac{m_k}{M}\nabla_{\xi_k}\right)\right]\phi_0(\mathbf{X})\psi_0(\boldsymbol{\xi})\mathrm{d}\tau_X\mathrm{d}\tau_\xi. \tag{18}$$

Using the orthogonality of the $\psi(\boldsymbol{\xi})$ and the $\phi(\mathbf{X})$ together with the explicit form (10) we find on integrating over the $\mathrm{d}\tau_X$ that

$$H_{\mathrm{f0}} = i\hbar\sqrt{\frac{\mu_0\hbar}{2k_{\mathrm{f0}}}}\int\psi_{\mathrm{f}}^*(\boldsymbol{\xi})\mathbf{u}\cdot\left[\sum_i\frac{q_i}{m_i}\sum_k{}'\left(\delta_{ik}-\frac{m_k}{M}\right)\nabla_{\xi_k}\right]\psi_0(\boldsymbol{\xi})\mathrm{d}\tau_\xi$$
$$\text{if } \mathbf{K}_{\mathrm{f}} = \mathbf{K}_0+\mathbf{k}_{\mathrm{f0}}, \tag{19}$$
$$= 0 \quad \text{if} \quad \mathbf{K}_{\mathrm{f}} \neq \mathbf{K}_0+\mathbf{k}_{\mathrm{f0}}$$

where $\mathbf{K}_0$ and $\mathbf{K}_{\mathrm{f}}$ are the initial and final vector wave-numbers of the centre of mass of the system. In eq. (19) the electric dipole approximation has also been employed, i.e.

$$\mathrm{e}^{i\mathbf{k}_{\mathrm{f0}}\cdot\boldsymbol{\xi}_j} \to 1$$

and

$$\exp[-i\mathbf{k}_{\mathrm{f0}}\cdot\sum_k{}' m_k\boldsymbol{\xi}_k/m_{\mathrm{N}}] \to 1.$$

Note that in eq. (19) the summation $i = 1, 2, \ldots, N$.

We insert into eq. (14) one factor H_{f0} given by eq. (19) and the other factor H_{f0} also given by eq. (19) but with the gradients removed by using eq. (13).

We now find

$$I = -\pi\mu_0\hbar c\sum_{\mathrm{f}}\langle 0|B^*|\mathrm{f}\rangle\langle\mathrm{f}|A|0\rangle, \tag{20}$$

where

$$A \equiv \mathbf{u}\cdot\left[\sum_i\frac{q_i}{m_i}\sum_j{}'\left(\delta_{ij}-\frac{m_i}{M}\right)\nabla_{\xi_j}\right] \equiv \sum_j{}'\left(\frac{q_j}{m_j}-\frac{Q}{M}\right)\mathbf{u}\cdot\nabla_{\xi_j}, \tag{21}$$

and

$$B \equiv \mathbf{u} \cdot \left[\sum_i \frac{q_i}{m_i} \sum_j{}' \left(\delta_{ij} - \frac{m_i}{M} \right) m_j \left(\xi_j + \sum_k{}' \frac{m_k}{m_N} \xi_k \right) \right] \equiv \mathbf{u} \cdot \left[\sum_j{}' \left(q_j - \frac{q_N}{m_N} m_j \right) \xi_j \right]; \tag{22}$$

Q is the total charge of the system.

Using the closure property of the $\psi(\xi)$ the summation over f may be performed giving

$$I = -\pi \mu_0 \hbar c \langle 0 | B^* A | 0 \rangle. \tag{23}$$

Eq. (11) may be used to show that

$$\int \psi_0^*(\xi) \mathbf{u}^* \cdot \xi_j \mathbf{u} \cdot \nabla_{\xi_k} \psi_0(\xi) d\tau_\xi = -\tfrac{1}{2} \delta_{jk}, \tag{24}$$

whence

$$I = \tfrac{1}{2} \pi \mu_0 \hbar c \left\{ \sum_i \frac{q_i^2}{m_i} - \frac{Q^2}{M} \right\}. \tag{25}$$

This reduces to the well-known result

$$I = \frac{\pi \mu_0 \hbar c e^2}{2 M_p} \frac{NZ}{A} \tag{26}$$

for a nuclear system, where M_p is the mass of a nucleon and Z, N are the proton and neutron numbers respectively, and $A = N + Z$.

For an atomic system, neglecting the nuclear system because of its high mass, we obtain the well-known result

$$I = \frac{\pi \mu_0 \hbar c e^2}{2 m_e} \cdot Z, \tag{27}$$

where m_e is the electronic mass.

3. Possible Extension to Exchange Forces

The presence of exchange forces has been attributed to the existence of mesons in the nucleus. If it is possible to find an equation of the Schrödinger type which includes directly the meson and nucleon system together, and which contains no terms other than the kinetic energy which fail to commute with the position coordinates of the mesons and nucleons, an equation of the form (25) may be expected to hold. The mesons, having a lighter mass than the nucleons, would increase the value of I above the value in eq. (26). In this case the increase in integrated cross section would be explained kinematically by the presence of charged mesons rather than the more usual way of Levinger and Bethe using exchange forces.

The author would like to thank Associate Professor C. B. O. Mohr and Dr. B. M. Spicer for their interest in the present work. He is also indebted to General Motors-Holden's Ltd. for a research fellowship.

References

1) W. Thomas, Naturwiss. **13** (1925) 627;
W. Kuhn, Zs. f. Phys. **33** (1925) 408;
F. Reiche and W. Thomas, Zs. f. Phys. **34** (1925) 510
2) J. S. Levinger and H. A. Bethe, Phys. Rev. **78** (1950) 115
3) H. A. Bethe, Revs. Mod. Phys. **9** (1937) 221
4) W. Heitler, Quantum Theory of Radiation (3rd Edit. Oxford, 1954) Ch. IV

7.B

Nuclear Physics **14** (1959/60) 512—516; © *North-Holland Publishing Co., Amsterdam*

Not to be reproduced by photoprint or microfilm without written permission from the publisher

THE CREATION OF FAST ELECTRON PAIRS BY HIGH ENERGY MUONS

P. H. STOKER and P. C. HAARHOFF

Department of Physics, University of Potchefstroom, Union of South Africa †

Received 1 September 1959

Abstract: The cross sections for the creation of fast electron pairs by high energy muons in lead are calculated, imposing a lower limit of 10 mc^2 on the energy of each electron of the pair.

1. Introduction

The evaluation of the differential and total cross sections for the creation of fast electron pairs in lead by cosmic-ray muons was required for the analysis of an experiment.

Formulas for the cross sections for pairs produced by charged fermions have been derived by Bhabha [1]) and recently more accurately by Murota *et al.* [2]) ††. Bhabha calculated the second order differential as well as the total cross section only for the cases in which $r \ll 1$ and $r \gg 1$, where $r = \mu\varepsilon/mE$; (m, ε) and (μ, E) being the rest mass and total energy of the electron pair and the incident particle, respectively. In M the second order expression was obtained for all values of r, but the total cross section was given only for the two above-mentioned cases. When the incident particle is an electron, r is generally small compared to unity, but for heavier particles such as muons or protons it varies from $r \ll 1$ to $r \gg 1$ and the region $r \approx 1$ consequently becomes important.

In order to find numerical values for the total cross section for certain energy ranges of the muons and electrons of interest, the formula in M for the cross section as the differential of the negaton and positon energies was simplified to an expression for the cross section as the differential of the total pair energy.

2. The Cross Section as the Differential of the Total Pair Energy

It is assumed in M that the energies of the participating particles are large compared to the respective rest mass energies. We will make the further assumption that $\varepsilon/E \ll 1$, as will be the case for most pairs. Under these conditions, taking the indefinite constant α [2]) as equal to unity, eq. (23) of M becomes

† This is part of the work supported by the South African C.S.I.R.

†† This article will be referred to as M.

$$d^2\sigma = \frac{2}{3\pi}(Z\alpha')^2 r_e^2 \left[\log\left(\frac{R(1-v^2)}{\gamma(1+x)^{\frac{1}{2}}}\right) - 1\right]\left[\{(2+v^2)+(3+v^2)x\}\log\left(1+\frac{1}{x}\right) - (3+v^2) + \frac{1-v^2}{1+x}\right]\frac{d\varepsilon}{\varepsilon}dv \quad (1)$$

where

σ = cross section,

Z = atomic number

$\alpha' = \frac{1}{137}$ = fine structure constant,

r_e = classical electron radius,

$\gamma = \mu c^2/E$, $\gamma_0 = 2mc^2/\varepsilon$,

$R = \gamma/\gamma_0 = \frac{1}{2}r$,

ε_+ = energy of positon,

ε_- = energy of negaton,

$v = \frac{\varepsilon_+ - \varepsilon_-}{\varepsilon_+ + \varepsilon_-} = \frac{\varepsilon_+ - \varepsilon_-}{\varepsilon}$,

$x = R^2(1-v^2)$.

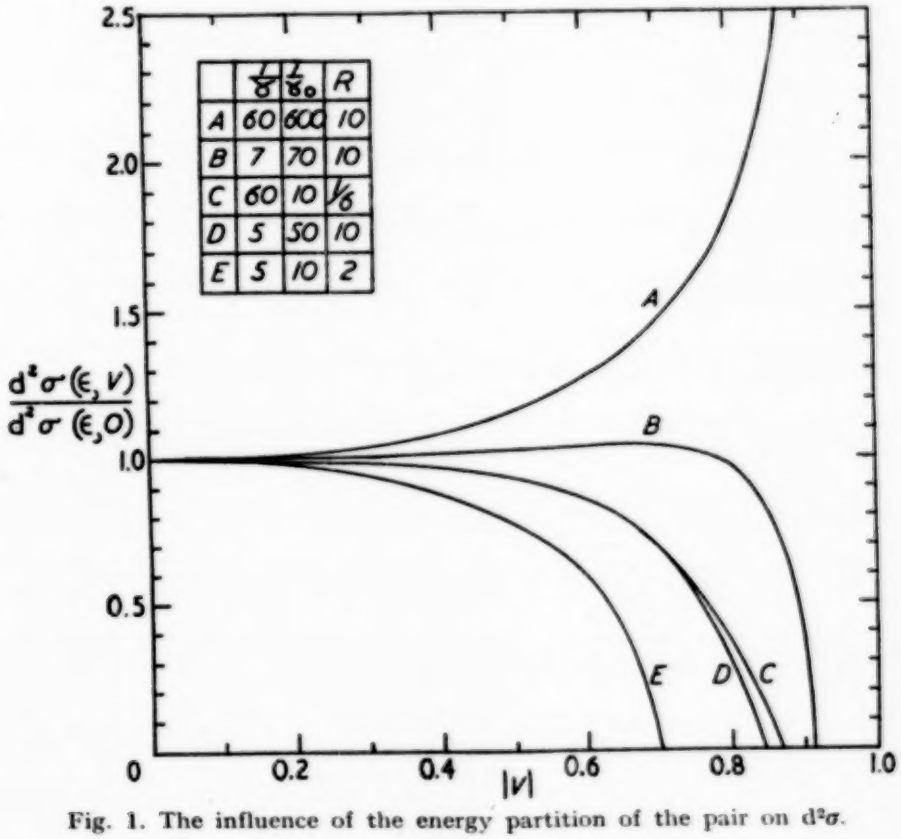

Fig. 1. The influence of the energy partition of the pair on $d^2\sigma$.

In fig. 1, $d^2\sigma(\varepsilon, v)$, normalized to the value at $v = 0$, is plotted against v for various values of γ and γ_0. It is obvious that for low values of ε, relatively few pairs occur in which one of the members has a small fraction of the total pair energy. When both ε and E are large, however, an asymmetric energy partition of the pair becomes probable.

The formula clearly does not hold for low values of ε_+ or ε_-; for $\gamma = \frac{1}{5}$ and $\varepsilon = 20\ mc^2$, e.g., σ becomes zero for ε_+ or $\varepsilon_- = 3\ mc^2$. This is due to the fact that the contribution of the indefinite number α, introduced in M for the derivation of $d^2\sigma$, becomes large in this region. Consequently, a definite lower limit for the individual energies of the negaton and the positon becomes necessary. Experimentally, this is also desirable for reliable measurements of the energies of the pair electrons.

We shall therefore consider only pairs in which each member has a minimum energy of 10 mc^2, i.e. $\varepsilon_+, \varepsilon_- \geqq 10\ mc^2$, $1/\gamma_0 \geqq 10$, and $-1+10\gamma_0 \leqq v \leqq 1-10\gamma_0$.

For the integration of (1) with respect to v, no general simplifying approximation can be made. The more direct approach is adopted of multiplying the value of $d^2\sigma$ at $v = 0$ with the interval $2(1-10\gamma_0)$, an empirical correction factor $1+C$ being introduced to compensate for the variation of $d^2\sigma$ with v. To facilitate the calculations, we require that $|v| \leqq 0.9$, i.e. $\varepsilon_+, \varepsilon_- \geqq 0.05\ \varepsilon$. This condition only becomes applicable for $\varepsilon \geqq 200\ mc^2$, and will thus have very little effect on the total cross section.

The parameter C is a function of γ and γ_0, given by

$$C = 0.023\left(\frac{1}{10\gamma_0} - 1\right) - \gamma^3\left(\frac{1}{100\gamma_0^2} - 1\right) \tag{2a}$$

for $\varepsilon \leqq 200\ mc^2$, i.e. for an interval $2(1-10\gamma_0)$, and by

$$C = 0.3 - 9\gamma_0 - 100\gamma^3 \tag{2b}$$

for $\varepsilon \geqq 200\ mc^2$, i.e. for a maximum interval of 1.8.

Eq. (2) is valid for $5 \leqq 1/\gamma \leqq 60$, corresponding approximately to 0.5 GeV $\leqq E \leqq$ 6 GeV for muons, $1+C$ being correct within 3 %. Values of $1/\gamma$ larger than 60 were not considered, as the effect of screening in lead becomes marked at higher energies [2]).

The formula for $d\sigma$ in terms of $d\varepsilon$ becomes

$$d\sigma = \frac{4}{3\pi}(Z\alpha')^2 r_e^2 \left[\log\left(\frac{R}{\gamma(1+R^2)^{\frac{1}{2}}}\right) - 1\right]\left[(2+3R^2)\log\left(1+\frac{1}{R^2}\right) - 3 + \frac{1}{1+R^2}\right] \times [I(1+C)]\frac{d\varepsilon}{\varepsilon} \tag{3}$$

where

$$I = 1-10\gamma_0 \quad \text{for} \quad \varepsilon \leqq 200\ mc^2,$$

$$I = 0.9 \quad \text{for} \quad \varepsilon \geqq 200\ mc^2.$$

In fig. 2, $d\sigma$ is plotted against R for $R \leqq 10$, i.e. approximately for $\varepsilon/E \leqq 0.1$, for various values of γ. The dashed line gives the value of $d\sigma$ for $\gamma = \frac{1}{5}$, when all pairs with total energy ε are taken into account, i.e. $\varepsilon_+, \varepsilon_- \geqq mc^2$.

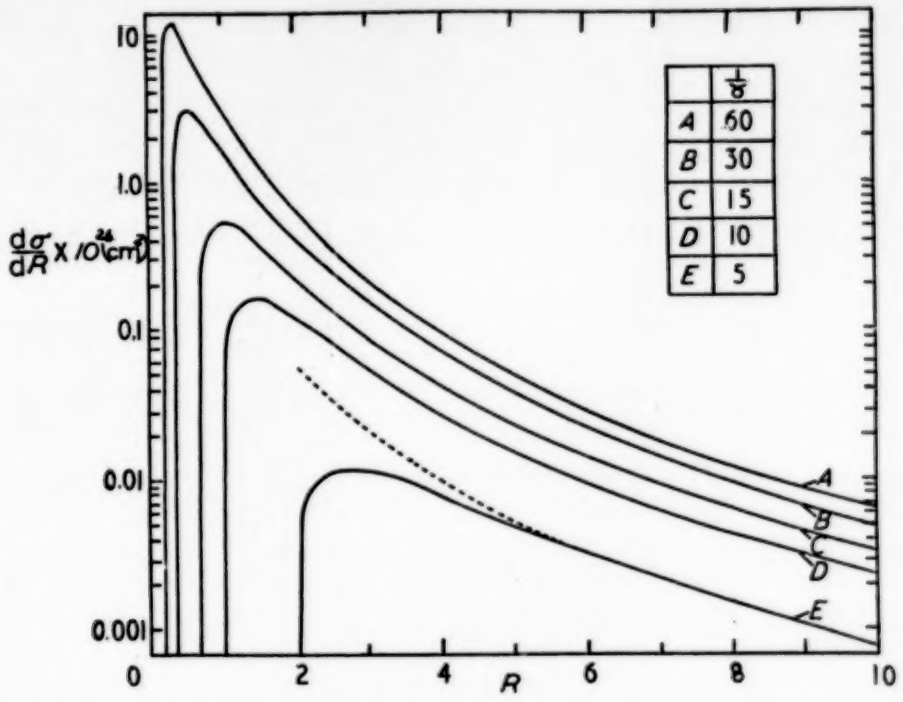

Fig. 2. The values of $d\sigma/dR$ in lead against R for $R \leqq 10$, and various values of γ. The dashed curve gives the value for $\gamma = 1/5$, when all pairs are taken into account.

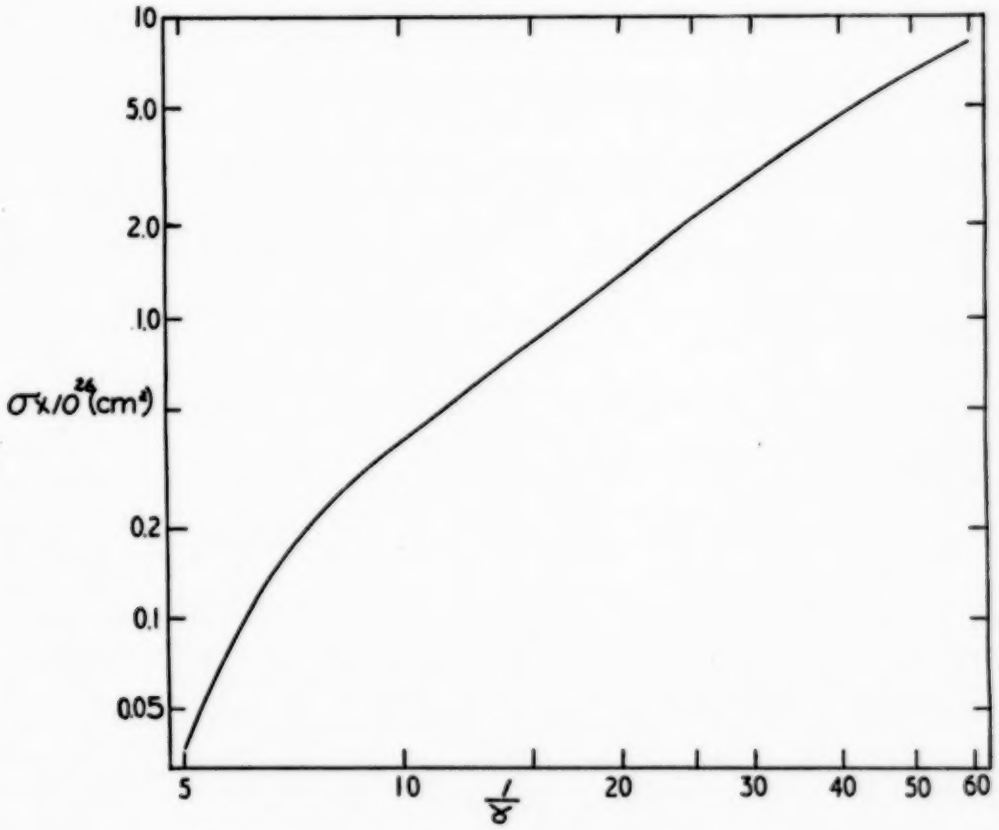

Fig. 3. The value of σ in lead against γ.

3. The Total Cross Section

The value of σ in lead is plotted against γ in fig. 3, the integration being performed numerically. When $\gamma \gg 1$, these values cannot be compared to those given by the corresponding formula in M, as M did not introduce a lower limit for the individual energies of the pair electrons. Integration of the dashed curve in fig. 2 gives a cross section of $\sigma = 0.10 \times 10^{-26}$ for $\gamma = \frac{1}{5}$ in lead, when all pairs with $\varepsilon \geqq 20\ mc^2$ are considered. As $\gamma \geqq 4$ in this case, eq. (38) in M is applicable, giving $\sigma = 0.39 \times 10^{-26}$ when the correct value [2]) of the constant β is taken.

It seems that large errors are introduced by the approximations in M for the integration of $d^2\sigma$, and a better estimate of σ should be obtained by our method. Even such a rough approximation as $C = 0$ gives a maximum error of 30 %.

P. C. H. would like to thank the Vacuum Oil Company of S. A. (Ltd.) for a very generous scholarship.

References

1) H. J. Bhabha, Proc. Roy. Soc. A **152** (1935) 559;
H. J. Bhabha, Proc. Camb. Phil. Soc. **31** (1935) 394
2) T. Murota, A. Ueda and H. Tanaka, Prog. Theor. Phys. **16** (1956) 482

7.A *Nuclear Physics* **14** (1959/60) 517—521; © *North-Holland Publishing Co., Amsterdam*
Not to be reproduced by photoprint or microfilm without written permission from the publisher

DISPERSION RELATIONS IN THE LEE MODEL

PAUL DE CELLES and GORDON FELDMAN
The Johns Hopkins University, Baltimore, Maryland †

Received 15 August 1959

Abstract: The self energy and the wave function renormalization constant in the Lee Model are calculated with the technique of dispersion relations. The results agree with those obtained in the usual manner.

1. Introduction

The technique of dispersion relations has been used recently in an attempt to calculate quantities of physical interest such as transition probabilities. In particular, Goldberger and Treiman [1]) have calculated the lifetime of the π-meson in this way. To support their analysis Goldberger and Treiman [2])†† have solved an analogous decay problem using a modified Lee Model. In addition to calculating transition probabilities, one might envisage the evaluation of quantities such as self energies and other renormalization constants within the framework of dispersion theory. To determine these constants one must assume the validity of the unsubtracted dispersion relations [3]). In this work we examine the self energy and the wave function renormalization constant for the V-particle in the Lee Model. We find that, indeed, the dispersion relations lead to the correct results.

2. Calculation of the Wave Function Renormalization Constant Z

In this section we write down the Hamiltonian for the Lee Model [4]). Then we proceed to calculate the V-particle wave function renormalization constant Z using dispersion relations.

The Hamiltonian H for the Lee Model is given by

$$H = m_V Z\psi_V^\dagger \psi_V + m_N \psi_N^\dagger \psi_N + \sum_k \omega_k a_k^\dagger a_k + g\psi_N^\dagger \psi_V A^\dagger + g\psi_N \psi_V^\dagger A + \delta m_V Z\psi_V^\dagger \psi_V . \quad (1)$$

All of the symbols are defined in GT. However, their modification has been left out, namely, the weakly coupled term H_2 has been set equal to zero.

From the anticommutation relations for ψ_V we obtain for Z the following

† Supported in part by the National Science Foundation.
†† Henceforth referred to as GT.

expression

$$1/Z = \langle 0|\{\psi_V, \psi_V^\dagger\}|0\rangle. \tag{2}$$

If we introduce a complete set of states in the usual way we obtain the expression

$$1/Z = \sum_n \{\langle 0|\psi_V|n\rangle\langle n|\psi_V^\dagger|0\rangle + \langle 0|\psi_V^\dagger|n\rangle\langle n|\psi_V|0\rangle\}. \tag{3}$$

The second term does not contribute because of the selection rules. Also, only the V-particle and N$+\theta$ scattering states contribute to the sum in the first term. Thus

$$1/Z = \langle 0|\psi_V|V\rangle\langle V|\psi_V^\dagger|0\rangle + \sum_k |\langle 0|\psi_V|N\theta_\omega\rangle|^2. \tag{4}$$

As in GT,

$$\langle 0|\psi_V|V\rangle = 1. \tag{5}$$

We define $L(\omega)$, where

$$L(\omega) = \frac{(2\omega\Omega)^{\frac{1}{2}}}{u(\omega)}\langle 0|\psi_V|N\theta_\omega\rangle. \tag{6}$$

Thus,

$$\frac{1}{Z} = 1 + \sum_k \frac{u^2(\omega)}{2\omega\Omega}|L(\omega)|^2. \tag{7}$$

The quantity $L(\omega)$ is similar to the vertex function $K(\omega)$ defined in GT. The procedure used to solve for $L(\omega)$ is analogous to that carried out for $K(\omega)$ in GT.

Using the formulation of Lehmann, Symanzik, and Zimmermann [5], we write $L(\omega)$ as follows:

$$L(\omega) = \frac{(2\omega\Omega)^{\frac{1}{2}}}{u(\omega)} i\int_{-\infty}^{\infty} dt e^{-i\omega t}\left(i\frac{d}{dt} + \omega\right)\langle 0|T(\psi_V a_k^\dagger(t))|N\rangle, \tag{8}$$

$$= i\int_{-\infty}^{\infty} dt e^{-i\omega t}\langle 0|T(\psi_V j^\dagger(t))|N\rangle, \tag{9}$$

where $j(t)$ is the θ-particle "current"

$$j(t) = \frac{(2\omega\Omega)^{\frac{1}{2}}}{u(\omega)}\left(-i\frac{d}{dt} + \omega\right)a_k(t), \tag{10}$$

and we have used

$$[\psi_V, a_k^\dagger(0)] = 0. \tag{11}$$

The T product can be written

$$T(\psi_V j^\dagger(t)) = [\psi_V j^\dagger(t)]\theta(-t) + j^\dagger(t)\psi_V. \tag{12}$$

Since

$$\langle 0|j^\dagger(t)\psi_V|N\rangle = 0, \tag{13}$$

we may write $L(\omega)$ as

$$L(\omega) = i\int_{-\infty}^{\infty} \mathrm{d}t e^{-i\omega t}\langle 0|[\psi_V j^\dagger(t)]\theta(-t)|N\rangle. \tag{14}$$

Because the Fourier transform of $L(\omega)$ is zero for $t > 0$, $L(\omega)$ is analytic everywhere in the upper half of the complex ω-plane. Therefore

$$L(\omega) = \frac{1}{\pi}\int_{-\infty}^{\infty} \frac{\operatorname{Im} L(\omega')}{\omega'-\omega-i\varepsilon}\,\mathrm{d}\omega'. \tag{15}$$

Again introducing a complete set of intermediate states, we can write $\operatorname{Im} L(\omega)$ as

$$\operatorname{Im} L(\omega) = -\pi g\delta(m_V-m_N-\omega) + \pi\sum_{k'}\langle 0|\psi_V|N\theta_{\omega'}\rangle\langle N\theta_{\omega'}|j^\dagger|N\rangle\delta(\omega-\omega'). \tag{16}$$

The first term in eq. (16) comes from the V-particle intermediate state, and we have used eq. (5) and $\langle V|j^\dagger|N\rangle = -g$.

The matrix element $\langle N\theta_{\omega'}|j^\dagger|N\rangle$ has been evaluated in GT using dispersion relations. Using GT, eq. (30), we can write

$$\operatorname{Im} L(\omega) = -\pi g\delta(m_V-m_N-\omega) + \tan\delta(\omega)\operatorname{Re} L(\omega)\theta(\omega-\mu), \tag{18}$$

where $\delta(\omega)$ is the $N+\theta$ scattering phase shift. Substituting eq. (18) into eq. (15) we arrive at the following integral equation:

$$L(\omega) = \frac{g}{\omega-m_V+m_N} + \frac{1}{\pi}\int_{\mu}^{\infty} \frac{\tan\delta(\omega')\operatorname{Re} L(\omega')}{\omega'-\omega-i\varepsilon}\,\mathrm{d}\omega'. \tag{19}$$

This is an equation of the type discussed by Omnès [6]). The solution which is regular at $\omega = \mu$ can be obtained from the particular solution of Omnès by means of an integration over the complex ω-plane. It is

$$L(\omega) = \frac{g}{1-\beta(\omega)}\cdot\frac{1}{\omega-m_V+m_N}, \tag{20}$$

where $\beta(\omega)$ is given by GT, eq. (43). Substituting eq. (20) into eq. (7) we obtain

$$1/Z = 1+g^2\sum_k \frac{u^2(\omega)}{2\omega\Omega}\frac{1}{|1-\beta(\omega)|^2}\cdot\frac{1}{(\omega-m_V+m_N)^2}. \tag{21}$$

This sum can be evaluated by going to the continuous limit. Aside from numerical factors the integral which arises is equivalent to I_1 of GT, eq. (57). Using their method of evaluation we obtain

$$g^2\sum_k \frac{u^2(\omega)}{2\omega\Omega}\frac{1}{|1-\beta(\omega)|^2}\frac{1}{(\omega-m_V+m_N)^2} = \frac{1}{1-\beta(\infty)} - 1. \tag{22}$$

Therefore,

$$Z = 1-\beta(\infty). \tag{23}$$

i.e.

$$Z = 1-g^2 \sum_k \frac{u^2(\omega)}{2\omega\Omega} \frac{1}{(\omega-m_V+m_N)^2}, \tag{24}$$

which is exactly the result originally obtained by Lee.

3. Calculation of the Self Energy

In this section we calculate the self energy of the V-particle. We define

$$f(t) = \left(-i\frac{d}{dt}+m_V\right)\psi_V(t). \tag{25}$$

From the Hamilton equations of motion it follows that

$$f(t) = -\delta m_V \psi_V - \frac{g}{Z}\psi_N A. \tag{26}$$

Using the fact that [7])

$$\langle 0|f(0)|V\rangle = 0, \tag{27}$$

and the formulation of Lehmann, Symanzik, and Zimmermann [5]), we find the following expression for δm_V:

$$\delta m_V = iZ\int_{-\infty}^{\infty} dt e^{-im_V t}\langle 0|\{f(0), f^\dagger(t)\}\theta(-t)|0\rangle. \tag{28}$$

We now define the function

$$\delta m_V(\xi) = iZ\int_{-\infty}^{\infty} dt e^{-i\xi t}\langle 0|\{f(0), f^\dagger(t)\}\theta(-t)|0\rangle. \tag{29}$$

Again, since $\delta m_V(\xi)$ is analytic in the upper half of the complex ξ-plane, we obtain the dispersion relation

$$\delta m_V(\xi) = \frac{1}{\pi}\int_{-\infty}^{\infty} \frac{\operatorname{Im}\delta m_V(\xi')}{\xi'-\xi-i\varepsilon} d\xi'. \tag{30}$$

Proceeding as before and using eq. (27), we obtain

$$\operatorname{Im}\delta m_V(\xi) = Z\pi \sum_k |\langle N\theta_\omega|f^\dagger|0\rangle|^2 \delta(\xi-m_N-\omega). \tag{31}$$

As in GT, eq. (22), we define the vertex function

$$K(\omega) = \frac{(2\omega\Omega)^{\frac{1}{2}}}{u(\omega)}\langle 0|f|N\theta_\omega\rangle. \tag{32}$$

They have shown that $K(\omega)$ satisfies an integral equation, the solution of which is

$$K(\omega) = -\frac{g}{1-\beta(\omega)}\frac{(1-\beta(\infty))}{Z}. \tag{33}$$

Using eq. (23) we have †

$$K(\omega) = -\frac{g}{1-\beta(\omega)}. \tag{34}$$

Using eqs. (30), (31), (32) and (34), we obtain

$$\delta m_{\mathrm{V}} = Zg^2 \sum_k \frac{u^2(\omega)}{2\omega\Omega} \frac{1}{|1-\beta(\omega)|^2} \frac{1}{(\omega - m_{\mathrm{V}} + m_{\mathrm{N}})}. \tag{35}$$

When we pass to the continuous limit this sum is equivalent to I_0 in GT, eq. (56). Using their method of evaluation we obtain

$$\sum_k \frac{u^2(\omega)}{2\omega\Omega} \frac{1}{|1-\beta(\omega)|^2} \frac{1}{(\omega - m_{\mathrm{V}} + m_{\mathrm{N}})} = \frac{1}{Z^2} \sum_k \frac{u^2(\omega)}{2\omega\Omega} \frac{1}{\omega - m_{\mathrm{V}} + m_{\mathrm{N}}}. \tag{36}$$

Therefore,

$$\delta m_{\mathrm{V}} = \frac{g^2}{Z} \sum_k \frac{u^2(\omega)}{2\omega\Omega} \cdot \frac{1}{\omega - m_{\mathrm{V}} + m_{\mathrm{N}}}, \tag{37}$$

which is Lee's result.

4. Conclusions

We have shown that the dispersion relation technique affords a means of evaluating such "unphysical quantities" as the self energy and wave function renormalization constant in the Lee Model. This was possible because we arrived at a finite set of coupled integral equations, which could be solved exactly. One might hope that in a more realistic theory some approximation would allow a solution not only for transition amplitudes but also for quantities such as self energies and other renormalization constants. Also, in a more realistic theory one would have to assume the validity of unsubtracted dispersion relations [3]). This is no problem in the Lee Model because all integrals exist owing to the presence of the cut-off.

† Since the vertex function $K(\omega)$ evaluated at $\omega = m_{\mathrm{V}} - m_{\mathrm{N}}$ is the coupling constant $-g$, we could have used this fact to show that $Z = 1-\beta(\infty)$. However, in a more realistic model $K(\omega)$ would depend not only on the wave function renormalization constant Z, but also on the vertex renormalization constant, which in this case is unity. Notice, also, that one can obtain $K(\omega)$ from $L(\omega)$, since $K(\omega) = (m_{\mathrm{V}} - m_{\mathrm{N}} - \omega)L(\omega)$. This follows from the definitions of $K(\omega)$ and $L(\omega)$ and eq. (25).

References

1) Goldberger and Treiman, Phys. Rev. **110** (1958) 1178
2) Goldberger and Treiman, Phys. Rev. **113** (1959) 1663
3) Drell and Zachariasen, Phys. Rev. **111** (1958) 1727
4) T. D. Lee, Phys. Rev. **95** (1954) 1329;
Källén and Pauli, Mat. Fys. Medd. Dan. Vid. Selsk. **30**, No. 7 (1955)
5) Lehmann, Symanzik and Zimmermann, Nuovo Cimento **1** (1955) 205
6) R. Omnès, Nuovo Cimento **8** (1958) 316
7) G. Källén, Handbuch der Physik Vol. V, Part 1 (Springer-Verlag, Berlin, 1958) p. 339

8.A

Nuclear Physics **14** (1959/60) 522—539; © *North-Holland Publishing Co., Amsterdam*

Not to be reproduced by photoprint or microfilm without written permission from the publisher

MECHANISM OF INTERACTION OF FAST PROTONS WITH NUCLEONS AND NUCLEI

V. S. BARASHENKOV, V. A. BELIAKOV, V. V. GLAGOLEV, N. DALKHAZHAV, YAO TSYNG SE, L. F. KIRILLOVA, R. M. LEBEDEV, V. M. MALTSEV, P. K. MARKOV, M. G. SHAFRANOVA, K. D. TOLSTOV, E. N. TSYGANOV and WANG SHOU FENG

Joint Institute of Nuclear Research, Dubna, USSR

Received 20 March 1959

Abstract: Angular and energy characteristics of interaction between 9 GeV protons and emulsion nuclei, as well as the production of strange particles have been investigated. The obtained experimental results reveal a better agreement with the cascade mechanism of nucleon-nucleus interaction than with the nucleon-tube model.

The average energy loss in a single nucleon-nucleon collision is estimated to be (40 ± 10) %. The size of a nucleon core is discussed. Through the optical analysis of nucleon-nucleon interactions the value $r_c \approx 0.6 \times 10^{-13}$ cm is obtained for the size of the nucleon core, while the fraction of peripheral collisions constitutes ≈ 20 %. Angular and energy distributions of slow K^+ and $\pi^\pm$ mesons have also been obtained. The production cross-section for K^+ mesons with energy up to 140 MeV on an average emulsion nucleus is $\sigma = 5 \pm 2$ mb.

1. Introduction

The interaction of fast nucleons with nuclei has been studied by many investigators both in the beam of accelerated particles (with energy $E \leqq 9$ GeV) and in cosmic rays [1]). The present work attempts an analysis of experimental results on the interaction of the 9 GeV protons with emulsion nuclei. The preliminary data were reported at the Geneva conference [2]).

In analysing nucleon-nucleus interactions two important factors should be kept in mind:

Firstly, the initial stage of proton-nucleus interaction may be represented either as a proton-nucleon collision or as an interaction of the proton with several nucleons of the nucleus simultaneously — the so called "tube" or "tunnel" which the incident proton cuts out in the nucleus. In the latter case the nucleon of the "tunnel" loses its individuality and the features of the initial stage must depend on atomic number. The conditions leading to "tube" interaction were formulated by E. L. Feinberg [3]). I. A Ivanovskaya *et al.*[4]), in analysing the results obtained in cosmic ray studies, came to the conclusion that the experimental data are consistent with the "tube "model.

Secondly, one should take into account the subsequent intranuclear interactions of particles produced in the first encounter. The probability of such interactions increases with atomic number.

Owing to these factors the interaction of a nucleon with light nuclei considerably differs from the interaction with heavy nuclei. The mechanisms of excitation and subsequent disintegration in light and heavy nuclei also have a number of distinctive features.

Therefore, in our analysis we divided all the observed nuclear interactions produced by incident protons in stripped emulsions into two groups:

1. interactions with light nuclei (C, N, O),
2. interactions with heavy nuclei (Ag, Br).

These groups differ in the number of nucleons by a factor of 7 and in the size of nuclei almost by a factor of 2.

2. Experimental Results

The greater part of the results analysed in this work was obtained with stack "A" consisting of 100 stripped emulsions NIKFI-R, 450 microns thick and 10×10 cm wide, the remaining part — with stack "B" similar to stack "A". These stacks were exposed to the internal beam of 9 GeV protons from the synchrophasotron of the Joint Institute of Nuclear Research.

The following notations are used:

s: shower particles with ionization $I \leqq 1.4\, I_0$, where I_0 is the ionization loss of 9 GeV protons;

g: particles with $I > 1.4\, I_0$ and a range $R > 3.73$ mm (grey tracks);

b: particles with $R \leqq 3.73$ mm (black tracks).

The s-particles consist mainly of pions produced in collision of particles within the nucleus, and of a small fraction of protons (≈ 0.5 per star); g and b particles are for the most part nuclear disintegration products.

The following criteria were used for singling out interactions with light nuclei:

a) the number of grey and black tracks in the star $n_g + n_b \leqq 7$;

b) the star does not contain any track with $R \leqq 10\mu$ i.e., there is no recoil nucleus;

c) there are no electrons in the residual nucleus disintegration;

d) among all tracks at least one has a range $10\mu < R \leqq 50\mu$.

(The emission from heavy nuclei of α-particles with $R < 50\mu$ is suppressed by the Coulomb barrier, the hardly probable tunnel effect being neglected.)

The criteria for selecting the interactions with heavy nuclei were the following

a) either $n_g + n_b > 8$; or

b) if $n_g + n_b \leqq 8$, the star should contain a recoil nucleus, i.e., a track with $R \leqq 10\mu$, and should not contain any track with $10\mu < R \leqq 50\mu$.

Thus, 53 stars out of 1260 found in track scanning and 66 stars out of 2060 found in area scanning were attributed to interactions with light nuclei; this constitutes 3.6 % of all stars. The experimental data obtained by other

investigators [5]) and the optical model analysis of the cross-section show that the interactions with light nuclei should constitute 25—30 % of the total number of interactions. Consequently, the chosen selection criteria are sufficiently rigid.

According to the above criteria, 67 stars out of 100 found in track scanning were ascribed to interactions with heavy nuclei. The obtained characteristics of interactions for light and heavy nuclei and for mixtures of nuclei found in track scanning are given in table 1:

TABLE 1

Characteristics of the interaction between 9 GeV protons and emulsion nuclei

	Light nuclei (C, N, O)	Heavy nuclei (Ag, Br)	Stars with $n_g+n_b \geqq 28$	Mixture of nuclei
$\bar{n}_s$	3.0± 0.2	3.5± 0.3	4.0±0.4	3.2± 0.2
$\bar{n}_g$	1.4± 0.1	4.1± 0.5	32	3.1± 0.4
$\bar{n}_b$	3.3± 0.1	6.1± 0.6		4.7± 0.5
$\theta^0_{s,\frac{1}{2}}$	22.5± 1	27.5± 1.5	53	25.0± 1.5
$\theta^0_{g,\frac{1}{2}}$	56.5± 3	65 ± 3	63	65 ± 3
$\theta^0_{b,\frac{1}{2}}$	–	84 ± 3	–	84.5± 3
$E_{s,\pi}$ (GeV)	–	–	–	1.0± 0.2
$E_{s,p}$ (GeV)	–	–	–	3.0± 0.5
$E_{g,\pi}$ (MeV)	–	–	–	40 ± 3
$E_{g,p}$ (MeV)	132 ±20	118 ±12	–	120 ±12
E_b (MeV)	≈6	12 ± 2	–	11 ± 1.0
$\bar{P}_{g\perp,p}$ (MeV/c)	344 ±20	354 ±20	–	350 ±20
$\bar{P}_{s\perp,\pi}$ (MeV/c)				370 ±70

1. the average numbers $\bar{n}_s$, $\bar{n}_g$, $\bar{n}_b$ of charged particles per star;

2. the angles $\theta_{s,\frac{1}{2}}$, $\theta_{g,\frac{1}{2}}$, $\theta_{b,\frac{1}{2}}$ which contain half of all particles, determined from the angular distributions plotted in figs. 1, 2, 3;

3. the mean kinetic energy for the different kinds of particles;

4. the average transverse momenta for pions and protons. The kinetic energies E_g and E_b for g and b particles were determined from the experimental energy distributions. Fig. 4 shows the energy distribution of g-particles for light and heavy nuclei. The energies of all stopping particles were determined from their range on the assumption that they are all either pions or protons †. The energy distribution of the escaped g particles as well as that of s particles was determined by ionization and multiple scattering measurements (see Appendix).

The average transverse momenta $\bar{p}_{s\perp,\pi}$ and $\bar{p}_{g\perp,p}$ for pions and protons

† The range-energy curves for the Ilford G-5 emulsions were used. The validity of these curves for the NIKFI-R emulsion is proved by the fact that the ranges of μ mesons from the π—μ decays agree well for both types of emulsions.

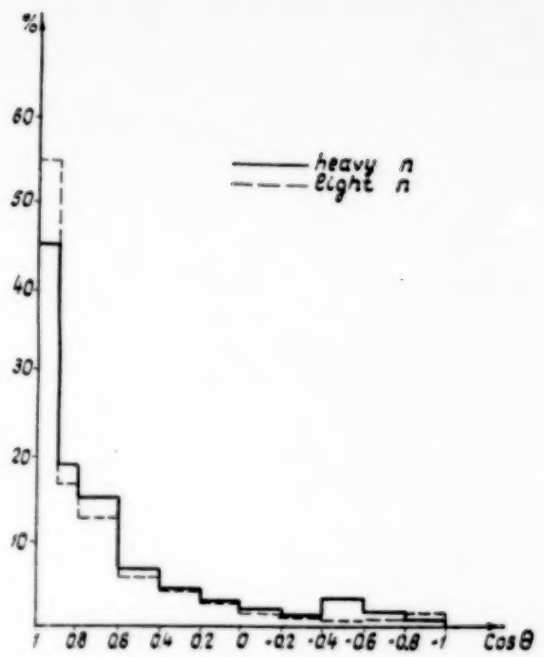

Fig. 1. Angular distribution of 3 particles. The solid line is for heavy nuclei, the dotted line for light nuclei.

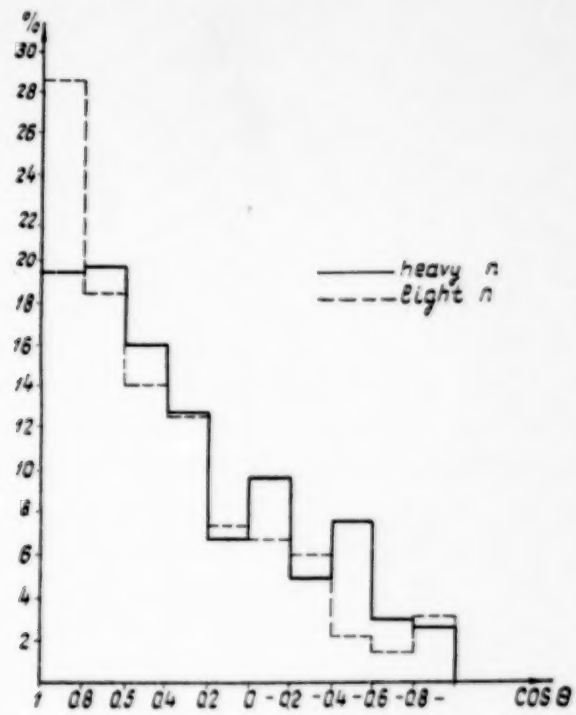

Fig. 2. Angular distribution of g particles. The solid line is for heavy nuclei, the dotted line for light nuclei.

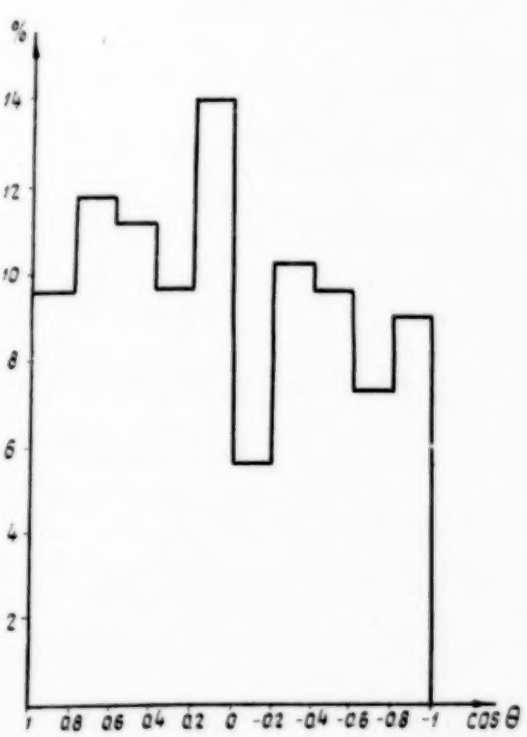

Fig. 3. Angular distribution of g particles on heavy nuclei.

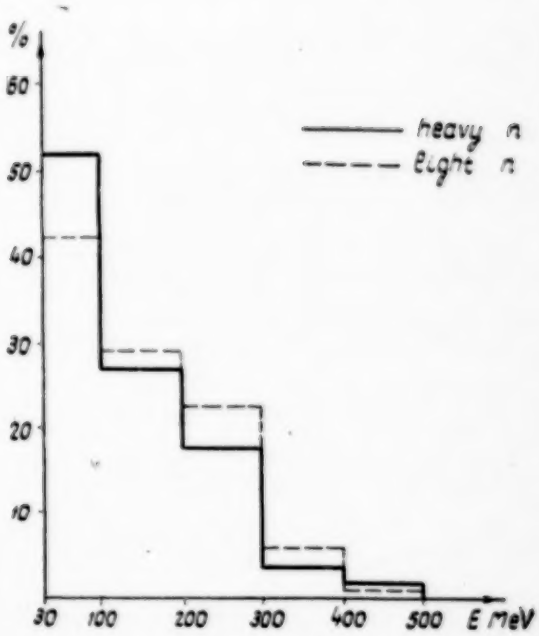

Fig. 4. Energy spectrum of g particles. The solid line is for heavy nuclei, the dotted line for light nuclei.

were obtained from the experimental values of their energies and angles. The values of average transverse momenta for nucleon-nucleon collisions calculated on statistical theory are 0.6 GeV/c and 0.45 GeV/c for nucleons and pions respectively.

The above-enumerated features of interactions with light and heavy nuclei and mixtures of nuclei allow us to calculate the overall energies ε_s, ε_b, ε_g carried away by s, b and g particles per star. The energy ε_g is given by

$$\varepsilon_g = (1+\eta)n_g(E_g+E_N)$$

where η is the ratio of the number of neutrons to protons, and E_N the average binding energy of a nucleon in the nucleus. The energy ε_b was calculated on the assumption either that all B particles are protons, or that the fraction of α particles consitutes 0.2—0.3 of the number of b particles [8]: in both cases ε_b happens to be practically the same.

The values for the energies ε_s, ε_g and ε_b, as well as for the energy $W = \varepsilon_g+\varepsilon_b$ transferred to the nucleus, are given in table 2 for the light, heavy and average nuclei of the emulsion.

TABLE 2

Values of energy $E_s E_g$ and E_b carried away by s, g and b particles and of energy $W = E_g+E_b$ transferred to the nucleus

	Mixture of nuclei	Heavy nuclei	Light nuclei
E_s (GeV)	7.5 ± 1.0	–	–
E_b (MeV)	180 ± 18	245 ± 25	≈ 90
E_g (MeV)	870 ± 90	1165 ± 120	390 ± 50
W (MeV)	1050 ± 100	1410 ± 140	480 ± 60

It should be noted that for the light nuclei our value $W_l = 480\pm 60$ MeV is in good agreement with the figure 440 ± 160 MeV obtained by N. L. Grigorov [9]) for cosmic ray radiation. It was also indicated by N. L. Grigorov that with variation of the incident particle (proton) energy within the 3—40 GeV range, W_l changes but little.

3. Mechanism of Interaction with Nucleus

It was pointed out in the introduction that a fast proton may interact either with a "tube" or with individual nucleons in the nucleus. In order to determine which of the two possible mechanisms actually takes place, accurate Monte Carlo calculations of nuclear cascades should be compared with the experimental data. Since such calculations are not yet completed we shall confine ourselves only to some qualitative considerations.

The assumption that the primary nucleon interacts with a "tube" leads to

values of $\theta_{s,\frac{1}{2}}$ angles $\approx 30°$ and $\approx 40°$ for light and heavy nuclei respectively †. These values considerably exceed the experimental ones. The probability of secondary interactions of particles produced in the nucleon-tunnel collision might only increase the calculated values of the angles.

Furthermore, if the initial stage of the nucleon-nucleus collision is a nucleon-tube interaction, the centre-of-mass velocity in the case of interaction with Ag and Br tubes will be much lower than for light nuclei, since on the average the tube is almost twice longer, and consequently the number of s particles must be considerably greater. In the experiments, however, the numbers of s particles produced on heavy and light nuclei are respectively equal to 3.5 ± 0.3 and 3.0 ± 0.2. Such a small difference can be explained by the cascade mechanism of interaction. Indeed, in the case of cascade collisions the energy of s particles decreases rapidly as the cascade proceeds, and this leads to a diminishing multiplicity of particles produced in these collisions.

Besides, the realization of the nucleon-tube mechanism would imply a considerable contamination of g particles by pions produced in the collision of a nucleon with the nuclear tube. The experimental data show, however, that g particles are almost exclusively nucleons, which can again be explained on the assumption of the cascade mechanism of the nucleon-nucleus interaction, according to which the majority of g particles are recoil nucleons. This agrees with the experiments on meson-nucleon collisions at $E > 0.5\,\mathrm{GeV}$ [10]), in which recoil nucleons of an energy corresponding to g particles were observed with a probability near unity.

The tube interaction model is of still less avail in explaining the events of nuclear disintegration with emission of more than 28 g and b particles ($\bar{n}_g + b = 32$) which are observed in $> 2\ \%$ cases and listed in table 1. In these disintegrations a complete decay of a nucleus into protons and neutrons with a small fraction of α-particles takes place, and the $\bar{n}_s$, $\theta_{g,\frac{1}{2}}$ and W values are nearly the same as the corresponding values for all cases of interaction with heavy nuclei.

The fact that the values of the transverse momentum $P_{g\perp}$ coincide for g particles produced on light and heavy nuclei, and also agree with the transverse

† The average number of nucleons in a tube,

$$n = \frac{\text{volume of tube}}{\text{specific volume per nucleon}} \approx \sqrt[3]{A},$$

with due consideration for the emulsion composition, is 2.4 and 4.6 for light and heavy nuclei. In calculating the $\theta_{s,\frac{1}{2}}$ angles a distribution of the produced particles isotropic in the centre of mass system was assumed and the laws of conservation of energy and momentum, baryon number and strangeness were taken into consideration. Account was also taken of the resonance interaction between the generated mesons and nucleons in a state with total and isobaric spins equal to $\frac{3}{2}$ at 200 MeV. Similar, but somewhat lower, values of the $\theta_{s,\frac{1}{2}}$ angles for light and heavy nuclei were also obtained by V. M. Maksimenko; we wish to thank V. M. Maksimenko for making the results of his calculations available to us prior to publication.

momenta of π-mesons (see table 1), also points to the cascade mechanism of interaction.

All other experimental results can also be explained on the assumption of the nuclear cascade.

4. Energy Losses in Nucleon Collisions

For the purpose of determining the average energy of s particles 83 particles with dip angle $< 3°$ were selected. The momenta of those particles were esti-

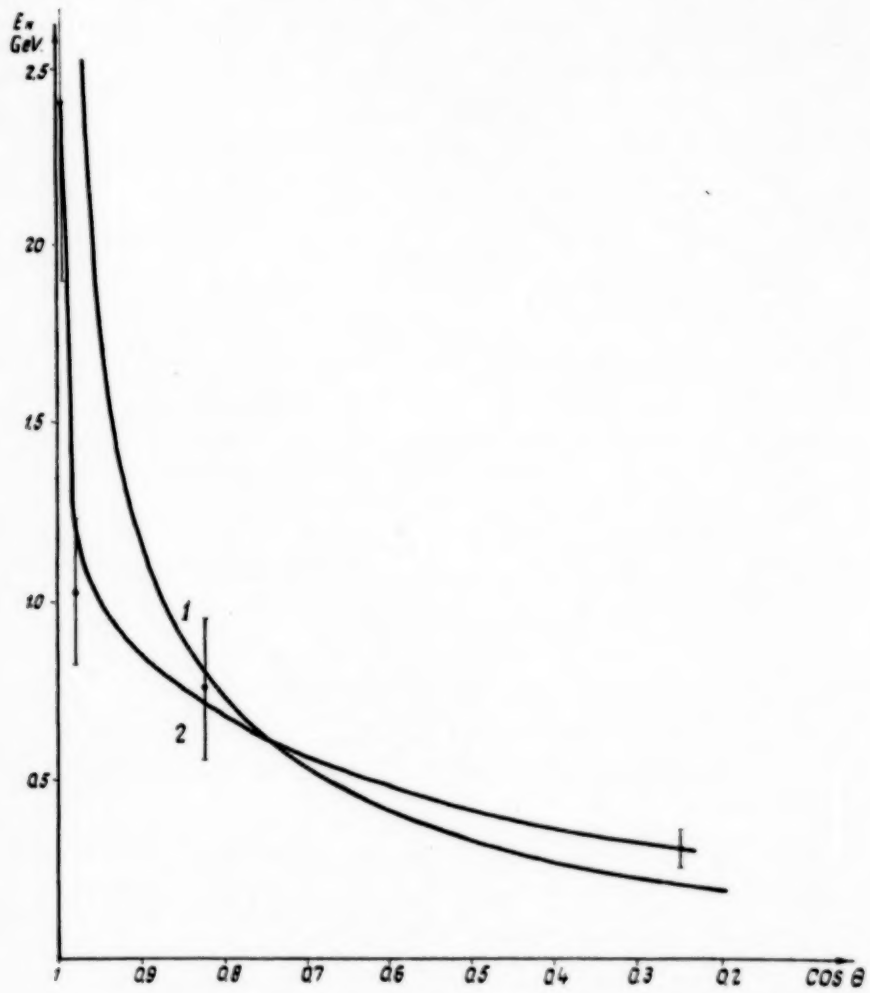

Fig. 5. Curve 2 represents the dependence of pion energy on the emission angle (mixture of nuclei). Curve 1 is a theoretical curve calculated from statistical theory for N—N collisions.

mated by multiple scattering measurements, and their masses were obtained from ionization losses (for more detail see Appendix). In the angular interval of 0—15° the mean energy of the protons was found to be 3 ± 0.5 GeV, while the ratio of the number of pions to the number of protons was ≈ 1, which corresponds to ≈ 0.5 proton per star. Then, the curve of the pion energy dependence

on the angle was obtained as plotted in fig. 5. Using this dependence and the angular distribution of s particles for the mixture of nuclei, and also taking into account the found fraction of protons, we obtained the mean total energy of mesons which, in the 0—30° angular interval, equals $\bar{E}_\pi = 1.3 \pm 0.25$ GeV (measurements were performed with chamber "B", see Appendix). The total energy averaged over all angles is $\bar{E}_\pi = 1.0 \pm 0.2$ GeV. Thus, the energy losses for meson production constitute 4.0 ± 0.8 GeV.

Together with the energy of nuclear disintegration the losses will be equal to 5.1 ± 0.8 GeV, i.e., 60 ± 10 %.

The number of collisions which the incident proton undergoes on the average in a light nucleus can be estimated from the measured values $\bar{n}_s = 3$ and $\bar{n}'_g = 2.8$ (including neutrons). It can be assumed that in the first collision the proton yields one g particle (0.5 proton and 0.5 neutron) and together with neutral mesons the total number of fast particles is

$$\bar{n}'_s = \tfrac{3}{2}(\bar{n}_{s,p} - 0.5) + 1 = 4.3,$$

where $\bar{n}_{s,p}$, the average number of s particles in proton-nucleon collisions, is [13]) equal to 2.7 (the coefficient $\frac{3}{2}$ takes into account the fraction of neutral pions). The number of secondary collisions will be

$$\frac{\bar{n}'_g - 1}{\bar{n}'_s} = 0.4.$$

Consequently, the primary proton on the average undergoes 1.4 collisions in a light nucleus. The number of collisions with Ag and Br nuclei, in accordance with the nucleus size, can be taken to be two times greater. Hence, on the average, the proton undergoes $\gtrsim 2$ collisions in the emulsion nucleus.

If the nucleon energy after one nucleon-nucleon collision is $E_1 = \xi E$, where E is the initial energy of the nucleon, then, after n collisions, the nucleon energy is $E_n = \xi^n E$. With $n = 2$, we obtain that the average energy loss in one nucleon-nucleon collision constitutes 35 ± 10 %.

The energy losses in nucleon-nucleon collisions can also be estimated in the following way. We have derived that the mean total energy of pions produced in collisions with nuclei is 1.0 ± 0.2 GeV. The experimental value $\bar{n}_s$ for p—p collisions was obtained in ref. [11, 12]). Considering that the mean pion energy in nucleon-nucleon collisions cannot be lower than in nucleon-nucleus collisions and that s particles contain ≈ 0.5 proton, we deduce that the energy loss in a nucleon-nucleon collision must be $\geqq 40 \pm 10$ %. Within the limits of experimental errors this value is not in contradiction with the theoretical one of 50 % obtained in statistical theory [12]). Peripheral collisions may slightly reduce this value.

It should be noted that in cosmic ray studies [9]) the average energy losses of a nucleon in collisions with air nuclei were found to be 30 ± 3 % in the 3—40 GeV

energy range. If the number of collisions in an average nucleus of the air is taken to be equal to 1.5, the energy losses for a single nucleon-nucleon collision must constitute 20 % of the primary particle energy.

The results obtained above, as well as the previously published data on nucleon interactions [12]) make it possible to offer some considerations pertaining to the size of the nucleon core.

The paper just mentioned [12]) reported some results on the nucleon-nucleon interactions at 9 GeV. It was shown that on the whole there is agreement with the statistical theory of multiple production [7]). However, there is a discrepancy in the region of small angles pointing to anisotropy in the centre of mass system. Similar experimental results were obtained by N. P. Bogachev *et al.* [11]). Further work [13]) established that only for stars with a small number of particles does anisotropy of angular distribution occur in the centre of mass system. The angular distribution of prongs in stars with a great multiplicity of particles may be considered isotropic within experimental errors.

In terms of a nucleon model consisting of a central core and peripheral meson cloud collisions with great multiplicity can be considered as core collisions. The statistical theory of multiple production is applicable for describing such collisions. As to the collisions with small multiplicity, they can be regarded as collisions of the core of one nucleon with the periphery of another, or as peripheral collisions of nucleons. Since the experimental number of s particles, their energy, angular distribution (with the exception of small angles) and the energy losses agree in the main with the statistical theory calculations, we are led to conclude that nucleon-nucleon collisions at $E \leqq 10$ GeV are for the most part collisions of their cores.

The optical analysis of proton-nucleon collisions in the 1—10 GeV energy range has shown that they occur with the greatest probability for an impact parameter

$$b = \lambda\!\!\!^{-}\sqrt{l(l+1)}$$

approximately equal to 0.6×10^{-13} cm. (There , $\lambda\!\!\!^{-}$ is $(2\pi)^{-1}$ times the wavelength in the centre of mass system, and l the corresponding angular momentum.) This can be seen from fig. 6, which represents the relative contribution to the cross-section of inelastic proton-proton collisions:

$$\Delta = \frac{\sigma_{\mathrm{in}}(b)}{\sigma_{\mathrm{in}}} = \frac{(2l+1)(1-\mathrm{e}^{-4\eta(l)})}{\sum_{l=0}^{\infty}(2l+1)(1-\mathrm{e}^{-4\eta(l)})},$$

due to interaction in the region b, $b+\lambda\!\!\!^{-}$, at energies $E = 1.5$, 4.4 and 10 GeV †, i.e. $\lambda\!\!\!^{-} = 0.24$, 0.14 and 0.091×10^{-13} cm.

† The values of absorption and refraction coefficients $K(r)$ and $U(r)$ are taken from ref. [6]). At 10 GeV, σ_{in} is assumed to be equal to 30×10^{-27} cm² in accordance with the results of ref.[14]).

If nucleon-nucleon collisions at 9 GeV are mainly collisions of the cores, we thus infer that the radius of a nucleon core r_c is $>\frac{1}{2}b$, i.e., $r_c > 0.3\times 10^{-13}$ cm, which agrees with the analysis of the electromagnetic size of the core [15]).

If one accepts that core collisions are most probable for the impact parameter $b \approx r_c$, then r_c is $\approx 0.6\times 10^{-13}$ cm. (The latter value gives the limit between large and small values of the absorption coefficient $K = K(r)$ [16]).) In this case the contribution of peripheral collisions constitutes ≈ 20 %. It should be noted that the anisotropy of angular distributions revealed by the experiments may

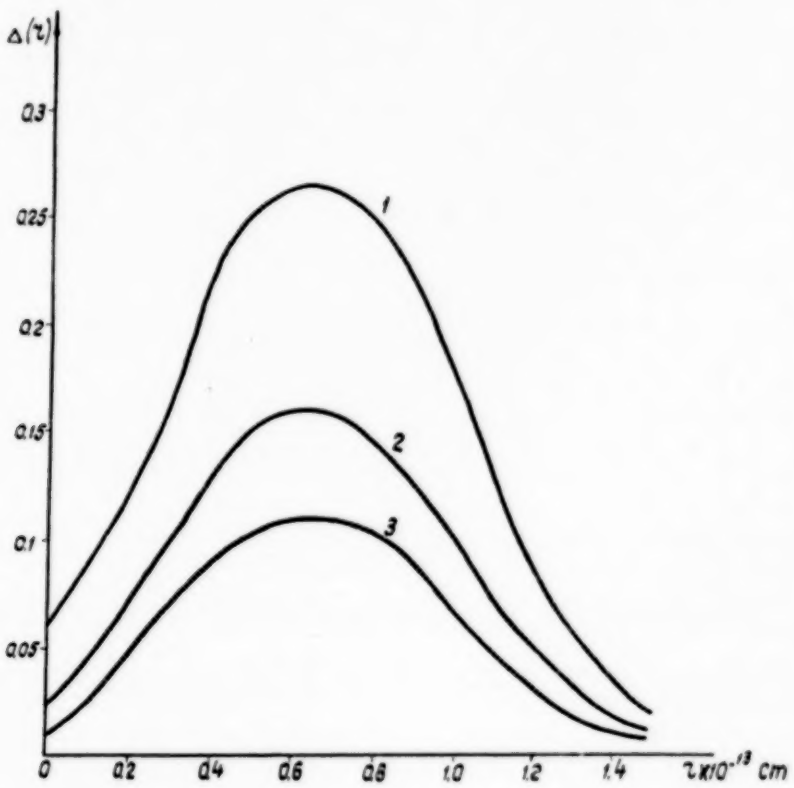

Fig. 6. Relative contribution to the cross-section of inelastic N—N collisions which is due to the interaction in the region $(b, b+\lambda\!\!\!^{-})$. The curves 2, 1, 3 describe the collisions at 1.5, 4.4, 10 GeV respectively (in the laboratory system).

in some part be due to the conservation of angular momentum. Both effects are being calculated at present.

The value of 80 % obtained in ref. [17]) for peripheral collisions was based on the unsound assumption that

$$\sigma_{\text{periph}} : \sigma_{\text{integral}} = \pi r_c^2 : \pi r_N^2, \qquad r_N \approx 10^{-13}\ \text{cm}$$

(cf. the graph $K = K(r)$ in ref. [16])), as well as on an inaccurate choice of the values of constants.

5. Production of Slow Strange Particles and Pions

In following up all prongs of the 100 stars found in track scanning not a single strange particle was registered. The systematic search for strange particles was carried out by area scanning. All the marked part (a circle 8.5 cm in diameter) of the 15 emulsion strips was twice scanned under the 200× magnification. The efficiency of single scanning was equal to 88 % for primary stars and 80 % for secondary stars. Altogether 2322 primary and 2361 secondary

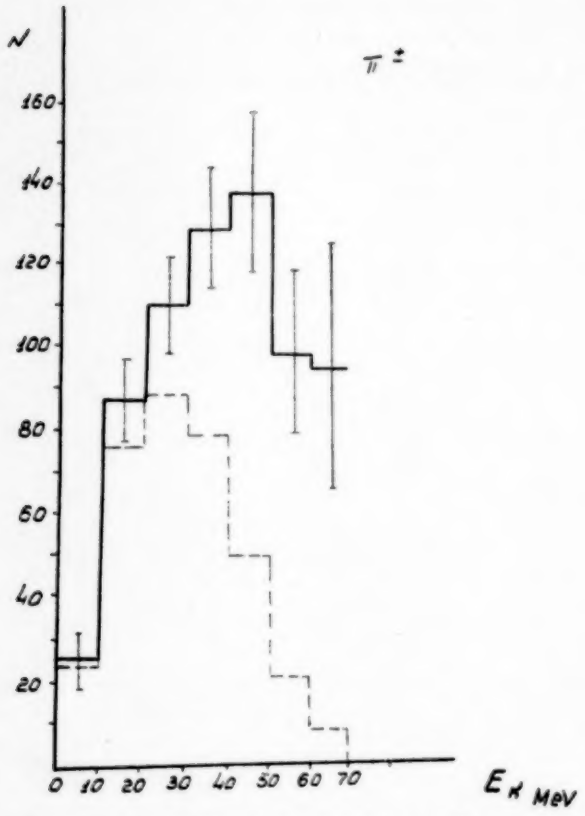

Fig. 7. Angular distribution of $\pi^{\pm}$ mesons. Solid curve includes geometrical corrections.

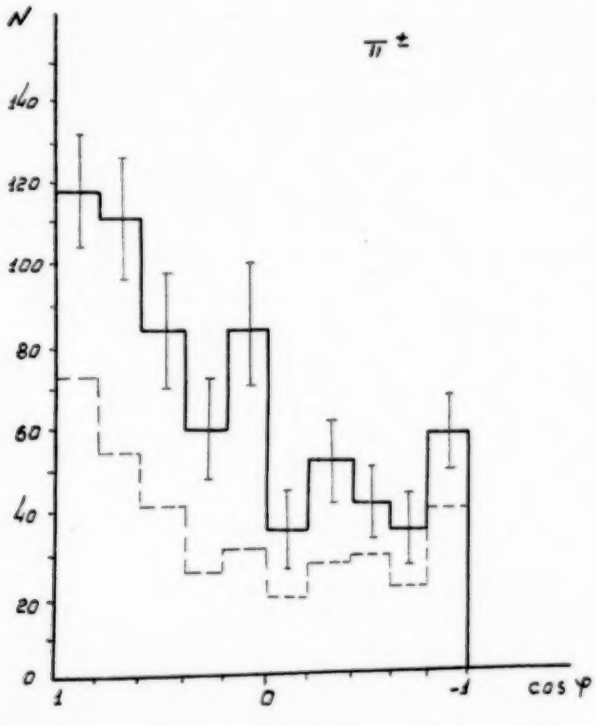

Fig. 8. Energy distribution of $\pi^{\pm}$ mesons. Solid curve includes geometrical corrections.

stars were found. In scanning 18 emulsions 387 stars and 386 $\pi^+ - \mu - e$ decays were detected. In following up these meson tracks it was discovered that 203 π^- and 146π^+ mesons were generated in the primary stars of the marked area of the chamber. Angular and energy distributions of these mesons proved to be similar. Their spectra were calculated with the corrections for the escapes due to the finite size of the chamber. These corrections were introduced by the method described in ref. [18]). Figs. 7 and 8 represent angular distributions of π^+ and π^- mesons and their energy spectrum with and without the geometrical corrections (solid and dotted lines respectively).

For the purpose of singling out strange particles all the two-prong events

were analysed. Identification was effected through the residual range and ionization by the method of blob and gap count. 32 strange particles were detected: 22 K^+ mesons, 1 K^-, 4$\Sigma^\pm$ hyperons and 5 Λ° particles. The values of their emission angles with respect to the beam and their kinetic energy are given in table 3. Only 18 parent stars were found for all strange particles (from among

TABLE 3

Summarized data on strange particles †

	Particle type	Parent star type $(n_g+n_b)+n_s$	Angle θ with respect to the proton beam	E_{kin} (MeV)	Q (MeV)	Remarks
1	K^+	8+4	150	84.9		
2	K^+	25+6	80	107		
3	K^+	15+5	0	10.7		
4	K^+	24+6	50	66		
5	K^+	12+6	43	54		
6	K^+	8+8	1	48		
7	K^+	16+2	95	22.6		
8	K^+	8+1	91	71		
9	K^+	5+2	47	44		
10	K^+	23+8	14	96		The parent star is outside the marked area
11	K^+	15+7	95	90		
12	K^+	14+3	102	38		
13	$\Sigma^\pm$	21+4				
14	$\Sigma^\pm$	10+1	6			
15	$\Sigma^\pm$	18+5	79	168		
16	Λ°	17+6	90	8	36.6	Found in area scanning and in following pion track; the range is 13.5 mm
17	Λ°	23+6	160	27	37.3	The range is 10.5 mm
18	Λ°	13+1	135	67	37.4	The range is 13 mm

† The table lists events which have parent stars.

them parent stars for 3 Λ° particles). For these stars $\bar{n}_g+\bar{n}_b = 15.6\pm4$, $n_s = 4.2\pm1.2$. These values exceed the average characteristics of stars found in track scanning. One event of simultaneous production of 2 strange particles was registered. Out of 22 K^+ mesons 12 were generated in primary stars and their mean energy equals 61 MeV. We shall now determine the cross-section of the K^+ production for this part of the spectrum. The efficienty of detecting the K^+ type events was estimated in the following way. All the two-prong events containing s and b or g particles (including K meson decays) were selected, the total number amounting to 57. Out of this number 37 relativistic particles are emitted in the interval of dip angles $0^\circ \leqq \alpha \leqq 36^\circ$ (0.59 of the total solid angle). If the angular distribution of these particles is isotropic 64.5 events ought to be observed, whence the relative efficiency over different dip angles is 0.88. A similar analysis of black prongs led to a relative efficiency of 0.90. It remains then to determine the detection efficiency for the events with the

black and relativistic prongs contained in the angular interval $0^0 \leqq \alpha \leqq 36°$. This efficiency was obtained by independent double scanning of one and the same emulsion area and was found to be 0.85.

The average density of the proton flux was equal to $(3.1 \pm 0.3) \times 10^3$ cm^2. The number of nuclei in one cm^3 of the emulsion is 7.83×10^{22}. Thus, the production cross-section for K^+ mesons with energy up to 140 MeV, on the average emulsion nucleus, corresponds to (5 ± 2)mb (with geometrical corrections). The angular distribution of the 12 K^+ mesons (also with geometrical correc-

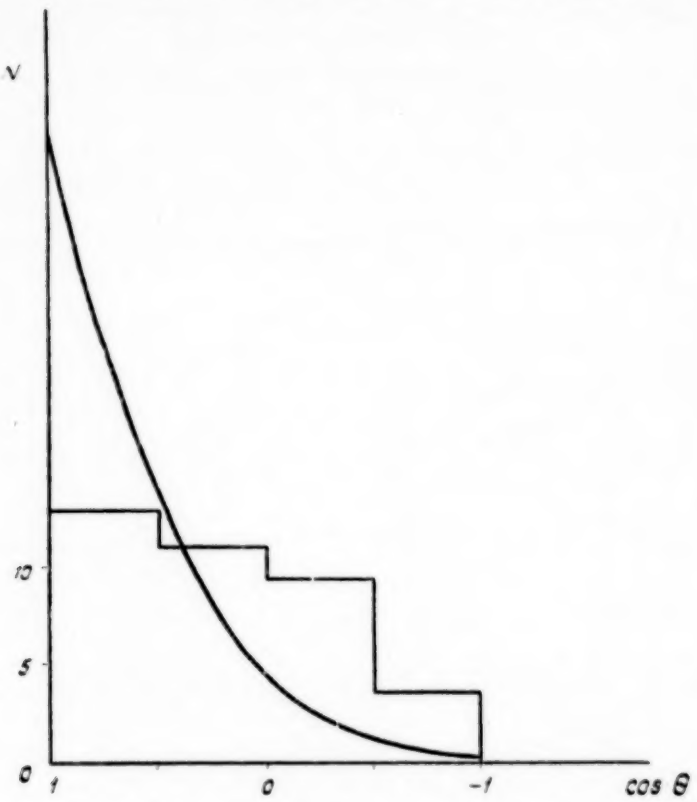

Fig. 9. Angular distribution of K^+ mesons produced in N—N collisions. The curve is calculated from the statistical theory.

tions) is given in fig. 9. The statistical theory curve for the angular distribution of K mesons produced in p—p collisions is plotted in the same figure. Comparison of the experimental and theoretical curves reveals a large discrepancy, which is difficult to explain only by K meson scattering in nuclei.

Indeed, in the energy interval up to 300 MeV the mean free path of K mesons in nuclear matter is 11×10^{-13} cm [19]). If we assume that the majority of K mesons was produced on heavy emulsion nuclei, and take their range to be of the order of the nuclear radius $1.2A^{\frac{1}{3}} \times 10^{-13}$ cm, we obtain that the number of interactions within the nucleus will be $< 1.2\sqrt[3]{94/11} \approx 0.5$ i.e., much less than for π mesons.

The combination of such facts as the high value of the production cross-

section, wide angular distribution and large size of parent stars support the inference that the greater part of strange particles is produced in the intranuclear cascade process, which is quite probable in view of the value ≈ 1 GeV for the mean energy of mesons. A similar conclusion was reached by C. Besson *et al.*[20]) who investigated the production of strange particles by π^- mesons at 4.3 GeV.

In conclusion the authors wish to thank G. Beznogikh, Z. Kuznetsova, N. Metkina, M. Prisnolova and V. Vaksina who were very helpful in scanning and also to acknowledge the aid in analysis by L. Popova. They would also like to express their gratitude to the Zeiss company, Jena, German Democratic Republic, which has manufactured a first-rate measuring microscope for nuclear research, to professor K. Rambush who was very helpful in making this microsope available to the Joint Institute and in particular to H. Bayer, H. Schüler and M. Sost who were in charge of the delivery and installation.

Appendix

MOMENTUM DETERMINATION FOR STRANGE PARTICLES BY MULTIPLE SCATTERING MEASUREMENTS

The following microscopes were used: MB1—8 with a modernized stage and a noise background $\approx 0.03\mu$ for a 2000μ cell; KSM-Karl Zeiss Jena with noises $\approx 0.008\mu$ for a 2000μ cell; Koristka with noises $\approx 0.02\mu$ for a 2000μ cell. Measurements were performed on two emulsion chambers: chamber "A" whose pellicles were processed in a free state, and chamber "B" whose emulsion strips were stuck to the plates before processing.

The average distortion level and quasi-scattering were evaluated by direct measurements of proton beam tracks. The value 1.5μ on a 1000μ cell was obtained for chamber "A" and 0.65μ on a 2000μ cell for chamber "B".

A rough estimate of the secondary particles energy made from their interaction with emulsion nuclei allowed us to infer that all the strange particles with θ angles $> 30°$ are comparatively slow. Therefore, chamber "A" despite great distortions proved to be suitable for scattering measurements of particles with θ angles $> 30°$.

For these particles the cell length was chosen in such a way that the ratio of the measurement signal to the distortion signal equalled 3 or more and there was no need to introduce corrections for distortion. The momentum of these particles was calculated from the formula

$$|D| = \frac{At^{\frac{3}{2}}}{p\beta c} \qquad (1)$$

where $A = 50.6$ for a scattering constant $K = 29$, and t is the cell length in units of 100μ.

TABLE 4

Results of energy measurements of secondary particles on chamber "B"

No.	Space angles θ°	Identification	$E \pm \Delta E$ (MeV)
1	1.9°	proton	$5.3^{+4.3}_{-1.5}$
2	5.9°	proton	$2.1^{+1.2}_{-0.5}$
3	1.5°	proton	$4.7^{+4.5}_{-1.4}$
4	3°	proton	$5.4^{+4.6}_{-1.7}$
5	1.3°	π-meson	$3.6^{+0.7}_{-0.5}$
6	4.5°	proton	$3.2^{+1.6}_{-0.9}$
7	10.3°	proton	$1.9^{+1.0}_{-0.5}$
8	1.3°	π-meson	$3.5^{+1.0}_{-0.5}$
9	7.6°	proton	$3.1^{+1.4}_{-0.9}$
10	3.1°	proton	$3.1^{+1.4}_{-0.9}$
11	0.6°	proton	$3.2^{+0.8}_{-0.6}$
12	1.4°	proton	8
13	10°	probably proton	$5.7^{+2.9}_{-1.5}$
14	1.5°	π-meson	$5.4^{+2.5}_{-1.3}$
15	5°	proton	$7.6^{+14}_{-3.4}$
16	8.1°	proton	$3.5^{+1.2}_{-0.8}$
17	4.4°	π-meson	$2.9^{+0.7}_{-0.5}$
18	4.3°	π-meson	$1.3^{+0.4}_{-0.2}$
19	14.1°	π-meson	$0.86^{+2.0}_{-0.2}$
20	12.4°	π-meson	$0.63^{+0.17}_{-0.14}$
21	6.4°	probably π-meson	$2.1^{+0.5}_{-0.4}$
22	4.8°	proton	$2.0^{+1.0}_{-0.6}$
23	2.4°	proton	$0.52^{+0.16}_{-0.07}$
24	9.7°	π-meson	$0.22^{+0.06}_{-0.03}$
25	22°	probably π-meson	$1.9^{+0.6}_{-0.4}$
26	13.1°	proton	$1.0^{+0.4}_{-0.2}$
27	14.8°	proton	$1.3^{+0.5}_{-0.3}$
28	11°	π-meson	$0.71^{+0.24}_{-0.11}$
29	30°	probably π-meson	$2.2^{+0.9}_{-0.6}$
30	2.2°	π-meson	$1.3^{+0.3}_{-0.2}$
31	9.7°	π-meson	$2.8^{+1.3}_{-0.7}$
32	9.5°	probably π-meson	$1.8^{+0.6}_{-0.4}$
33	11.8°	π-meson	$0.69^{+0.17}_{-0.09}$
34	29.8°	π-meson	$2.5^{+1.1}_{-0.7}$
35	18.8°	π-meson	$0.15^{+0.03}_{-0.03}$
36	5.9°	proton	$0.51^{+0.18}_{-0.06}$
37	9.7°	probably proton	$1.6^{+0.9}_{-0.4}$

TABLE 4
(continued)

No.	Space angles $\theta°$	Identification	$E^{+}_{-}\Delta E$ (MeV)
38	16.6°	π-meson	$0.88^{+0.17}_{-0.13}$
39	5.3°	π-meson	$1.3^{+0.3}_{-0.2}$
40	15.3°	π-meson	$0.54^{+0.14}_{-0.09}$
41	2.5°	proton	$2.3^{+1.5}_{-0.7}$
42	11.8°	probably proton	$1.1^{+0.5}_{-0.3}$
43	1.6°	probably proton	$1.4^{+0.5}_{-0.3}$
44	2°	probably π-meson	$1.9^{+0.5}_{-0.3}$
45	4°	probably proton	$1.9^{+0.6}_{-0.4}$
46	0.9°	π-meson	$1.4^{+0.3}_{-0.2}$
47	1.1°	proton	$1.1^{+0.3}_{-0.2}$
48	4.2°	π-meson	$0.4^{+0.07}_{-0.05}$
49	13.3°	π-meson	$0.71^{+0.13}_{-0.09}$
50	5.5°	proton	$2.3^{+0.8}_{-0.5}$

Tracks with flat θ angles $< 30°$ were measured on stack "B". Here the particles were divided into two groups: $p\beta c < 2$ GeV and $p\beta c\ 2 > 2$ GeV. The momenta of particles with $p\beta c < 2$ GeV were calculated from formula (1), quasi-scattering was eliminated through the formula

$$\bar{D}^2_{\text{Coul}} = \bar{D}^2_{\text{meas}} - \bar{D}^2_{\text{quasi}}; \tag{2}$$

$\bar{D}_{\text{quasi}}$ was averaged over all emulsion strips in which the measurements were made.

For particles with $p\beta c > 2$ GeV noises and distortions were eliminated through the formula [21, 22])

$$|\bar{D}|_{\text{Coul+quasi}} = 0.715\sqrt{\bar{D}_i{}^2 + \bar{D}_i\bar{D}_{i+1} - 2\bar{D}_i\bar{D}_{i+2}} \tag{3}$$

and quasi scattering through formula (2). Quasi-scattering was measured on beam particles all along a secondary track, i.e., along five-or six-beam tracks.

All the measurement results are summarized in table 4.

ERRORS

The total error in momentum measurements was respectively made up of the statistical error of direct measurements ($\Delta = 0.86/\sqrt{n}$ in accordance with ref.[1])) and of the error due to the elimination of quasi-scattering.

In determining the nature of secondary particles a blob count method was additionally used. The results are plotted in fig. 10.

The a—a′ lines mark an area in which protons cannot be separated from pions by their ionization. This area contains 9 particles. We roughly estimated

that half of them are protons because in the neighbouring areas the ratio of protons to pions is of the order of a unity.

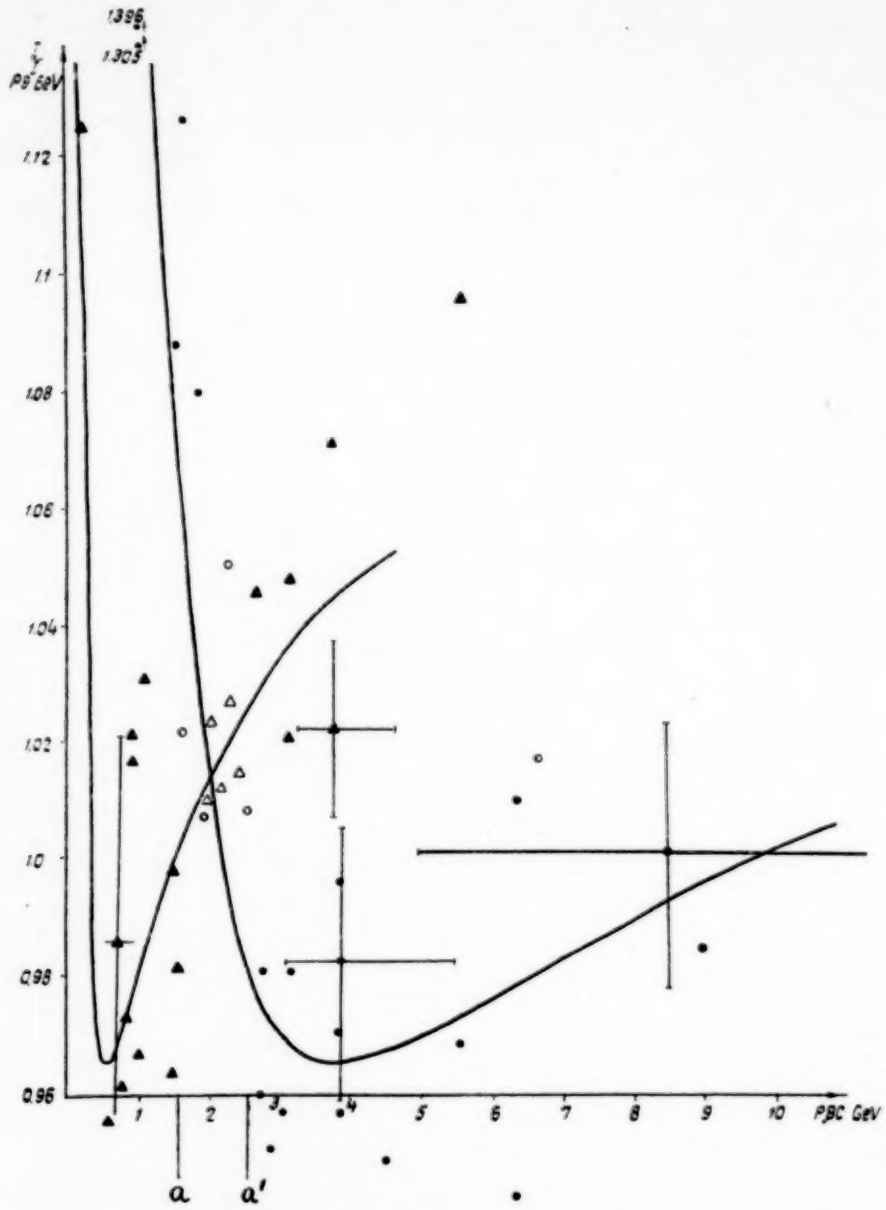

Fig. 10. The momentum versus ionization curves for protons and π^- mesons (on the basis of Barkas' tables) and the experimental data on s particles.
● — proton, ○ — probably proton; ▲ — π meson, △ — probably π meson.

Further, it turned out that among the identifiable particles all protons have angles $\leqq 15°$, therefore the particles with angles $> 15°$ in the a—a′ area were transferred from the proton group to the meson group †.

† It should be noted that the procedure of particle identification in the a—a′ area does not practically affect the obtained value of mean energy, because the energy values in this area are close to the mean energy.

References

1) N. P. Bogachov *et al.*, Atom. Energ. **4** (1958) 281;
W. R. Johnson, Phys. Rev. **99** (1955) 1049
2) V. Beliakov *et al.*, Annual International Conference on High Energy Physics at CERN (1958) p. **309**
3) E. L. Feinber, JETP **28** (1955) 241; Usp. Fiz. Nauk **58** (1956) 193
4) I. A. Ivanovskaya and D. S. Chernavsky, Nuclear Physics **4** (1957) 29
5) E. L. Grigoriev and L. P. Solovyova, JETP **31** (1956) 932
6) V. S. Barashenkov and Huan Nian Nin, JETP (in press)
7) V. S. Barashenkov, B. M. Barbashov and E. G. Bubelev, Nuovo Cimento **7**, Suppl. 1 (1958)117
8) W. O. Zock, P. V. Murch and R. M. Keague, Proc. Roy. Soc. **231** (1955) 368
9) N. L. Grigorov, Usp. Fiz. Nauk **58** (1956) 599
10) W. D. Walker and J. Crussard, Phys. Rev. **98** (1955) 1416;
J. E. Crew and R. D. Hill, Phys. Rev. **110** (1958) 177;
M. Blan and A. R. Oliver, Phys. Rev. **102** (1956) 489
11) N. P. Bogachev, S. A. Buniatov, Y. P. Merekov and V. M. Sidorov, Dokl. Akad. Nauk SSSR **121** (1958) 617
12) V. S. Barashenkov *et al.*, Nuclear Physics **9** (1958) 74
13) N. P. Bogachev *et al.*, private communication
14) V. S. Barashenkov and Huan Nian Nin, JETP **36** (1959) 1319
15) D. I. Blokhintsev, V. S. Barashenkov and B. M. Barbashov, Usp. Fiz. Nauk (in press)
16) D. I. Blokhintsev, V. S. Barashenkov and V. G. Grishin, Nuovo Cimento **9** (1958) 249; V. G. Grishin, JETP **35** (1958) 50
17) E. G. Bubelev, JETP **33** (1957) 539
18) V. V. Alpers *et al.*, JETP **30** (1956) 1025
19) M. F. Kaplon, Annual International Conference on High Energy Physics at CERN (1958) p. **173**
20) C. Besson *et al.*, Nuovo Cimento **6** (1957) 1168
21) B. d'Espagnat, J. Phys. et le Radium **13** (1952) 74; Comptes Rendus **232** (1951) 800
22) A. G. Ekspong, Arkiv för Fysik **9** (1955) 49

8.B

Nuclear Physics **14** (1959/60) 540—544; © *North-Holland Publishing Co., Amsterdam*

Not to be reproduced by photoprint or microfilm without written permission from the publisher

ON EXCITATION OF NUCLEI BY μ-MESONS

D. F. ZARETSKY and V. M. NOVIKOV

Atomic Energy Institute, USSR, *Academy of Sciences*

Received 27 May 1959

Abstract: Excitation of heavy nuclei in μ-mesic atom 2p—1s transitions is considered. The effect is connected with the electromagnetic interaction between the meson and nucleus. The ratio of the probability of emission of a γ-quantum during the indicated transition to the probability of transfer of all the transition energy to the nucleus with subsequent dissipation of the energy through nuclear channels is computed. The case is considered when the distance between the nuclear levels is much greater than the width of the levels for the indicated excitation energy.

1. Introduction

The last phase of capture of μ-meson onto atomic shells is the transition from the 2p to the 1s state [1]). It has been shown in ref.[2]) that in such elements as uranium or thorium this transition may be accompanied by radiationless excitation of the nucleus. In this case the 2p—1s transition energy is directly imparted to the nucleus. The excited nucleus can then disintegrate by various nuclear channels. For the nuclei indicated above the energy of the 2p—1s transition is 6.3 MeV. An excitation energy of this magnitude is sufficient for emission of a neutron, radiation of a γ-quantum or fission of the nucleus. Moreover, under certain conditions, the energy can be transferred back to the μ-meson which then returns to the 2p-state and the nucleus to the ground state. This inverse transition is appreciable for $\rho\Gamma_n \ll 1$ where ρ is the nuclear level density corresponding to the transition energy and Γ_n the total nuclear width. The results of ref.[2]) are valid for $\rho\Gamma_n \gg 1$, i.e. when the inverse transition can be neglected. In this limiting case the ratio of the probability W_γ for γ-quantum emission by the μ-meson in a 2p—1s transition to the probability W_n of energy dissipation through nuclear channels is

$$\frac{W_\gamma}{W_n} = \frac{\Gamma_\gamma}{\Gamma_{r.l.}} \tag{1}$$

where Γ_γ is the radiation width for γ-quanta produced by the meson and

$$\Gamma_{r.l.} = 2\pi|V_{2p-1s}|^2\rho,$$

where V_{2p-1s} is the matrix element for a 2p—1s meson transition involving excitation of the nucleus with an energy equal to that of the 2p—1s transition.

The ratio W_γ/W_n is computed in the present paper for the case when $\rho\Gamma_n \ll 1$. The calculations are carried out under the assumption that $\Gamma_{r.l.} \gg \Gamma_\gamma$. For example, according to ref.[2]), for U^{238} the ratio $\Gamma_{r.l.}/\Gamma_\gamma \approx 10$.

2. Theory

Consider a conservative system consisting of a meson and a nucleus. This means that all processes leading to dissipation of energy of the system are neglected in a first approximation. The calculation will be performed in the non-relativistic approximation. The wave function for the meson-nucleus system can then be written in the form

$$\varphi(t) = C_{op}(t)\psi_0 U_p e^{-\frac{i}{\hbar}E_p t} + \sum_c C_{cs}(t)\psi_c U_s e^{-\frac{i}{\hbar}E_c t} \tag{2}$$

where ψ_0 and ψ_c are respectively the nuclear wave functions of the ground state and of an excited state of energy E_c; U_p and U_s are correspondingly the 2p and 1s meson wave functions E_p is the energy of a system in a state with a wave function $\psi_0 U_p$. The initial condition can be formulated in the form

$$\varphi(0) = \psi_0 U_p. \tag{3}$$

The Hamiltonian of the meson+nucleus system is

$$\mathscr{H} = H + H_\mu + V, \tag{4}$$

where H is the Hamiltonian of the nucleus and $H_\mu = T_\mu + V_\mu$, T_μ being the kinetic energy operator of the meson and

$$V_\mu = -\left\langle \psi_0 \left| \sum_{i=1}^{z} \frac{e^2}{|\mathbf{r}_i - \mathbf{r}_\mu|} \right| \psi_0 \right\rangle \tag{5}$$

(summation is carried out over all protons in the nucleus). Furthermore,

$$V = \left\langle \psi_0 \left| \sum_{i=1}^{z} \frac{e^2}{|\mathbf{r}_i - \mathbf{r}_\mu|} \right| \psi_0 \right\rangle - \sum_{i=1}^{z} \frac{e^2}{|\mathbf{r}_i - \mathbf{r}_\mu|}. \tag{6}$$

From the Schroedinger equation we find

$$\begin{aligned} i\hbar\dot{C}_{op} &= \sum_c V_c e^{\frac{i}{\hbar}(E_p - E_c)t} C_{cs}, \\ i\hbar\dot{C}_{cs} &= V_c^* e^{\frac{i}{\hbar}(E_c - E_p)t} C_{op}, \end{aligned} \tag{7}$$

where

$$V_c = \langle \psi_0 U_p | V | \psi_c U_s \rangle.$$

Solutions of eq. (7) with the initial condition (3) leads to the expressions (see, e.g. ref.[3]))

$$C_{\mathrm{op}}(t) = -\frac{1}{2\pi i}\int_{-\infty}^{+\infty} \mathrm{d}E \, \frac{\mathrm{e}^{\frac{i}{\hbar}(E_{\mathrm{p}}-E)t}}{E-E_{\mathrm{p}}+\frac{1}{2}i\hbar\Gamma(E)} \tag{8}$$

$$C_{\mathrm{cs}}(t) = -\frac{1}{2\pi i}\int_{-\infty}^{+\infty} \mathrm{d}E \, \frac{V_{\mathrm{c}}^*}{E-E_{\mathrm{p}}+\frac{1}{2}i\hbar\Gamma(E)} \cdot \frac{\mathrm{e}^{\frac{i}{\hbar}(E_{\mathrm{c}}-E)t}-1}{E_{\mathrm{c}}-E} \tag{9}$$

$$-\tfrac{1}{2}i\hbar\Gamma(E) = \sum_{\mathrm{c}} |V_{\mathrm{c}}|^2 \zeta(E-E_{\mathrm{c}}), \quad \zeta(x) = \lim_{\sigma\to+0} \frac{1}{x+i\sigma}.$$

In order to evaluate the integral (8) we close the integration contour in the lower half-plane. Then

$$C_{\mathrm{op}}(t) = \sum_{k} \frac{\mathrm{e}^{-\frac{i}{\hbar}(E_k-E_{\mathrm{p}})t}}{1+\sum_{\mathrm{c}} \frac{|V_{\mathrm{c}}|^2}{(E_k-E_{\mathrm{c}})^2}} \tag{10}$$

where the E_k are roots of the equation

$$E-E_{\mathrm{p}}-\sum_{\mathrm{c}} \frac{|V_{\mathrm{c}}|^2}{E-E_{\mathrm{c}}+i\sigma} = 0. \tag{11}$$

The sums over c in (10) and (11) are evaluated in the appendix. In calculating the sums it has been assumed that the nuclear levels are equidistant and the quantity $|V_{\mathrm{c}}|^2$ constant in the energy interval $\Delta E = |E_{\mathrm{c}}-E_{\mathrm{p}}| \approx \Gamma_{\mathrm{r.l.}}$. After the summation, the following relation between the sums over c in (10) and (11) has been obtained:

$$\sum_{\mathrm{c}} \frac{|V_{\mathrm{c}}|^2}{(E_k-E_{\mathrm{c}})^2} = \frac{1}{|V_k|^2}\left[\pi^2\rho^2|V_k|^4 + \left(\sum_{\mathrm{c}} \frac{|V_{\mathrm{c}}|^2}{E_k-E_{\mathrm{c}}}\right)^2\right]. \tag{12}$$

Combining (10), (11) and (12) we get

$$C_{\mathrm{op}}(t) = \sum_{k} \frac{|V_k|^2}{|V_k|^2+\pi^2\rho^2|V_k|^4+(E_k-E_{\mathrm{p}})^2} \mathrm{e}^{\frac{i}{\hbar}(E_k-E_{\mathrm{p}})t} \tag{13}$$

It can easily be shown that if $\rho\Gamma_{\mathrm{r.l.}} \gg 1$ the roots E_k of eq. (11) are equidistant and the distance between them is $1/\rho$. In this case we have

$$C_{\mathrm{op}}(t) = \sum_{k=-\infty}^{\infty} \frac{|V_k|^2}{\left(E_{k_0}-E_{\mathrm{p}}+\frac{k}{\rho}\right)^2+\pi^2\rho^2|V_k|^4} \mathrm{e}^{-\frac{i}{\hbar}\left(E_{k_0}-E_{\mathrm{p}}+\frac{k}{\rho}\right)t} \tag{14}$$

where E_{k_0} is the root closest to E_p. Evidently $|E_{k_0}-E_p| < 1/\rho$. No large error will be introduced by assuming $\rho\Gamma_{r.l.} \gg 1$ if $|E_{k_0}-E_p| = 1/\rho$. Taking account of the assumptions previously made we obtain

$$C_{op}(t) = \sum_{k=-\infty}^{\infty} \frac{\rho^2|V_{2p-1s}|^2}{k^2+\pi^2\rho^4|V_{2p-1s}|^4} e^{-\frac{i}{\hbar}\frac{k}{\rho}t}. \tag{15}$$

It can be seen from (15) that $C_{op}(t)$ is a periodic function with a period $T = 2\pi\rho\hbar$. The sum of series (15) can be evaluated in the interval $0 < t < T$. The result is

$$|C_{op}(t)|^2 = \frac{\mathrm{ch}^2\left(\frac{\Gamma_{r.l.}t}{2\hbar} - \frac{1}{2}\pi\rho\Gamma_{r.l.}\right)}{\mathrm{sh}^2\frac{1}{2}\pi\rho\Gamma_{r.l.}}. \tag{16}$$

In the following we shall need the mean value

$$\overline{|C_{op}(t)|^2} = \frac{1}{T}\int_0^T |C_{op}(t)|^2 dt = \frac{1}{\pi\rho\Gamma_{r.l.}} + O\left(\frac{1}{\rho^2\Gamma_{r.l.}^2}\right). \tag{17}$$

Within the limits of our problem we obtain for the ratio of interest to us

$$\frac{W_\gamma}{W_n} = \frac{\overline{|C_{op}(t)|^2}\Gamma_\gamma}{\sum_c \overline{|C_{cs}(t)|^2}\Gamma_n} = \frac{\Gamma_\gamma}{\Gamma_{r.l.}}\frac{1}{\pi\rho\Gamma_n}. \tag{18}$$

Of all quantities entering (18) only Γ_γ and $\Gamma_{r.l.}$ can be computed provided that the cross section for photo-excitation on the given nucleus is known for an energy equal to the transition energy E_p. As mentioned above, for U^{238} one has $\Gamma_\gamma/\Gamma_{r.l.} \approx 1/10$. Knowing this ratio and having determined experimentally W_γ/W_n. We can estimate the magnitude of the very interesting quantity $\rho\Gamma_n$.

As an example, the following experiment for determination of the indicated ratio can be suggested. The yields of 2p—1s transition γ-quanta during irradiation of lead and uranium by μ-mesons are compared. In the first case $W_\gamma/W_n = \infty$. Thus, for γ-quanta emitted in the indicated transition the decrease of the yield of γ-quanta per meson stopped in uranium gives the fraction of transitions which occur with energy dissipation through nuclear channels.

Appendix

Let the nuclear levels be denoted as in fig. 1; E_{c_0} is the level closest to

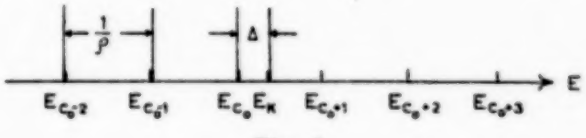

Fig. 1.

$E_k (E_k \neq E_c)$, and $\Delta = E_k - E_{c_0}$. Then

$$\sum_{\mathfrak{c}} \frac{|V_{\mathfrak{c}}|^2}{E_k - E_{\mathfrak{c}}} = \frac{|V_{\mathfrak{c}_0}|^2}{\Delta} + \frac{|V_{\mathfrak{c}_0-1}|^2}{\Delta + \frac{1}{\rho}} + \ldots + \frac{|V_{\mathfrak{c}_0-m}|^2}{\Delta + \frac{m}{\rho}} + \ldots + \frac{|V_{\mathfrak{c}_0+1}|^2}{\Delta - \frac{1}{\rho}} + \ldots + \frac{|V_{\mathfrak{c}_0+m}|^2}{\Delta - \frac{m}{\rho}}. \quad (19)$$

Suppose that the quantity $|V_{\mathfrak{c}}|^2$ is constant in the interval $|E_{\mathfrak{c}} - E_{\mathfrak{c}_0}|^2 \approx \rho |V_{\mathfrak{c}_0}|^2$, which is the characteristic energy interval for our problem. Then, combining the terms corresponding to $E_{\mathfrak{c}_0+m}$ and $E_{\mathfrak{c}_0-m}$ in (19) and extending the sum to infinitely large values of m, we get

$$\sum_{\mathfrak{c}} \frac{|V_{\mathfrak{c}}|^2}{E_k - E_{\mathfrak{c}}} = \rho |V_k|^2 \left\{ \frac{1}{\rho\Delta} - 2\rho\Delta \sum_{m=1}^{\infty} \frac{1}{m^2 - (\rho\Delta)^2} \right\} = \rho |V_k|^2 \pi \operatorname{ctg} \pi\rho\Delta \quad (20)$$

where

$$|V_k|^2 = |V_{\mathfrak{c}_0}|^2.$$

Similarly, we calculate

$$\sum_{\mathfrak{c}} \frac{|V_{\mathfrak{c}}|^2}{(E_k - E_{\mathfrak{c}})^2} = \rho^2 |V_k|^2 \left\{ \frac{1}{(\rho\Delta)^2} + 2 \sum_{m=1}^{\infty} \frac{m^2 + (\rho\Delta)^2}{[m^2 - (\rho\Delta)^2]^2} \right\} = \rho^2 |V_k|^2 \frac{\pi^2}{\sin^2 \pi\rho\Delta}. \quad (21)$$

Eliminating Δ from (20) and (21) we obtain (12).

Note added in proof: Recently the excitation of the uranium nuclei in 2p—1s μ-meson transition was observed by B. Pontecorvo *et al.* in Dubna. The results were presented at the Kiev Conference on High Energy Physics.

References

1) V. L. Fitch and J. Rainwater, Phys. Rev. **92** (1953) 789
2) D. F. Zaretsky, Report at 2nd Geneva Conference on Peaceful Uses of Nuclear Energy
3) W. Heitler, The quantum theory of radiation

8.A

Nuclear Physics **14** (1959/60) 545—564; © *North-Holland Publishing Co., Amsterdam*

Not to be reproduced by photoprint or microfilm without written permission from the publisher

CONTRIBUTION A L'ÉTUDE DE L'ANNIHILATION DES ANTIPROTONS DANS LES NOYAUX COMPLEXES

A. BERTHELOT, C. CHOQUET, A. DAUDIN, O. GOUSSU et F. LÉVY

Centre d'Études Nucléaires de Saclay, Gif-sur-Yvette (S & O)

Reçu le 4 août 1959

Abstract: 207 stars resulting from $\tilde{p}$ annihilation have been analyzed in the present paper. Results are given concerning the mean free path for annihilation as well as the main characteristics of annihilation stars.

The proportion of stars which are effectively accompanied by at least *one* visible K meson is (4.6 ± 0.5) % in the present work. The error quoted does not take into account the statistical uncertainty.

The average numbers are finally compared to the last Berkeley results.

1. Introduction

Depuis la découverte des antiprotons [1–4]), leurs propriétés et leurs interactions ont fait l'objet d'un grand nombre de travaux dont la plupart ont été effectués à Berkeley.

Il a paru nécessaire d'étudier d'abord les sections efficaces d'interaction dans l'hydrogène. Ce problème a été exploré par les techniques de compteurs qui, utilisant des cibles variées (eau ordinaire, eau lourde, hydrogène liquide) dans la bande de 0 à 700 MeV, ont permis de mesurer les sections efficaces de diffusion et d'annihilation [5–8]).

Parallèlement, les groupes d'émulsions photographiques ont recherché les sections efficaces sur les noyaux complexes [9–10]); ce sont eux qui, les premiers, ont étudié le phénomène d'annihilation. Leurs résultats concernant l'émission de mésons π dans ce processus, leur multiplicité, leur énergie moyenne, ont été récemment confirmés par les premiers résultats obtenus par les groupes de chambres à bulles: chambre à hydrogène [11]), chambre à propane [11]).

Cependant, les statistiques dans ce domaine sont encore si pauvres, si longues à accumuler qu'il paraît nécessaire de conjuguer tous les efforts. Certains problèmes nécessitent encore une attention particulière: le spectre d'énergie des mésons π émis, la création de particules étranges dans l'annihilation. Ce dernier phénomène est si rare qu'il faudra sans doute une longue accumulation de résultats avant d'en tirer des conclusions évidentes et interprétables en ce qui concerne à la fois la fréquence d'émission de ces particules, leur énergie à l'émission, le rapport π^+/π^-, le rapport K^+/K^-, etc.

Le présent travail se situe dans ce cadre.

2. Matériel Expérimental

Un empilement de 130 feuilles d'émulsion K_5 de 15×20 cm^2 a été exposé en février 1958 au faisceau d'antiprotons du bévatron de Berkeley. Les émulsions K_5 ont été choisies à cause de la petitesse des grains d'argent permettant de meilleures possibilités de suivage. Afin de préserver la sensibilité des émulsions et éviter le fading, le paquet a été emballé, à l'aller comme au retour, dans la neige carbonique [12]).

Le faisceau d'antiprotons utilisé était un faisceau séparé au moyen de trois analyseurs magnétiques et deux absorbants. La valeur nominale de l'impulsion à l'entrée dans l'empilement était 740 MeV/c, ce qui correspond, pour les antiprotons, à une énergie de 255 MeV.

Pendant la durée de l'irradiation (11.5 h), 2.15×10^{14} protons sont tombés sur la cible, ce qui correspond, dans les émulsions, à 4.7 ± 0.4 antiprotons par cm^2 de surface exposée.

Après l'exposition, une trame a été photographiée sur chaque émulsion dans le but de faciliter le suivage des traces. Cette trame imprimée à Berkeley par une méthode publiée antérieurement [13]) permet de passer très facilement d'une émulsion à la suivante. La précision du marquage étudiée pour des traces plongeantes, sur plusieurs plaques de l'empilement, est de 30μ.

Le collage des émulsions sur verre, de même que le développement ont été effectués au C.E.N. de Saclay par une méthode publiée antérieurement [14]).

Les résultats exposés dans le présent article correspondent seulement à l'exploitation d'une partie de l'empilement (47 plaques) et sont limités, dans leur ensemble, à l'étude du phénomène d'annihilation.

3. Critères d'Identification des Antiprotons

3.1. CRITÈRES A L'ENTRÉE

Le dépouillement a été effectué par détection des traces à 7 mm de l'entrée dans la plaque et suivage de celles qui ont été identifiées comme traces d'antiprotons. D'après la valeur nominale indiquée plus haut, l'énergie à ce point est de 246 MeV. Ceci correspond, pour le parcours résiduel et l'impulsion, à des valeurs $R = 14.5$ cm, $p = 725$ MeV/c. Il en résulte, pour les antiprotons, une valeur $g/g_0 = 1.65$ qui définit leur granulation à l'entrée. Le minimum d'ionisation (21 blobs) observé nous a conduits à sélectionner à l'entrée les traces pour lesquelles $g = 36 \pm 4$ blobs. Pour la rapidité du travail, nous avons décidé de suivre seulement les traces ayant au minimum une longueur de 5 mm dans la plaque d'entrée, ce qui correspond à un angle inférieur à 7° en profondeur. En suivant ces traces et en observant l'évolution de leur allure, on identifie facilement celles qui sont des antiprotons.

3.2. IDENTIFICATION DES ANTIPROTONS

Une ambiguïté ne se présente, à vrai dire, que pour les traces pour lesquelles la variation (ΔR, Δg) indique une masse protonique. Autrement dit, le problème est d'écarter, parmi les antiprotons, une contamination toujours possible de protons parasites.

3.2.1 *Les antiprotons au repos et leurs caractéristiques*

Le problème est relativement simple lorsqu'il s'agit d'antiprotons qui interagissent au repos. Alors qu'un proton positif se présente généralement en fin de parcours comme une trace noire, sans interaction, un antiproton produit le plus souvent une étoile visible. Cette étoile résulte, on le sait, du phénomène d'annihilation, c'est-à-dire de la destruction d'un système nucléon-antinucléon à l'intérieur du noyau, et de la libération sous forme visible, ou non, d'une énergie de 1868 MeV. Des travaux précédents [9, 10]) ont indiqué que l'émission de mésons π chargés accompagne l'annihilation au repos dans 98 % des cas environ. Cependant, certains travaux ont souligné l'existence d'annihilations

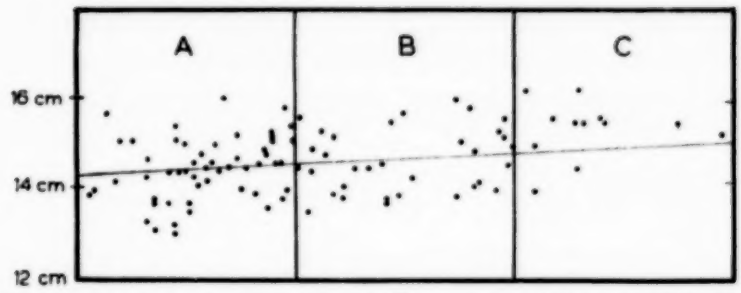

Fig. 1. Position et parcours des $\bar{p}$ au repos (plaques 24 à 70)

conduisant seulement à des mésons π_0 et à des neutrons [15]). C'est ce que nous appellerons des phénomènes du type $\tilde{p}_\rho$, phénomènes analogues à ceux que l'on rencontre dans la capture des mésons π^- et K^-. Les trajectoires d'antiprotons qui les produisent présentent toutes les caractéristiques des trajectoires de protons. Nous parlerons d'abord des antiprotons donnant une étoile d'annihilation visible et expliquerons par la suite la méthode adoptée pour indiquer au moins un ordre de grandeur des événements $\tilde{p}_\rho$.

La méthode de suivage indiquée ci-dessus a permis d'identifier 104 antiprotons se terminant au repos par une étoile visible. Ce chiffre n'implique aucune coupure et n'élimine aucune des annihilations produites soit sur le bord de l'empilement, soit près de la surface ou du verre.

La figure 1 indique la distribution de leurs parcours, de même que leur position par rapport aux bords de la plaque. Les parcours correspondant aux trois zones A, B, C, définies par $\bar{R}_A = (144 \pm 2)$ mm, $\bar{R}_B = (146 \pm 2)$ mm, $\bar{R}_C = (152 \pm 2)$ mm, ne semblent pas indiquer une variation importante de l'impulsion sur la largeur du paquet ($\approx$ 2 à 3 %). A l'intérieur de chaque zone, les fluctuations sont petites autour de la valeur moyenne. On en déduit que le

parcours moyen des antiprotons dans la plaque

$$\bar{R} = (146.5 \pm 1) \text{ mm}$$

correspond à une énergie cinétique $\bar{T} = 250$ MeV à l'entrée dans la plaque, conforme à l'énergie nominale.

3.2.2. *Les interactions en vol des antiprotons*

Pour éviter tout biais possible, il n'a pas été tenu compte des interactions en vol qui sont à une distance inférieure à 1.5 cm de l'entrée (énergie résiduelle $\approx$ 233 MeV).

Les antiprotons peuvent subir en vol deux espèces d'interactions:

a) celles d'où l'antiproton émerge sous forme d'antinucléon. Ce sont les diffusions élastiques ou inélastiques, avec ou sans échange de charge ($\tilde{p}$, $\tilde{p}$ ou $\tilde{p}$, $\tilde{n}$) selon que l'antiproton a échangé sa charge, ou non, avec un nucléon du noyau. La diffusion peut être accompagnée, ou non, d'une petite étoile d'évaporation.

b) les annihilations en vol, qui ne diffèrent pas, dans leur principe, des annihilations au repos. Ces événements se manifestent par une étoile, comportant le plus souvent des mésons π chargés. Le nombre de mésons π émis peut varier d'une interaction à l'autre, comme dans le cas des annihilations au repos. Mais le problème est moins simple ici. En effet, un proton parasite, d'une énergie au moins égale à 200 MeV, peut, dans certaines conditions favorables, créer un méson π. L'émission d'un tel méson résultant d'une collision nucléon-nucléon à l'intérieur du noyau peut conduire à des confusions entre les phénomènes recherchés et certaines collisions proton-noyau. L'étude énergétique des quelques étoiles en cause a toujours permis de lever l'ambiguïté.

Enfin, certaines annihilations en vol peuvent conduire seulement à une émission de particules nucléoniques, soit que le processus primaire ait libéré uniquement des mésons π_0, soit que les mésons chargés émis aient été réabsorbés dans le noyau. Il est utile, pour ces étoiles, de faire le bilan d'énergie: elles sont classées dans la catégorie antiprotons si l'énergie libérée est supérieure à l'énergie *cinétique* de la particule incidente.

3.2.3. *Remarque importante*

Une remarque s'impose à ce point. Si l'on rassemble tous les antiprotons certains, identifiés comme il a été dit précédemment, qu'ils interagissent en vol ou au repos, et si l'on étudie leur distribution horizontale par rapport à la direction moyenne du faisceau, on obtient les courbes de la fig.2. Celles-ci, déterminées sur un échantillonnage, correspondent, on le voit, à une bonne collimation définie par la direction moyenne

$$\alpha = 2.5 \pm 1.5°.$$

Ceci suggère une méthode pour donner au moins un ordre de grandeur de celles qui, parmi les interactions douteuses, peuvent être dues aux antiprotons.

Celles-ci rassemblent les particules protoniques qui s'arrêtent au repos sans interaction visible, pour lesquelles le parcours R est à l'intérieur des limites définies par $\bar{R} \pm \sigma$, les disparitions en vol et celles qui, parmi les étoiles en vol, conduisent seulement à une faible évaporation ($T < T_{\tilde{p}}$).

L'angle α a été calculé à l'entrée de la plaque pour chacune de ces traces et nous avons rejeté comme traces parasites celles pour lesquelles α est extérieur à l'intervalle $-2° < \alpha < 7°$. Après cette élimination il subsiste:

a) 4 événements du type $\tilde{p}_\rho$,

b) deux étoiles ne donnant à l'annihilation qu'une faible évaporation.

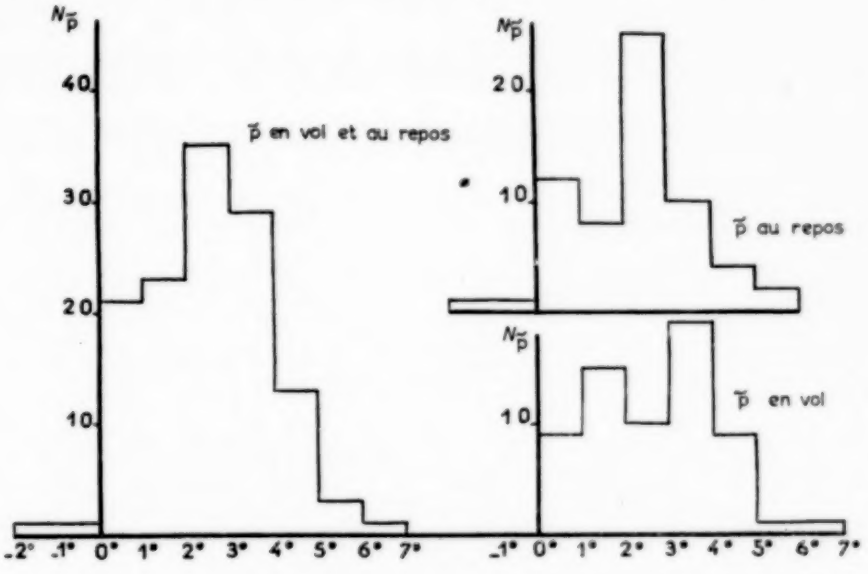

Fig. 2. Angles à l'entrée; distribution en projection horizontale.

Nous n'avons trouvé aucun procédé permettant de conclure avec certitude si le primaire était un proton ou un antiproton. En conséquence, nous avons exclu ces six événements de la statistique.

Un doute subsiste encore pour quelques rares étoiles produites près du bord d'entrée et présentant en outre un méson π rapide émis vers l'arrière, dans la direction du faisceau. Il est alors difficile d'affirmer lequel, du méson π ou du nucléon (p ou $\tilde{p}$), est la particule incidente. Dans ce cas, c'est encore généralement la bonne collimation de l'une ou de l'autre des particules qui permet de décider.

4. Résultats Expérimentaux

104 antiprotons interagissant au repos et 101 antiprotons interagissant en vol ont été observés jusqu'à ce jour dans le présent travail. Comme on le verra plus loin, certaines coupures ont été faites selon les phénomènes recherchés.

4.1. SECTION EFFICACE D'ANNIHILATION. LIBRE PARCOURS MOYEN

La discussion relative à la section efficace d'annihilation doit, en toute rigueur, tenir compte de tous les événements relevés quelle que soit leur position par rapport au verre. Cependant, nous avons éliminé ici 7 antiprotons (6 s'annihilant au repos et 1 en vol) parce qu'ils subissent, avant leur annihilation, une diffusion inélastique. Cette interaction modifie leur parcours résiduel de façon trop notable pour qu'on puisse leur appliquer le raisonnement suivant sans biaiser la statistique.

La discrimination entre annihilations au repos et annihilations en vol a été faite par inspection visuelle. C'est-à-dire que, vraisemblablement, nous avons

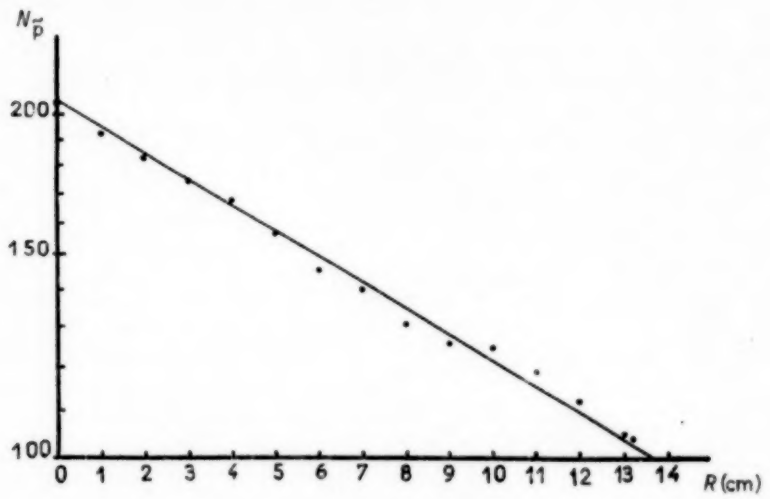

Fig. 3. Libre parcours moyen.

classé dans la catégorie "au repos" un certain nombre d'événements en vol, au voisinage de la fin de leur parcours. Si l'on admet que la distinction entre les deux catégories n'est possible que pour un parcours résiduel supérieur à 6 mm, toutes nos annihilations au repos sont en fait des phénomènes pour lesquels on a: 12.6 cm $\leqq R \leqq$ 13.2 cm (on tient compte de la coupure à 1.5 cm de l'entrée).

La fig. 3 représente, en coordonnées semi-logarithmiques, la décroissance du nombre N des antiprotons, due au phénomène d'annihilation en vol, en fonction de leur parcours dans la plaque, dans le domaine $0 \leqq R \leqq 13.2$ cm. C'est cette courbe qui est utilisée pour le calcul du libre parcours moyen. Elle est sensiblement linéaire sauf peut-être dans la région 8 cm $\leqq R \leqq$ 10 cm, mais il faudrait sans doute enrichir notablement la statistique avant d'affirmer qu'il y a dans ce domaine un écart à la linéarité.

On peut rappeler ici la définition classique du libre parcours moyen:

$$\lambda = \frac{\mathrm{d}R}{\mathrm{d}P},$$

où $\mathrm{d}P$ représente la probabilité d'une interaction sur une distance $\mathrm{d}R$.

Si on a initialement N particules d'énergie E (correspondant au parcours total $R_0 = 13.2$ cm) et si $n(R)$ est le nombre de celles qui restent après un parcours R, on a

$$dP = \frac{dn}{n},$$

d'où

$$\lambda = \frac{n}{dn} dR.$$

Si l'on admet que, dans un domaine donné, λ est une quantité constante, on a

$$n = Ne^{-R/\lambda}.$$

L'examen de la courbe 3 permet de conclure que dans le domaine exploré,

$$\lambda_{ann} = 19 \text{ cm}.$$

4.2. L'ÉMISSION DES MÉSONS π DANS L'ANNIHILATION

Le phénomène d'annihilation se traduit, dans la plupart des cas, par une émission de mésons π accompagnés le plus souvent de branches nucléaires. Les 104 antiprotons dont on observe l'annihilation au repos, après élimination des $4\tilde{p}_\rho$ mentionnés au paragraphe 3.2.3, produisent tous des mésons π chargés. En ce qui concerne les événements en vol, 5 étoiles n'ont que des branches noires sans π; 4 d'entre elles seulement, dans lesquelles l'énergie libérée est supérieure à l'énergie cinétique de la particule incidente, sont incluses dans la statistique. Ceci revient à dire que le phénomène d'annihilation est accompagné d'une émission de π dans 96 % des cas, au moins.

Pour éviter les biais dus à une perte possible de traces au minimum, une coupure a été faite à 20 μ de la surface et à 20 μ du verre; une autre coupure a été faite à 1.5 cm du bord latéral de la plaque sur plusieurs étoiles où les mesures auraient été entachées de trop larges erreurs. Ceci nous a conduits à limiter à 165 événements (89 au repos, 76 en vol), l'analyse suivante concernant l'émission de π; 9 événements contenant des mésons K ont été écartés à dessein: nous en parlerons plus loin. Sur ces 165 événements, toutes les traces au-dessus du minimum ont été suivies jusqu'à la fin de leur parcours, ou leur sortie de l'empilement.

Parmi les traces au minimum, le suivage a été limité à celles dont le parcours par plaque était supérieur à 3 mm (angle de 11° avec le plan d'observation). Une mesure de diffusion multiple a été effectuée sur ces traces, de sorte que le spectre d'énergie des mésons π émis a été mesuré sur un échantillonnage homogène.

Pour les angles supérieurs à 11°, toutes les traces au minimum ont été considérées comme mésons π.

4.2.1. *Nombre de mésons π chargés émis dans l'annihilation*

Les histogrammes (fig. 4) représentent la distribution du nombre d'étoiles à 1, 2, 3, 4, 5 mésons π chargés. Les traits pleins sont relatifs au présent travail: on a tracé en pointillé, pour la comparaison, les résultats de Berkeley ((700 ± 20) MeV/c à l'entrée dans l'émulsion). Les nombres moyens de mésons π observés dans les étoiles d'annihilation au repos et en vol sont respectivement (2.54 ± 0.17) et (2.22 ± 0.17).

4.2.2. *Spectre d'énergie des mésons π*

La figure 5 représente le spectre d'énergie des mésons π émis dans les annihilations au repos, en vol, et pour l'ensemble des deux catégories de phénomènes.

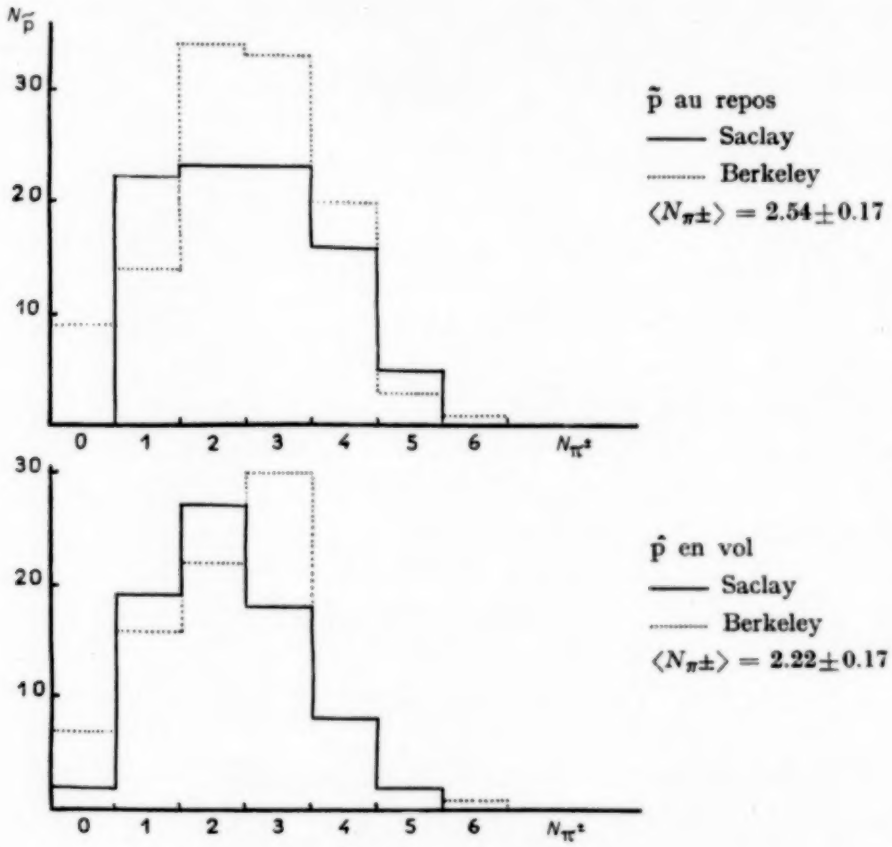

Fig. 4. Nombre de mésons π par étoile.

Ce spectre a été limité pour *tous* les mésons à l'intervalle angulaire $\pm11°$ mentionné plus haut.

L'énergie moyenne des mésons π issus des annihilations au repos $T_\pi = (226\pm21)$ MeV est supérieure à celle, $T_\pi = (184\pm24)$ MeV, des mésons π issus des interactions en vol. Ceci peut s'expliquer si l'on admet que le phénomène primaire est le même, mais que, dans les annihilations en vol, les anti-

protons pénètrent plus profondément dans le noyau, favorisant ainsi la probabilité de réactions secondaires. Ces réactions secondaires peuvent se traduire, soit par une diminution de l'énergie des π initialement émis (diffusions inélastiques), soit par une absorption. Ceci expliquerait aussi que le nombre moyen de mésons π visibles émis,

$$\langle N_\pi \rangle_{\text{vol}} = 2.22 \pm 0.17,$$

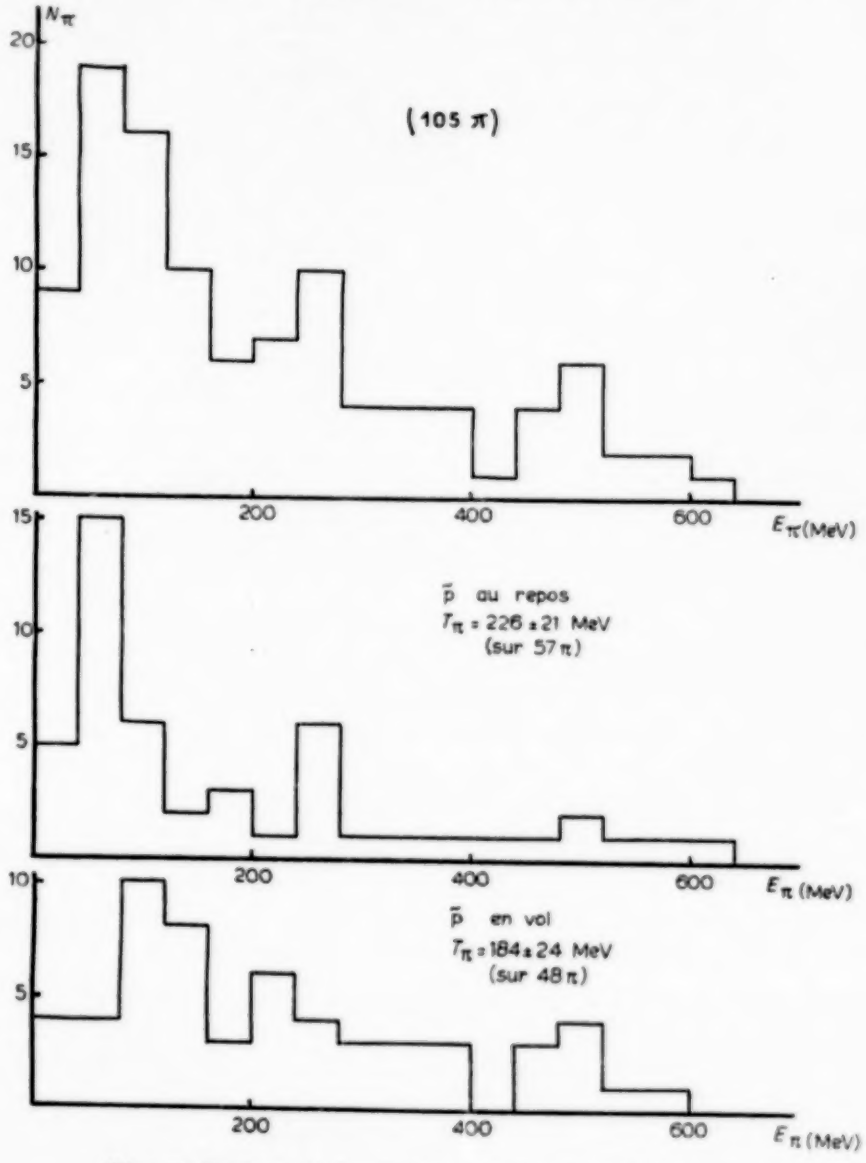

Fig. 5. Spectre d'énergie des mésons π émis (105 π)

soit inférieur à

$$\langle N_\pi \rangle_{\text{repos}} = 2.54 \pm 0.17.$$

Le tableau 1 exprime l'énergie cinétique moyenne des mésons π chargés émis, en fonction de leur multiplicité. Les fluctuations statistiques sont grandes, car le nombre de mésons mesuré dans chaque catégorie est petit, mais si les chiffres

ci-dessus devaient être confirmés par la suite, il faudrait conclure, au moins pour les événements au repos, que l'énergie des mésons π émis varie en raison inverse de leur multiplicité.

TABLEAU 1

Energie cinétique moyenne des mésons π chargés émis, en fonction de leur multiplicité

N_π/étoile	en vol			au repos		
	Nombre d'étoiles	Nombre de π mesurés	T_π(MeV)	Nombre d'étoiles	Nombre de π mesurés	T_π(MeV)
5	2	4	119±41	5	4	227.5±40
4	8	7	212±45	16	18	154 ±23
3	18	12	126±28	23	15	227 ±45
2	27	17	218±46	23	14	259 ±41
1	19	8	206±77	22	6	357.5±55

4.2.3. *Rapport* N_{π^+}/N_{π^-}

Le suivage des mésons π, tel qu'il est indiqué en 4.2, a permis d'identifier 23 mésons π^+ pour 35 mésons π^- (voir leurs caractéristiques dans le tableau 2). Ces chiffres correspondent à un suivage complètement indépendant de l'angle de plongée; les mésons π^+ ont été identifiés par le classique π—μ—e en fin de parcours, les mésons π^- par leur absorption au repos, avec ou sans étoile visible.

TABLEAU 2

Caractéristiques des mésons π^+ et π^- émis, identifiés par suivage

	Nombre de π^+	$\overline{T_{\pi^+}}$ (MeV)	Nombre de π^-	$\overline{T_{\pi^-}}$ (MeV)
repos	14	54±6	16	40.4±11.5
vol	9	41±6.5	19	46 ± 5

Ceci correspond à un rapport $N_{\pi^+}/N_{\pi^-} = 0.66\pm0.18$ plus voisin que le rapport de Berkeley (0.45 ± 0.12) de la valeur théorique 0.76 calculée à partir de la composition de l'émulsion en supposant que les protons et les neutrons jouent un rôle analogue dans l'annihilation.

Une bonne discussion a été publiée antérieurement à ce sujet[10]) et nous y renvoyons le lecteur. Ajoutons cependant qu'il serait intéressantd'obtenir plus de précision sur la valeur du rapport N_{π^+}/N_{π^-}. Ce rapport est en effet sensible à

1) une distribution différente des protons et des neutrons à l'intérieur du noyau,

2) une différence de spectre énergétique des mésons π primaires selon leur état de charge.

Une telle étude est actuellement impossible à l'aide des émulsions photographiques, où le phénomène primaire est masqué par les phénomènes secondaires, mais elle sera facilitée par les résultats obtenus avec les chambres à bulles à hydrogène.

TABLEAU 3

Caractéristiques des mésons K^+ et K^- émis, identifiés par suivage

No de l'év.	β	R	T_K (MeV)	Méthode d'identification	signe	β'
$\tilde{p}_{13}$	+ 6° (surf.)	612 μ	8	désint. au repos	+	−22° (verre)
$\tilde{p}_{79}$	+32° (surf.)	3.6 cm	83	R, g; désint. repos	+	+44° (surf.)
$\tilde{p}_{152}$	+ 9°30′ (surf.)	14.6 mm	48.5	désint. au repos; $m = 900^{+425}_{-225} m_e$	+	+38° (surf.)
$\tilde{p}_{177}$	−36° (verre)	9974 μ	39	désint. au repos	+	−31°30′ (verre)
$\tilde{p}_{132}$	+ 5°30′ (surf.)	7.6 cm	≈220	$p\beta$, g; sort du paquet	?	−
$\tilde{p}_{61}$	− 4°30′ (verre)	1.5 cm	≈72	$p\beta$, g (incertain)	?	−
$\tilde{p}_{262}$	− 8° (verre)	9 cm	142	$p\beta$, g; désint. repos	+	− 3° (verre)
$\tilde{p}_{234}$	−25° (verre)	63 μ	?	interact. sec. vol	−	−
	−27°13′ (verre)	1384 μ	94	désint. en vol	+	+54° (surf.)
$\tilde{p}_{245}$	+ 5°52′ (surf.)	1396 μ	12.9	interact. sec. repos	−	−

TABLEAU 4

Caractéristiques des étoiles d'où sont issus des mésons K

No de l'étoile	13	79	152	177	132	61	262	234	245
Signe des K	1 K^+	1 K^+	1 K^+	1 K^+	1?	1?	1 K^+	1 K^-	K^+ et K^-
N_π	2	0	1	0	0	0	3	2	2
N_H	4	1	3	5	0	11	7	2	0
ΣE_K	502	577	542	533	714	566	636	>494	1095
ΣE_π	>476	0	>220	0	0	0	>583	>395	>400
ΣE_H	>140	>104	111	172	0	422	130	36	0
$E_{vis.}$	>1118	>681	>873	705	714	988	>1349	>925	>1495
$T_{\tilde{p}}$	0	0	0	0	0	215	186	0	0
Energie cinét. des K (MeV)	8	83	48.5	39	220^{+40}_{-28}	$72^{+16}_{-\ 7}$	142	>0	94; 12.9
Energie cinét. des π (MeV)	96; ≧ 100	0	>80	0	0	0	>60; >60; 43	>60; 55	>60; >60
$\Sigma E_K/W$	0.27	0.31	0.29	0.28	0.38	0.27	0.31	>0.26	0.58
$\Sigma E_\pi/W$	>0.25	0	>0.12	0	0	0	>0.28	>0.21	>0.21
$\Sigma E_H/W$	>0.075	>0.056	0.06	0.09	0	0.20	0.063	0.019	0
$\Sigma E_{vis.}/W$	>0.6	>0.36	>0.47	0.38	0.38	0.47	>0.65	>0.49	>0.79

4.3. L'ÉMISSION DE MÉSONS K

Comme il a été dit plus haut, toutes les traces au-dessus du minimum d'ionisation ont été suivies jusqu'à la fin de leur parcours ou de leur sortie du paquet: 192 étoiles, parmi les 205 relevées au dépouillement,ont pu être analysées de cette façon. La coupure de 13 étoiles correspond à celles, situées trop près du bord latéral, pour lesquelles un suivage trop court n'aurait apporté aucune information sur la nature des secondaires.

Le suivage jusqu'à la fin du parcours a permis de reconnaître 6 mésons K^+, identifiés par la présence d'un secondaire au minimum d'ionisation et 2 mésons K^-, identifiés par leur interaction. D'autre part, des mesures systématiques de $(p\beta, g)$ effectuées sur toutes les traces ($g > 22$) sortant du paquet, pour lesquelles l'inclinaison β était inférieure à 20°, ont permis d'identifier deux autres mésons K.

Le tableau 3 résume leurs caractéristiques (β est l'angle d'inclinaison du méson K, R son parcours, T_k l'énergie cinétique à l'émission, β' l'angle d'émission de la particule secondaire).

Les caractéristiques des étoiles d'où sont issus des K sont rassemblées dans le tableau 4.

Plusieurs de ces événements ayant été décrits dans une publication antérieure [17]) nous ne répéterons pas ici les remarques déjà exprimées. Nous nous limiterons aux événements $\tilde{P}_{234}$, $\tilde{P}_{245}$ et $\tilde{P}_{262}$ contenant chacun un ou deux mésons K. On trouvera les deux premiers d'entre eux photographiés sur la page ci-contre.

$\tilde{P}_{234}$. L'étoile primaire résulte d'une annihilation au repos qui se manifeste par l'émission de 2 mésons π chargés (l'un se désintègre au repos en donnant la cascade π—μ—e), de deux branches d'évaporation et d'une branche grise. Celle-ci ($g \approx 50$ blobs) donne, après 63μ, une interaction en vol d'où sortent un électron, une trace noire et un méson π^-. Celui-ci est capturé au repos après un parcours de 50 mm et produit une étoile à 4 branches. Son parcours R_π correspond à des valeurs $E_\pi = 62$ MeV, $g_\pi = 28$ grains au point d'émission. Le fait que g_π soit inférieur à g exclut ici un phénomène de diffusion. Il faut donc penser à la capture classique d'un méson K^-, avec formation d'un méson π et d'un hypéron qui n'est pas visible.

$\tilde{P}_{245}$. L'étoile primaire est également une annihilation au repos. Elle se manifeste par deux mésons π au minimum d'ionisation, 2 reculs et 2 traces grises. Les deux mésons π sont si plongeants qu'aucun suivage systématique, ni aucune mesure de leur énergie, n'ont pu être effectués. L'une des traces grises (marquée K^- sur le cliché) conduit, après 1396 μ, à une interaction au repos d'où partent 2 reculs et une trace grise. Celle-ci a été suivie sur 4 cm jusqu'à sa sortie de l'empilement et identifiée comme proton (ΔR, Δg). Son énergie cinétique à l'émission (200 MeV) permet d'exclure la possibilité d'une capture Σ^- et de penser qu'il s'agit vraisemblablement de la capture d'un méson K^- au repos.

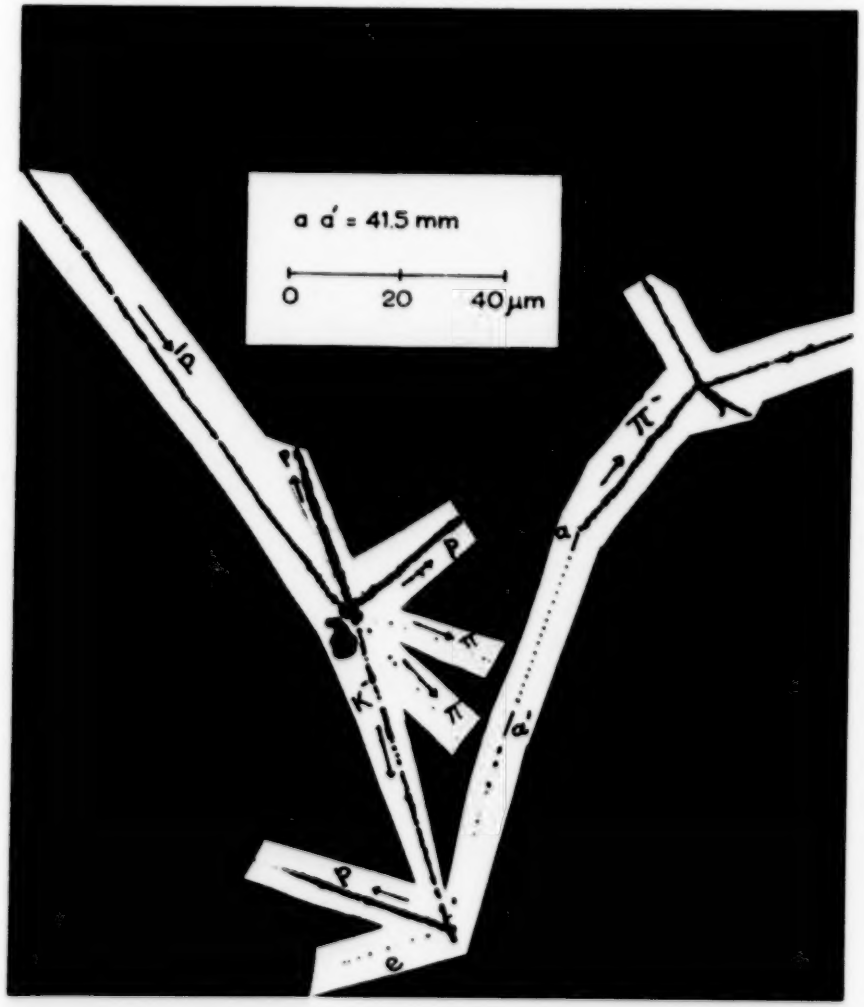

P244

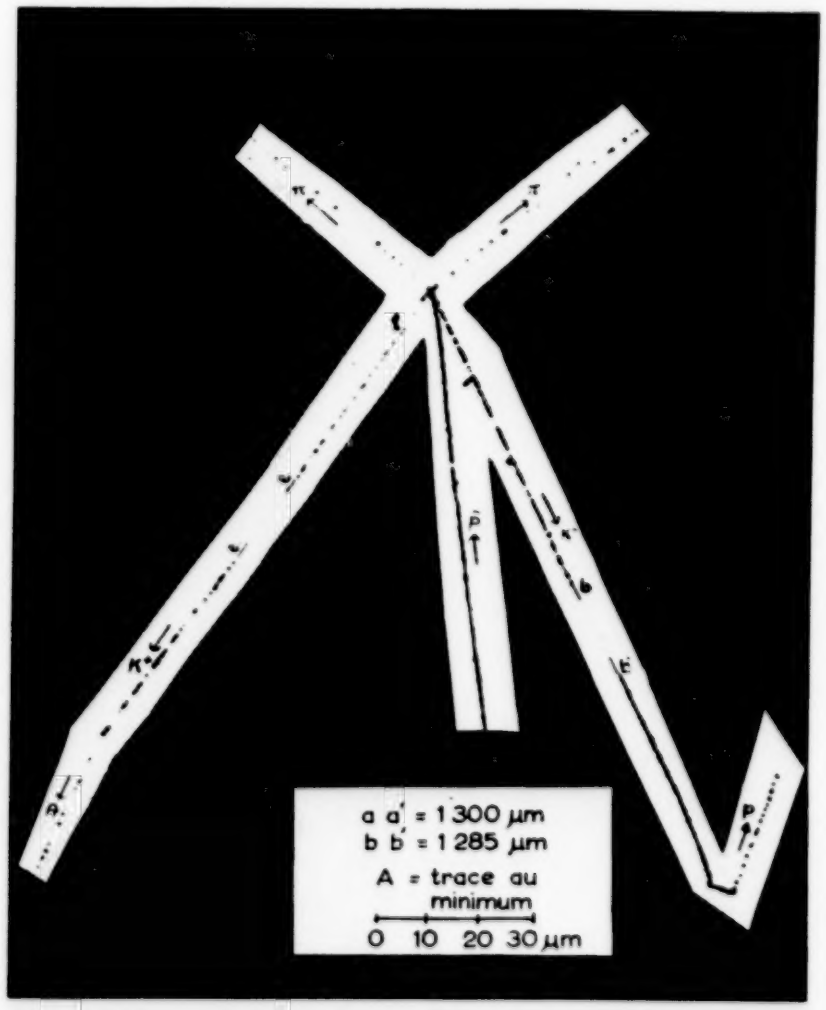

P245

Les deux mosaïques ont été effectuées par Mlle L. Berthelot du C.E.N. de Saclay.

L'autre trace grise ($g \approx 42$ grains) se désintègre en vol après 1384μ pour donner un secondaire au minimum d'ionisation. L'hypothèse de la conservation de l'étrangeté permet d'exclure immédiatement une désintégration Σ^+ et de penser qu'il s'agit ici d'une désintégration K^+.

On peut donc affirmer que, dans ce cas particulier, l'annihilation s'est produite sur un seul nucléon du noyau, vraisemblablement selon un schéma

$$\tilde{p}+p \rightarrow K^+ + K^- + \pi^+ + \pi^- + n\pi^0.$$

L'idée d'une annihilation sur l'hydrogène, considérée a priori, a dû être rejetée à cause d'écarts importants dans le bilan des impulsions, comme le laissait d'ailleurs prévoir la présence des deux reculs.

$\underline{\tilde{p}_{262}}$. L'étoile primaire est une annihilation en vol d'où sortent trois mésons-π, 7 branches noires et une branche grise qui donne au repos un secondaire au minimum. Ce secondaire n'est accompagné d'aucun blob, ni recul, ce qui favorise, a priori, l'hypothèse d'une désintégration.

La valeur de $p\beta$ à l'émission,

$$p\beta = 245 \begin{matrix} \nearrow 208 \\ \searrow 299 \end{matrix} \text{ MeV}/c,$$

correspondrait, pour des mésons π et μ, à des valeurs

$$R_\pi = 21.5 \begin{matrix} \nearrow 16.5 \\ \searrow 30 \end{matrix} \text{ cm}, \qquad E_\pi = 166 \begin{matrix} \nearrow 138 \\ \searrow 215 \end{matrix} \text{ MeV};$$

$$R_\mu = 25.5 \begin{matrix} \nearrow 20 \\ \searrow 35 \end{matrix} \text{ cm}, \qquad E_\mu = 178 \begin{matrix} \nearrow 148 \\ \searrow 230 \end{matrix} \text{ MeV}.$$

Parmi les processus possibles, on peut envisager une désintégration $\Sigma^+ \rightarrow \pi^+ + n$, ou la désintégration d'un méson K^+.

La désintégration $\Sigma^+ \rightarrow \pi^+ + n$ se trouve exclue rapidement si l'on considère que l'énergie théorique (100 MeV) du méson π^+ émis est extérieure à la zone des valeurs possibles pour E_π.

Il en est de même de la désintégration K_{π_2} qui correspond, pour les mésons π émis, à une énergie cinétique de 106 MeV.

Par contre, les modes de désintégration K_{β_2}, K_{μ_3}, K_{μ_2} correspondent à des particules μ, e, dont l'énergie est à l'intérieur de la bande $p\beta$ mentionnée ci-dessus.

Il est donc raisonnable de penser qu'il s'agit ici de la désintégration d'un méson K qui pourrait correspondre à l'un de ces schémas.

Une autre possibilité qu'on ne peut pas entièrement exclure est celle d'une réaction

$$K^- + p \rightarrow \Sigma + \pi$$

ou

$$K^- + p \rightarrow \Lambda^0 + \pi$$

non accompagnée de branches visibles.

Les mésons π correspondant à la première réaction $\left(E_\pi = 82 \begin{matrix} \nearrow 94 \\ \searrow 49 \end{matrix} \text{MeV}\right)$ sont en dehors de la zone des énergies possibles; ceux qui correspondent à la seconde $\left(E_\pi = 142 \begin{matrix} \nearrow 166 \\ \searrow 99 \end{matrix} \text{MeV}\right)$ sont dans cette zone.

Cependant, si l'on considère la proportion des étoiles de mésons K^- qui conduisent à un seul méson π visible (< 10 %), on peut conclure qu'il s'agit d'un phénomène très improbable.

On peut penser qu'au cours du présent travail un certain nombre de mésons $K^\pm$ ont été perdus. Cette perte résulterait d'une efficacité imparfaite (90 %) dans la détection des secondaires au minimum d'ionisation, et du fait qu'un certain nombre de mésons $K^\pm$ existent parmi les traces non mesurables (trop plongeantes) qui sortent du paquet. On estime qu'un méson K au plus a été perdu de cette façon.

Les chiffres signalés ci-dessus permettent de fixer à (4.6 ± 0.5) % la proportion des étoiles d'annihilation observées dans le présent travail qui sont *effectivement* accompagnées d'au moins un méson K visible. Pour connaître la proportion exacte d'étoiles émettant au moins un méson K, il faut tenir compte de l'émission $K^0\overline{K}^0$ et de l'émission K^-K^0 où le méson K^- est réabsorbé dans le noyau. Si l'on admet, comme des auteurs précédents [10, 18]), que ces phénomènes représentent 24 % du nombre d'étoiles émettant un couple $K\overline{K}$, on doit en conclure que, toute fluctuation statistique mise à part, la fraction réelle d'étoiles accompagnées de mésons K est de (6 ± 0.7)% dans le présent travail. On ne tient pas compte ici de la possibilité de la création simultanée d'un K et d'un hypéron qui demanderait l'intervention de deux nucléons dans la réaction d'annihilation.

Le tableau 4 permet de fixer à 566 MeV l'énergie moyenne des mésons K

TABLEAU 5

Nombre moyen de branches nucléoniques par étoile et énergies moyennes correspondantes

Repos				Vol			
Nbre de branches étoile		En./étoile (MeV)	En./branche (MeV)	Nbre de branches étoile		En./étoile (MeV)	En./branche (MeV)
évap.	2.14 ± 0.17	38.1	17.8	évap.	3.67 ± 0.22	67.9	18.5
k.o.	1.08 ± 0.11	101.7	94	k.o	1.99 ± 0.16	195.6	98.3
tot.	3.22 ± 0.2	139.8 ± 13	43.5	tot.	5.66 ± 0.28	263.5 ± 27	46.5

émis dans l'annihilation. Ceci implique que l'énergie moyenne $\overline{E_{K\bar{K}}}$ émise par étoile sous forme de mésons K visibles et neutres est de (68 ± 23) MeV où l'erreur est l'erreur statistique.

4.4. BRANCHES NUCLÉONIQUES

Aucune tentative n'a été faite pour distinguer des protons les particules plus lourdes: deutérons, tritons, particules α. Toutes ont été suivies jusqu'à la fin de leur parcours, à l'exception des branches sortant du paquet. La détermination de leur énergie repose sur l'hypothèse que toutes sont des protons. Ces protons sont classés en deux catégories selon que leur énergie cinétique est supérieure à 35 MeV (protons de choc direct ou "knock-on") ou inférieure à cette valeur (particules d'évaporation).

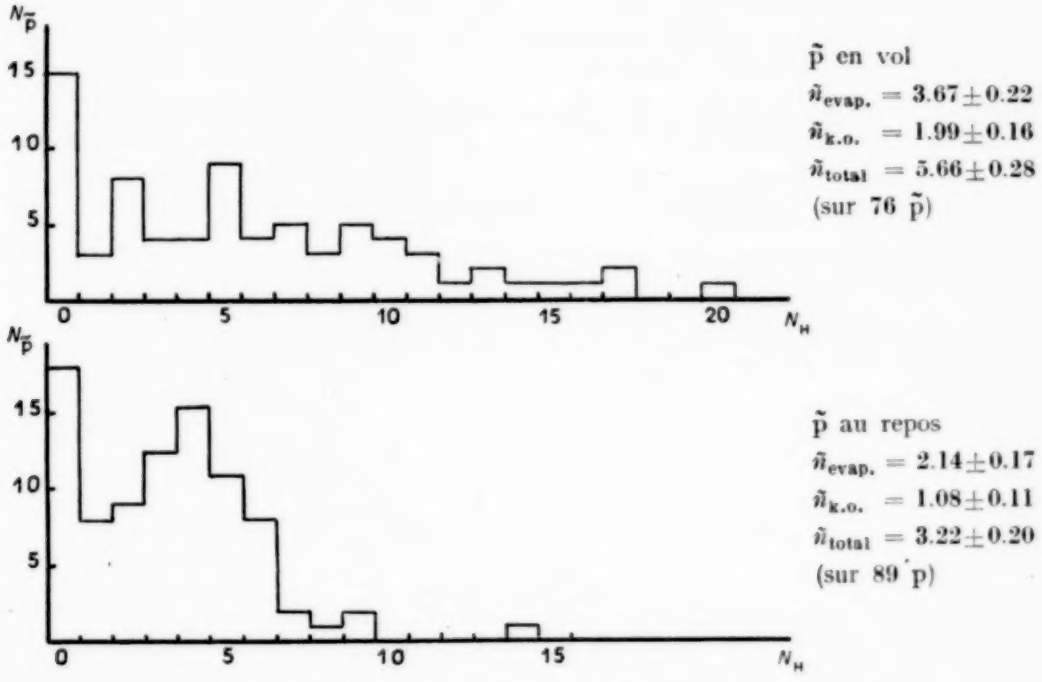

Fig. 6. Spectre du nombre N_H des particules lourdes (p, d, t, α)

4.4.1. *Nombre de branches par étoile et énergie moyenne des branches*

La figure 6 représente le spectre du nombre de branches à allure protonique pour les antiprotons au repos et en vol. On trouvera, indiqués en regard, les nombres moyens de branches d'évaporation et de choc direct dans les deux catégories de phénomènes.

La figure 7 exprime l'énergie moyenne des branches nucléoniques par étoile d'annihilation: celle-ci est relative, d'une part à l'énergie moyenne en protons directs ($\bar{E}_{k.o.}$), d'autre part à l'énergie moyenne en protons d'évaporation ($\bar{E}_{evap.}$).

Les résultats sont résumés dans le tableau 5 qui exprime en même temps

l'énergie moyenne par "évaporation" et par "knock-on" dans le cas des antiprotons au repos et des antiprotons en vol (on a tenu compte, dans tous les cas, de l'énergie de liaison).

Alors que le nombre moyen de branches est systématiquement plus élevé pour les étoiles en vol que pour les étoiles au repos, l'énergie moyenne par branche est sensiblement la même dans les deux cas. Ces résultat, très similaires à ceux obtenus précédemment par le groupe de Berkeley, semblent indiquer que

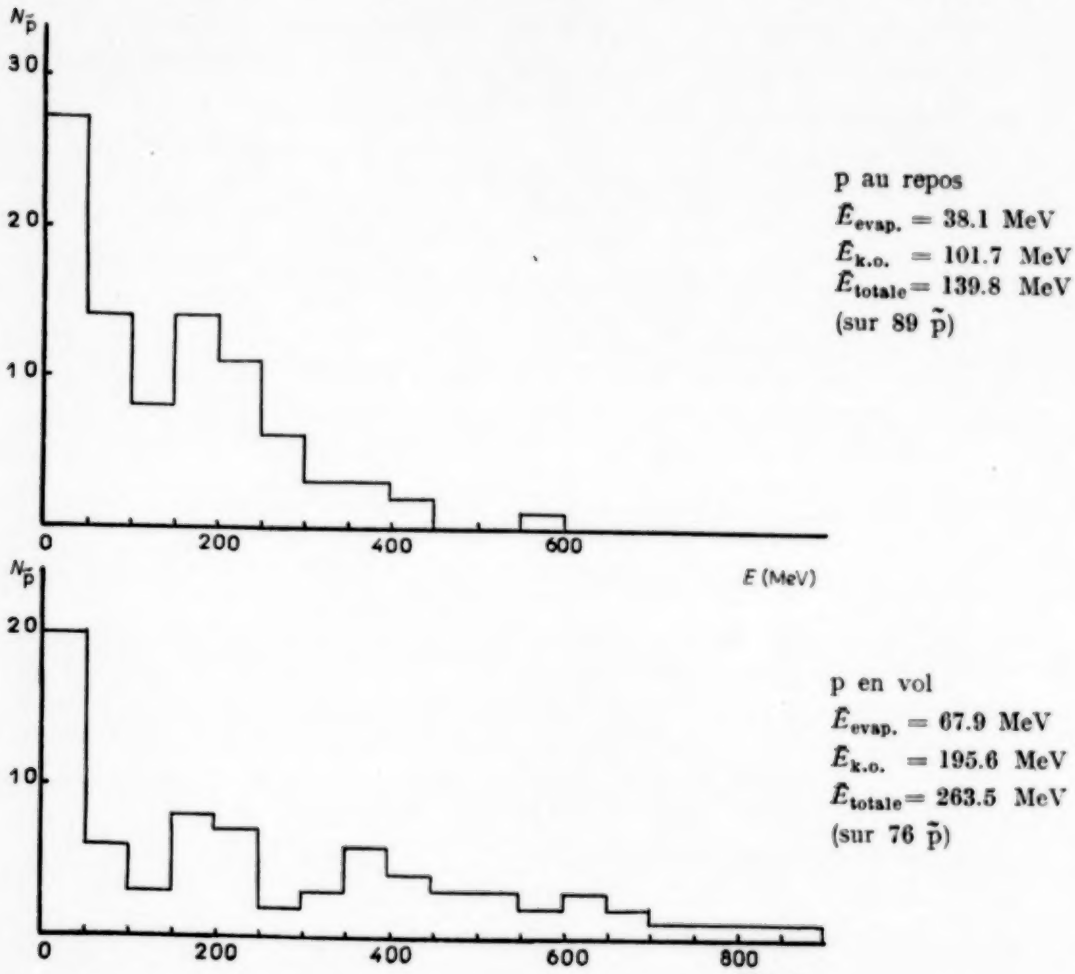

Fig. 7. Spectre de l'énergie totale des particules lourdes (p, d, t, α) (par étoile de p)

les branches nucléoniques résultent d'un processus secondaire (absorption ou diffusion des mésons π primaires), plus fréquent dans les annihilations en vol que dans les annihilations au repos.

Une autre façon de rechercher cette dépendance consiste à établir la figure 8 qui illustre l'énergie émise sous forme nucléonique en fonction du nombre de mésons π observés. Les courbes, établies séparément pour les antiprotons au repos et en vol, indiquent en parallèle l'énergie nucléonique sous forme d'évaporation et de "knock-on". Le tableau 6 résume les résultats.

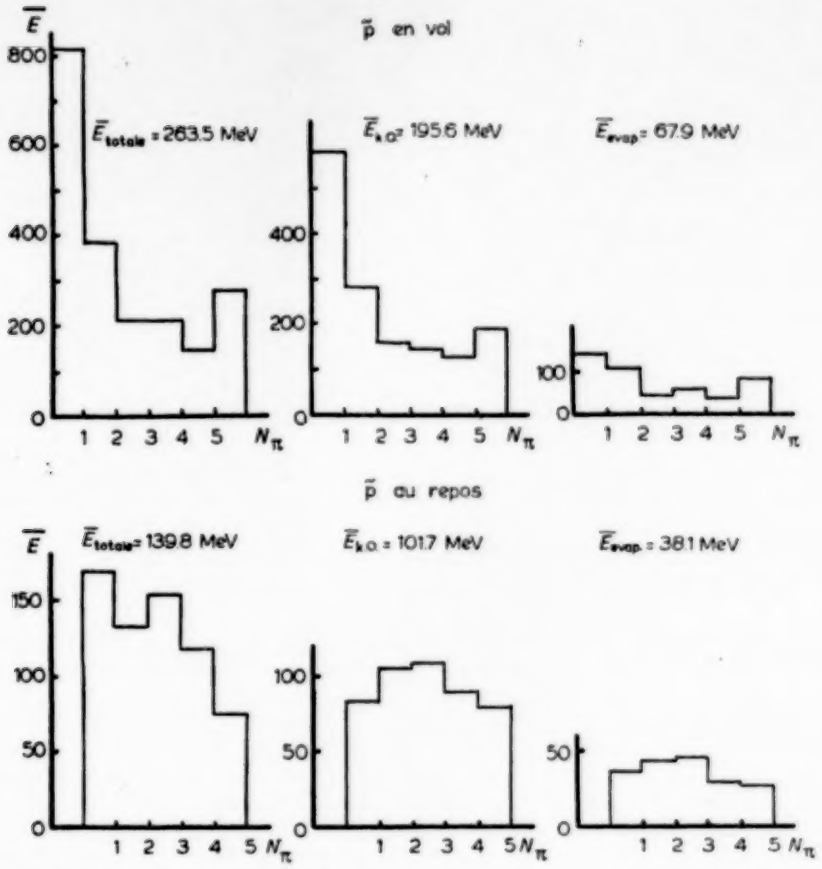

Fig. 8. $\bar{E}$ (par étoile) des particules lourdes (p, d, t, α) en fonction du nombre de mésons π émis.

TABLEAU 6

Nombre moyen de branches nucléoniques par étoile et énergies moyennes correspondantes, en fonction du nombre de mésons π observés dans l'annihilation

		Repos			Vol		
		Nbre branches étoile	En. moyenne par étoile (MeV)	En. moyenne par branche (MeV)	Nbre branches étoile	En. moyenne par étoile (MeV)	En. moyenne par branche (MeV)
1π	évap.	1.95	36.2	18.6	5.4	106.2	19.7
	k.o.	1.6	>131.8	>82.4	3.5	>281	>80.3
	tot.	3.55	>168	>47.3	8.5	>384	>45.18
2π	évap.	2.55	43.4	17.02	2.7	47.6	17.6
	k.o.	0.85	>88.8	>104.5	1.3	>160.4	>123.4
	tot.	3.4	>132.2	>38.9	4	>208	>52
3π	évap.	2.35	45.1	19.2	3.4	60.7	17.9
	k.o.	1	>108.6	>108.6	1.8	>147.9	>82.2
	tot.	3.35	>153.7	>45.9	5.2	>208.6	>40.1
4π	évap.	1.85	29.3	15.8	2.25	40.5	18.0
	k.o.	1	88	88	1.25	>131	>104.8
	tot.	2.85	>117.3	>41.15	3.5	>171.5	>49
5π	évap.	1.6	26.8	16.75	4	83	20.7
	k.o.	0.6	>46.8	78	1.5	>192	>128
	tot.	2.2	>73.6	33.4	5.5	>275	>50

4.4.2. *Energie des neutrons émis*

Il est intéressant d'évaluer, à partir des chiffres ci-dessus, l'énergie transférée aux neutrons dans le processus d'évaporation. Il existe, en effet, parallèlement aux protons de choc direct, des neutrons correspondant au même phénomène, et parallèlement aux protons d'évaporation, des neutrons d'évaporation. On a proposé des chiffres variés [9, 10, 16]) pour évaluer les fractions respectives n/p de choc direct et d'évaporation. Nous nous limiterons au chiffre le plus récent n/p = 1.6, auquel nous ne donnerons ici qu'une valeur indicative. Ce chiffre permet néanmoins, à partir du tableau 6, d'estimer la contribution des neutrons dans l'annihilation et d'en déduire l'énergie totale émise dans l'annihilation sous forme nucléonique (tableau 7).

TABLEAU 7

Contribution des neutrons dans l'annihilation calculée pour n/p = 1.6

	Repos		Vol	
	Nbre de branches/étoile	Energie/étoile (MeV)	Nbre de branches/étoile	Energie/étoile (MeV)
Chargées	3.22±0.2	139.8±13	5.66±0.28	263±27
Neutres	5.15±0.32	224.2±21	9.06±0.45	421±43
Nucléons	8.37±0.52	364.0±34	14.72±0.73	684±70

5. Comparaison avec les Résultats de Berkeley

Les 207 étoiles d'annihilation qui sont l'objet de ce travail ont finalement été analysées au moyen de la méthode de Berkeley (réf.[10]), section 4).

A partir des valeurs expérimentales brutes (tableau 8), on tire les valeurs dérivées (tableau 9). Dans les deux tableaux, on a indiqué en regard les valeurs de Berkeley. Pour la définition détaillée des symboles, nous renverrons le lecteur à la réf. [10]).

On remarque que les valeurs de Saclay sont, dans tous les cas, à l'intérieur des erreurs signalées par Berkeley. Ceci indique qu'il faudrait augmenter sensiblement la statistique pour obtenir une meilleure précision.

Le paquet d'émulsions utilisé a pu être exposé grâce à la courtoisie du Dr. Lofgren et à l'amabilité du Prof. Segrè qui a bien voulu autoriser l'irradiation dans le faisceau qu'il avait réalisé. Nous leur en exprimons notre reconnaissance.

L'irradiation et le marquage des émulsions ont été effectués grâce à la collaboration des Drs. G. Goldhaber et H. Heckmann de l'Université de Berkeley, et de notre collègue J. F. Detoeuf du C.E.N. de Saclay. Nous les prions de croire à notre reconnaissance amicale.

Le paquet a été développé grâce à l'aide efficace et amicale de Mmes Mathieu-Faraggi et A. Garin de la Section des Réactions Nucléaires à Moyenne Energie

TABLEAU 8

Tableau récapitulatif des résultats obtenus à Berkeley et à Saclay

	Saclay		Berkeley	
	Au repos	En vol	Au repos	En vol
$\langle W \rangle$ Energie totale disponible par étoile dans l'annihilation	1868	2024	1868	2009
$\langle E_\pi \rangle$ Energie moyenne des π chargés observés (énergie totale)	366 $\pm$21	324 $\pm$24	324 $\pm$21	361 $\pm$30
ΣE_n Energie moyenne par étoile sous forme nucléonique visible	140.1 $\pm$13	263 $\pm$27	144.5 $\pm$15	220.3 $\pm$26
$\Sigma E_{K\bar{K}}$ Energie moyenne émise par étoile sous forme de particules étranges	68 $\pm$23	68 $\pm$23	50 $\pm$25	50 $\pm$25
N_n Nombre moyen de branches lourdes par étoile	3.22 $\pm$ 0.2	5.66 $\pm$ 0.28	3.33 $\pm$ 0.34	5.09 $\pm$ 0.6
$N_{\pi\pm}$ Multiplicité moyenne des π chargés par étoile	2.54 $\pm$ 0.17	2.22 $\pm$ 0.17	2.50 $\pm$ 0.26	2.30 $\pm$ 0.28

TABLEAU 9

	Saclay		Berkeley	
	Au repos	En vol	Au repos	En vol
$\langle E'_\pi \rangle$ Energie moyenne des π issus du processus primaire (énergie totale)	322 $\pm$25	343 $\pm$23	337 $\pm$21	367 $\pm$25
$\langle U \rangle$ Energie moyenne par étoile des particules nucléoniques (chargées et neutres)	364 $\pm$34	684 $\pm$70	393 $\pm$36	612 $\pm$45
$\langle N_\pi \rangle$ Multiplicité moyenne des π	5.59 $\pm$ 0.30	5.7 $\pm$ 0.35	5.39 $\pm$ 0.34	5.33 $\pm$ 0.4
ν Nombre moyen de π interagissant à l'intérieur du noyau	1.29 $\pm$ 0.13	2.26 $\pm$ 0.14	1.32 $\pm$ 0.14	1.93 $\pm$ 0.14

du C.E.N. de Saclay. Au cours des opérations de développement, elles n'ont pas cessé de nous prodiguer leur temps et leurs conseils: nous les en remercions vivement.

En terminant, nous désirons exprimer notre gratitude à l'équipe des dépouilleuses du laboratoire d'émulsions à haute énergie, dirigée par M. Bernheim. Elles ont consacré de longs mois à la recherche fastidieuse des événements et nous voulons reconnaître ici l'enthousiasme et la discipline qu'elles ont témoignés dans leur travail. Mlle C. Patou de l'Université de Caen, qui a effectué un stage de plusieurs mois au laboratoire au cours du présent travail, y a apporté une collaboration que nous tenons à souligner.

Bibliographie

1) Chamberlain, Segrè, Wiegand et Ypsilantis, Phys. Rev. **100** (1955) 947
2) Chamberlain, Chupp, Ekspong *et al.*, Phys. Rev. **102** (1956) 921 (L)
3) Chamberlain, Chupp, Goldhaber *et al.*, Nuovo Cimento **3** (1956) 447
4) Hill, Johansson et Gardner, Phys. Rev. **101** (1956) 907
5) Cork, Lambertson, Piccioni et Wentzel, Phys. Rev. **107** (1957) 248
6) Chamberlain, Keller, Mermod, Segrè *et al.*, Phys. Rev. **108** (1957) 1553
7) Button, Elioff, Segrè, Steiner *et al.*, Phys. Rev. **108** (1957) 1557
8) Combes, Cork, Galbraith, Lambertson et Wentzel, Phys. Rev. **112** (1958) 1303
9) Barkas, Birge, Chupp, Ekspong *et al.*, Phys. Rev. **105** (1957) 1037
10) Chamberlain, Goldhaber, Jauneau *et al.*, Phys. Rev. **113** (1959) 1615
11) 1958 Annual International Conference on High Energy Physics at C.E.R.N., p. 85, 86
12) Bhowmik, Davies, Evans et Prowse, Nuovo Cimento **7** (1958) 712
13) Goldhaber, Goldsack et Lannutti, U.C.R.L. 2928 (23 mars 1955)
14) A. Garin, M. Levi et H. Faraggi, Rapport intérieur C.E.A., S.R.N.M.E., no 4 (1959)
15) Frye, Phys. Rev. Letters **1** (1958) 14
16) K. J. Le Couteur, Proc. Phys. Soc. A **63** (1950) 259
17) A. Berthelot, C. Choquet *et al.*, C.R. Acad. Sci. **248** (1959) 94—97
18) J. Sandweiss, Thèse, U.C.R.L. **3577** (octobre 1957)

NORTH - HOLLAND BOOKS

Paul Ehrenfest

COLLECTED SCIENTIFIC PAPERS

XII + 632 pages

Guilders 45.00 (90s.)

This volume makes widely scattered publications readily available. All Dutch articles appear here in English; the German publications in the original language.

Sole Agency for U.S.A.: Interscience Publishers Inc. – New York

Send your order to your bookseller or to:

NORTH-HOLLAND PUBLISHING COMPANY-AMSTERDAM

NORTH - HOLLAND BOOKS

Bruno Vitale

CERN-GENEVA

A Bibliography

on

Heavy Mesons and Hyperons

1946-1958

It has become difficult nowadays either to find a useful information or a pertinent reference in the field of "strange" particles. Now the aim of this bibliography is to classify and arrange in chronological order all the available papers on this matter. The book could be used also as a list of the problems that have been, or are at present discussed about "strange" particles.

6½×9½" VIII + 142p. Guilders 9.50 19s. $2.50

Send your order to your bookseller or to:

NORTH-HOLLAND PUBLISHING COMPANY — AMSTERDAM